Drop Formation and Rupture in Shearing during processing of Highly Concentrated Emulsions

by

SIPHO MDLEMBE

Thesis submitted in fulfilment of the requirements for the degree MASTER TECHNOLOGIAE: Chemical Engineering

In the Department of Chemical Engineering
Cape Peninsula University of Technology

DROP FORMATION AND RUPTURE IN SHEARING DURING PROCESSING OF HIGHLY CONCENTRATED EMULSIONS

SIPHO MUDEME

DROP FORMATION AND RUPTURE IN SHEARING DURING PROCESSING OF HIGHLY CONCENTRATED EMULSIONS

BY

SIPHO MUDEME

B Tech. (Chemical Engineering) (Cape Peninsula University of Technology)

Thesis submitted in fulfilment of the requirements
For the degree of
Master Technologiae

In the Department of Chemical Engineering
Cape Peninsula University of Technology

Supervisor: Prof. Irina. Masalova

Co-supervisor: Prof. R Haldenwang.

Cape Town, South Africa

March 2009

ABSTRACT

The purpose of emulsification process is to create numerous small droplets from a large and homogenous oil phase. The emulsion used for this study is new thermodynamically unstable multi-component water-in-oil (w/o) explosive type with an internal phase ratio of approximately 94% (wt), i.e. far beyond the close packing limit of spherical droplets of 74%. However, little work has been done for this system, pertaining to the literature explaining what physical phenomena plays a major role in the process of drop formation during highly concentrated emulsion (HCE) manufacturing. This thesis is devoted to develop an understanding of what parameters control drop formation and rupture during processing of highly concentrated emulsions.

The material used for the study consisted of three Pibsa derivatives (MEA, IMIDE and UREA), one mixture (MEA/SMO, 10:1) and SMO. Two concentrations were used namely 8% and 14% and the two fuel phase material were Mosspar-H and Shellsol. The Pibsa IMIDE was carried out in both oil phases. To carry out the study, the Hobart N50 mixer coupled with a power and harmonic analyser to record power as a function of time was used to manufacture all samples for the study.

Droplet size distributions from the Malvern Matersizer 2000 were modelled to determine the critical dimensions: diameter, width of distribution and time at which these dimensions are obtained. A Paar Physica MCR 300 rheometer with sand blasted plate – plate geometry to remove slip was used to measure flow curves and viscoelastic properties. The yield stress from the Herschel-Bulkley model and viscoelstic properties were measured at 30°C. Using the same geometry, the emulsion viscosity was measured at 70°C. Sand blasted bob and cup geometry was used to determine the viscosity of the dispersed phase at 85°C. Dynamical equilibrium interfacial tension between the two phases was measured on the Kruss K100 tensiometer at 70°C for all formulations and characterisation of droplet disruption was done using a power law model for formulations in Mosspar-H starting with similar droplet size distributions. Finally the single drop master curve (Grace curve) was used to prove/disprove that it is a good estimate for the system under study.

It was found that the average droplet size and width of distributions decrease exponentially with increase in energy density (KJ/Kg). The sauter mean diameter was found to decrease

exponentially with increase in energy density for all formulations. To manufacture similar droplet size, higher surfactant concentration required less energy. The critical diameter was found to be lower for high surfactant concentration. Comparison of calculated experimental energy input into making emulsions was found to be larger than the actual droplet surface energy. Rheological measurements indicated that both yield stress and viscoelastic properties increase with increase in energy density. The elastic modulus was found to be proportional to d_{32}^{-2}. Characterisation of droplet disruption was carried out for formulations in Mosspar-H. The disruption coefficient *C* was found to be lower for high surfactant concentrations. All calculations of capillary number, Ca and viscosity ratio, $\lambda(\eta_d/\eta_e)$ were done for all Pibsa derivatives. Plotting of Ca(λ) on the Grace curve (master curve for single drop) showed that the majority of points were in the breaking region, with some collecting close to the critical capillary region points. This generally confirmed that the master curve can be used as a good estimate for the system under study.

DECLARATION

I, Sipho Mudeme, hereby declare that, to the best of my knowledge, this thesis represents my own work and has not been submitted previously for examination toward any degree or diploma qualification at any other University. Further more it represents my own opinions and not necessarily those of the Cape Peninsula University of Technology.

.....

Sipho Mudeme

March 2009

DEDICATION

This thesis is dedicated to the following important persons:

My mother, Mudeme Ivy, the pillar of my strength, encouragement and a beacon of light to me,

My father, Mudeme Joseph, for his fatherly advice, motivation and support,

My brother and his wife (Ereck and Kefilwe), Lerato, the twins and her husband, Ketumetsi, Matsidiso, close relatives, and friends for their support, encouragement and advice.

And finally to my Lord, my Saviour, my guide and spiritual teacher, from whom I derived all my strength, perseverance, motivation and health,

ACKNOWLEDGEMENTS

I hereby wish to pass my sincere gratitude to the following people and organisations for their contribution towards completion of this thesis:

Prof. Slatter, head of the Flow process research centre who gave me the opportunity to pursue my goal, and allowed me to research in his research unit, his constant motivational speeches and in-depth knowledge in this field,

Prof. Irina Masalova, for her guidance, insight in the field, encouragement, moral and technical support, and motherly advice,

African Explosive Limited, the company that provided all the research material, and permission to use their Experimental Test Facility, as well as to make known results of this study,

The Cape Peninsula University of Technology Research Development Department for their financial assistance,

The Flow process research centre staff and students, for their assistance and support,

My family and friends (Reza, Fahimeh, Hamat, Samantha, Rose) for their moral support, love and prayers.

NOMENCLATURE

Symbol	Description	Unit
ΔA	Change in interfacial area	m^2
Ca	Capillary number	...
Ca_{crit}	Critical capillary number	...
C_e	Centreline distance between agitator and bowl	m
$\%C_{surf}$	Concentration of surfactant	%
cmc	Critical micelle concentration	%
d	Droplet size	m
d_{max}	Maximum droplet size	m
d_s	Mean solid size	m
D_{50}	Average droplet size	m
d_{32}	Sauter mean diameter	m
D_A	Diameter of agitator	m
D_B	Diameter of bowl	m
D_0	Initial droplet size	m
D	Deformation	s^{-1}
D_s	Surface diffusivity	m^2s^{-1}
D_{cal}	Calculated diameter	m
D_{crit}	Critical diameter	m
E	Elasticity number	
E_v	Energy per volume	$J\ m^{-3}$
E_p	Energy density	$J\ g^{-1}$
E_{exp}	Energy calculated from experiment	$J\ g^{-1}$
E_{thoe}	Theoretical energy	$J\ g^{-1}$

E_a	Activation energy	J/mol
G	Velocity gradient	s^{-1}
G*	Complex shear modulus	Pa
G'	Storage modulus	Pa
G"	Loss modulus	Pa
G'_P	Plateau modulus	Pa
ΔG	Change in Gibbs energy	J mol^{-1}
∇_S	Surface gradient operator	...
$\nabla_S\sigma$	Marangoni stress	Pa
H	Height of mixing zone	m
j_n	Net flux	kg/m^2s
K	Fluid consistency index	$Pa.s^n$
K_G	Elasticity coefficient	$Pa.\mu m^n$
L	Length of cylinder	m
p	Laplace pressure	N/m^2
Δp	Difference in Laplace pressure	N/m^2
P_{es}	Peclet number	...
P_V	Net power density	Wm^{-3}
R	Radius	m
R_a	Gas constant	J/mol K
R_1	Principal radii of curvature	m
R_2	Principal radii of curvature	m
r	Radius of cylinder	m
S.A	Surface area	m^2
ΔS	Change in entropy (specific)	J/Kg

T	Temperature	°C
T_a	Absolute temeperature	K
T_c	Congelation temperature	°C
T_d	Crystallisation temperature or Fudge Point	°C
T_{hn}	Homogenous nucleation temperature	K
t_{mixing}	Mixing time	min
t_{ads}	Adsorption time	min
V_D	Volume of emulsion droplets	m^3
V_E	Total volume of the emulsion	m^3
X	Surface coverage	...

Greek symbols

β	Constant	...
Γ	Surface excess per unit area	$1/m^2$
Γ_∞	Surface excess per unit area at infinity	$1/m^2$
δ	Phase angle	rad
$\dot{\gamma}$	True shear rate	s^{-1}
$\dot{\gamma}_{Ave,Hob}$	Average shear rate of Hobart N50 mixer	s^{-1}
$\dot{\varepsilon}$	Elongation rate	s^{-1}
η	Shear viscosity	Pa.s
η_0	Zero shear rate	Pa.s
η_c	Continuous phase viscosity	Pa.s
η_d	Dispersed phase viscosity	Pa.s
η_e	Emulsion viscosity	Pa.s
η_{eff}	Effective viscosity	Pa.s

θ	Characteristic time	min
λ	Viscosity ratio	...
ρ	Density	$Kg.m^{-3}$
σ_0	Initial interfacial tension	$N.m^{-1}$
σ	Interfacial tension	$N.m^{-1}$
σ_{eq}	Equilibrium interfacial tension	$N.m^{-1}$
τ	Shear stress	Pa
τ_y	Yield stress	Pa
ϕ	Internal phase ratio or volume fraction	...
ϕ_{eff}	Effective volume fraction	...
ϕ_m	Maximum volume fraction	...
ϕ_s	Volume fraction of solids	...
ω_0	Initial width of droplet size distribution	...
ω_{crit}	Critical width of droplet size distribution	...
ω_{cal}	Calculated width of droplet size distribution	...

ABBREVIATIONS

AN	Ammonium nitrate solution
Moss	Mosspar-H

Terms and Concepts Cited

Term	Definition
Capillary number	Ratio between the viscous stress which acts to deform the droplet and stabilising Laplace pressure
Critical capillary number	Capillary number at which droplets are just able to break up
Emulsion explosive	High internal phase water-in-oil emulsion of a concentrated solution of nitrate salts in water emulsified into an oil base.
Flow curve/Rheogram	Curve relating shear stress to the true rate of shear.
Interfacial tension	Measurement of cohesive (excess) energy present at an interface arising from the imbalance of forces between molecules at an interface (gas / liquid, liquid / liquid, gas / solid, liquid / solid)
Marangoni stress	Liquid motion caused by movement of surfactant in the Interface in the direction of higher interfacial tension due to the difference between dynamic and static tension.
Newtonian fluid	Any fluid that has a direct proportionality between shear stress and shear rate
Peclet number	Dimensionless group which relates forced convection of a system to its heat conduction
Rheology	Science of deformation and flow of matter, it deals with the deformation of materials as a result of an applied stress
Rheological Model	An idealised relationship of rheological behaviour expressible in mathematical, mechanical or electrical terms
Rheometer	An instrument for measuring rheological properties.

Sauter mean diameter	The ratio of volume to surface area of the dispersed phase droplets.
Shear rate	Rate of shear deformation, change of shear deformation per unit time.
Shear stress	Component of stress parallel or tangential to the direction of flow.
Storage modulus	The quotient of the part of the stress in phase withthe strain divided by the strain under sinusoidal conditions
Viscosity	The property of a material to resist deformation increasingly with increasing shear rate, a measure of this property is defined as the quotient of shear stress divided by shear rate in steady flow.
Viscous	The tendency of a liquid to resist flow as a result of internal friction. During viscous flow, mechanical energy is dissipated as heat and the stress that develops depends on the rate of deformation
Viscoelastic material	Material exhibiting both viscous and elastic effects under the action of outside stresses in the absence of time dependence
Yield stress	Stress corresponding to a yield point.

TABLE OF CONTENTS

LIST OF FIGURES

LIST OF TABLES

CHAPTER 1

Introduction

1.1 Background

The subject of this study is highly concentrated emulsion explosives. The emulsions investigated are dispersions of an aqueous phase (up to 85% by volume) in an oil phase. The dispersed droplets consist of an aqueous solution of nitrate salts that is supersaturated at room temperature, comprising less than 20% water by mass. Compounds of this kind are thermodynamically unstable and their instability is related to the coarsening of the emulsion (droplet coalescence) and phase transition (crystallisation) in the dispersed phase.

It is well known that liquid droplets dispersed in another liquid can be ruptured with the formation of smaller droplets. The classical theory of this effect was first proposed by Rayleigh (1879, 1882) and Bohr (1909) and then the modern version of the theory was developed by Tomokita (1935, 1936). They considered the problem of instability of a liquid thread, which finally, under the action of surface forces, destructed into individual droplets. It was shown in many visual investigations (Milliken and Leal, 1991) that a droplet initially is stretched into a thread and, after that, the Rayleigh-Tomokita mechanism of rupture takes place. The Rayleigh-Tomokita theory relates to a single droplet, so destruction of a liquid stream due to surface tension is determined by the ratio of viscous stress to interfacial stress and this phenomenon is ruled by the capillary number, *Ca*.

It was shown by Grace (1982) that there is some critical number value Ca_{crit} at which the droplet rupture can occur and this Ca_{crit} value depends on the ratio of viscosities λ of both components of an emulsion. The dependence of Ca_{crit} (λ) was found theoretically for a wide range of λ values. Experimental evidences by Jackson and Tucker (2003) completely confirms theoretical predictions for a range of λ from 10^{-6} to 10^{2}. Later model experiments were carried out by Mason and Bibette (1996) for a single droplet, which clearly demonstrated that the dependence of the final radius (after shearing) depends on shear rate according to the scale rule:

$$R = \frac{C\sigma}{\eta_{eff}\dot{\gamma}} \quad , \qquad \textbf{Equation 1.1}$$

where *C* is a geometrical constant of order of unity which corresponds to the existing conception.

Meanwhile, it is important to develop our understanding of the problem from the behaviour of a single droplet in shearing to the rupture of droplets in concentrated emulsions. Several works were carried out along this line. The most comprehensive is the publication by Jansen *et al.*, (2001) in which the authors worked not with a single droplet but with emulsions of different concentrations. They have demonstrated that the analogous approach (as in the case of a single droplet) can be applied with some modification of the determining factors. First of all they proposed to substitute the viscosity of a droplet in the definition of the capillary number, *Ca* by viscosity of emulsion and the viscosity ratio of liquid drop to emulsion viscosity. In this approach the authors obtained the universal dependence of Ca_{crit} on λ valid in the whole range of concentration of emulsions from 0 to 70% but below the concentration of the maximal dense packing φ^*. It is interesting to mention that the minimal value of Ca_{crit} on the $Ca_{cr}(\lambda)$ dependence equals 0.41 for the whole concentration range. In their publication (Jansen *et al.*, 2001) the problem of droplet influence of shear on the final size of droplets size was also discussed and experiments were carried out for the whole concentration range (below the limit of the maximal dense packing, φ^*). As in previous models of a single droplet, it was found that the same scaling law is valid and the rule:

$$\dot{\gamma}_{crit} = const \qquad \textbf{Equation 1.2}$$

was fulfilled. However, in all these cases only classical emulsions were discussed, in which the concentration of a dispersed phase was below the limit of the maximal dense packing φ^*.

The current research study is devoted to developing the existing conception of droplet instability in shearing, where concentration of a dispersed phase exceeds the limit φ^*, as one is dealing with so-called "compressed" emulsions and rheological methods of testing; characterisation and correlation of the flow properties of highly concentrated w/o emulsions. At present, rheological characterisation of many complex fluids is well documented, therefore the use of this knowledge as a base for analysis of the flow properties of these emulsion systems it was expected to obtain fruitful results. Knowledge of both shear and storage-induced structure instabilities, as well as the prediction of pumping characteristics from rheometry could be established from such a study.

1.2 Problem statement

When the study was commenced, there was no fundamental theory for the break-up of droplets in highly concentrated emulsions. It was deemed likely that hydrodynamic interactions play an important role between closely neighbouring droplets during the interfacial instabilities.

1.3 Objectives of the study

The main objective of this study was to:

- Correlate the influence of energy input in the emulsification process on droplet size and droplet size distribution.
- Determine the critical diameter and width of size distribution with prolonged mixing time.
- Determine the effect of surfactant concentration and type on droplet size.
- Determine and compare experimentally calculated energy with theoretical energy needed to expand an interfacial area in the emulsification process.
- Determine droplet disruption coefficients from power law dependence of droplet size versus energy.
- Correlate the influence of energy input on yield stress and shear modulus.
- Determine elasticity-droplet size dependency
- Determine the capillary number as a function of viscosity ratio of the dispersed phase to emulsion viscosity.

1.4 Research design and methodology

To accomplish these objectives, the research was conducted in the manner outlined below.

1.4.1 Manufacture of samples using the Hobart N50 mixer

Different droplet sizes from each formulation were manufactured by varying the emulsifying time from:

- Five surfactants: Pibsa-MEA, Pibsa-IMIDE, Pibsa-UREA, Pibsa-MEA/SMO (10:1), SMO.
- Oxidiser - Ammonium nitrate (AN).
- Two continuous phases of oil– Mosspar-H and Shellsol.

1.4.2 Measurement of power and time using Power and harmonic analyser

- Power and time were recorded during the emulsification process for each formulation.
- Energy was computed for all formulations by integration of power versus time.

1.4.3 Measurement of particle size distribution

- Samples manufactured were measured on the Malvern Mastersizer 2000 for droplet size and droplet size distribution.

1.4.4 Determination of critical diameter and critical width of droplet size distribution

- The Gauss equation was used to model the width of the size distributions for all formulations.
- Different droplet sizes from each formulation were modelled by using a proposed model to find the critical diameter and characteristic time.
- Widths from Gauss fitting for different mixing times for each formulation were modelled using a similar equation to the latter to find the critical width and characteristic time.

1.4.5 Rheological experiments using Rheometer MCR 300, Anton Paar

- Two geometries were used, namely plate-plate and bob cup.
- Using the plate-plate geometry, the following were measured:
  - Flow curves (200-$10^{-4}s^{-1}$) were measured at 30°C to determine the yield stress.
  - Oscillatory measurements (0.01- 200%) at 30°C.
  - Emulsion viscosity (800-$50s^{-1}$) was measured at 70°C corresponding to the Hobart N50 average shear rate.
- Bob and cup geometry was used to determine the ammonium nitrate solution viscosity at 85°C corresponding to the Hobart N50 average shear rate from a temperature sweep.

1.4.6 Measurement of interfacial properties

- Interfacial tension between the two phases was measured by means of the Kruss K100 tensiometer.

This study was expected to provide a better understanding of the droplet formation and rupture during shear and behaviour of highly concentrated w/o explosive emulsions and to also give much insight into the efficient processing conditions for preparation of highly concentrated explosive emulsions, as well as their transportation in chemical engineering processing.

The thesis is subdivided into the following chapters:

- **Introduction (Chapter 1)**

Serves as an introduction to this thesis.

- **Literature Review (Chapter 2)**

Relevant literature on highly concentrated emulsion formation and droplet break-up is reviewed in this chapter. This includes different methods of emulsion formation and also the role of a surfactant in the emulsification process. The most relevant literature was the work of Walstra (1983), McClements (2004) and Karbstein and Schubert (1995). Fundamentals of droplet break formation, deformation and break-up are presented, which include the equations governing droplet deformation and break-up which are presented in detail.

- **Experimental Work (Chapter 3)**

A discussion of the material used for the study, as well as the instrumentation used to carry out the study, is presented in this chapter. Models to characterise the results and experimental methods used to analyse errors and the inherent discussions pertaining to their corrections are also outlined.

- **Results and Discussions (Chapter 4)**

Chapter 4 deals with the analysis of results and the discussion of these results includes comparison with the findings obtained from the literature.

- **Conclusions and Recommendations (Chapter 5)**

This chapter summarises the thesis. Conclusions are drawn from results discussed in Chapter 4 and recommendations are outlined.

CHAPTER 2

Literature Review

2.1 Introduction

This chapter outlines the relevant fundamental theory concerning droplet formation and rupture under shear stress of highly internal phase ratio emulsion explosives.

The following topics are covered in this chapter: (1) definition of emulsions; (2) rheology of highly concentrated emulsion (HCE); (3) rheology of explosive emulsions (EM); (4) drop formation by emulsification; (5) influence of surfactant; (6) theory of droplet break-up; (7) break-up in concentrated emulsions; (8) role of surfactant in drop deformation and break-up.

2.2 General definition of emulsion and emulsion explosives

Emulsions are categorised according to the distribution of their oil and aqueous phases. The distribution of oil droplets dispersed in an aqueous medium constitutes what is referred to as an oil -in -water emulsion (o/w) and the distribution of water droplets in an oil medium constitutes what is called a water-in-oil emulsion (w/o).

The mixing process of two immiscible fluids to form an emulsion is known as homogenisation. The possibility of homogenising pure oil and pure water is met with rapid phase separation which consists of two layers, with oil at the top (lower density) and water at the bottom (higher density) and this is due to neighbouring droplets merging as they collide, which finally separates into two phases. The mechanism behind this phase separation between water and oil droplets is the unfavourable energy (Israelachvili, 1992) that renders emulsions thermodynamically unstable. The availability of an interface causes unequal forces that affect the energy of particles at or close to the interface, giving particles in that zone a net energy higher than those in the bulk.

To form kinetically stable emulsions for a reasonable period of time, the droplets must be prevented from coalescing together after they have been formed (Walstra, 1983) and this is achieved by including an emulsifier and/or thickening agent during the homogenisation process. The mechanism leading to the lowering of energy of the system emanates from the availability of the interface, which results from the adsorption of materials such as emulsifiers at the interfaces. The action of the adsorbed materials in lowering the surface energy reduces the amount of

energy required to generate a new interfacial area and therefore facilitates the preparation of emulsified systems.

Concentration of droplets has been shown to vitally influence some characteristics of an emulsion such as texture, stability, appearance and cost of emulsified products. Droplet concentration is described in terms of the volume of the dispersed phase (ϕ), formulated by emulsion droplet volume (V_D) divided by the total volume of the emulsion volume (V_E): $\phi = V_D/V_E$. The composition of the emulsion is conveniently described in terms of mass fraction of the dispersed phase (ϕ_m), which, in turn, is in relation to the volume fraction given by the equation:

$$\phi_m = \frac{\phi \rho_2}{\phi \rho_2 + (1-\phi)\rho_1}$$ **Equation 2.1**

where ρ_1 is the continuous phase density and ρ_2 is the aqueous phase density.

An interesting effect is the inversion of an oil in water emulsion to a water- in- oil emulsion. Generally speaking, the methods whereby inversion may take place involve introducing a condition such that the opposite type of the emulsion would normally be the stable one. First, an emulsion would have to invert if ϕ exceeded 0.74, if the inner phase consisted of a uniform rigid sphere and this value ϕ represented the point of close packing. Actual emulsion droplets are deformable, and not monodispersed. Continuous addition of the inner phase may result in inversion, but the effect is not assured and certainly will not be controlled by the theoretical ϕ value of 0.74.

Becher (1965) showed that the volume fraction of a stable emulsion can be increased to a certain value, beyond which inversion or breakage of an emulsion is observed. The theory of phase volume by Ostwald (1910) reveals that this is the point at or near 0.74, which is the hexagon packing of spheres which are in distorted configuration. Stable emulsions of considerably higher volume fraction of the dispersed phase, or highly concentrated emulsions (HCE), or high internal phase emulsions are known to exist under the following conditions:

- When the emulsion is strongly heterodispersed, the interstices between the spherical droplets can be filled successively by smaller ones. This would, in principle, allow the dispersed phase volume fraction to closely approach unity. In practice this peculiar kind of heterodispersity will rarely, if ever, be encountered.

- Under the influence of a centrifugal field, the emulsion can be compressed (Mittal, 1975). Under this compression, deformation of droplets results, i.e. they flatten in those areas where they make "contact" and assume the shape of polyhedra with rounded edges and corners.
- Emulsions with volume fractions of an aqueous phase close to 0.99 have been studied. In this system, extensive work has been done, notably by Princen (1979, 1980), Nixon and Beerbower (1969) and Lissant (1966, 1970, 1973, 1974). Such high values of high volume fraction of an aqueous phase were obtained with no application of a field from the centrifugal and does not explain on the basis of heterodispersity. The authors stress the importance of surfactants. Lissant (1966, 1970, 1973, 1974) postulated and demonstrated that the droplets are deformed into polyhedral structures of particular types.

Emulsion explosives (EM) have a high volume fraction of dispersed phase water in oil emulsion. The water phase consists of high concentration salts from Group 1 and Group 2 metals, namely sodium, calcium and magnesium, blended in a hydrocarbon oil phase. Commercially made emulsions traditionally use three types of explosives (namely: nitroglycerinenitro-glycerine dynamite, dry blasting agents and slurries or water gels), which are composed mainly of intimate mixtures of group 1 and group 2 metal salts of nitrates mainly sodium, magnesium calcium as condensed oxidisers, blended in a hydrocarbon oil or wax, as well as buffers. Buffers control pH, physiochemical and detonation properties.

Emulsion explosives show interesting characteristics. The capability to detonate and the velocities of explosion are influenced by the mixed components described in the previous paragraph and droplets in the order of about 1μm in size are used in practice. Since water proves to be a good reducing agent for detonation, the degree of responsiveness to the presence of water is managed by monitoring the level of water in the emulsion formulation. As a result, the required stoichiometry for the reduction-oxidation reactions manifest a reaction that is solved by means of large amounts of highly concentrated salt solution, finally emulsified in an oil phase. In industry, an ammonium nitrate solution makes up about 70% by volume of the emulsion composition. The aqueous phase constitutes about 90% by mass. The aqueous phase is sometimes made up of other nitrate salts of sodium and calcium mixed in hydrocarbon oil or wax (7 to 10%). Other supplements are included, for instance glass, aluminium powder, plastic micro bubble, as sensitizers.

The particle size distribution indicates that, independent of method of preparation, the explosive emulsion can be considered a blend of (usually) three generations of log-normal distribution, the largest $\overline{D_m}$ is the most homogenous and the generation with smallest $\overline{D_m}$ is the most polydispersed. Studies reveal that the droplet size distribution of the aqueous phase is a blend of three generations of log-normal distributions [$\varphi(1)$, $\varphi(2)$ and $\varphi(3)$] in the following proportions 22%, 58%, and 20% respectively, and that the mean droplet sizes and standard deviations for these generations are as follows $\overline{D_m}(1):\overline{D_m}(2):\overline{D_m}(3)=1:0.69:0.37$ and $\sigma(1):\sigma(2):\sigma(3)=1:1.3:3.5$ and that 0.1μm is the limiting droplet size for these systems. The property function of the explosive emulsion is related to some rheological and explosive properties. Since the volume fraction of the aqueous phase is in the range of 0.88 to 0.94, the microstructure is described as being polydispersed as opposed to monodispersed.

To serve as a complete theoretical description of emulsion, a theory must be able to explain and predict all aspects of emulsion formation, stability and type, the influence of environmental factors such as temperature and pressure, the role of emulsifiers and stabilisers and the chemical structures of the immiscible phases, as well as the effects of additives in each phase. That is a very tall order, as illustrated by the fact that even though a vast amount of experimental data relating to each of these issues are available, no general applicable theory has been presented.

2.3 Theory and Rheology of highly concentrated emulsions

Emulsions with a high volume fraction of aqueous phase or high packing are referred to as high internal phase ratio emulsions (or simply HIPRE emulsions) in which the aqueous phase occupies more than the maximum packing volume fraction of 0.74 for spheres having the same diameter (Tai *et al.*, 2001). The aqueous phase droplets are arranged hexagonally in packing. This arrangement enhances droplet-droplet interaction, which makes movement of droplets difficult due to 'friction' between moving droplets. Similar findings by Pal (1999) showed that, when the aqueous phase volume is greater than maximum packing, such droplets are no longer spherical, but are deformed against their neighbours and take the shape of a polyhedron. In such systems extensive aggregation or flocculation of the dispersed phase droplets occur, which results in a stable, weak, gel-like particulate network (Jager-Lezer *et al.*, 1998; Partal *et al.*, 1997).

Since the rheological properties of HIPREs are governed by a three-dimensionally interconnected network structure of thin liquid films of the continuous phase, they show very complex rheological behaviour. They show a plastic-like response under deformation and, when subjected to small shear deformation, they exhibit strong modulus and yield stress, with the applied force linearly changing proportional to the strain. Deformations of drops below the yield stress are insufficient to allow a flow in a global movement and, consequently, elastic behaviour, whereas the deformations above the yield stress are sufficient to induce a flow, which is characterised by the predominance of the viscous effect. Their viscoelastic properties have been shown to depend on drop size, polydispersity, interfacial tension and volume fraction (Jager-Lezer *et al.*, 1998).

Emulsion systems with a high volume fraction of the dispersed phase tend to show or exhibit strong non-Newtonian behaviour, which is characterised by both shear thinning and elastic behaviour. The flow properties of highly concentrated emulsions are controlled by different interacting forces that occur within them and these forces depend on the dispersed phase fraction, the concentration and nature of the emulsifier, the chemical composition of the continuous phase and interfacial properties. The non-Newtonian behaviour is characterised by the existence of yield behaviour and a strong shear-thinning region, in which the apparent viscosity is dependent on the rate of shear or shear stress. The yielding behaviour is due to flocculated droplets in the dispersed phase undergoing deformations when the applied shear stress exceeds the dynamic yield stress and this takes place as the flocs deform in the direction of flow and that of the flow gradient. When the latter occurs, the disintegration of flocs into spheres with an increase in the rate of shear or shear stress takes place and droplet-droplet interaction forces a decrease, thus lowering the emulsion viscosity (Mezger, 2002; Pal, 1999). It was demonstrated that highly concentrated emulsion systems exhibit a lower Newtonian shear viscosity and thus behave like elastic solids at this low shear rate region (also referred to as the zero-shear viscosity,η_0) (Cross, 1965; Ultracki; 1980; Kozicki and Kuang, 1993).

The problem discussed in many research papers is the influence of the size of the droplet on the properties of rheology. The influence of the size of the droplet in relation to viscoelasticity was studied by Otsubo and Prud'homme (1994a) and they found that viscosity (especially at high concentration of a phase) strongly depends not only on the average droplet size but is influenced by the breadth of droplet size, although for relatively narrow distribution; this effect can be neglected (Barnes, 1999; Lacroix *et al.*, 1997). Masalova *et al.*, (2003b) investigated the

complete rheological characterisation of highly concentrated emulsions by doing a full set of rheological measurements including steady flow, transient regimes of deformation and viscoelastic measurement. The droplet sizes of emulsions were quantitatively defined and the influence of droplet size on rheology was clearly determined. Among the variables, the drop size has been shown to strongly influence rheological properties. A model predicting the rheological properties of high internal phase emulsions on drop size was proposed by Princen and Kiss (1989) and several authors observed the dependence of elastic modulus on reciprocal diameter, based on this model principle (Pal, 1999; Babak *et al.*, 2001; Pal, 2002). However, the results from Malkin *et al.*, (2004) showed that the elastic modulus measured in oscillatory tests and the droplet size is inversely proportional to the square of drop diameter.

Meanwhile the current interest in studies of the rheological properties of emulsions has been focused on highly (or super-) concentrated emulsions with the content of the dispersed phase exceeding this limit. Viscoelastic properties of such emulsions were measured (Pons et al., 1992, 1995) and treated in the frames of simplest Maxwellian relaxation mode and the model of flow of such emulsions was also proposed (Schwartz and Princen, 1987). The viscoelasticity of HCE is strongly influenced by the concentration of the aqueous droplets and this was discussed in work concerning Princen's theory (Ponton *et al.*, 2001).

In summary: the effect of droplet size in emulsions which are highly concentrated on the rheological properties reveal that the drops cannot remain spherical, they are deformed into polyhedral shapes and a thin liquid film (interface) is formed between the deformed droplets (Princen, 1979). The rheological properties of such emulsions are controlled by the network structure of the thin liquid film of the continuous phase. When the emulsion is subjected to shear forces, the liquid films must stretch or shrink until a critical strain is achieved, which results in steady flow. Most rheological properties of these emulsions are related to the Laplace pressure (σ/R). Thus, with the decrease in droplet size, the yield stress, viscosity and elastic modulus are expected to increase (Princen, 1979, 1985; Princen and Kiss, 1986, 1989).

Based on latter, the following general conclusion can be drawn regarding the effect of droplet size:

- For dispersions of deformable spherical particles, the rheological properties are governed by a network of thin films of the continuous phase if the particle concentration is above the close-packed configuration. The rheological parameters of such emulsions increase with a decrease in droplet size (Pal, 1996b).

2.3.1 Viscoelastic properties of highly concentrated emulsions

In defining viscoelastic properties, two important properties are taken into account namely elastic and dissipative losses. It has been considered that the development of delayed stress gives rise to viscoelasticity. This deformation with respect to time and delay should not be confused with other effects like inertia, which have been shown to be specifically characterised with a time lag. Viscoelastic property can be described by three experiments:

- Creep – delayed development of deformations under action of constant force (or stress)
- Relaxation – slow delay of stresses at preserving constant deformation
- Periodic Oscillation – harmonic changing of stresses or deformations with relative shift of deformation in relation of stress.

The characteristics of linear viscoelasticity of a material are interrelated by algebraic equations and can be mutually recalculated. That is why the linear theory of viscoelasticity is a closed theory, containing all necessary equations in order to estimate mechanical behaviour of a material in an arbitrary stress deformation situation based on measurements of any fundamental characteristic of viscoelastic properties of the material (Malkin, 1994).

One of the most powerful methods of investigating interactions between droplets in concentrated emulsions is the measurements of viscoelastic properties of these systems (Tadros *et al.*, 1990). By measuring viscoelasticity dependence on the aqueous phase volume of droplets or as a function of some other parameters, useful information is gathered and this is interpreted in terms of the interactions between droplets (Pons *et al.*, 1995). By modifying these interactions, bulk rheological properties of emulsions can be modified.

The theory of linear viscoelasticity is used for:

- Obtaining objective characteristics of a material which can be correlated with their structure and/or content.
- Verification of conclusions from theories, which give grounds for understanding the structure of a material and inter particle interactions.
- Calculation of mechanical behaviour of a material in arbitrary regimes of their exploitation (but rather low levels of stress) (Malkin, 1994).

Experiments as well as theory on HIPREs (highly compressed emulsions) have been investigated, where the dispersed phase droplets are very close to each other and separated by a thin film of continuous phase formed at each point where droplets touch (Barry, 1975; Princen, 1979, 1980, 1983, 1985; Aronson and Petko, 1993; Bibette, 1992; Benali, 1993; Reinelt and

Kraynik, 1993; Otsubo, 1994a, Princen and Kiss, 1986, 1989). Their viscoelastic properties have been shown to be strongly influenced by the average size of dispersed phase droplets, how the droplets are polydispersed, interfacial tension between the two phases and, mainly, the volume fraction of the aqueous phase.

In oscillatory shear, the evolution of the linear viscoelastic functions in the frequency range between 10^{-2} and 10^{2} rad/s, for highly concentrated emulsions, is characterised by the appearance of a minimum in the loss modulus at intermediate frequencies and a "plateau region" in the storage modulus. In addition, the frequency dependence of both moduli is clearly dependent on the emulsion concentration, processing conditions and nature of the emulsifier used (Franco *et al.*, 1995, 1997; Tadros, 1994). The plateau region of G', according to Guerrero *et al.*, (1998), has been related to a network structure due to the interaction between emulsifier particles positioned at the oil-water interface of nearby droplets (Dickson, 1989; Franco *et al.*, 1995; Bird *et al.*, 1987). Ferry (1980), in polymer rheology, described the plateau region as an entanglement network among polymer chains in which the neighbouring molecules constrain the movement of molecules. This defines the elastic region. The change from elastic to viscoelastic domain was defined precisely by noting the stress (or strain) when G" reaches a maximum, this critical stress being considered a yield stress. The G" peak confirms and elucidates the transition from the elastic to the viscoelastic region. From a micro structural point of view, this peak probably means that the dissipation energy is maximal when the droplets are deformed and flattened enough to allow flow despite the crowding. This behaviour has been generally found for highly flocculated o/w emulsions such as mayonnaise (Gallegos *et al.*, 1992; Guerrero and Ball, 1994), salad dressing stabilised by egg proteins (Franco *et al.*, 1995; Moros *et al.*, 2003; Munoz and Sherman, 1992) and concentrated emulsions stabilised by vegetable proteins (Bengoechea *et al.*, 2006; Franco *et al.*, 1998, 2000; Raymundo *et al.*, 2002). The occurrence of a well-developed plateau region, where a very low frequency dependence for G' can be observed, has been a result of the formation structural network that confers a high stability to the emulsion (Dickson, 1989; Franco *et al.*, 1995).

Whatever the volume fraction studied, a plateau zone appears, and it becomes extended for higher volume fractions. It has been shown in results obtained by Jager-Lezer *et al.*, (1998) that a decrease in the volume fraction is accompanied by a decrease of elasticity, expressed by values of G* (complex shear modulus) and δ (phase angle), which are a reflection of a less and less compact organisation, especially when $\phi < 70\%$.

Finally, Malkin *et al.*, (2004) and Masalova and Malkin (2007) have proved experimentally that the storage modulus, G' is constant over a wide range of amplitudes and frequencies, and it is significantly compared to the loss modulus. Therefore this plateau value of G_p' can be considered as shear modulus of material. An almost linear relationship between plateau modulus (from frequency sweep, Figure 2.1) and agitation speed was established using an oil in water emulsion which was highly concentrated and stabilised with crayfish flour (Romero *et al.*, 2008). Only the emulsion prepared at the highest agitation speed deviated from this tendency.

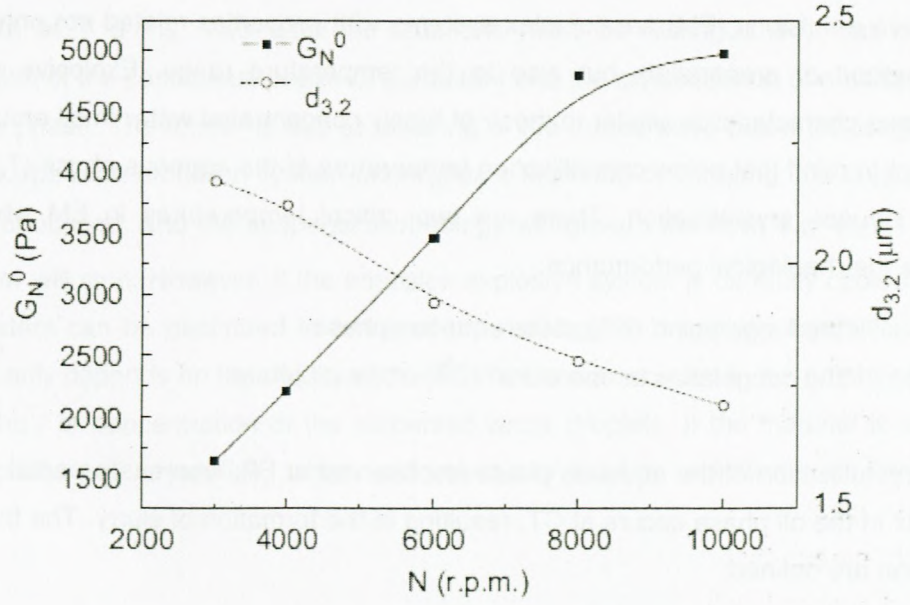

Figure 2.1: Evolution of plateau modulus and d_{32} (Adapted from Romero *et al.*, 2008)

2.3.1.1 Elasticity – Droplet size effect

Previously published experimental data (Malkin *et al.*, 2004) obtained for various droplet sizes demonstrated that the G(D) and τ_y dependencies comply with rules $G \propto D^{-2}$ and $\tau_y \propto D^{-2}$ rather than linear dependencies, which have been shown by some researchers (Babak *et al.*, 2001; Pal , 2002; Princen and Kiss, 1986), as well as by the work of other researchers (Pons *et al.*, 1992; Langenfield *et al.*, 1999; Aronson and Petko, 1993) for other emulsions, not to correspond to the experimental data measured by Malkin *et al.*, (2004). The experimental data was approximated by the empirical equation:

$$G = k_G D^n \qquad \textbf{Equation 2.2}$$

where the numerical value of the coefficient k_G is approximately 10^5 (Pa.μm^2). The reason for the discrepancy of the experimental results from other researchers was related to the type of

emulsion used (emulsions in the other studies were not as highly concentrated as the one in this study), as well as the difference in the averaging procedure for the polydispersed samples. Interestingly, studies by Mougel *et al.*, (2006) on the ageing of an unstable w/o gel emulsion with non-ionic surfactant SMO found that elastic modulus (G') dependence with average droplet size radius R for different volume fractions was better correlated to $1/R^2$, especially for volume fractions greater than 75%.

2.4 Theory and Rheology of highly concentrated explosive emulsions (EM)

Explosive emulsions (EM) are complex systems with properties related not only to composition and method of preparation, but also to the temperature range. Explosive emulsions have numerous characteristics similar to those of highly concentrated water in oil emulsions, provided it is kept in mind that below crystallisation temperature of the aqueous phase (T_d), impartation of shear induces crystallisation. There are two critical temperatures in EM which significantly change the rheological performance:

i) "the fudge point" (FP) of the aqueous phase
ii) "the congelation temperature" (CT) of the oil phase

Bulk crystallisation of the aqueous phase is observed at FP, whereas a partial crystallisation of the wax in the oil phase occurs at CT, resulting in the formation of slurry. The following states of emulsion are defined:

a) true emulsion at T> FP > CT
b) suspension-emulsion at FP > T > CT
c) "solid froth" at FP > CT > T

There are two factors influencing emulsion viscosity, and these are the total effective volume fraction of the dispersed phase, ϕ_{eff} (the higher the value of ϕ_{eff}, the higher the viscosity, η), and the deformability of the droplets (the larger the size of the droplets, the higher is their deformability, and the lower is the viscosity). Emulsion explosives are considered as supercooled, aqueous-phase dispersions (with volume a fraction of about 0.90 or more) in a partially crystallised oil phase. Partial crystallisation of the aqueous phase by a heterogeneous nucleation mechanism at a temperature, $T_d \cong 65 - 70^0C$ occurs due to high degree of supercooling. Consequently, the system changes to a suspension-emulsion system, whose properties are intermediate between those of suspensions, and those of emulsions. In this case,

the emulsion playa the role of the continuous phase, while the solid particles play the role of the aqueous phase. If kept for a period of time, gradual changes of crystals take place structurally from a multi crystalline form to a well-defined crystal. In the absence of nuclei, the droplets that remain can be supercooled to the homogenous nucleation temperature, T_{hn} (°K):

$$T_{hn} = k(T_d + 273) \qquad \textbf{Equation 2.3}$$

where k = 0.82 ± 0.02, and T_{hn} = -3°C to 11°C.

The rate of this crystallisation process changes proportionally with droplet size. It decreases with temperature at $T \leq T_{hn}$. Two different situations must be distinguished, that is, the shear crystallisation of the continuous phase or surfactant and the crystallisation of a component of the continuous phase. The former is due to lowering of the temperature below its congelation point T_c. If the suspension-emulsion system undergoes a high rate of shearing, the crystallisation will be very pronounced, and the suspension rheology will govern the flow, e.g. $\phi_{eff} \rightarrow \phi_m$, $\eta \rightarrow \infty$ and the flow will stop. However, if the emulsion explosive system is carefully cooled to $T_{hn} < T < T_c$, the system can be described in terms of the rheology of a partially crystallised oil phase, which primarily depends on the rigidity of the matrix, the wax content in the oil phase, but not on the size and / or concentration of the dispersed water droplets. If the material is sheared, the aqueous phase will crystallise, which will eventually lead to solidification of the emulsion explosive.

Little work has been reported on the rheology of high internal phase suspo-emulsions. However, the following conclusions pertaining to the rheology of suspo-emulsions can be drawn from studies conducted by Pal and colleagues (1990, 1991): (a) At a lower volume fraction of the solids, i.e. $\phi_s < 0.1$, the size of the solid particles exerts little effect on the rheology of emulsion systems. However, at $\phi_s > 0.1$, the solid particle size effect is more pronounced, and the smaller the size the larger the size effect. (b) Addition of solids to emulsion systems leads to bimodal size suspo-emulsion systems with higher viscosities than the parent monomodal emulsion systems. (c) The emulsion systems act as a continuous phase towards the solids, when the solids are much larger than the emulsion droplets, i.e. when the size ratio of solids to droplets $\frac{\bar{d}_s}{\bar{d}} > 3$. In such systems, Barnea and Mizrahi's (1973) equation can be used to describe the viscosity of the suspo-emulsion relative to that of solid-free emulsions, provided the shape of the

solid particles is spherical and $\phi_s \leq 0.04$. (d) In general, suspo-emulsions always have higher viscosities than solid-free emulsions at the same total concentration of the dispersed phase. (e) The effect of solid shape on the viscosity decreases as the shear stress increases, and the more the solid shape deviates from that of a sphere, the higher the viscosity of the suspensions (Utracki, 1980; Bampfield and Cooper, 1988, Pal *et al.*, 1990, 1991).

2.4.1 Stability of emulsions

When discussing the stability of an emulsified system, it is important to have a clear idea of the physical condition of components and the terminology employed. Physicochemical mechanisms are responsible for the instability observed in the emulsion. The mechanisms involved in the instability of emulsions are:

- Breaking
- Coalescence
- Creaming
- Flocculation

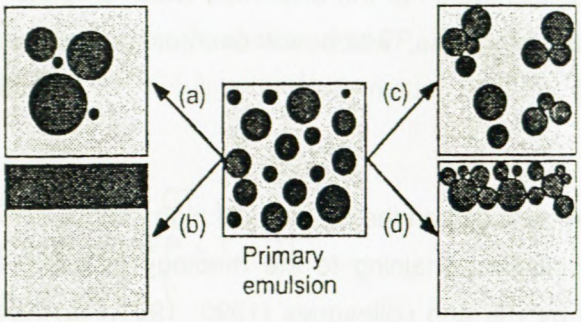

Figure 2.2: Mechanisms of emulsion instability (Adapted from Myers, 1992): (a) coalescence (b) breaking (c) flocculation (d) creaming

From Figure 2.2 coalescence is a mechanism that occurs as a result of two or more droplets coming together and coalescing into a larger single droplet. The flocculation mechanism is a result of two or more droplets coming together and aggregating, but keeping their individual identities. Creaming describes the upward movement of droplets due to a difference in densities between droplets and the environment. Breaking refers to complete separation of two phases.

2.4.2 Stability of emulsion explosive

The stability of explosive emulsions is not connected to hazard. The presence of supersaturated droplets, emulsion explosives comprise an inherently metastable system. This super saturation may break down completely if the emulsion is cooled to a sufficiently low temperature. At temperatures well above from those at which spontaneous nucleation becomes a problem, one must be concerned with droplet coalescence and heterogeneous crystal nucleation on dust particles as instability mechanisms.

With many commercial formulations, a spectacular demonstration of nucleation can result from a sharp blow on the emulsion. The shear induces nucleation in the product, resulting in crystallisation as well as a rise in temperature. This action results in the hardening of material within a short space of time. Emulsion explosives with bigger droplets are not responsive or sensitive to being 'explosive' and the critical diameters of such explosive emulsions are bigger in explosive than explosive emulsions with small droplets. The reaction involving a reaction mixture of oil phase and oxidiser is retarded by an increase in the time of diffusion. As a result of the coalescence of droplets which occurs, this leads to poor quality of the detonation properties. Bigger droplets increase the probability of the presence of nuclei being heterogeneous, and chances of crystallisation increases.

Cameron and Cooper (1978) have described emulsions stabilised by alkyd polymeric surfactants, while Nippon Oil and Fats (1980) describe an ethylene oxide-propylene oxide copolymer. Wade (1978) discovered increased stability when a blend of microcrystalline wax and paraffin wax is used, rather than either alone, while Ikeda *et al.*,(1983) claimed high stability for emulsions containing a high melting point wax containing a high proportion of urea non crude hydrocarbon component. Yorke *et al.*, (1983) showed the advantages of using a crude hydrocarbon mixture (e.g., slack wax) of wide molecular weight distribution. Binet *et al.*, (1982) claimed increased stability in emulsions containing at least one conventional water in oil emulsifier and at least one amphipathic synthetic graft, block or branch polymeric emulsifier. The increased stability was ascribed to the highly ordered and stable film formed in the presence of the polymeric emulsifier and this assertion was supported by calorimetric measurements.

Much effort has gone into improving the stability of emulsions. The above only outlines few improvements made by manufacturer claims. The literature only sheds light on a handful of

examples of progress claimed with regard to stability, particularly those involving chemical or physical influence employed to stabilise emulsions.

2.5 Drop formation by the emulsification process

Emulsification is the process whereby water in oil emulsions are formed. The mechanism by which emulsifiers aid emulsification was first clearly expounded by Van den Tempel (1960), but this and the dynamics of emulsification were poorly understood until the 1990s. It was not recognised until recently that the basics of water in oil emulsification were understood in the surfactant industry. To prepare emulsions, oil, water, a surfactant and energy are needed. Figure 2.3 shows the processes involved in the emulsification process in brief.

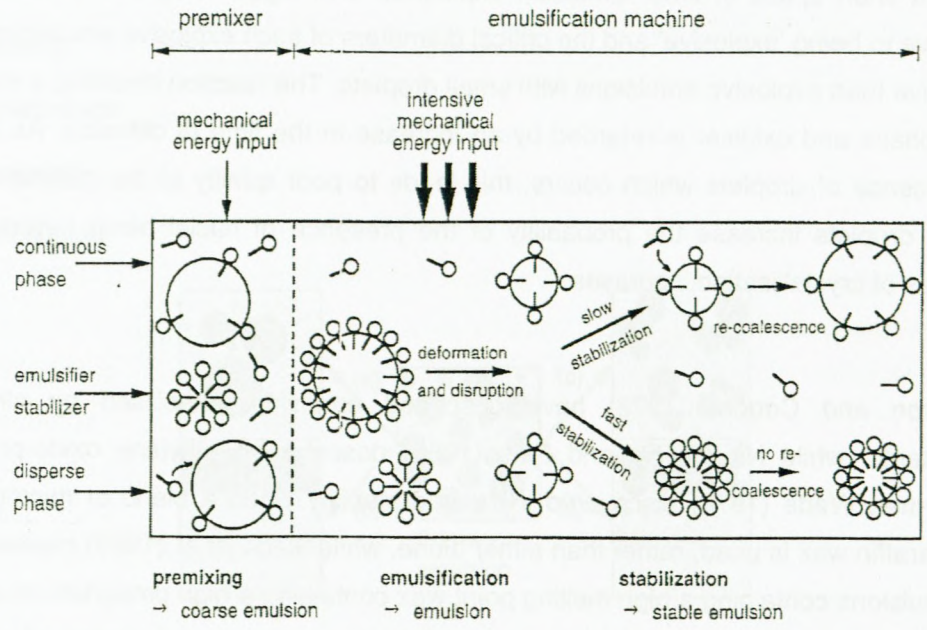

Figure 2.3: Emulsification process (Adapted from Karbstein and Schubert, 1995)

2.5.1 Different emulsification methods

The mechanism of blending or emulsifying two immiscible fluids to form an emulsion is known as homogenisation and a mechanical device designed to carry out this process is called a homogeniser.

2.5.1.1 High speed blenders

The fluids to be homogenised are placed in a vessel (Figure 2.4) which may contain as little as a few cubic centimetres or several cubic meters of liquid and are then agitated by a stirrer which

rotates at high speeds (typically 20 to 2000 rpm). The rapid rotation of the blade generates a combination of longitudinal, rotational and radial velocity gradients in the liquids which disrupts the interface between the oil and water and causes the liquids to become intermingled, breaking the larger droplets into smaller ones (Fellows, 1988). Homogenisation is achieved when the horizontal and vertical flow profiles distribute the liquid evenly throughout the vessel. This can be facilitated by fixing baffles to the inside walls of the vessel (Gopal, 1968).

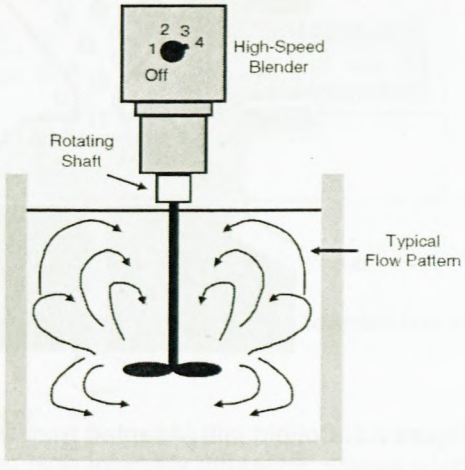

Figure 2.4: High-speed blender (Adapted from McClements, 2005)

The design of the stirrer also determines the efficiency of the homogenisation process. A number of different types are available for different situations (blades, propellers and turbines) (Fellows, 1988). Blending in general results in temperature increase in an emulsification process because some of mechanical energy is converted into heat due to viscous dissipation. High-speed blenders are particularly useful for preparing emulsions with low or intermediate viscosities. The droplet size usually decreases as the homogenisation time or the rotation speed of the stirrer is increased until a lower limit is achieved. This is influenced by the nature as well as the amount of material used. Typically, the droplets produced by a high-speed blender range between about 2 and 10μm in diameter.

2.5.1.2 Colloid mills

The fluids to be homogenised are fed into the colloid mill (Figure 2.5) in the form of a coarse emulsion, rather than as separate oil and aqueous phases. The emulsion is then fed into the homogeniser and flows through a narrow gap between two disks: the rotor (a rotating disk) and the stator (a static disk). The rapid rotation of the rotor generates shear stress in the gap which causes the larger droplets to be broken down into smaller ones. The intensity of the shear

stresses can be altered by varying the thickness of the gap between the rotor and stator (from about 50 to 1000μm), varying the rotation speed (from about 1000 to 20000 rpm) or by using disks that have roughened surfaces or interlocking teeth (Gopal, 1968).

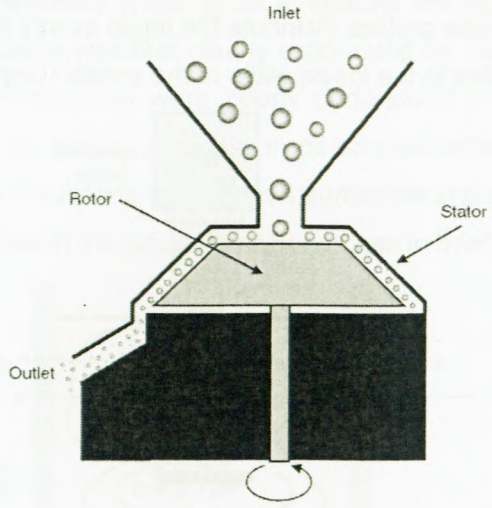

Figure 2.5: Colloid mill (Adapted from McClements, 2005)

Droplet disruption can also be enhanced by increasing the length of time that the emulsion spends in the colloid mill. This is achieved by decreasing the flow rate or passing the emulsion many times through the emulsifying equipment. Colloid mills are more suitable for homogenising intermediate and high viscosity fluids and typically are used to produce emulsions with droplet diameters between about 1 and 5μm.

2.5.1.3 High pressure valve homogenisers

A coarse emulsion is usually produced by using a high-speed blender and is then fed directly into the input of the higher pressure valve homogeniser. The homogeniser has a pump which pulls the coarse emulsion into a chamber on its backstroke and then forces it through a narrow valve at the end of the chamber on its forward stroke (Figure 2.6). As the coarse emulsion passes through the valve, it experiences a combination of intense shear, cavitational and turbulent flow conditions which cause the larger droplets to be broken into smaller ones (Phipps, 1985). Decreasing the gap size increases the pressure drop across the valve, which causes a greater degree of droplet disruption and smaller droplets are produced. On the other hand, narrowing the gap increases the energy input required to form an emulsion, thereby increasing

manufacturing costs. Emulsion droplets with diameters as small as 0.1μm can be produced using this method.

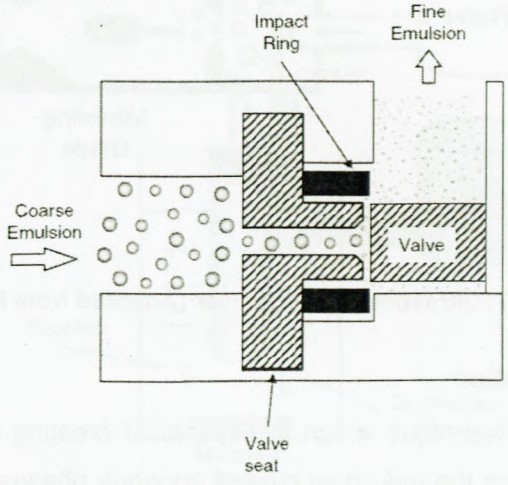

Figure 2.6: Higher pressure valve homogeniser (Adapted from McClements, 2005)

2.5.1.4 Ultrasonic homogeniser

This type of homogeniser utilises high intensity ultrasonic waves which generate intensive shear and pressure gradients within a material that disrupt the droplets, mainly due to cavitational effects. The ultrasonic transducer consists of a piezoelectric crystal contained within a protective metal casing which is tapered at the end. A high-intensity electrical wave is applied to the transducer, which causes the piezoelectric crystal to oscillate rapidly and generate an ultrasonic wave which is directed towards the tip of the transducer, where it radiates into the surrounding liquids and generates intense pressure and shear gradients (mainly due to cavitational effects), which causes liquids to be broken up into smaller fragments and intermingle with one another. The major advantages of this device are that it can be used for the continuous production of emulsions; it can generate very small droplets and is more energy efficient than a high pressure valve homogeniser. Even so, the vibrating blade is prone to erosion because of the ultrasonic field, which means that it has to be replaced frequently.

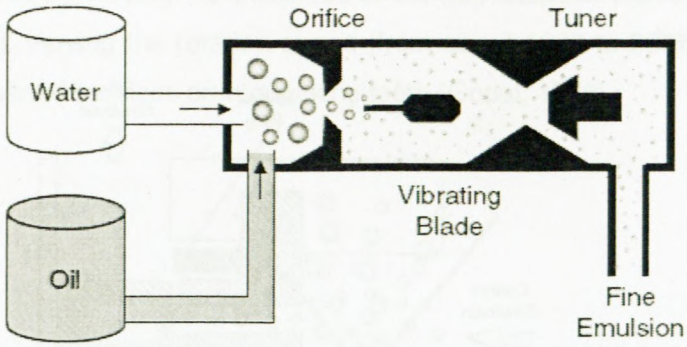

Figure 2.7: Ultrasonic homogeniser (Adapted from McClements, 2005)

2.5.1.5 Micro fluidisation

Micro fluidisation is a technique which is capable of creating emulsions with extremely small droplet size directly from the individual oil and aqueous phases (Dickinson and Stainby, 1988). Separate streams of the oil and aqueous phases are accelerated to a high velocity and then made to simultaneously impinge on a surface, which causes them to be intermingled with each other and broken up into droplets (Figure 2.8). Extremely small emulsion droplets can be produced by recirculation an emulsion through the micro fluidiser a number of times (Strawbridge *et al.*, 1995).

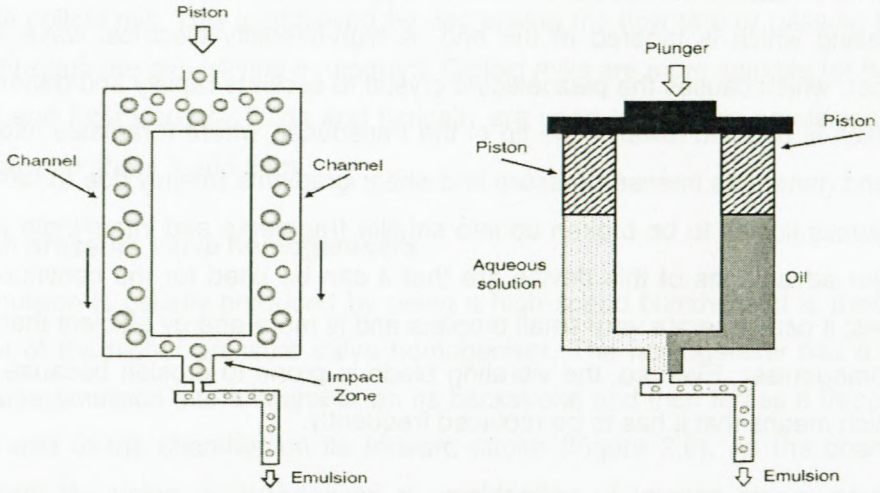

Figure 2.8: Oil and Aqueous brought together at high velocity in a micro fluidiser (Adapted from McClements, 2005)

2.5.1.6 Membrane homogeniser

An emulsion is formed by forcing one immiscible liquid into another through a glass membrane which contains a uniform pore size (Figure 2.9). The size of the droplets formed depends on the

diameter of the pores in the membrane and the interfacial tensions between the oil and water phases (Kandori, 1995).

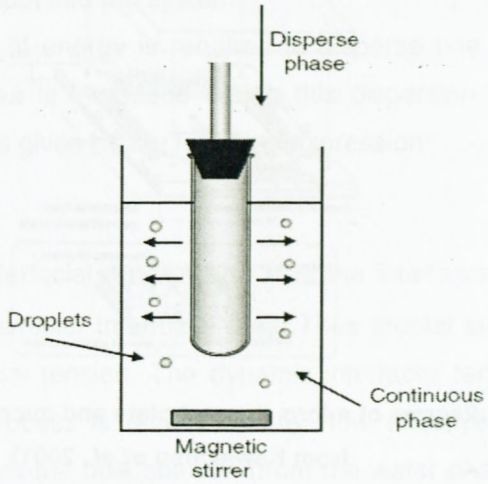

Figure 2.9: Batch version of a membrane homogeniser (Adapted from McClements, 2005)

The membrane must be sufficiently strong so that it is not broken by the pressure applied to the fluids during the process.

2.5.1.7 Micro channel homogeniser

This type of homogeniser works on the same principle as the membrane homogeniser. The only difference is that the dispersed phase is forced through the micro channel (Figures 2.10 and 2.11) with well-defined geometries and the droplets detach due to the Laplace instability mechanism (Schubert and Lambrich, 2003).

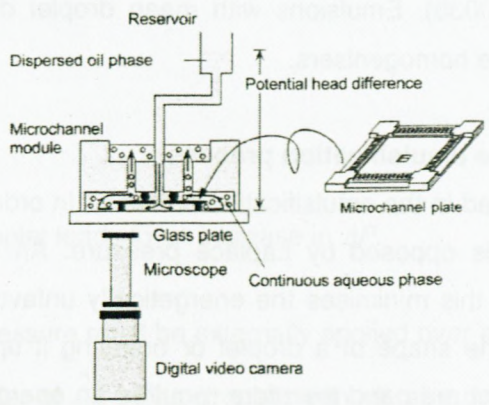

Figure 2.10: Schematic diagram of micro channel homogeniser

(Adapted from Kawakatsu *et al.*, 2001)

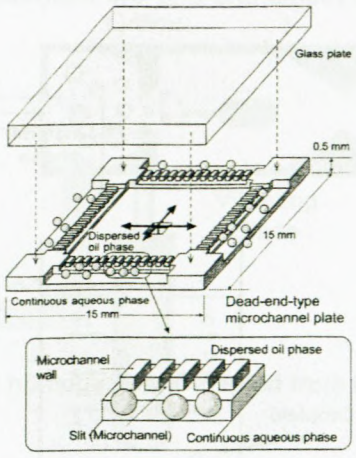

Figure 2.11: Schematic diagram of micro channel plate and micro channel emulsification (Adapted from Kawakatsu *et al.*, 2001)

This technique has proved to be particularly useful for producing droplets with very narrow particle size distributions (Kawakatsu *et al.*, 1997; Kobayashi *et al.*, 2003). These instruments can be used to manufacture oil in water, water in oil and multiple emulsions by selecting a material with appropriate polarity from which to make the membrane or micro channels (Schroder and Schubert, 1999; Suzuki *et al.*, 1999; Kawakatsu *et al.*, 2001; Christov *et al.*, 2002; Sugiura *et al.*, 2004). The major advantages of this type of homogeniser are the ability to produce emulsions with narrow droplet size distributions and the fact that they are highly energy efficient because much less energy is lost due to viscous dissipation (Vladisavljevic and Schubert, 2003a, 2003b). Emulsions with mean droplet diameters as low as 0.3μm can be produced using these homogenisers.

2.5.2 Energy in the emulsification process

Why is energy needed in the emulsification process? In order to break up a drop it must first be deformed and this is opposed by Laplace pressure. An emulsion droplet tends to retain a spherical shape, as this minimises the energetically unfavourable contact area of an oil-water system. Changing the shape of a droplet or breaking it up into a number of smaller droplets increases this contact area and therefore requires an energy input (Walstra, 1993). This is due to excess free energy associated with the surface of emulsion droplets. The excess surface energy arises as a result of the cohesive forces between the molecules of an individual liquid being greater than adhesive forces between the liquids (Banker and Rhodes, 1979; Martin *et al.*,

1993). On dispersion, the interfacial area of the dispersed phase liquid increases considerably compared to that of the continuous phase liquid. The dispersed droplet diameter is also conditioned by the energy input into the system.

During emulsification, a lot of energy is required to disperse one liquid into another as small droplets. The interfacial area is increased during this dispersion process. The work done to expand the interfacial area is given by the following expression:

$E_{theo} = \sigma A$ **Equation 2.4**

Where σ is the dynamic interfacial tension and A is the interfacial area. For constant E_{theo}, a greater value of σ yields a smaller interfacial area. Thus droplet size of an emulsion increases with an increase in interfacial tension. The dynamic interfacial tension between oil and water during the emulsification process is determined by how effectively the emulsifier monomers adsorb into the interface from the bulk solution (from the water phase for O/W emulsions, from the oil phase for W/O emulsions).

The interfacial force responsible for keeping a droplet in a spherical shape is characterised by the Laplace pressure, which acts across the oil water interface toward the centre of the droplet so that there is a larger pressure inside the droplet than outside of it:

$$\Delta P = \frac{\sigma}{\left(\frac{1}{R_1} + \frac{1}{R_2}\right)}$$ **Equation 2.5**

where σthe interfacial tension and R1, R2 represent radii. For a spherical droplet of r this becomes

$$\Delta P = \frac{\sigma}{\left(\frac{1}{R_1} + \frac{1}{R_2}\right)} = \frac{2\sigma}{R}$$ **Equation 2.6**

and any deformation of the droplet leads to an increase in ΔP.

To disrupt the droplet, such pressure must be externally applied over a distance, *r,* which means a pressure gradient of the order of $\frac{2\sigma}{r^2}$. The droplets can also be deformed by viscous forces exerted by the surrounding liquid and the viscous stress $G\eta_c$ should be overcome, i.e. should be of the same magnitude as the Laplace pressure. *G* is the velocity gradient (rate of strain) and η_c,

the continuous phase viscosity. The velocity gradient or pressure gradients needed are mostly supplied by agitation. The smaller the droplets, the more intense the agitation should be to disrupt them. It is seen from Equation 2.6 that the stress and, consequently, the amount of energy needed to deform and thereby break up the droplets is less if the interfacial tension is lower, which can be achieved by adding a sufficient amount of a suitable surfactant. The surfactant prevents immediate re-coalescence of newly formed drops, as well as reduces mechanical agitation energy.

The most widely used method to characterise the energy efficiency of homogenisers consists of evaluating the relationship between sauter mean diameter obtained after emulsification and the amount of energy supplied (McClements, 2004; Schubert and Engel, 2004; Walstra, 1983). The amount of energy supplied to an emulsion during the homogenisation process is often referred to as the energy density, which has been defined as the energy input per unit volume of emulsion, or the power input per unit volume flow rate emulsion (Schubert et al., 2003). In general, the energy density is given by the following function (Walstra and Smulder, 1998):

$$E_v = \int P_v(t)\,dt \qquad \textbf{Equation 2.7}$$

where P_V is the net power density and t is emulsification time. Droplet disruption does not take place unless P_V exceeds some critical value, which depends on the Laplace pressure of the droplets. If the net power density is below this critical value in any region within the homogeniser, droplet disruption cannot occur and the energy is wasted (McClements, 2004).

The size of droplets in an emulsion is reduced by increasing the intensity or duration of the disruptive energy supplied during homogenisation as long there is sufficient emulsifier available to cover the interfaces generated in the emulsification process (McClements, 2004). The final droplet size distribution (DSD) of any emulsion results from the dynamic equilibrium between droplet disruption and coalescence, both favoured by intense agitation (Walstra, 1983). An increase in energy input generally produces a displacement toward smaller sizes since droplet disruption becomes predominant over coalescence, although coalescence is also promoted (Sanchez *et al.*, 1998). As there is a huge energy input, droplet disruption would be considerably higher and more severe within the interaction chamber. The differences in DSD could be directly correlated to the energy density, which is specific volumetric energy input. The higher the energy density, the smaller the droplets. The difference in span might be related to emulsification time and emulsion volume in the dispersing zone of the emulsifying device.

Studies by Karbstein and Schubert (1995) on different units have shown that the results of size reduction mainly depend on the energy density and viscosity of the dispersed phase. It has been shown that size reduction decreases exponentially as a function of energy density. Since the droplet size decreases with increasing energy input, the surface-volume ratio of the dispersed phase is shifted to higher values. As a result, the number of emulsifier molecules adsorbed on the surface increase, resulting in smaller droplet size.

Adding a suitable surfactant may considerably reduce the agitation energy needed to obtain a certain droplet size. Very roughly one may state that:

- With a higher surfactant concentration, less energy is needed.
- At low energy density, type and concentration of surfactant vary.

It has been shown, by Fradette *et al.* (2007) and Othmer (1994) that the energy spent to form an emulsion is larger than the actual droplet surface energy in the actual product. The reason is that most of the energy is actually lost as heat (thermal dissipation) or converted into momentum for phase contacting (hydrodynamic mixing). In practice, however, a lot of energy is lost during emulsification through heating, either because of viscous dissipation for a mechanical energy supply or through diffusion or convection for a chemical energy supply. Reduction of this high amount of lost energy is a real challenge in industrial emulsion production. From a more fundamental point of view, the mixture obtained is in a metastable state and therefore the properties of an emulsion depend not only on the state variables (temperature and composition), as in the case of a thermodynamic system, but also on the preparation method. For this reason, emulsification is of the utmost importance. Different emulsification routes can be distinguished.

In emulsification devices usually employed, droplet disruption of a coarse premix is induced by various mechanisms. Shear forces in laminar flow and shear or inertial forces in turbulence are predominant in the case of rotor-stator systems (Karbstein, 1994; Stang, 1998). Depending on the respective predominant effect, droplet disruption (C in the power law equation) is influenced by several physical parameters, like viscosity of the dispersed and continuous phase, interfacial tension or density of the liquids (Walstra, 1993; Walstra and Smulders, 1997). Besides, power density (power input per unit volume) and residence time of the emulsion in the dispersing zone of a continuously operated apparatus are key process parameters which influence the emulsification results (Koglin *et al.*, 1981).

The concept of energy density was proved suitable for droplet disruption in continuous mechanical emulsification (Karbstein and Schubert, 1994) depends on the type of forces acting on the droplet and therefore on the flow pattern (Brosel and Schubert, 1999). According to experimental results, the mean droplet diameter of an emulsion can be described as a function of both power density and residence time by a power law (Stang *et al.*, 2001):

$$d_{32} = CE_{\rho}^{-b}$$ **Equation 2.8**

where d_{32} is the volume-surface mean droplet size (sauter diameter). The value of the characteristic exponent b contains information about the droplet disruption mechanism and the characteristic exponents are often similar in describing the type of flow (turbulent or laminar). Typically, values are found between b = 0.35 (turbulent inertial forces) and b = 1 (laminar shear or elongational flow) (Schubert and Ax, 2001; Walstra and Smulders, 1997).

In conclusion, calculations of the energy needed to increase the specific area of collective droplets by a certain amount of area show that very little energy is needed to increase the surface area, but very high energy must be used in the emulsification machine to achieve small droplets. One reason for this energy is that it is needed to create flow which acts to deform droplets.

2.5.2.1 Influence of energy input on the yield stress

An increase in the input energy density increases the yield stress. This increase cannot be explained, either by an increase in the phase volume ratio ϕ or by synergistic effects of ingredients that approach each other. Since the droplet size decreases with increasing energy input, the surface-volume ratio of the dispersed droplets is shifted to higher values. As a result, the number of emulsifier molecules adsorbed on the surface increases, resulting in an increase in interparticulate interactions for a constant phase volume ratio ϕ. Therefore the yield point can be used to make integral statements on the internal structure of dispersed multi substance mixtures. However, they provide no information on the microstructure or molecular causes of structural breakdown. A linear relationship between the energy input and yield stress has been recognised (Figure 2.12). With increasing energy input, the yield stress also increases. The plot of yield stress vs droplet size clearly shows that the shear stress needed to initiate flow of an emulsion increases with decreasing droplet size (Brummer, 2006).

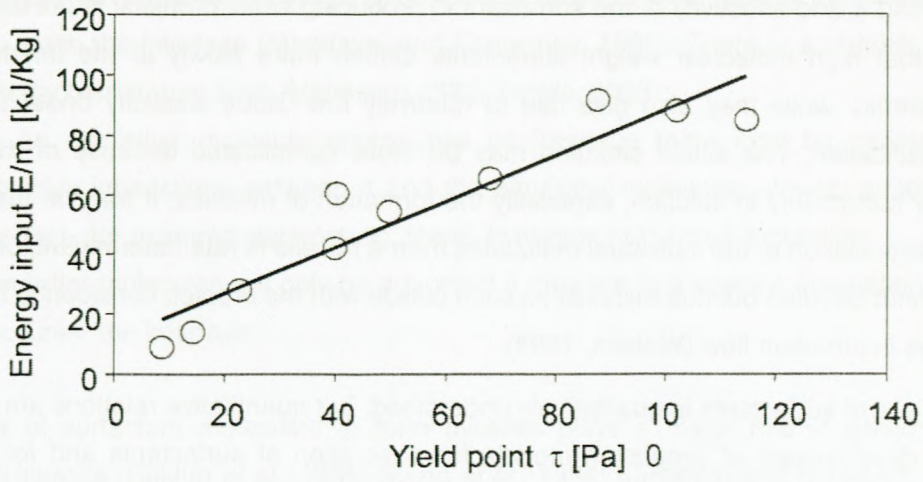

Figure 2.12: Influence of energy on yield stress (Adapted from Brummer, 2006)

2.6 Influence of surfactant in the emulsification process

The surfactant has two main roles to play: it lowers the interfacial tension, thereby facilitating drop break-up and it prevents re-coalescence (to a varying degree). Moreover, if the surfactant concentration is high and the resulting interfacial tension very low, it may cause "spontaneous emulsification" under some conditions, due to the strong interfacial tension gradients induced. Such a droplet break-up without putting much mechanical energy into it is only of importance in the earlier stages of emulsion formation and has little to do with the final droplet size obtained. Different surfactants lower σ to a different degree and this should affect the final droplet size. For a surfactant giving a lower σ, less energy is thus needed to obtain a certain droplet size (Walstra, 1993). Droplet shredding naturally occurs easiest when the interfacial tension is very low, which may be the case for some surfactants if present in high concentration. It is not known to what extent this facilitates disruption. A large amount of emulsifier provides a larger surface area between emulsion droplets and the continuous phase and thus allows the formation of smaller droplets (Rusli *et al.*, 2007).

It is also useful to consider the time needed for the surfactant to reach the droplet surface, t_{ads}. This is not determined by diffusion; at the prevailing conditions of very high velocity gradients or very intense turbulence, transport towards the droplets is almost entirely by convection (Levich, 1962). In the author's opinion, this implies that experiments in which the decrease in surface tension at a microscopic surface above a solution of the surfactant is measured as a function of time are irrelevant to emulsification. That correlations are sometimes found between the rate of

lowering σ and affectivity of the surfactant in producing small droplets, is presumably due to the fact that high molecular weight surfactants diffuse more slowly to the interface in the tests performed, while they also give rise to relatively low Gibbs elasticity under the conditions of emulsification. The actual situation may be more complicated because of the association of many surfactants in solution, especially the formation of micelles. It may be that in some cases the dissociation of the individual molecules from a micelle is rate determinant, on the other hand, it cannot be ruled out that micelles as such collide with the droplet, considering the strong inertial forces in turbulent flow (Walstra, 1993).

The role of surfactants is qualitatively understood, but quantitative relations are hardly available. The development of simulation models for adsorption of surfactants and for the phenomena occurring during a close approach of droplets would be very useful. The role that Gibbs elasticity plays needs further study, especially its dependence on the time scale for different surfactants.

In summary, the role of the surfactants during emulsification are:

- They decrease the surface tension involving two phases, thereby reducing the amount of free energy required to deform and disrupt the droplets.
- They form a protective coating around the droplets that prevents them from coalescing with each other.

2.6.1.1 Adsorption rate

The rate at which an emulsifier adsorbs to an interface is one of the important factors determining its efficiency (Magdassi and Kamyshny, 1996; Walstra, 1996a; 1996b). It has been shown that the adsorption rate depends on molecular characteristics of the emulsifier (e.g. size flexibility, conformation and interactions), the nature of the bulk liquid (e.g. viscosity, polarity) and the prevailing environmental conditions (e.g. temperature and flow profile). Adsorption is divided into two stages:

- **Movement of the emulsifier molecules from the bulk liquid to the vicinity of the interface.**

In this case it is assumed that the emulsifier is adsorbed to an interface as soon as it encounters it, therefore, that there are no energy barriers that retard adsorption.

- **Attachment of the emulsifier molecules to the interface.**

In this case there maybe one or more energy barriers that must be overcome before a molecule adsorbs and so only a fraction of the encounters between an emulsifier and an interface lead to adsorption (Damodaran, 1990, 1996; Magdassi and Kamyshny, 1996; Norde, 2003). Adsorption

kinetics may be governed by the height of the energy barrier, rather than by the rate at which the molecules reach the interface (Magdassi and Kamyshny, 1996). There is a number of reasons why an energy barrier may exist (Malmsten, 2003; Norde, 2003):

- As an emulsifier molecule approaches an interface there may be various types of repulsive interactions between it and the emulsifier molecules already adsorbed to the interface, for example electrostatic, steric, hydration or thermal fluctuation.
- Emulsifier molecules will only be adsorbed if they are in a specific orientation when they encounter the interface.

The ability of surfactant molecules to form micelles plays a major role in determining their adsorption kinetics (Dukhin *et al.*, 1995; Stang *et al.*, 1994; Karbstein and Schubert, 1995). The adsorption kinetics therefore depends on the concentration of monomers and micelles present, as well as on the dynamics of micelle formation-disruption (Karbstein and Schubert, 1995; Kabalanov and Weers, 1996). According to Windhab *et al.*, (2005), the emulsifier adsorption has to be considered in the context of four different steps:

- emulsifier de-micellation in the bulk fluid;
- diffusive/convective transport to the interface;
- interfacial adsorption; and
- structural changes.

Adsorption kinetics at the interface plays a vital part during the mixing process for the following reasons:

- The more rapidly the new interfaces are reoccupied by emulsifier molecules, the simpler the subsequent disruption of the droplets.
- Insufficiently covered droplets show a higher tendency to coalesce, resulting in a lower degree of emulsification.

Three steps must be considered in the adsorption of emulsifier molecules from the bulk phase (Miller and Kretzschmar, 1991):

- Macroscopic (mixing, convection) and microscopic (diffusion) transport of emulsifier molecules from the bulk phase to the subsurface.
- Transfer of emulsifier molecules or parts of them from the solute to the adsorbed state (adsorption itself).
- Structural changes in the emulsifier molecules at the interface, rearrangement, unfolding of complex structures.

2.6.1.2 Importance of micelle kinetics in emulsification process

Since the pioneering work of Ward and Tordai (1946), many theories have been suggested to describe the kinetics of non-ionic surfactant adsorption at a fluid-fluid interface (Kretzschmar and Miller, 1995). In chemistry, the critical micelle concentration (cmc) is defined as the concentration of surfactants above which micelles are spontaneously formed. Above this critical micelle concentration (cmc), surfactant molecules associate into micelles which are in equilibrium with free monomers whose concentration is approximately equal to the cmc. Adding more monomers to the solution leads to the formation of new micelles. In the presence of an interface it is usually assumed that free surfactants adsorb, because the adsorption energy of micelles is too high (Mukerjee and Bunsenges, 1978).

The importance of the micelle break-up process involving an increase in the interfacial area was first reported by Mijnlieff and Ditmarsch (1965). The increase in the interfacial area has to be stabilised by surfactant molecules. The surfactant molecules originate from the bulk solution; it contains surfactant monomers and micelles if it is above the cmc value. The formation of a new interface means that monomers are transported to this new interface and in this process the balance between monomers being broken up to supply the new interfaces and the used to cover newly formed interfaces is disturbed. As a result of this imbalance, existing micelles are broken up to provide extra monomers to the interface. To argument flux, micelles need not be very stable to cover the new droplets formed. By the same token, if micelles are relatively unstable, the break-up of micelles supplies the depleted monomers and a reduction of interfacial tension results. The role of micelles has been shown to include solubilising and transport through the aqueous phase; this has a significant effect on the physicochemical properties of emulsions and can lead to time-dependent changes in droplet concentration, size distribution and composition (McClements and Fairley, 1992; McClements and Dungan, 1993; Weiss *et al.*, 1996).

2.6.2 Effect of surfactant on distribution size of droplets and mean diameter

Adding surfactants to the aqueous (dispersed) phase leads to lowering or reduction of interfacial tension, which reduces the energy necessary to produce small drops and also introduces repulsive forces on the droplet surface to prevent coalescence. In several studies the surfactant concentration has been varied; the droplet size generally decreased with increasing concentration (Walstra,1983; Ostberg *et al.*,1995), but droplet size also depends strongly on the type of surfactant and it is poorly correlated with σ, as this is measured under static conditions (Walstra,1983). Walstra (1983) has shown that the droplet size is only weakly dependent on the

interfacial tension, so, in principle, the type/concentration of surfactant can be treated as one process variable allowing manufacture of drops/particles in a required size range. However, as the current theories describing maximum stable drop size can only account for the presence of a surfactant via the reduction of interfacial tension, whereas it is well known that surface charges have a much stronger effect of the behaviour of the dispersion, the effect of surfactants on drop size / size distribution has to be determined experimentally. As the concentration of surfactants is increased, the particle size distribution narrows and the mean particle size gradually decreases. The observations that have been made showed clearly that, by proper selection of type / concentration of surfactant and hydrodynamic conditions, the particle size can be controlled effectively (Mu *et al.*, 2005). Generally,with more surfactant added, one obtains smaller droplets, hence a greater number of disruptions and the increase in emulsification time is not surprising. If more surfactant causes smaller droplets, the time needed to obtain equilibrium droplet size also increases.

The size of the droplets produced during emulsification therefore depends on a number of characteristics of the emulsifier (McClements, 2004):

- The ratio of emulsifier to the dispersed phase - there must be sufficient emulsifier to completely cover the new interfaces of the droplets formed.
- Time required for the emulsifier to move from bulk phase to the drop surface – the faster the adsorption time, the smaller the droplet size.
- Probability that an emulsifier will be adsorbed to the surface of a droplet during an encounter between it and the droplet – the greater the adsorption efficiency, the smaller the droplet size.
- Amount by which the emulsifier reduces the interfacial tension – the greater the amount, the smaller the droplet size.
- The extent to which the emulsifier alters the dynamic interfacial rheology – the greater the resistance to deformation, the more difficult is droplet disruption (larger size) and the less likely is droplet coalescence (smaller size).

Studies on the influence of emulsion formulation and parameters controlling the emulsification process in droplet size distribution have been documented. Variables involve the type of mixer; intensity of mixing; concentration of surfactant and type of surfactant; and ratio by volume of aqueous phase to continuous phase (Sanchez and Villa-Jatta, 1993; Poncelet and Neufeld, 1989; Jeyanthi *et al.*, 1997; Benita *et al.*, 1997; Boisdron *et al.*, 1995; Witschi and Doelker, 1998). However, little information is available on the dynamic changes in droplet size that occur

during emulsification. In fact, emulsification is a complicated process that involves the deformation of an interface between two immiscible liquid phases: the formation of primary emulsion droplets and their subsequent break-up and coalescence. The complexity of this process has presented an obstacle to studying real changes in droplet size over the course of emulsification.

In summary: the drop size distribution obtained in an emulsification process is a result of the competition between two opposite processes, drop breakage and drop-drop coalescence (Walstra, 1983; Narsimham and Goel, 2001; Nienow, 2002; Coulaloglou and Tavlarides, 1977; Walstra *et al.*, 1999). Droplet break-up and coalescence are the result of strong external shear stress supplied by intensive agitating of the mixture of oil and water in the mixing vessel or chamber. The result of the emulsion process is strongly influenced by four types of factors namely:

- The viscosity ratio of the two phases of oil and water;
- The type and concentration of used emulsifier;
- The volume fraction of the oil and water phases;
- hydrodynamic conditions in the mixing device.

2.6.2.1 Influence of surfactant type on droplet size

Goloub and Pugh (2003) showed in their study that the initial process of emulsification was rather fast, resulting in a reduction of droplet size, but then a steady state was reached where the droplet size remained nearly constant. The origin of these kinetic effects on droplet size during emulsification is discussed elsewhere (Groeneweg *et al.*, 1994; Polat *et al.*, 1999). It has been suggested that the break-up of droplets takes place in the eddies in the boundary layer of an impeller, which comprises a relatively small volume in the tank. As a result, the total volume of the emulsion has to pass through zones before a steady state is reached. As shown by DeRoussel et al. (2001), two zones are identified in the mixer, a strong and a weak zone. The strong zone represents the regions of the mixer in which stretching and break-up during flow occurs. Droplet distributions are generated by means of sub zones and each sub zone is characterised by its own stretching rate, shear rate and residence time. The weak zone represents the regions of the mixer where coalescence and break-up at rest occurs. In their results on the effect of interfacial tension on droplet size, Goloub and Pugh (2003) showed that droplet size decreases with an increase in the surfactant concentration up to the cmc. However, at concentrations above cmc, the droplet size is no longer concentration dependent. In this

surfactant concentration region, both the mean droplet size and the size distribution vary considerably with type of surfactant and head group.

Inhomogeneities in the flow in this region would explain the range of particle distribution. Earlier studies utilising circulation mode emulsification (Djakovic *et al.*, 1987; Sanchez *et al.*, 2001; Oh *et al.*, 1993; Tornberg, 1978, 1980), have shown that changes in the drop size distribution and a decrease in mean drop size occur prior to reaching a steady state. The rate of achieving the steady state depended on the hydrodynamic conditions and on the properties of the emulsifier (concentration, kinetics of adsorption, etc.). The mechanism behind this is also understood by taking into consideration that deformation of emulsion droplets under external stress is opposed by the Laplace pressure that is trying to preserve the original shape and does so by opposing the deformation. The Laplace pressure is inversely related to the radius of droplets and, hence, their size ($\Delta P = \frac{2\sigma}{R}$), where σ is the interfacial tension and R is the radius of an undeformed droplet). Therefore, it is possible that an increase in emulsion viscosity is accompanied by both. A decrease in the size of droplets and long periods of mixing result in synergic resistance against movement to break up emulsion droplets (Yogita and Hongkee, 2000).

2.6.2.2 Surfactant-electrolyte interactions in concentrated emulsions

Ganguly *et al.* (1992) studied interactions between polymeric surfactants, Pibsa Mea and SMO, specifically. Their results showed that any effect of dissolved salts in the aqueous phase on interfacial tension values for SMO could only be attributable to hydrogen bonding type interactions between the polar head group and the salts, mediated through water. With Pibsa MEA it appeared that the interactions are so strong, even at low electrolyte concentrations, that they could be "masking" any further changes due to possible bulk hydrogen bonding effects which are entirely concentration dependent. The head groups of surfactants consisting of two surfactants had hydrogen bonding that was moderate to strong, although the group that is polar in the polymeric emulsifier (MEA) may have stronger hydrogen bonding relative to the group in SMO which is non-ionic.

2.7 Theory of drop break-up

The theory of droplet deformation and break-up by viscous shear was first formulated by Taylor (1934) and further developed by others (Khakar and Ottino, 1987; Stone, 1994; Bentley and Leal, 1986; Briscoe *et al.*, 1999). Much effort was made in the early 1970s and 1980s to develop various models using the fluid circulation approach. However, the majority of these models were

restricted to particular situations imposed, whether by flow, type and intensity of flow, or by the rheological properties of the system under consideration.

The breaking of single droplets has been the subject of many investigations since the early work undertaken by Taylor (1934). Models involving the deformation of droplets have been developed and are based on Newtonian components, but with using larger and more complex deformations. The inclusion of non-linear ties in their model was tried by of Maffettone and Minacle (1998), by inclusion of a phenomenological term that contains the capillary number Ca. The small deformation type theories by Barthes-Biesel and Acrivo (1973) and Rallison (1980, 1984) were limited to weak flow fields with a small capillary number, while large deformation type theories (Acrivos and Lo, 1978; Hinch and Acrivos, 1979; Khakhar and Ottino, 1986) were restricted to a very small viscosity ratio ($\lambda = \frac{\eta_d}{\eta_c}$). These restrictions were mainly due to the techniques used to solve the equations of droplet deformation.

While Newtonian fluids predominate in nature, non-Newtonian fluids occur in a myriad of important industrial and biological applications. The deformation and break-up of non-Newtonian fluid is largely unexplored. The effect of non-Newtonian properties on the shape of a deformed drop was considered by Chin and Han (1979) and Vanoene (1972).

The viscous behaviour of emulsions is intimately linked to the deformation and orientation of droplets suspended in the continuous phase. The equilibrium shape of the droplet, as well as its orientation with respect to the flow direction is governed by a balance between two competing stresses, namely hydrodynamic ($\sim \eta_c \dot{\gamma}$) and interfacial stress ($\sim \frac{\sigma}{R}$), where η_c is the viscosity of the external phase (matrix), σ represents interfacial tension between the phases and R represents the radius of the droplet. The hydrodynamic stress tends to stretch the droplet into a filamentary shape, whereas the interfacial stress tends to contract the droplet into a sphere of radius R. The ratio of hydrodynamic stress to interfacial stress is referred to as the capillary number, *Ca*, formulated as:

$$Ca = \frac{\eta_c \dot{\gamma} R}{\sigma} = \frac{\tau R}{\sigma} \qquad \textbf{Equation 2.9}$$

where τ is the shear stress and $\dot{\gamma}$ is the shear rate defined as $\dot{\gamma} = \sqrt{2D:D}$, D being the rate of deformation tensor. (Note that in 2D and 3D elongation flow, $\dot{\gamma}$ equals 2 $\dot{\varepsilon}$ and $\sqrt{3}\dot{\varepsilon}$ respectively, with $\dot{\varepsilon}$ being the elongation rate. For each viscosity ratio, there is a capillary

number above which the drop will rupture. This critical capillary is of order unity for viscosity ratios close to one and increases steadily as λ decreases, where $\lambda = \frac{\eta_d}{\eta_c}$. At the other end, $\lambda > 1$, the critical capillary number rapidly increases and reaches an asymptote for $\lambda \approx 3.8$. The master curve for single droplet break-up is usually referred to as the Grace curve (Grace, 1982) and can be written as

$Ca_{crit} = f_{Grace}(\lambda)$ **Equation 2.10**

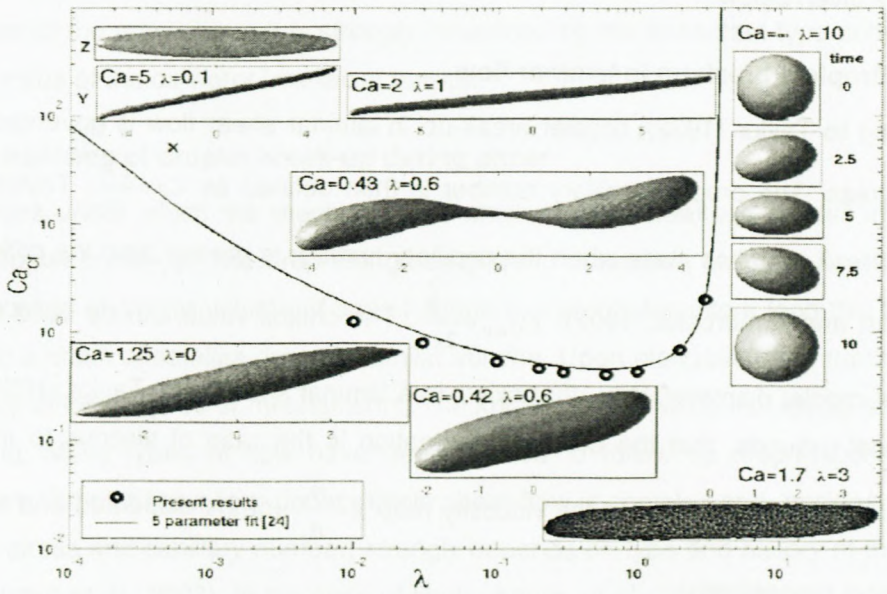

Figure 2.13: Critical capillary number for simple shear flow as a function of viscosity ratio (Adapted from Bazhlekov *et al.*, 2006)

At a critical capillary, Ca_{crit}, defined as the largest capillary number for which there exists a steady drop shape. The study by Stone (1994) pointed out that the critical capillary number was strongly influenced by the type and history of flow, as well as by the viscosity ratio of the two components. Experiments by Jansen *et al.* (2001) proved that, in simple shear flow, the critical capillary number decreased with an increase in the volume fraction of the aqueous phase droplets. Correspondingly, the critical deformation is the deformation at the critical number when droplets break up. Studies on fibrils or blends recorded in the work of Loewenberg and Hinch (1996) showed that, under deformation, droplets elongate into long filaments which break up due to instability of the interface, the mechanism changes. The influence of viscous shear stress causes droplets to elongate, increasing the capillary number in the process. They can be

regarded as liquid cylinders susceptible to capillary instability in which the interfacial tension is the main factor behind the droplet break-up of the cylinders into spherical drops with a smaller total surface area (Van de Ven, 1989; Schmitt *et al.*, 2003).

In summary: droplet break-up is determined by competition between external stress acting on the interface and Laplace pressure trying to preserve by resisting deformation. It can be characterised and quantified by a dimensionless capillary number, including the effect of the viscosity of the dispersed phase. A brief review of the models proposed for laminar and turbulent flows are given below.

2.7.1 Droplets break up in laminar flow

According to Taylor (1932), droplet break-up in laminar shear flow is governed by the viscous shear stress. The droplet capillary number is then defined as $Ca = \frac{\tau R}{\sigma}$. Taylor suggested that droplet break-up takes place when the capillary number is greater than the critical number, Ca_{cr} (Schubert and Armbruster, 1992): $Ca_{crit} = \frac{\tau R}{2\sigma}$. The critical value can be used to determine the maximal droplet diameter, $d_{max,}$, that exists in a laminar shear field. Taylor (1934) has stated, on theoretical grounds, that the droplet deformation is the ratio of viscous to interfacial tension forces, leading to a function of the viscosity ratio $\lambda = \frac{\eta_d}{\eta_c}$ (of the dispersed and continuous phase viscosities, respectively).

2.7.2 Droplet break-up in turbulent flow

Turbulence occurs when the flow rate of a fluid exceeds some critical value, which is largely determined by its viscosity (Curle and Davies, 1968; Walstra, 1983, 1993; Phipps, 1985). Turbulence is characterised by rapid and chaotic fluctuations in the velocity of the fluid with time and location. The disruption of droplets under turbulent flow conditions is caused by the extremely large shear and pressure gradients associated with eddies generated in the fluid (Walstra, 1993). An eddy is a region within a fluid where there is a close correlation between the fluid velocity of the different elements (Curle and Davies, 1968). The shear and pressure gradients associated with these eddies increase as their size decreases (Walstra, 1983). As a consequence, large eddies are believed to be relatively ineffective at disrupting emulsion droplets. Very small eddies are also believed to be relatively ineffective at breaking droplets because they generate such high shear stresses that most of their energy is dissipated through

viscous losses, rather than through droplet disruption. For these reasons, intermediate-sized eddies are thought to be largely responsible for drop disruption under turbulent flow conditions (Walstra, 1983; 1993). The turbulent fluid mostly is not quite homogeneous and the resulting droplets will thus show a spread in size.

Theoretical analysis and experimental work showed that, in turbulent flow and excess emulsifier (the so-called 'surfactant rich regime') (Taisne *et al.*, 1996), the mean droplet size is influenced by the energy density input into the mixing vessel as well as the interfacial tension of oil and water. In this regime, the average size of the droplet is not strongly influenced by the concentration of the emulsifier but is strongly influenced by the surfactant type achieved via the equilibrium value of the oil-water interfacial tension.

2.7.3 Mechanisms of droplet break-up during shear

The conditions under which the mechanism at which droplet breakage follows influences the history of droplet break-up. The drop elongates under deformation and may break up into two daughter droplets of similar volume. If stretched more, it elongates into a long thin thread which ruptures into a chain of satellite drops of similar volume. Upon elongation, the rupturing process is affected by different types of mechanisms. The known mechanisms include tip streaming and end pinching. Many types of flow have been studied to follow up droplet behaviour under different flows. Droplet behaviour under simple shear flow is complex and, besides the viscosity ratio, shear stress and capillary number, strongly depends on type and history of the shear flow created (Schmitt *et al.*, 2003). In the case of fibrils, Knops *et al.* (2001) showed that interactions are quite complicated.

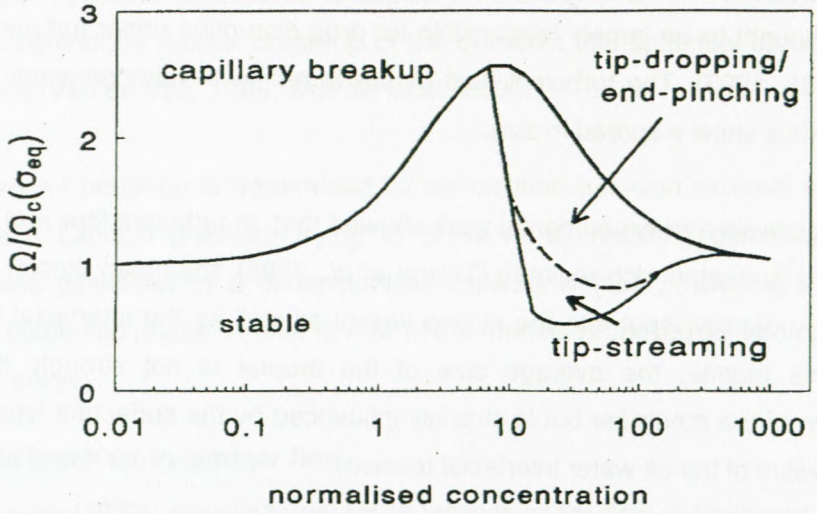

Figure 2.14: Typical break-up behaviour of w/o systems as a function of capillary number (based on σ_{eq} and bulk concentration) (Adapted from Janssen *et al.*, 1994)

2.7.3.1 Tip streaming

Tip streaming refers to the development of pointed ends at the sigmoidal droplet, which eject a continuous stream of tiny fragments. Tip streaming is caused by the presence of surfactants (DeBruijn, 1989; 1993). Several experiments (Taylor, 1934; Grace, 1971) have shown that a low viscosity ratio, typically $\lambda < 0.1$, gives rise to droplets with pointed ends that develop under steady deformation, with small drops jetting off from the pointed ends. DeBruijn (1989, 1993) shed some light on this subject via a comprehensive and careful set of experiments. A convincing qualitative explanation was presented which described tip streaming as the result of surfactants being swept toward the narrow ends of the drop, so that the ends become rigid at high enough surface concentrations and viscous stresses tear the narrow end regions away.

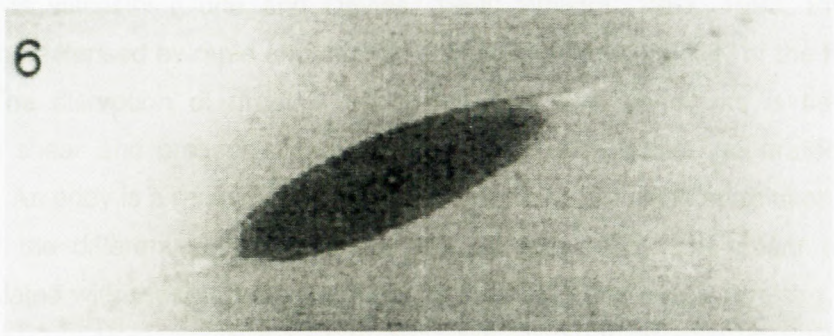

Figure 2.15: Tip streaming mechanism (Adapted from Ha and Yang, 1999)

2.7.3.2 Necking

Drop or fluid filament fragmentation, whether by growth of capillary instabilities or via end pinching because of the finite size of the drop, results in a distribution of drop sizes. In between the largest visible drops are smaller satellite drops and, on still smaller scales, there are sub satellite drops. Tjahjadi *et al.,* (1992) reported a detailed study documenting sub satellite drop formation through growth from the capillary instabilities on the surface of long, stationery, viscous fluid thread.

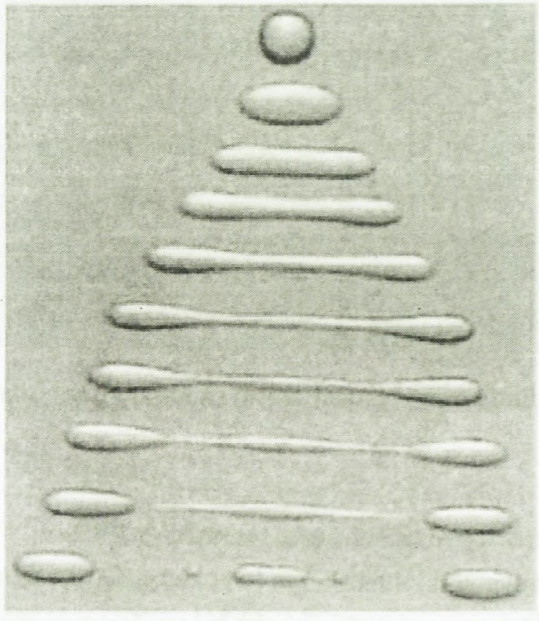

Figure 2.16: Necking mechanism (Adapted from Changzhi and Liejin, 2007)

2.7.3.3 End pinching

Experiments by Taylor (1934) and Grace (1971) observed the end pinching mechanism. Grace mentioned capillary wave instabilities as an explanation for this mode of fragmentation, though it is proper to describe the break-up of modestly deformed drops in terms of a deterministic interfacial tension driven flow dominated by end effects. End pinching is a result of an interfacial tension driven flow associated with curvature variations along the surface of the finite drop. The drop attempts to return to a spherical shape, though fluid motions produced by internal pressure gradients lead to break-up. Higher drop viscosities dampen internal flows, while lower external viscosities increase the speed with which the ends of the drop retract through the surrounding fluid, It therefore follows that higher λ drops are able to sustain much higher initial elongations prior to break-up during the relaxation process.

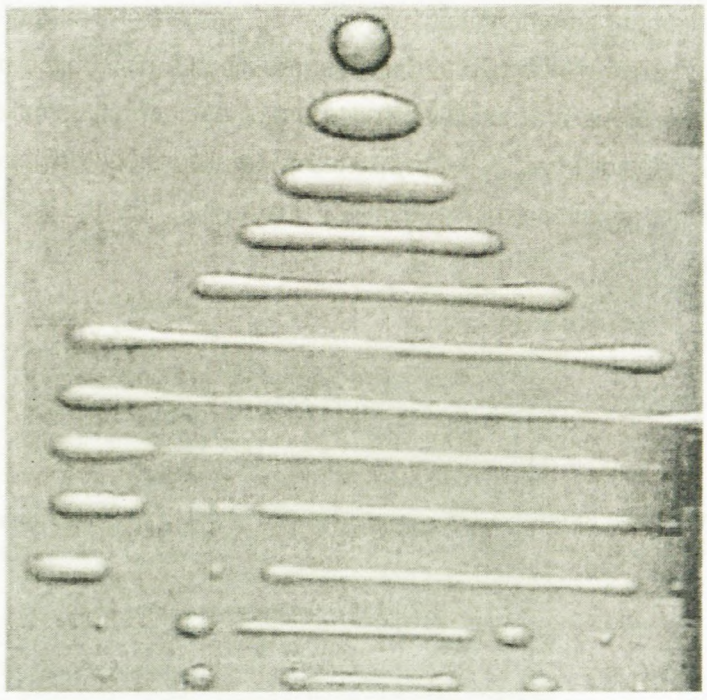

Figure 2.17: End pinching mechanism (Adapted from Changzhi and Liejin, 2007)

2.8 Break-up in concentrated emulsions

In more concentrated systems, the relation (Ca_{crit} = f $_{Grace}$ (λ)) cannot be expected to hold without modification. Droplets frequently interact with their neighbours, which will destabilise the drops and thus the critical break curve is expected to shift toward smaller capillary numbers. The most detailed work on the effect of concentration on interdroplet interaction, hydrodynamic stresses and break-up are the recent numerical studies by Loewenberg and Hinch (1996) and Loewenberg (1998). They presented a three-dimensional simulation of a concentrated emulsion in shear flow, using a boundary integral formulation which allowed for a disordered dynamic microstructure. They calculated how the average (normal) forces and the drop deformation and orientation change with increasing capillary number for a volume up to 30%. From their simulations it follows that the critical capillary number decreases by about 20% at maximum, which suggests that the effect of concentration on break-up is relatively small (at least for volume fractions from 0% to 30%).

Experimental studies, however, show that at higher volume fractions, the effect of concentration on break-up can be quite pronounced. Wieringa *et al.*, (1996) considered 80% oil in water emulsions and followed the change in drop size distribution after emulsion fraction in a colloid mill. Their experimental results were compared with a population balance model in which droplet break-up is predicted using a critical capillary number based on the emulsion viscosity. The model predictions agreed well with the experiments, which confirmed the idea that break-up is caused by the average emulsion stress rather than the local stress in the continuous phase layers.

Jansen *et al.*, (2001) in their results (Figure 2.18) showed how the critical capillary number varies with the viscosity ratio for emulsions at different volume fractions (0 – 70%) and they found that break-up is easier in concentrated emulsions (the curves shift downward).The reduction in the critical capillary number for 70% emulsions was about a factor of 10.

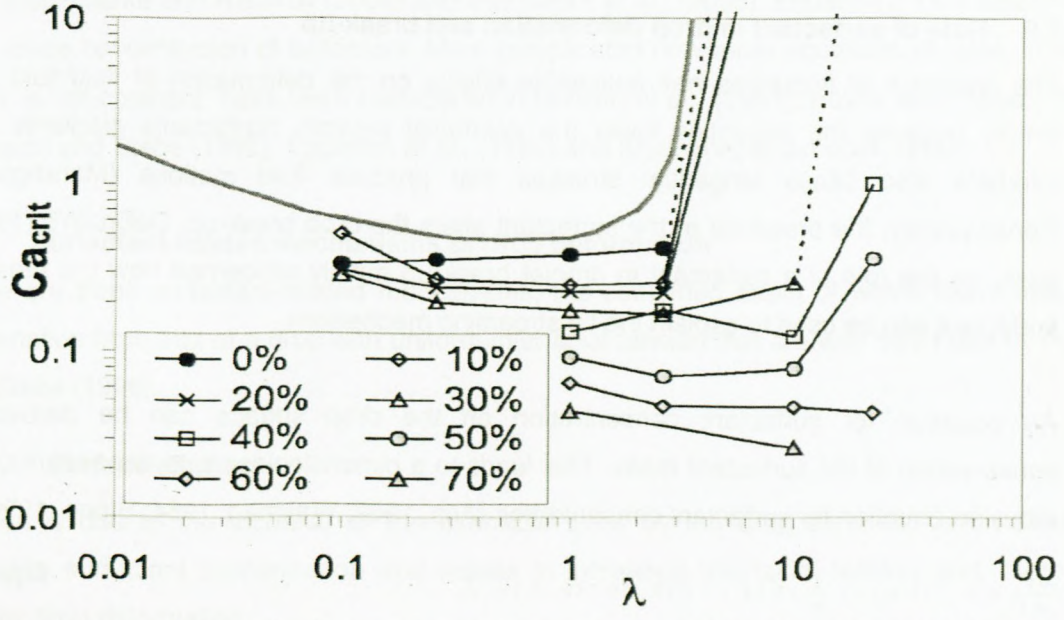

Figure 2.18: Critical capillary number for emulsions of different viscosity ratio and different volume fractions (Adapted from Jansen *et al.*, 2001)

The variations in emulsion viscosity with the viscosity of the continuous phase as well as with the dispersed phase ratio (ϕ) is quite complex (Mason, 1999; Pal, 2003; Jansen *et al.*, 2001). At low ϕ, the viscosity of the continuous phase determines the viscosity of the emulsion as well as the emulsion properties. With increasing ϕ, the structure of emulsions shifts from simple liquid-liquid dispersions to emulsions consisting of close-packed dispersed droplets separated by a thin layer

of continuous phase. As a result of a high internal phase ratio of concentrated emulsions, their viscosities are enormously increased. In such a case the viscous emulsion itself acts as the continuous phase for rupturing the drops. As a result, the rupturing of drops in the concentrated emulsion is boosted. This leads to formation of fine drops. Wieringa *et al.*, (1996) and Janssen and Meijer (1995) took into account the influence of the surrounding droplets by replacing the viscosity of the continuous phase for the apparent emulsion viscosity throughout the model. Mathematically:

$$Ca = \frac{\eta_e \dot{\gamma} R}{\sigma}$$ **Equation 2.11**

and $\lambda = \frac{\eta_d}{\eta_e}$ **Equation 2.12**

where η_d and η_e are the viscosities of dispersed phase and emulsion respectively.

2.9 Role of surfactant in drop deformation and break-up

The presence of impurities has noticeable effects on the deformation of fluid-fluid interfaces simply because the impurities lower the interfacial tension. Surfactants gradients along the interface also cause tangential stresses that produce fluid motions (Marangoni flows). Consequently, the presence of the surfactant alters the drop break-up. DeBruijn's (1989, 1993) study on the role of a surfactant in droplet break-up mainly concerned how the presence of a surfactant can be used to explain the tip streaming mechanism.

An equation for surfactant concentration on the drop surface can be derived through conservation of the surfactant mass. This leads to a dimensionless time dependent convection-diffusion equation for surfactant concentration (Aris, 1962; Waxman, 1984; Stone, 1990),

$$\frac{\partial \Gamma}{\partial t} + \nabla_s \cdot (\Gamma u_s) = \frac{1}{\alpha} (\nabla_s^2 \Gamma) - \Gamma (\nabla_s \cdot n)(u \cdot n) + j_n$$ **Equation 2.13**

where $u_S = (\delta - nn) \cdot u$ is the tangential velocity on the interface and j_n represents the net flux of surfactant for the interface. The parameter α is defined by $\alpha = (R\ \sigma_0)/(\eta_c D_s) = P_{es}/Ca$, where D_s is the surface diffusivity and $P_{es} = \frac{R^2 \dot{\gamma}}{D_s}$ is the surface Peclet number. This parameter controls the relative roles of diffusion and convection in the transport of surfactant on the interface. A small α corresponds to diffusion-dominated surfactant mass transfer on the interface, while a large α

corresponds to convection-dominated surfactant mass transfer. The larger α is, the more surfactant is transported along the interface by convection.

Assuming that the interfacial tension $\sigma = \sigma(\Gamma)$ varies linearly with surfactant concentration, according to Adamson (1976)

$$\sigma(\Gamma) = \sigma_0 (1 - \beta\Gamma) \qquad \textbf{Equation 2.14}$$

where the constant $\beta = - d(\sigma/\sigma_0)/d\Gamma$ is defined as $\beta = (T_0 R_g T_a)/(\sigma_0)$, where R_a and T_a are gas constant and absolute temperature respectively. It can be seen that a small value of β implies that interfacial tension decreases slowly as the excess surfactant concentration increases, while a larger value of β implies a rapid decrease of interfacial tension. When no surfactant is present, $\beta = 0$. Linear equations of the state of the form in Equation 2.14 have been considered in Stone and Leal (1990), Milliken and Leal (1994), Li and Pozrikidis (1997), Renardy *et al.*, (2002a), Drumright-Clarke and Renardy (2004) and Vlahovska *et al.*, (2005). Equation 2.14 is strictly valid for a dilute concentration of surfactant. More complicated non-linear equations of state, in which $d\sigma/d\Gamma$ is not constant, have been considered in Milliken et al., (1993), Pawar and Stebe (1996), Eggleton and Stebe (1998), Eggleton *et al.*, (1999) and Kruijt-Stegeman *et al.*, (2004).

2.9.1 Surfactant-related mechanisms of drop deformation

There are three surfactant-related mechanisms, the combined effect of which alters the drop deformation from that of a drop with uniform interfacial tension that are well described by Pawar and Stebe (1996).

2.9.1.1 Surface dilution

Dilution is due to the increase of the interfacial area as the drop deforms, which tends to decrease surfactant concentration and results in increased interfacial tension and, therefore, smaller drop deformation.

2.9.1.2 Marangoni stress

The Marangoni stress is defined as a product of the partial derivative of interfacial tension with respect to the concentration of the surfactant on the surface of the droplet and the concentration gradient

$$\nabla_S \sigma = -\frac{\partial \sigma}{\partial \Gamma} \nabla_S \Gamma \qquad \textbf{Equation 2.15}$$

and the interfacial derivative is $\frac{\partial \sigma}{\partial \Gamma} = \frac{X\,E\,\ln(1-X\,\Gamma)}{(1-X\,\Gamma)(1+\ln(1-X))}$,

where X is the surface coverage ($\Gamma_{eq}/\Gamma_{\infty}$), E is the elasticity number (RT Γ_{∞} /σ_0), Γ is emulsifier concentration per unit interfacial area and ∇_s is the gradient surface operator. The Marangoni stress retards the convective flux and thus opposes the interface velocity. Depending on the initial coverage, one or both multipliers in Equation 2.15 can contribute significantly to the total Marangoni stress (Pawar and Stebe, 1996). For small surfactant coverage initially, at uniform surfactant distribution, the interfacial derivative is very weak, as is the concentration gradient. This allows for the interface velocity to build up a significant gradient in surfactant concentration. For large X (surface coverage close to the maximum value), the surface tension derivative is also large, even for small concentration gradients. Thus the Marangoni stress is significant and a nearly uniform surfactant concentration is maintained.

2.9.1.3 Stretching

In studies by Hu and Lips (2003), the stretching is considered as purely tip stretching (a higher deformation at the tips compared to that of drops with a constant interfacial tension). Pawar and Stebe (1996) defined the difference between the local interfacial pressure and σ as a measure for tip stretching.

2.9.2 Effect of surfactant at small viscosity ratio, λ

Milliken *et al.*, (1993) and Milliken and Leal (1994) found that the effect of the surfactant is most pronounced when λ is smaller as the Marangoni stress hinders the interfacial velocity, causing the system to act essentially as if the drop has a higher viscosity. On the other hand, surfactants have little effect on droplets with a higher viscosity ratio. The shape of a droplet at break-up depends upon the viscosity ratio. Figure 2.19 shows a schematic diagram of different droplet shapes at sub and super critical shear rates. A lower λ generally leads to a more elongated shape. At low viscosity ratios, droplets become extremely elongated in the flow field at higher shear rates (Figure 2.19c). In the presence of surface-active species they develop cusped ends from which small droplets are ejected (Figure 2.19a). At intermediate viscosity ratios the droplets remain almost elliptical as the capillary number is approached. Break-up is preceded by the formation of a dumbbell shape (Figure 2.19b).

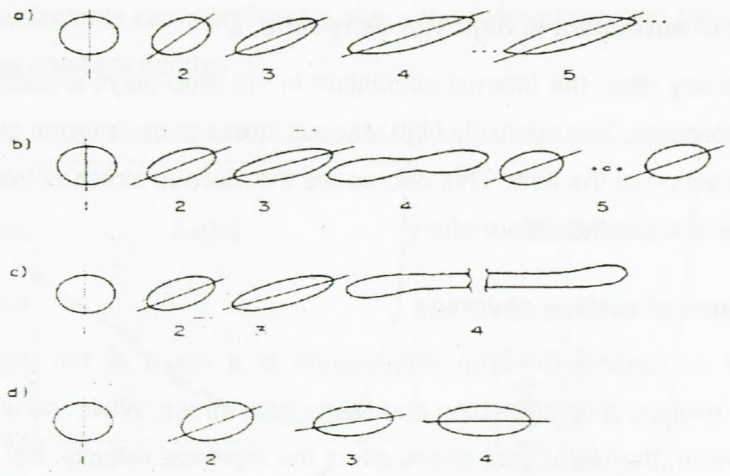

Figure 2.19: Evolutions of the droplet shape in simple shear at constant shear rate (Adapted from Williams *et al.*, 1997)

For systems with a viscosity ratio greater than 4, droplet break-up in simple shear flow has been found to be impossible. This is because the time scale of deformation is so high that the drop cannot readjust its shape as quickly as the flow fluid can cause rotation. This causes the long droplet axis to be aligned close the flow axis, where stretching is relatively weak. The droplet reaches a maximum deformation and is aligned with the flow field at higher capillary numbers (Figure 2.19d).

For small viscosity ratios ($\lambda < 0.1$), pointed drop tips with high curvature are formed. Such a shape plays an important role for the stability of the drop. In the presence of surfactants, their concentration increases at the tips of the drop, leading to interfacial tension reduction and resulting in stretching at the tips and if capillary number is sufficiently large, tip streaming occurs. Two competing processes in droplet deformation have been found in the presence of surfactants:

- **Surfactant convection:** this is due to the transport of surfactants along the interface by flow. It tends to increase surfactant concentration toward the tips of the drop, which decreases the interfacial tension at the tips, resulting in increased drop deformation.
- **Surfactant dilution:** this mechanism works to hinder drop deformation and surfactant convection, which works to enhance drop deformation. This mechanism is due to the increase of the interfacial area as the drop deforms, which tends to decrease surfactant concentration and results in increased interfacial tension and smaller drop deformation.

2.9.3 Effect of surfactant at high viscosity ratio, λ

At a high viscosity ratio, the internal circulation in the drop plays a stabilising role in addition to the interfacial tension. The relatively high viscous stress of the internal circulation also aligns the drop in the direction of the flow. This decreases the viscous stresses from the external flow and once more favours smaller deformation.

2.9.4 Influence of surface coverage

The effect of surfactants on drop deformation is a result of the combined action of three mechanisms: dilution, drop stretching and Marangoni stress. While the first two directly affect the interfacial tension; the Marangoni stress alters the interface velocity. For small surface coverage initially, at uniform surfactant distribution, the interfacial tension derivative is weak, as is the concentration gradient. This allows for the interface velocity to build up a significant gradient in surfactant gradient.

At high surface coverage (Figure 2.21), the Marangoni stress significantly alters the interface velocity to a pattern leading to a more uniformly distributed surfactant. It is also seen that the Marangoni stress affects the external flow around the drop. It should be mentioned, however, that the influence of the surface coverage decreases with an increasing viscosity ratio. At a high viscosity ratio, the viscous stresses of the internal drop circulation become dominant, suppressing the influence of surfactants. In summary: Marangoni stress can significantly alter the pattern of the interface velocity and, consequently, the velocity inside the drop. A typical vector field of the Marangoni stress is shown below in Figure 2.20 for relatively large surface coverage. It should be expected that Marangoni stress with such a pattern retards the drop deformation, especially in the tip regions

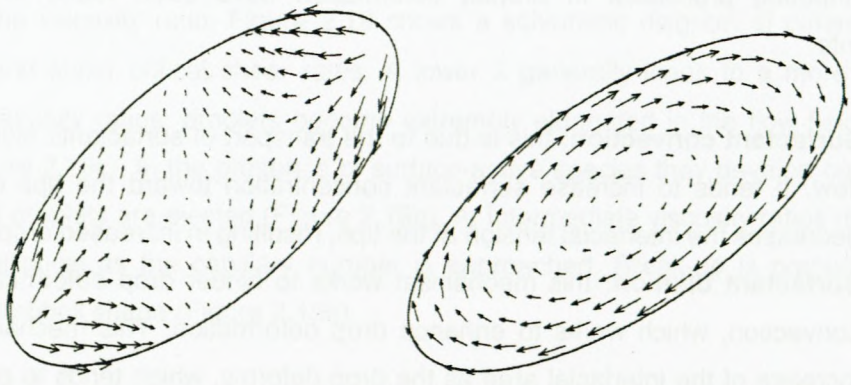

Figure 2.20: Marangoni stress $\nabla_s\sigma$ and interfacial velocity (Adapted from Bazhlekov *et al.*, 2006)

The presence of surfactants can significantly alter drop deformation and break-up and therefore also alter the critical capillary number.

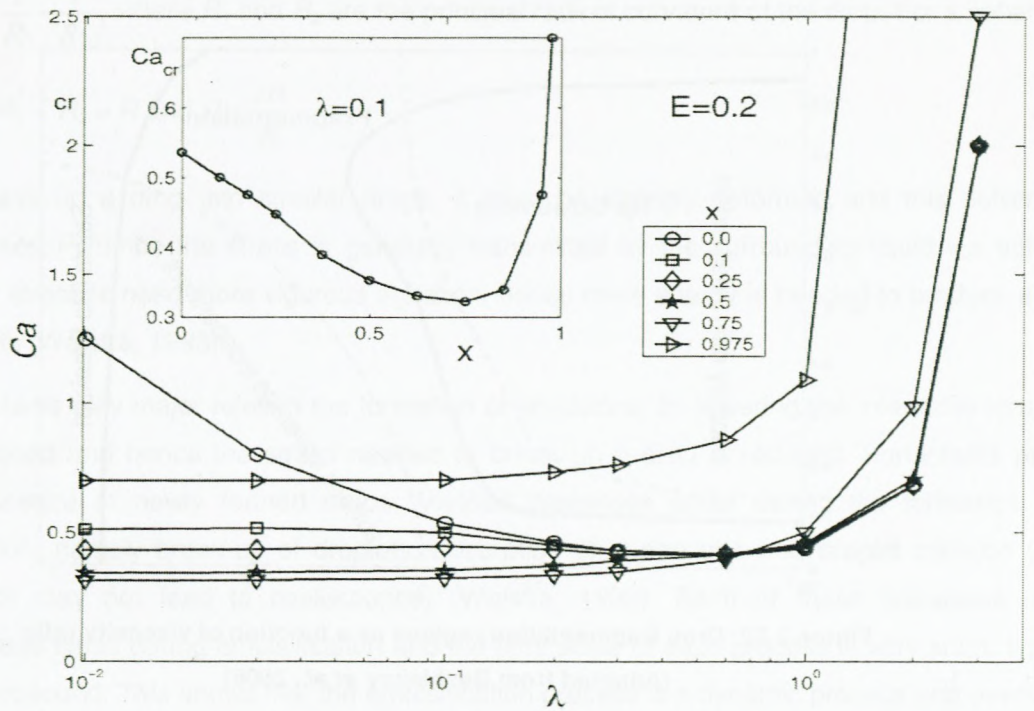

Figure 2.21: Critical capillary number as a function of the viscosity ratio for different surfactant coverage (Adapted from Bazhlekov *et al.*, 2006)

It can be seen that for small values of λ the presence of surfactants on the drop interface leads to a decrease in the critical capillary number; Ca_{crit} due to tip streaming and this is the case even for an extremely small surface coverage. The Grace curve in the presence of surfactants is shown (Figure 2.21) to have a plateau region (viscosity ratio independent) at small values of λ. At large surfactant coverage and λ the critical capillary number increases due to the effect of dilution. It should be remembered that Ca, and Ca_{crit} are based on σ_{eq}, which depends on the surface coverage.

Figure 2.22 illustrates regions of different modes of break-up by the solid lines. As is well known for large viscosity ratios in the absence of surfactants, break-up cannot occur independently of the capillary number. In the presence of surfactants, this is broadened at large X due to the stabilising effect of the Marangoni stress and dilution. Drop fragmentation appears at intermediate viscosity ratios for all surface coverage or at small viscosity in combination with

small ($X \leq 0.1$) or large ($X \geq 0.95$). The tip streaming mode is typical for small λ and intermediate surface coverage ($0.1 < X < 0.95$).

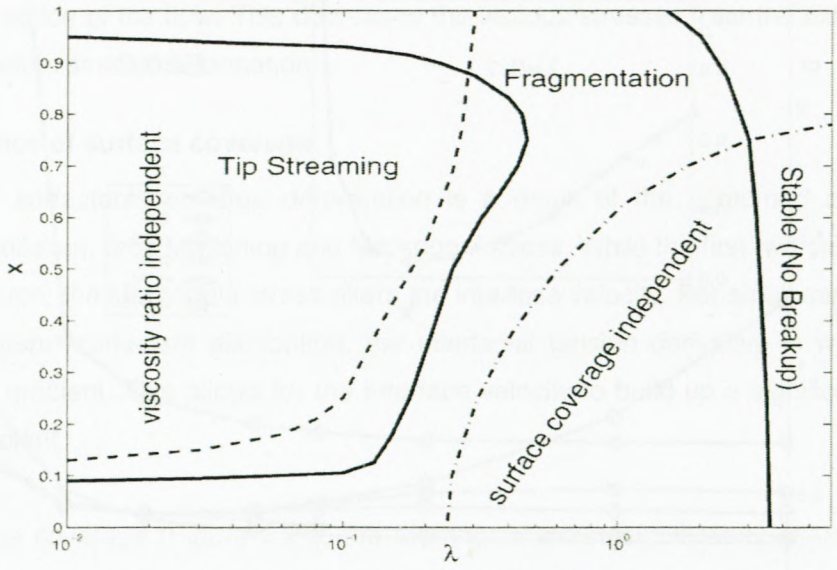

Figure 2.22: Drop fragmentation regions as a function of viscosity ratio (Adapted from Bazhlekov *et al.*, 2006)

The regions where drop deformation is independent of the viscosity ratio (dashed line) or surface coverage (dash dotted line).

2.10 Summary

Oil, water, surfactant and energy are needed to prepare an emulsion. This can be considered from the point of view of the energy required to expand the interface, $\Delta A\sigma$, where ΔA represents a change in interfacial area when bulk oil with area A_1 produces a large number of droplets with area A_2; $A_2 >> A_1$, σ is the interfacial tension). Since σ is positive, the energy to expand the interface is large and positive. This energy term cannot be compensated by the small entropy of dispersion $T\Delta S$ (which is also positive) and the total free energy of formation an emulsion, ΔG is positive, $\Delta G = \Delta A\sigma - T\Delta S$. Thus emulsion formation is non-spontaneous and energy is required to produce the droplets. The formation of large droplets (few micrometers) as is the case for macro emulsions is fairly easy and hence high speed stirrers such as the Ultraturrax or Silverson mixer is sufficient to produce emulsion.

The energy required for the formation of an emulsion can be understood from a consideration of Laplace pressure p (the difference in pressure between inside and outside the droplet, $P=\sigma\left(\frac{1}{R_1}+\frac{1}{R_2}\right)$ where R_1 and R_2 are the principal radii of curvature of the drop. For a spherical drop, $R_1 = R_2 = R$ and $P=\frac{2\sigma}{R}$.

To break up a drop into smaller drops, it must be strongly deformed and this deformation increases *P*. Since the stress is generally transmitted by the surrounding liquid via agitation, higher stresses need more vigorous agitation, hence more energy is needed to produce smaller droplets (Walstra, 1993).

Surfactants play major roles in the formation of emulsions: by lowering the interfacial tension, p is reduced and hence the stress needed to break up a drop is reduced. Surfactants prevent coalescence of newly formed drops. Various processes occur during the formation of an emulsion, namely break-up of droplets, adsorption of surfactants and droplet collision (which may or may not lead to coalescence) (Walstra, 1993). Each of these processes occurs numerous times during emulsification and the time scale of each process is very short, typically a microsecond. This shows that the emulsification process is a dynamic process and events that occur in a microsecond range could be very important. To describe emulsion formation, one has to consider two main factors: hydrodynamics and interfacial science.

- Emulsification involves the break-up of large drops of the dispersed phase into droplets in the 1 to 10μm range. With few exceptions, current hydrodynamic treatments of such drop break-up ignore the effects of emulsifiers other than their direct effect on the capillary or Laplace pressure, $\Delta P = 2\sigma/R$, where σ is the interfacial tension and *R* the radius of the drop before break-up. These treatments assume that:
- The interface transmits tangential stresses undiminished i.e. interfacially, the elasticity/viscosity is negligible and the interfacial tension is constant and uniform.

If reduction of capillary pressure were the only function of emulsifiers, one would expert the size of emulsion drops to vary linearly with the interfacial tension, σ, during emulsifications in shearing flow, under given conditions of rate and bulk viscosities. At least two factors arising from the dynamic character of any emulsification process can disturb this simple picture.

- During break-up, the interfacial tension of drops is neither constant nor uniform. The average value of σ will be higher than at equilibrium because of the necessary overall extension of the interface, but some parts of the drop may have much lower values than other parts since the deformation is not homogeneous.
- In many emulsifying machines, conditions of flow are such that zones of low shear exist side by side with highly sheared regions. After break-up in the high shear rate regions, drops almost always spend some time in the zones where they re-coalesce if their dynamic stability is low. This leads to a larger average drop size, particularly in a relatively inefficient emulsifying apparatus. As a result, a simple proportionality of average drop size with equilibrium interfacial tension is unlikely even in the simplified case of laminar flow.

Three important stages can be distinguished in the emulsification process:

- The extension of initially spherical drops of the dispersed phase in the applied flow field. If the applied flow is simple shear, the drop extension is moderate; in elongational flow, drops can be extended into very long cylindrical threads.
- The break-up of extended drops, into either a few relatively large drops (as in simple shear) or a multitude of tiny droplets (as in elongational flow).
- The re-coalescence of drops will occur, especially in emulsions with low concentrations of poor emulsifiers (Lucassen-Reynders and Kuijpers, 1992).

If the applied flow is simple shear (Rumscheidt and Mason, 1961; Grace, 1982; DeBruijn, 1989), it is generally found that a drop will eventually break up into two or three fragments when Ca is greater than Ca_{crit}. Experimentally, the numerical value of the critical capillary number turns out to depend on the viscosity ratio of the two phases, with a minimum value of the order 0.1 found for equal viscosities (Van den Tempel, 1960; Grace, 1982). If the applied flow is elongational (Grace, 1982; Rumscheidt and Mason, 1962; Tomokita, 1935), which is more efficient for emulsification purposes (Jurlaanse *et al.*, 1990), the initially spherical drops with radius R are extended into cylinders with length L and radius r. The final drop size depends on the L/r ratio and the question arises as to which factors determine the value of this ratio.

A controlled addition of surfactant leads to tip streaming for $\lambda < 0.1$, provided the surfactant concentration is large enough. Surfactants have significant effect on drop deformation at smaller viscosity ratios, but little effect at larger viscosity ratios is consistent with other studies (Milliken et al, 1993 and Milliken and Leal, 1994). Surfactants are found to facilitate the formation of

pointed ends during drop stretching and this may explain the observation of tip streaming in experiments with viscoelastic drops. The deformation of the drop increases with capillary number up to a limit (the critical capillary number), above which there is no steady drop shape (the drop stretches and "breaks up"). The effect of the viscosity ratio on the deformation of a surfactant-free drop is well established (Bentley and Leal, 1986). For moderate to high ratios (λ > 0.5), the deformation of the drop is largely insensitive to the viscosity ratio and the critical capillary number and critical deformation (the largest steady deformation of the drop) are also, approximately, independent of λ. For $\lambda < 0.5$, on the other hand, the critical capillary number and critical deformation increase significantly with a decrease in λ.

2.11 Research issues identified

The main shortcomings in current knowledge of processing or manufacture of highly concentrated explosive emulsions concerning the absence of systematic experimental data, especially regarding:

- What are determining factors that influence the break-up of droplets in highly concentrated explosive emulsions?
- Does the shape of the droplet size distribution change in shearing?
- What are the quantitative regularities that determine the kinetics of droplet break-up in highly concentrated explosive emulsions?
- What is the role of the surfactant in shearing of highly concentrated explosive emulsions?

It must also be mentioned that, among the numerous published works devoted to emulsions, a limited number touch on emulsions of the type investigated in this project, i.e. emulsions in which the dispersed phase is formed by a supercooled water solution of inorganic salts.

The interest in such highly concentrated emulsions is great because they have numerous potential technological applications in cosmetics, mining, oil recovery and explosives. The results of studies on the rheological properties of highly concentrated emulsions are published rather rarely, though some interesting exceptions are known.

Little knowlwdge is known or published concerning the fundamental theory or extensive experimental work that is done on this system (highly concentrated explosive emulsions). This problem is dominant because only an understanding of the structural processes of emulsions will

enable one to follow the evolution of the rheological properties, which determines their application value.

Against this background, the main objective of this study was to:

- Correlate the influence of energy input in the emulsification process with droplet size and droplet size distribution.
- Determine the critical diameter and width of size distribution with prolonged mixing time in changes to these parameters which are not noticeable.
- Determine the effect of surfactant concentration and type on droplet size.
- Determine and compare experimentally calculated energy with energy needed theoretically to expand an interfacial area in the emulsification process.
- Determine the droplet disruption coefficient from power law dependence of droplet size versus energy.
- Correlate the influence of energy input with yield stress and shear modulus.
- Determine the elasticity-droplet size dependency.
- Determine the capillary number as a function of the viscosity ratio of the dispersed phase to emulsion viscosity.

CHAPTER 3

Experimentation

3.1 Introduction

This chapter provides a comprehensive description of the experimental methodology adopted for this study; the procedures used in the statistical analyses of experimental random errors and the precautionary measures that were taken in order to eliminate experimental systematic errors, as well as a description of the instrumentation used.

3.2 Objectives

The objectives of this study were to:

- Correlate the influence of energy input in the emulsification process with droplet size and width of size distribution for different Pibsa-based surfactants and SMO in the explosive emulsions.
- Determine the critical diameter and width of size distribution with prolonged mixing time in changes to these parameters is not noticeable.
- Determine effect of surfactant concentration and type on droplet size.
- Determine and compare experimentally calculated energy with energy theoretically needed to expand an interfacial area in the emulsification process.
- Determine the droplet disruption coefficient from power law dependence of droplet size versus energy.
- Correlate the influence of energy input with yield stress and shear modulus.
- Determine the elasticity - droplet size dependency.
- Determine the capillary number as a function of viscosity ratio of the dispersed phase to emulsion viscosity.

3.3 Methodology

The methodology involved the following:

- Measurement of power consumption during mixing process using NanoVip Plus MEM meter.
- Calculating the energy input used for manufacturing emulsion samples as a function of time.
- Measurement of droplet size and droplet size distribution by laser diffraction and characterising the size distributions for all formulations.

- Measuring the rheological properties of prepared emulsions.
- Analysing time and energy evolution of rheological properties.
- Determining emulsion and dispersed phase viscosity from rheometry.
- Measurement of interfacial tension with the Kruss K100 tensiometer.
- Calculating capillary number and viscosity ratio.

3.4 Material

The materials used to manufacture the emulsion samples are summarised in the following table (Table 3.1).

Table 3.1: Materials used for manufacturing emulsion

Material	$\%C_{surf}$	dispersed phase	Fuel (continuous phase)
Pibsa-MEA	8	80% solution of AN in water	Mosspar-H
	14		Mosspar-H
Pibsa-IMIDE	8		Mosspar-H
	14		Mosspar-H
	8		Shellsol
	14		Shellsol
Pibsa-MEA/SMO	8		Mosspar-H
	14		Mosspar-H
Pibsa-UREA	8		Mosspar-H
	14		Mosspar-H
SMO	8		Mosspar-H
	14		Mosspar-H

The emulsion was prepared using a solution of surfactants in hydrocarbon oils (density of app. 0.9 g/ml) and an aqueous solution of inorganic salt. The aqueous phase was a solution of inorganic nitrate salt, mainly ammonium nitrate (AN). Water comprised less than 20% by mass of the solution. The crystallisation temperature (fudge point) of the aqueous phase was approximately 60°C. The density of the aqueous solution was about 1.4 - 1.5 g/ml. Trace

amounts (< 0.5%) of pH-buffering additives and acids were also present. Two types of surfactants, namely Pibsa-based and non-Pibsa SMO were used, as shown in Table 3.1. The pibsa surfactants are based on organic derivatives of PIBSA, especially alkanolamine derivatives. (PIBSA is an industry acronym for poly (isobutylene) succinic anhydride, which, when derivatised, forms an open-chain carboxylate). The PIBSA has a molecular mass in the range of 900 to 1300. The hydrocarbons are straight chain paraffins and cycling naphthanes. They are wax-like compounds with a chain length higher than 16. The hydrophile/lipophile balance is low (between 2 and 4).

3.5 Instrumentation

The instruments used in the study are described in this section, together with the procedures to operate them.

The following instruments were used in the study:

- Hobart N50 mixer
- Power and harmonic analyser
- Malvern Mastersizer 2000
- MCR 300 Paar Physica rheometer
- Kruss K100 tensiometer

3.5.1 Hobart N50 Mixer

The Hobart N50 mixer (Figure 3.1) was used to manufacture the samples under study. In its simplest form, it consists of a 'D' wire whisk (Figure 3.2) which can be operated at three different mixing speeds and a bowl for mixing (Figure 3.1 and Table 3.2).

Figure 3.1: Hobart N50 mixer

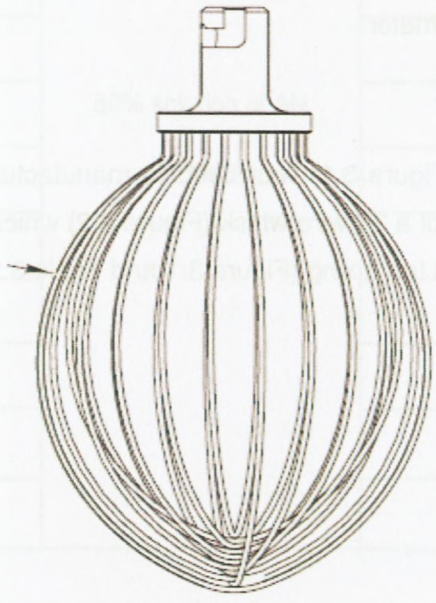

Figure 3.2: 'D' wire whisk

Table 3.2: Speeds of Hobart N50 mixer

	Agitator (RPM)	Attachment (RPM)
Low	136	160
intermediate	281	124
High	588	255

The first modification was made to the mixing bowl. An annular casing of stainless steel was made around the bowl, without changing its dimensions. This allowed the glycol bath supplied by the Haake temperature controlled system to circulate around the bowl to provide heat for the emulsification process.

The second minor modification involved the connection of the main power cable of the Hobart N50 mixer to the Nanovip Plus MEM meter. The live wire from the mixer was clamped, using a power clamp which measured current, insulation resistant, temperature and power going into socket 2 (Figure 3.3)

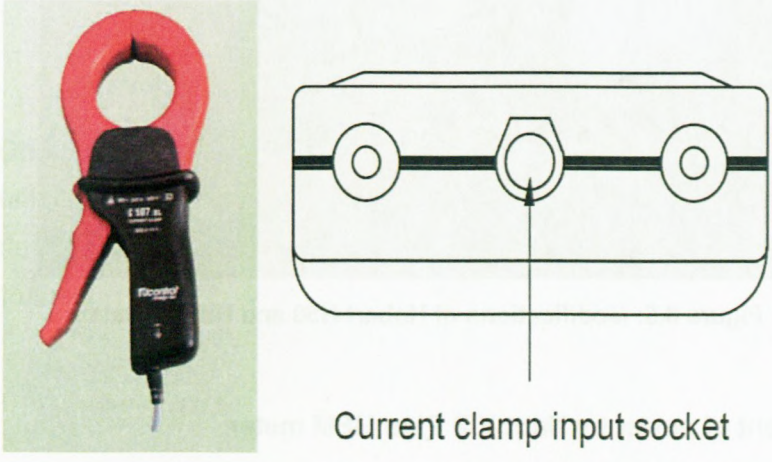

Figure 3.3: Clamp meter

The voltage measuring connection was done using the safety voltage leads provided with protected banana plugs for connection to the instrument Figure. 3.4).

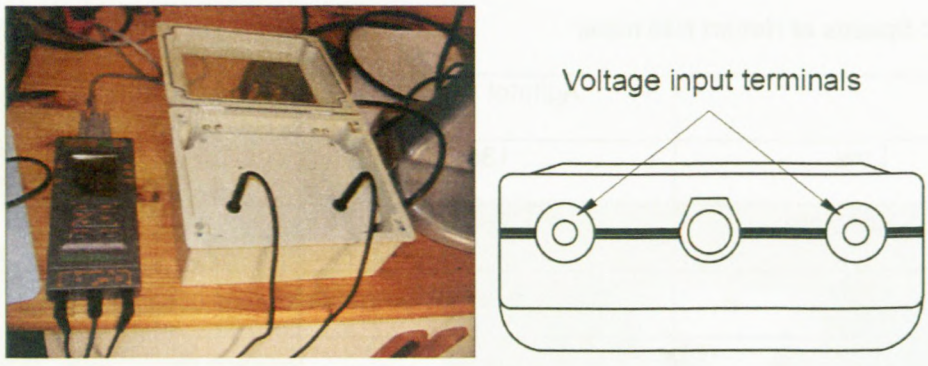

Figure 3.4: Voltage measuring connections

The complete setup is shown in Figure 3.5.

Figure 3.5: Modifications of Hobart N50 and Haake system

3.5.2 Measurement of power by NanoVIP Plus MEM meter

NanoWin is a software package designed to manage NanoVIP Plus and NanoVIP Plus MEM handheld analysers. NanoWin allows one to read all the measurements stored in the instrument and perform either manual or automatic measuring surveys (used in this study). When used together a with a NanoVIP Plus MEM analyser (Figure 3.6), one can download, catalogue and file the measuring surveys contained in the internal memory of the analyser, as well manage them just like rms surveys executed on the PC directly by NanoWin. A single configuration set-

up window allows one to display, modify and update all set-up parameters of the instrument , including PT and CT ratio, manual or automatic configuration of the amperometric clamp, standard (STD) and co-generation COG) meter power, enabling/disabling of harmonic analysis and auto scrolling of harmonics. Programmable CT and PT ratios allow automatic calculation of actual reading when NanoVIP-Plus is connected to the secondary circuits of preinstalled current and potential transformers. The program can operate in two modes outlined in the following sections.

Figure 3.6: NanoVIP Plus MEM meter

3.5.2.1 On line mode

The instrument must be connected to the RS232 serial port of the PC (Figure 3.7) by using the appropriate cable to display measurements, launch surveys and download the internal memory of the instrument.

Figure 3.7: Connection of power and harmonic analyser to RS232 serial port of PC

3.5.2.2 Off-line mode

The off-line mode is used to analyse previously saved data sets; an instrument does not necessarily have to be connected to the PC. The measuring session can be active at any given time.

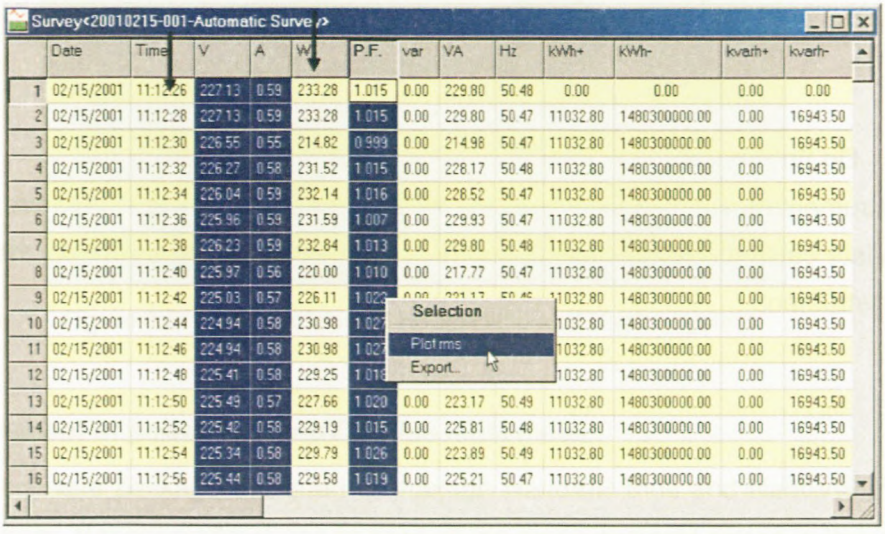

	Date	Time	V	A	W	P.F.	var	VA	Hz	kWh+	kWh-	kvarh+	kvarh-
1	02/15/2001	11:12:26	227.13	0.59	233.28	1.015	0.00	229.80	50.48	0.00	0.00	0.00	0.00
2	02/15/2001	11:12:28	227.13	0.59	233.28	1.015	0.00	229.80	50.47	11032.80	1480300000.00	0.00	16943.50
3	02/15/2001	11:12:30	226.55	0.55	214.82	0.999	0.00	214.98	50.47	11032.80	1480300000.00	0.00	16943.50
4	02/15/2001	11:12:32	226.27	0.58	231.52	1.015	0.00	228.17	50.48	11032.80	1480300000.00	0.00	16943.50
5	02/15/2001	11:12:34	226.04	0.59	232.14	1.016	0.00	228.52	50.47	11032.80	1480300000.00	0.00	16943.50
6	02/15/2001	11:12:36	225.96	0.59	231.59	1.007	0.00	229.93	50.47	11032.80	1480300000.00	0.00	16943.50
7	02/15/2001	11:12:38	226.23	0.59	232.84	1.013	0.00	229.80	50.48	11032.80	1480300000.00	0.00	16943.50
8	02/15/2001	11:12:40	225.97	0.56	220.00	1.010	0.00	217.77	50.47	11032.80	1480300000.00	0.00	16943.50
9	02/15/2001	11:12:42	225.03	0.57	226.11	1.023	0.00	221.17	50.46	11032.80	1480300000.00	0.00	16943.50
10	02/15/2001	11:12:44	224.94	0.58	230.98	1.023				11032.80	1480300000.00	0.00	16943.50
11	02/15/2001	11:12:46	224.94	0.58	230.98	1.023				11032.80	1480300000.00	0.00	16943.50
12	02/15/2001	11:12:48	225.41	0.58	229.25	1.018				11032.80	1480300000.00	0.00	16943.50
13	02/15/2001	11:12:50	225.49	0.57	227.66	1.020	0.00	223.17	50.49	11032.80	1480300000.00	0.00	16943.50
14	02/15/2001	11:12:52	225.42	0.58	229.19	1.015	0.00	225.81	50.48	11032.80	1480300000.00	0.00	16943.50
15	02/15/2001	11:12:54	225.34	0.58	229.79	1.026	0.00	223.89	50.49	11032.80	1480300000.00	0.00	16943.50
16	02/15/2001	11:12:56	225.44	0.58	229.58	1.019	0.00	225.21	50.47	11032.80	1480300000.00	0.00	16943.50

Figure 3.8: A typical output of the results from the Nanowin soft ware measurements

3.5.2.3 Operation procedure for Hobart mixer

- Switch on the oil circulator and set the temperature at not less than 15°C above the fudge point of the oxidiser solution.
- Ensure that the circulator valve is open in order to heat the bowl.
- Weigh the oxidiser solution ingredients into a metal jug.
- Weigh the fuel phase ingredients in a separate container.

It takes one hour for the circulator to reach a temperature of 85°C and afterwards to stabilise. The oxidiser salts in the metal beaker need to be stirred often in order to prevent boiling over of the ingredients.

3.5.2.4 Preparation of the mixer:

- Select speed on the mixer by moving the gear shift handle with the motor turned "off"
- Firmly attach the 'D'-wire loop on the agitator shaft, ensuring that the whip is safely secured onto the shaft.
- Locate the back pin of the bowl in its proper place on the column assembly.
- Snap down back locating lugs over the retaining pins.
- Move the bowl lift handle forward to lift the bowl.

3.5.2.5 Preparation of the base emulsion

- Transfer the fuel phase into the preheated bowl. Allow 5 minutes for the fuel phase to heat up.
- Switch "on" the mixer at speed 1.
- Slowly transfer the oxidiser solution into the bowl by running the solution into the bowl by means of a spatula.
- Ensure that an emulsion is formed.
- Continue adding the entire oxidiser solution.
- Stop the mixer and switch to speed 3.
- Cover the mixing bowl with plastic or with the aluminium cover to stop the emulsion from splashing.
- Let the mixer run at speed 3 while frequently sampling samples of about 10g at different times.

3.5.2.6 Determination of energy input into processing of explosive emulsions

Before emulsion samples were manufactured it was necessary to determine the losses in the Hobart N50 mixer at speed 3 without any sample. This was done by running the unloaded Hobart mixer for forty minutes. By using the mean power calculated from this process, multiplied by the different emulsification times for making emulsions, this energy was subtracted from the energy input given by:

$$E = \int_a^b P\,dt - \frac{\int_0^{40} P\,dt_{air\ run}}{\underbrace{40}_{Mean\ power}} \times t_{mixing} \qquad \textbf{Equation 3.1}$$

where *a* and *b* represent the initial and final times of the emulsification process.

3.5.3 Mastersizer 2000 (Malvern Co)

The droplet size distribution was measured using the Malvern Mastersizer 2000 instrument. The procedure is based on sample dispersion under software control and the measurement of angle dependence of the intensity of scattering of a collimated He-Ne laser beam. Particle size in the range from 0.02 to 2000 μm can be measured; this range is much wider than the droplet size distribution of the real samples used in this work. The particle size distribution calculations were based on the rigorous Mie theory and the use of the standard software applied to the instrument. The emulsion sample was prepared in a cylindrical (unbaffled) vessel with a turbine type stirrer. The vessel was connected to a flow-through cell (Hydro 2000 M). A known amount of reagent was added to the agitation vessel in the form of a pulse input and the time of addition was set as zero time. The sample was diluted in the oil of the continuous phase, just before the measurements were taken. The flow-through cell was placed on the laser beam of the light scattering measurement device for *in situ* size measurements. The agitation speed was maintained at 2000 rpm with an accuracy of 1rpm using a hand digital tachometer. Size distribution measurements were made at desired time intervals. The data acquisition time for each size distribution measurement was about 5s. All measurements were performed at 20°C.

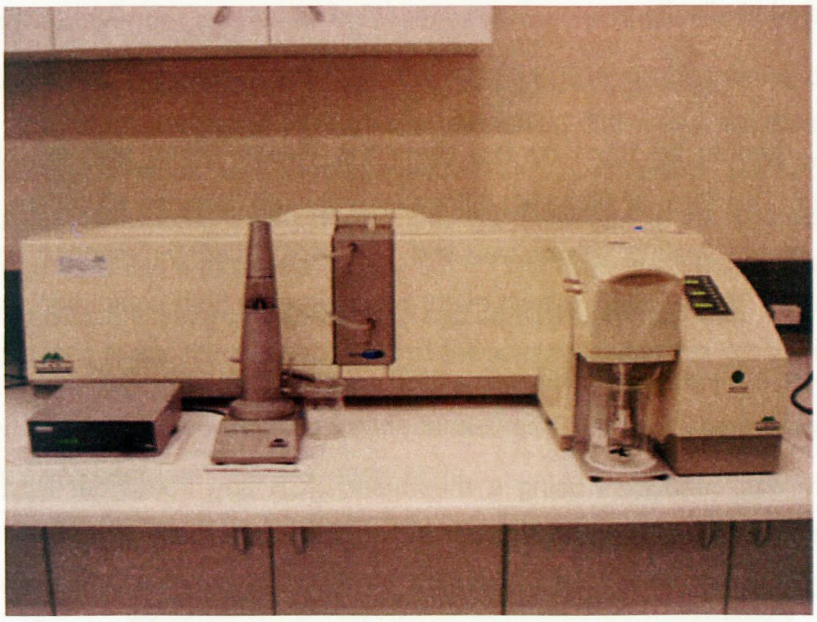

Figure 3.9: Malvern Mastersizer 2000

3.5.3.1 Determination of width (ω) of size distributions

The Gauss equation used to fit the distributions is given by:

$$f = \frac{A}{\omega\sqrt{\pi/2}}\, e^{\frac{2(D-D_0)^2}{\omega^2}} \qquad \text{Equation 3.2}$$

where f represents the density of the distribution function, D is the argument (droplet size), D_0 is the position of the maximum (semi log scale), ω is the dispersion characterising the width of the distribution and A is a normalising factor.

3.5.3.2 Determination of critical diameter (D_{crit}) and critical width (ω_{crit}) of size distribution

The critical diameter is defined as the diameter at which no further refinement of droplets is observed with increase in mixing time. The following equation was used to determine the critical diameter:

$$D_{cal} = D_{crit} + e^{-(t/\theta)}(D_0 - D_{crit}), \qquad \text{Equation 3.3}$$

where D_{cal} must be matched with D_{exp} (d_{32}) by changing the critical diameter, D_{crit}, and characteristic time, θ, respectively, which are fitting parameters, with D_0 being the initial diameter of the droplet.

The critical width distribution (ω_{crit}) was calculated using:

$$\omega_{cal} = \omega_{crit} + e^{-(t/\theta)}(\omega_0 - \omega_{crit}), \qquad \textbf{Equation 3.4}$$

where ω_{exp} had to be fitted by ω_{cal} (from the Gauss fitting) with ω_0, ω_{crit} and θ as fitting parameters. This form of fitting equations is proposed, besides all others, to demonstrate the existence of the limiting values ω_{crit} and D_{crit}, which can be reached as the final result of emulsification. The θ values (which might be different in both equations) are characteristic time parameters of the emulsification process in the chosen conditions of shearing.

3.5.4 Rheometry

Rheometry was conducted using a rheometer MCR 300 from Paar Physica. The MCR 300 rheometer is a research grade rotational drag flow instrument designed according to Searle's measuring principle, and is equipped with a permanent magnet synchronous drive that allows both CR and CRS rheological tests to be done in the same instrument. The complete MCR 300 rheometer assembly consists of an MCR 300 rheometer, an air compressor, air regulator, the temperature control units, (equipped with in-built heating and cooling systems), a computer data processing unit and US200 software, as shown in Figure 3.10.

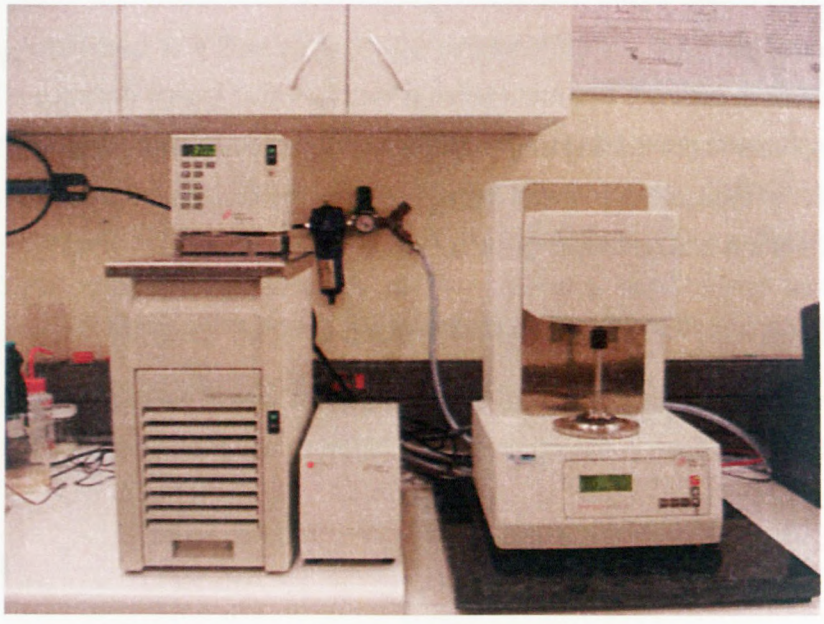

Figure 3.10: Modular compact Rheometer (MCR) 300

3.5.4.1 Concentric cylinder and plate – plate measuring systems

One of the measuring geometries used in this study was a concentric or coaxial cylinder geometry (CC 27), which consisted of a smooth cylindrical cup and a sandblasted cylindrical bob. The sandblasted surfaces were used to alleviate the wall slip effect. The bob was based on the Mooney-Couette or Mooney-Ewart design (i.e. the lower end of the bob was shaped as a truncated cone) to minimise end effects (Figure 3.11). The measuring bob diameter was 27mm and the gap measurement distance between the cup and the bob was 1mm.

Another geometry used for rheometry was a PP50 – TEK150AC (plate – plate geometry shown in Figure 3.12). This geometry was used for the measurement of flow curves (viscosity vs shear rate, shear stress vs shear rate) and oscillatory tests.

Figure 3.11: Concentric cylinder geometry CC27

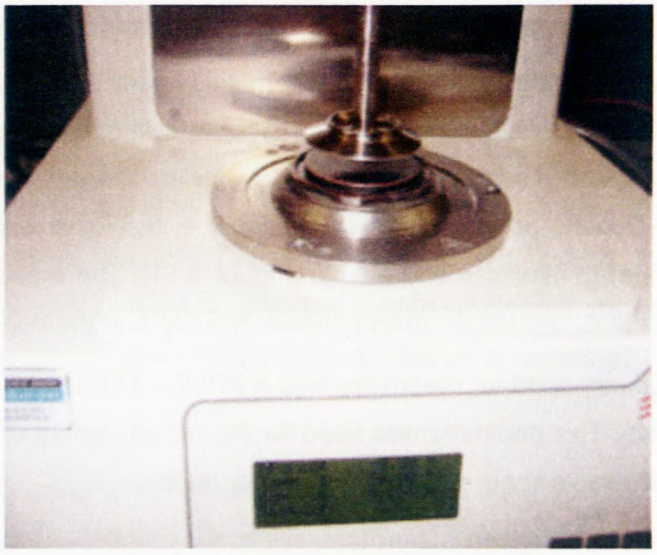

Figure 3.12: CC27plate – plate geometry

3.5.4.2 Experimental procedure

Some of the rheological studies were conducted on a rotational dynamic rheometer MCR 300 with CC27 measuring geometry. Samples for rheological measurements were taken from experiments, and were tested. Only a single region of deformation was used to determine the flow properties:

- Steady state flow-measuring flow curves (shear stress versus shear rate) in the shear rate control mode were used for the measurement of an ammonium nitrate solution at 85°C, using the CC27 and bob system.
- The plate – plate geometry (50mm) with a sandblasted surface (the plate diameter was 50mm) was used for the measurement of flow curves and oscillatory measurements. This geometry was used for:
  - Determining the emulsion viscosity with shear rates varying from 800 to 50s^{-1} by plotting shear viscosity as a function of shear rate at 70°C.
  - Oscillatory measurements for measuring strain amplitude dependences of the (storage and loss) components of dynamics modules were done from 0.01% - 200% at 30°C.
  - Flow curves (shear stress vs. shear rate) for determining yield stress were carried out from 200 – 1x0^{-6} s^{-1} at 30°C.

3.5.4.3 Experimental procedure

Some of the rheological studies were conducted on a rotational dynamic rheometer MCR 300 with CC27 measuring geometry. Samples for rheological measurements were taken from experiments, and were tested. Only a single region of deformation was used to determine the flow properties:

- Steady state flow-measuring flow curves (shear stress versus shear rate) in the shear rate control mode were used for the measurement of an ammonium nitrate solution at 85°C, using the CC27 and bob system.
- The plate – plate geometry (50mm) with a sandblasted surface (the plate diameter was 50mm) was used for the measurement of flow curves and oscillatory measurements. This geometry was used for:
  - Determining the emulsion viscosity with shear rates varying from 800 to 50s^{-1} by plotting shear viscosity as a function of shear rate at 70°C.
  - Oscillatory measurements for measuring strain amplitude dependences of the (storage and loss) components of dynamics modules were done from 0.01% - 200% at 30°C.
  - Flow curves (shear stress vs. shear rate) for determining yield stress were carried out from 200 – 1x0^{-6} s^{-1} at 30°C.

3.5.4.4 Determination of Dispersed phase viscosity, η_d

In order to determine the viscosity of an AN solution at 85°C which is Newtonian, a temperature sweep was performed at shear rate of 5s^{-1} in a range of temperatures from 100 to 60^{0}C (Figure 3.13),

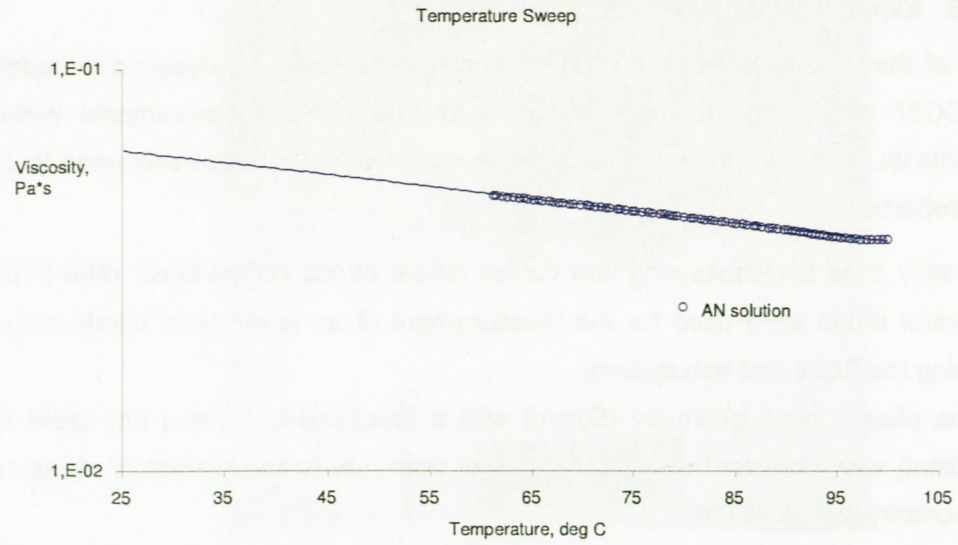

Figure 3.13: Temperature sweep of ammonium nitrate (AN) solution with approximation by the Arrhenius equation

and the Arrhenius equation was chosen to fit the experimental results and it is given by:

$$Y = \eta = A \cdot e^{\left(\frac{E_a}{RT}\right)} \qquad \textbf{Equation 3.5}$$

where A is the constant and E_a is the activation energy. Linearisation of equation 3.5 yields Equation 3.6, which is then used to determine the values of A and E_a:

$$\ln \eta = \ln A + \frac{E_a}{R}\frac{1}{T} \qquad \textbf{Equation 3.6}$$

where A = 0.004 is the regression parameter; E_a = 6.95 kJ/mol is the activation energy; R is the universal gas constant, and T is the absolute temperature. The temperatures and the corresponding values of viscosity are represented in Table 3.3.

Table 3.3: Results of prediction from the Arrhenius equation

T, °C	η, Pa*s
60	0.049
70	0.046
80	0.043
85	0.041
90	0.039
100	0.037

3.5.4.5 Determination of Emulsion viscosity, η_e

The prepared emulsions that were manufactured were tested by the MCR 300 for determination of the emulsion viscosity at 70°C, as this was the operation window for processing, and a flow curve (FC) of the emulsion was measured by using sandblasted plated – plate geometry. It should be noted that no breakage of emulsion, that is separation into two phases, was observed. The average shear rate at speed 3 of the Hobart N50 from the specification was estimated to be $380s^{-1}$.

In order to calculate the shear rate of complicated geometries like the Hobart mixer analytically, some simplifying assumptions are necessary (Bird *et al.*, 2007). Thus, for any section of the mixing chamber, the following assumptions were made to calculate the average Hobart shear rate, $\dot{\gamma}_{Ave,Hob}$:

- The gap was the main shearing zone
- Non-slip conditions at walls
- Negligible effect of curvature
- With the agitator both rotating and translating circularly in the bowl, the problem becomes a complicated moving boundary condition. If one could assume that the agitator only rotated, for including its translational velocity, it could be assumed that the bowl rotated in the opposite direction. This is a usual assumption in fluid dynamics (Bird *et al.*, 2007).

Therefore, the following parameters were obtained:

- The rotational wall speed of agitator (m/s): $\pi D_A N_R$ where D_A is the agitator diameter (m), and N_R is the rotational speed of agitator in the chosen gear for mixing (RPS)
- The imaginary wall speed of bowl (m/s): $\pi D_B N_T$ where D_B is the bowl diameter (m), and N_T is the translational speed of agitator in the chosen gear for mixing (RPS)
- The shearing gap between bowl and agitator, H (m): $(D_B - D_A - 2C_e)/2$ where C_e is the centre line distance between the agitator axis and the bowl axis (m).

Finally, the shear rate for each section was defined as follows:

$$\dot{\gamma} = 2\frac{\pi D_A N_R + \pi D_B N_T}{D_B - D_A - 2C_e} \qquad \textbf{Equation 3.7}$$

But, as D_A, D_B and h, and therefore $\dot{\gamma}$, were all dependent on the selected cross section (or on the height), one had to define an average shear rate as follows:

$$\bar{\dot{\gamma}} = \frac{\int_0^H \dot{\gamma}\, dH}{H}, \qquad \textbf{Equation 3.8}$$

where H was the height of the mixing zone, and this therefore became:

$$\dot{\gamma}(depth) = \frac{\pi D_A(depth) N_R + \pi D_B(depth) N_T}{\left(D_B(depth) - D_A(depth) - 2C_{Off}\right)/2} \qquad \textbf{Equation 3.9}$$

Integrating Equation 3.8 from 0 to H using the Matlab program version 7.0, the average shear rate was found to be $380 s^{-1}$

$$\dot{\gamma}_{ave}(depth) = \frac{1}{H}\int_0^H \dot{\gamma}(depth)d(depth) \approx 380 \ s^{-1}$$

The emulsion viscosity could be determined at this operation window for all formulations, as typically shown in Figure 3.14.

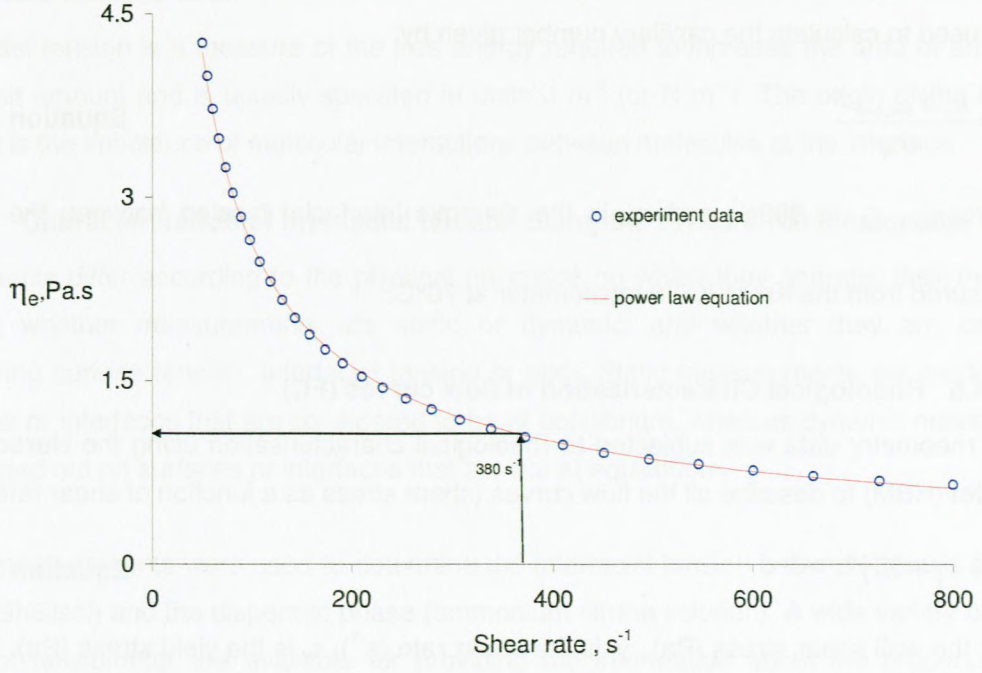

Figure 3.14: Typical fitting using Equation 3.11

Then, the experimental data of the flow curve were described according to the power law model

$$\eta = K\,\dot{\gamma}^{n} \qquad \textbf{Equation 3.10}$$

where η is the shear viscosity (Pa.s); $\dot{\gamma}$ is shear rate (s^{-1}); K is the fluid consistency index; and n is the power law index. n provides information about the material behaviour. Three value ranges could be identified for n:

i. $n < 1$, the system is shear thinning – the lower the value of n, the more shear thinning the emulsion is. Systems that are weakly flocculated or have thickeners added to them are usually shear thinning (Tadros, 2004).
ii. $n = 1$, flow in the emulsion is Newtonian.
iii. $n > 1$, the system is shear thickening.

The results shown in Table 3.3 relate specifically to the viscosity at 85°C for the ammonium nitrate solution and the emulsion viscosity calculated from the model at a Hobart average shear rate of 380s^{-1} and 70°C was used to calculate the viscosity ratio, λ given by: $\lambda = \frac{\eta_d}{\eta_e}$

Because the Hobart N50 shear rate is not constant, the value ($380s^{-1}$) estimated by the equation was used to calculate the capillary number given by:

$$Ca = \frac{\eta_e \dot{\gamma}_{Ave,hob} R}{\sigma_{eq}} \qquad \textbf{Equation 3.11}$$

where $\dot{\gamma}_{Ave,Hob}$ is $380s^{-1}$ and σ_{eq} is the dynamic interfacial tension between the two phases measured from the Kruss K100 tensiometer at 70°C.

3.5.4.6 Rheological Characterisation of flow curves (FC)

The rheometry data was subjected to rheological characterisation using the **Herschel-Bulkley model** (HBM) to describe all the flow curves (shear stress as a function of shear rate) obtained.

$$\tau_w = \tau_y + K.\dot{\gamma}^n \qquad \textbf{Equation 3.12}$$

τ_w is the wall shear stress (Pa), $\dot{\gamma}$ is the shear rate (s^{-1}), τ_y is the yield stress (Pa), K is the fluid consistency index ($Pa.s^n$), and n is the flow behaviour index. The Herschel-Bulkley model predicts both the yield stress (τ_y) and the shear-thinning behaviour of the overall fluid flow behaviour. It describes the behaviour of yield pseudoplastic fluids with reasonable accuracy, except at low and high shear rates. The shear thinning behaviour shows non-linearity of the flow behaviour, and can be seen clearly from the convexity of the rheogram curvature. The flow consistency coefficient (K) and the flow behaviour index (n) describe the rheogram curvature. All the flow model constants are empirical, which means that they are not formulated on the basis of the structure of the material, in fact, the τ_y value obtained often differs from the value of the ' true' dynamic and static yield stresses (Larson, 1999).

The advantage of the Herschel-Bulkley model is that it incorporates the features of the pseudoplastic model (rheogram curvature) and the Bingham plastic model (yield stress), (Slatter, 1999). In fact, this model can be used to characterise all time-independent flow behaviour, including Newtonian fluids. The major disadvantage of this flow model is that it is in direct opposition to the notion that there exist Newtonian asymptotes at both the low and the high rate of shear (Cross, 1965; Kozicki and Kuang, 1993; Slatter, 1999; Utracki, 1980).

3.5.5 Interfacial tension

Interfacial tension is a measure of the free energy required to increase the area of an interface by a unit amount and is usually specified in units J m^{-2} (or N m^{-1}). The origin of the interfacial tension is the imbalance of molecular interactions between molecules at the interface.

3.5.5.1 Characterisation of interfacial tension using the Kruss K100 tensiometer

Instruments differ according to the physical principles on which they operate; their mechanical design; whether measurements are static or dynamic; and whether they are capable of measuring surface tension, interfacial tension or both. Static measurements are carried out on surfaces or interfaces that are considered to be at equilibrium, whereas dynamic measurements are carried out on surfaces or interfaces that are not at equilibrium.

Static measurements were used to determine the interfacial tension between the oils (Mosspar-H and Shellsol) and the dispersed phase (ammonium nitrate solution). A wide variety of different types of tensiometer are available for providing the information about the properties of the surfaces and interfaces. Different methods are used for equilibrium measurements of interfacial tension; they include:

- Du Nouy ring
- Wilhelmy plate
- Pendant drop
- Sessile drop
- Spinning drop

Only the Wilhelmy plate method was used for determining the interfacial tension in using the Kruss K100 tensiometer and this is discussed in more detail in this section. The Kruss K100 (Figures 3.15 and 3.16) is a rapid, precise and accurate measuring device with flexible software control. The instrument has different add-in modules to measure surface tension, critical micelle concentration, contact angle, density, sedimentation and penetration measurements.

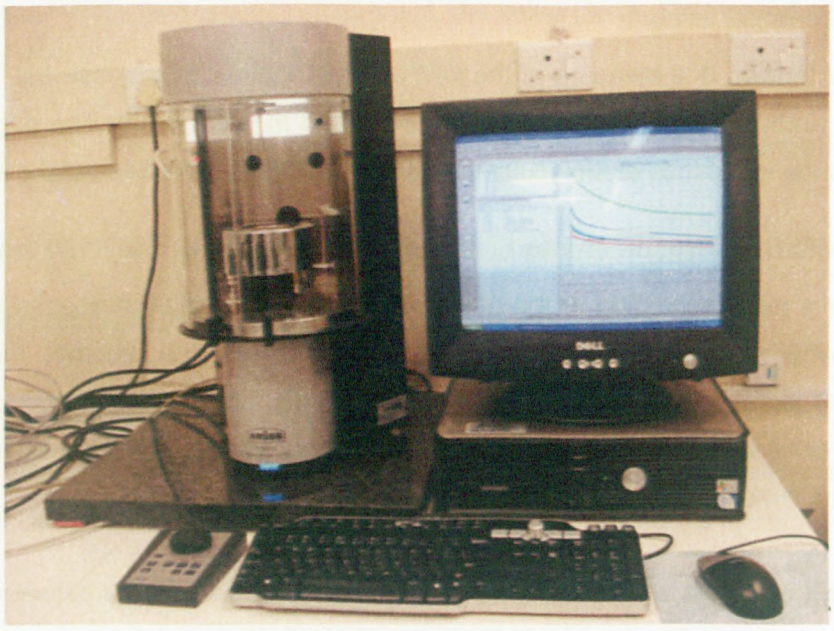

Figure 3.15: Kruss K100 Tensiometer

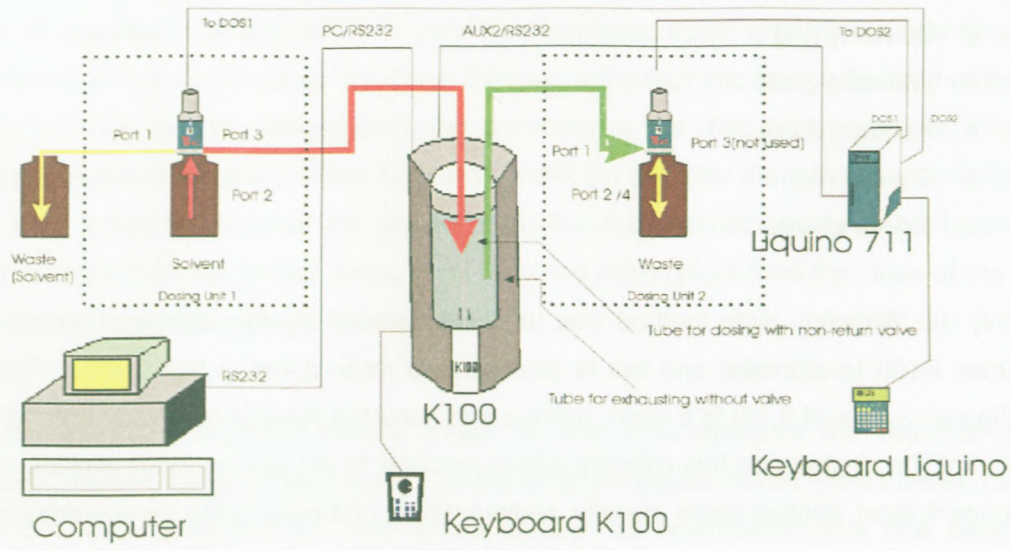

Figure 3.16: Connections: schematic overview

The Wilhelmy plate can be used to determine the interfacial tension between two liquids (Hiemenz and Rajagopalan, 1997). A vertical thin plate is used in this technique. Plates are often

constructed of materials that give a contact angle close to zero, such as roughened platinum or platinum/iridium, as this facilitates the analysis ($\cos\theta = 1$). The metal must be cleaned from organic contaminants by an organic solvent and flamed before experiments. Both roughening and cleaning of the plate surface are used to maintain good wetting of the plate by the test liquid. The plate is positioned so that its bottom edge is parallel to the interface between the two bulk liquids and the force measuring device is zeroed when the plate is located in the less dense liquid (usually oil). The force vertically acting on the plate by the liquid meniscus is measured by using a microbalance. The force applied to the plate is equal to the weight of the liquid meniscus uplifted over the horizontal surface. The force required to keep it positioned at the surface of the liquid is recorded as a function of time. The measuring procedure is static, which means that the plate can be held at zero level any time. This makes the continuous measurement of the surface or interfacial tension possible (Hubbard, 2002).

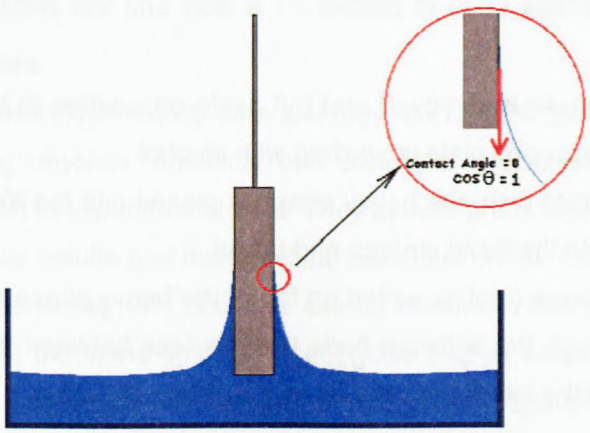

Figure 3.17: Wilhelmy plate technique

3.5.5.2 Experimental procedure for measuring interfacial tension

Before measurements are made, the plate should be:

- Washed with organic solvents and flamed before measurements are carried out.
- Checked as to whether the lower edge of the plate is straight. This can be done by placing the plate on a plane surface. The light gap between the plate and surface must be parallel and not wedge-shaped (Figure 3.18).
- Suspended from the hook on the instrument. The sample vessel should be filled with water, placed on the sample stage and moved upwards until the plate does not touch the

surface of the liquid. The light gap between the plate and the liquid must also be exactly parallel.

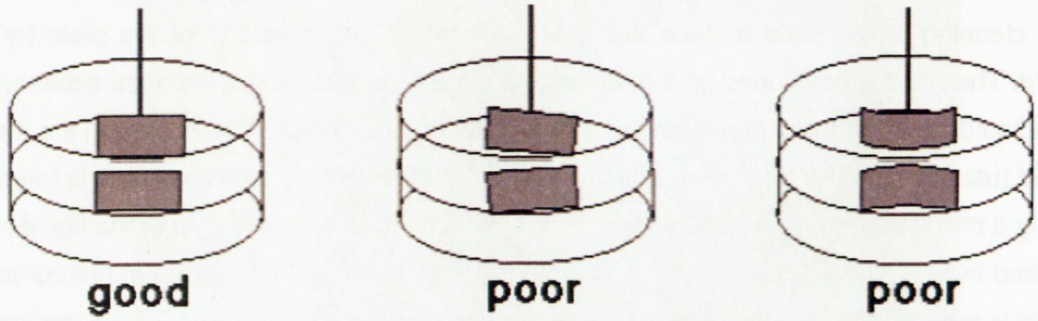

Figure 3.18: Alignment and shape check

- The light phase (fuel) is placed on a dish and the plate is lowered into the dish and tarred.
- The light phase is removed and put aside on a stove to keep the temperature at 70°C, and the measuring plate is washed with alcohol
- On a separate dish, the heavy phase is placed into the Kruss tensiometer and the plate is lowered to the liquid surface and tarred.
- The light phase (fuel) is added on top of the heavy phase and lowering of the plate of the Kruss through the software finds the interface between the oil and the aqueous phase and record the interfacial tension as a function of time.

The results of the procedure described above are shown in Table 3.4.

Table 3.4: Summary of results of interfacial tension measured at 70°C

Material	fuel	dispersed phase	Interfacial tension,mN/m
8% Pibsa MEA	Mosspar-H	AN	2.8
14% Pibsa MEA			
8% Pibsa IMIDE			1.0
14% Pibsa IMIDE			
8% Pibsa IMIDE	Shellsol		1.1
14% Pibsa IMIDE			
8% Pibsa UREA	Mosspar-H		3.7
14% Pibsa UREA			
8% Pibsa MEA/SMO (10:1)	Mosspar-H		0.6
14% Pibsa MEA/SMO (10:1)			

3.6 Experimental errors

Engineers constantly utilise experimental data and they rely on their theoretical understanding of the principles governing physical, chemical and biological processes. They test theoretical predictions by comparison to experimental data. They assess process performance by analysing experimental performance results and make critical decisions on the basis of their interpretation of measured data. Consequently, the ability to extract maximum information from engineering data is very important. At the same time, they recognise that all measurements are subject to errors which may affect their conclusions and must therefore be quantified. A primary goal is to identify the reliability of the measurements, and a secondary objective is to identify the limitations in the physical property measurements. Thus, steps must be taken to evaluate measurement errors. There are three steps in error analyses of most experiments: the first is the propagation of errors, which can be performed before the experiment is performed and the second is the determination of the errors which is done during the experiment. Lastly, comparison with true accepted values is performed after the experiment is completed (Poshusta, 2004). Experimental errors are grouped into three categories: gross, systematic and random errors.

Gross errors are errors due to blunders, equipment failure and power failures, and these are immediate cause for rejection of measurements.

Systematic errors are errors that result in a constant in an experimental measurement. These can result from improperly calibrated devices or a systematic effect on the measurement. With systematic error, one can repeat the experiment many times and always get the same results. Systematic errors are often identified by independent calibration of measurements. The accuracy of the measuring instrument is the measure of the deviation of the experimental result from the true accepted value. The most obvious sources of systematic errors in the case of both pipe watt meter and rotational rheometry are due to known conditions, and these conditions might be:

- o Instrumental (improperly calibrated device and incorrect alignment of the experimental setup
- o Personal (poor techniques and mistakes)
- o Experimental conditions
- o Imperfect technique

Random errors are errors due to experimental instrumental precision and imperfectly performed experiments. They affect the precision of a measurement. Precision is sometimes called "repeatability" or "reproducibility", and is a measure of the variation between repeated measurements. In most cases, precision is improved by increasing the sample size (i.e. number of repeated measurements). Often, under certain conditions, fluctuations due to this error obey the Gaussian distribution and this is referred to as statistical errors. Thus, averaging repeated measurements would often improve the precision of the measurements, provided $\left|\frac{x_i}{\bar{x}}\right| < 2$, for $\bar{x}$ is the arithmetic mean, and x_i is the measurement. The precision of the measurement is indicated by the least significant figures reported as associated with the error of the measurement, e.g. 4.235 ± 0.009 kg. The distribution of the values will depend on the physical system, but will generally assume a normal or Gaussian distribution (see Appendix J).

3.6.1 Accuracy of measurements

The statistics used to evaluate the accuracy, as well as the comparative performance, of various (rheological) models make use of a larger number of performance indicators, in the form of error equations. To name a few of these error equations, there is the log square error, standard error, absolute error, relative error, mean relative squared error, etc. For this study, only the mean

relative squared error was used as a measure of accuracy, and for comparing the performance of the models.

$$E = \frac{1}{N}\sqrt{\sum_{n=1}^{N}\left(\frac{\tau_{\exp} - \tau_{calc}}{\tau_{\exp}}\right)^2} \qquad \textbf{Equation 3.13}$$

In this equation, $\tau_{\exp}$ is the experimental value of the emulsion viscosity from rheometry and $\tau_{calc,}$ is the emulsion viscosity value predicted by the model. The degree of accuracy is indicated by the value of the error obtained; the smaller the value the more accurate is the model

3.7 Summary

A comprehensive description of both the emulsification process using the Hobart N50 and the rheometry has been presented. The summary describes in detail the instrumentation used for several types of measurement (i.e. the Kruss K100 tensiometer and concentric cylinder rheometry) and the experimental methodology adopted for the study. Analyses of experimental errors associated with rheological measurements have also been addressed. No corrections to the experimental data obtained were needed, as precautionary measures had been taken in advance to eradicate experimental systematic errors.

CHAPTER 4

Results and Discussion

4.1 Introduction

This chapter provides a comprehensive description of the procedures used in the analysis of results, and the inherent discussions pertaining to the experimental findings are also presented. The primary purpose of this chapter is to analyse, compare and discuss the test results obtained from the Hobart N50 mixer experiments.

The results include the following:

- Evolution of droplet size and droplet size distribution (DSD)
- Comparison of experimental energy and theoretical energy
- Characterisation of droplet disruption
- Effect of surfactant concentration on droplet size
- Effect of surfactant type on droplet size
- Effect of energy density on rheological properties
- Elasticity-droplet size dependency
- Capillary number and viscosity ratio of explosive emulsions.

It should be noted that in the following sections, the results are preferred to be presented typical for Pibsa-MEA in Mosspar-H as their characteristics for all formulations are similar and for other formulations they are shown in the Appendices.

4.2 Evolution of droplet size and droplet size distribution (DSD)

For evaluating the effectiveness of the influence of energy input on droplet size reduction during the emulsification process, it was necessary to determine their width of distribution. The droplet size distribution (DSD) of the samples that were manufactured was described by the Gauss equation. The equation is formulated below:

$$f = \frac{A}{\omega\sqrt{\pi/2}}\, e^{\frac{2(D-D_{50})^2}{\omega^2}}$$

Equation 3.2

This is characterised by three parameters: the width of DSD, ω, A, the normalising factor and the mass mediam diameter, D_{50}. Figure 4.1 (linear scale) shows the fitting of 8% Pibsa-MEA in Mosspar-H at 16 and 40 minutes of mixing to illustrate the characterisation of width of distribution, since the same procedure was followed for all formulations (see Appendix A). All the fitting parameters for all formulations in the study are summarised in Table 4.1.

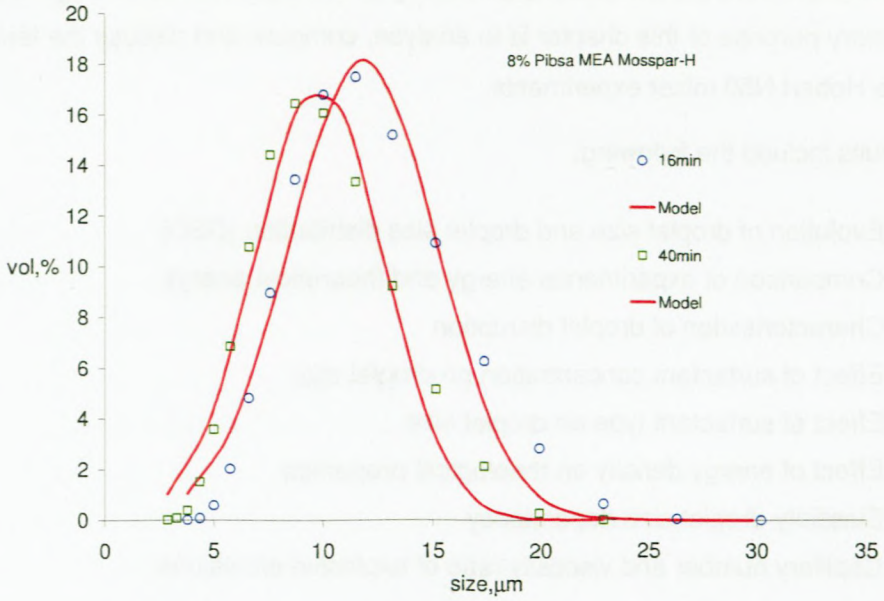

Figure 4.1: Gauss fitting for 8% Pibsa-MEA

In all cases under study, it was found that DSDs after emulsification were well described by the Gauss function as shown in Figure 4.1. This means that one can operate with time evolution of these two parameters, width of size distributions (ω) and mass mediam diameter (D_{50}). Both change in the process of emulsifying.

The changes in characteristics of parameters ω and D_{50} continue in such a way that some limiting value of both exists. Therefore it was useful to introduce the limiting value of those parameters that are achieved as the limit $t \rightarrow \infty$.

The critical width (ω_{crit}) of the size distribution refers to the width at which no further narrowing of the distribution is observed with increased mixing time. The model used to determine the critical width of the distributions for all formulations under study is given by:

$$\omega_{cal} = \omega_{crit} + e^{-(t/\theta)}(\omega_0 - \omega_{crit})$$ **Equation 3.4**

where ω_{exp} must be fitted by ω_{cal} (from the Gauss fitting) with ω_{crit} and characteristic time (θ) as fitting parameters, respectively, and ω_0 is the initial width distribution.

Typical experimental results illustrating the evolution of the width of DSD are shown Figure 4.2. As can be seen, the width of distribution decreases exponentially as the mixing time increases and approaches a constant value (see Appendix B for graphs).

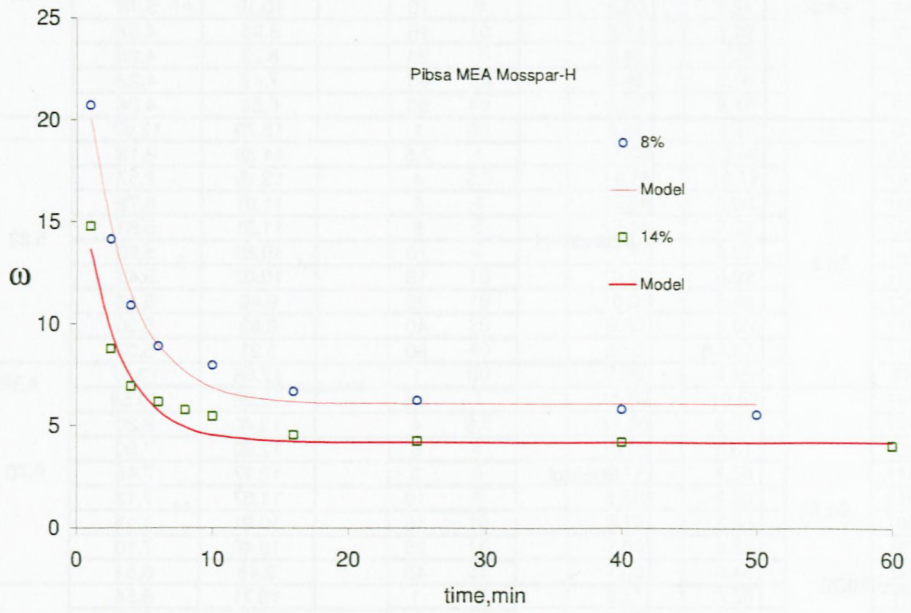

Figure 4.2: Width of size distribution as a function of time

Table 4.1: Change of mixing time with droplet size

Surfactant type	%C_{Surf}	Fuel	t_{mixing},mins	D_{50},μm	ω	ω_{crit}	A	θ,min
Pibsa-MEA	8	Mosspar-H	1	21.73	20.73	6.09	288.16	3.15
			2.5	18.04	14.15		236.68	
			4	15.84	10.91		205.22	
			6	14.50	8.91		187.18	
			10	13.15	7.98		170.88	
			16	11.78	6.69		152.30	
			25	10.62	6.26		137.31	
			40	9.683	5.83		125.70	
			50	8.93	5.59		115.59	
	14		1	18.87	14.79	4.20	249.36	2.78
			2.5	14.42	8.78		186.76	
			4	12.60	6.94		162.33	
			6	11.36	6.17		146.74	
			8	10.70	5.79		138.33	
			10	10.19	5.48		131.87	
			16	8.96	4.57		115.46	
			25	8.25	4.26		106.30	
			40	7.49	4.22		96.80	
			60	6.88	4.04		88.90	
Pibsa-IMIDE	8	Mosspar-H	1	18.79	12.97	5.23	244.23	2.81
			2.5	14.39	8.18		185.37	
			4	13.16	7.57		170.49	
			6	11.91	6.72		153.79	
			8	11.31	5.83		145.71	
			10	10.88	5.89		139.92	
			16	10.02	5.45		129.37	
			25	9.46	5.12		119.95	
			40	8.99	5.06		111.04	
			60	8.21	5.02		104.51	
		Shellsol	1	17.56	12.67	6.70	228.81	2.74
			2.5	15.28	10.53		198.88	
			4	13.40	8.20		173.67	
			6	12.90	7.90		167.15	
			8	12.17	7.46		157.28	
			10	11.67	7.13		150.76	
			16	10.91	7.11		137.24	
			25	10.48	7.10		136.39	
			40	9.43	6.51		122.56	
	14	Mosspar-H	1	13.71	8.54	4.03	177.63	2.55
			2.5	11.03	6.07		142.22	
			4	9.85	5.09		127.08	
			6	9.01	4.87		116.30	
			8	8.57	4.64		110.78	
			10	8.13	4.14		104.66	
			16	7.57	4.05		97.72	
			25	6.93	3.95		92.16	
			40	6.67	3.95		86.10	
			60	6.39	3.95		81.61	
		Shellsol	1	13.781	8.50	3.74	178.06	2.55
			2.5	10.79	5.90		138.92	
			4	9.73	5.28		125.71	
			6	8.69	4.73		112.26	
			8	8.19	4.42		105.38	
			10	7.88	4.13		101.32	
			16	7.14	3.82		92.15	
			25	6.65	3.56		85.87	
			40	6.27	3.53		79.18	

Surfactant type	%C_{Surf}	Fuel	t_{mixing},min	D_{50},μm	ω	ω_{crit}	A	θ,min
Pibsa-MEA/SMO (10:1)	8	Mosspar-H	0.5	18.79	13.26	3.70	245.20	2.32
			1	15.32	9.64		198.49	
			2.5	12.46	6.86		160.56	
			4	11.28	5.62		145.24	
			6	10.17	5.00		131.11	
			8	9.52	4.65		122.69	
			10	9.05	4.41		116.85	
			16	8.29	4.01		106.90	
			25	7.62	3.69		98.21	
			40	7.07	3.48		90.94	
			60	6.62	3.45		85.48	
	14		0.5	14.19	9.65	2.60	184.84	1.55
			1	11.47	6.40		147.92	
			2.5	8.84	4.39		113.95	
			4	7.75	3.78		99.90	
			6	7.08	3.41		91.27	
			8	6.69	3.21		86.25	
			10	6.39	3.02		82.27	
			16	5.88	2.76		75.85	
			25	5.46	2.54		70.24	
			40	5.07	2.47		62.65	
			60	4.69	2.37		60.53	
Pibsa-UREA	8	Mosspar-H	1	17.02	13.60	4.87	223.09	4.37
			2.5	14.78	10.17		193.05	
			4	12.98	8.00		168.43	
			6	12.14	7.32		156.90	
			8	11.47	6.87		148.91	
			10	10.83	5.92		139.49	
			16	10.05	5.46		130.05	
			25	9.30	5.05		119.91	
			40	8.55	4.67		110.51	
			60	7.96	4.65		99.13	
	14		1	15.02	10.52	3.50	195.88	2.44
			2.5	11.50	6.37		148.09	
			4	10.25	5.61		132.39	
			6	9.17	4.58		118.15	
			8	8.60	4.20		110.81	
			10	8.19	3.98		105.60	
			16	7.60	3.68		98.05	
			25	7.03	3.44		90.44	
			40	6.51	3.39		79.54	
			60	6.05	3.37		77.95	
SMO	8	Mosspar-H	1	9.89	5.39	2.50	128.47	2.71
			2.5	7.86	3.82		101.41	
			4	7.06	3.37		90.91	
			6	6.54	3.09		84.27	
			8	6.28	2.95		80.82	
			10	5.95	2.79		76.79	
			16	5.52	2.57		70.92	
			25	5.26	2.52		67.64	
			40	5.06	2.48		59.27	
			50	4.89	2.46		54.85	
	14		1	7.88	4.69	1.70	101.77	2.63
			2.5	6.09	3.17		77.02	
			4	5.26	2.43		67.84	
			6	4.87	2.24		60.28	
			8	4.57	2.08		59.03	
			10	4.38	1.99		56.55	
			16	4.08	1.84		52.42	
			25	3.90	1.81		48.02	
			40	3.69	1.75		39.56	
			50	3.54	1.72		39.35	

Analogous to Equation 3.4, the critical diameter, D_{crit}, refers to the diameter at which no further refinement of droplet size with increase in energy/mixing time is observed .The following model was used to determine the critical diameter:

$$D_{cal} = D_{crit} + e^{-(t/\theta)}(D_0 - D_{crit}) \qquad \textbf{Equation 3.3}$$

where D_{exp} (d_{32} in this study) must be fitted by D_{cal}, with D_{crit} and characteristic time (θ) as fitting parameters, respectively, and D_0 is the initial droplet size. Typical experimental results illustrating the evolution of the droplet size are shown in Figure 4.3 (see Appendix C for all formulations for fittings). The θ values (which might be different in both Equation 3.3 and 3.4) are characteristic time parameters of the emulsification process in the chosen conditions of shearing.

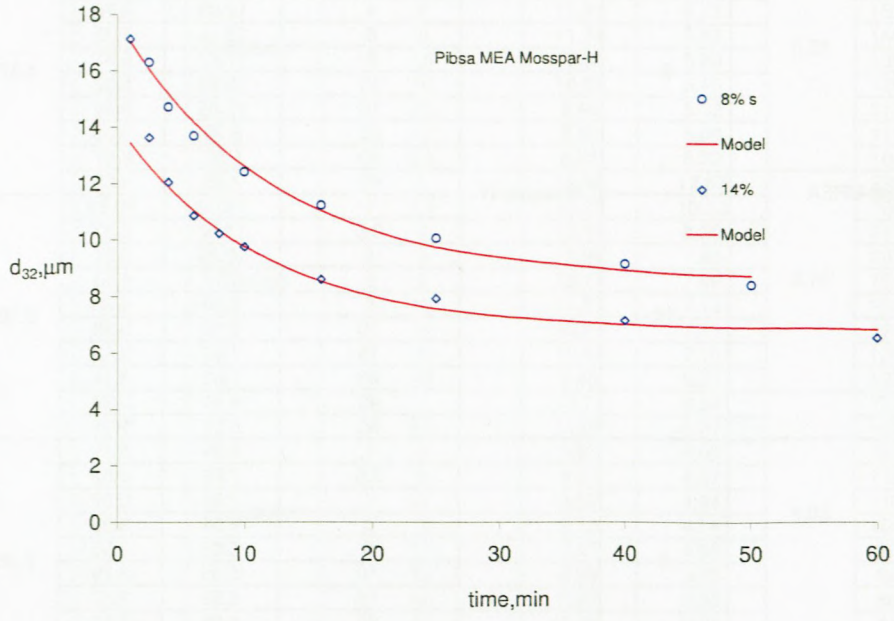

Figure 4.3: d_{32} as a function of time for determination of critical diameter

For comparison, the values of ω_0 and ω_{crit} from Table 4.1, as well as D_0 and D_{crit}, are all summarised in Table 4.2.

Table 4.2: Summary of results from fitting models

Surfactant type	Surfactant conc. %	D_0 / D_{crit}	ω_0 / ω_{crit}	θ_ω/θ_D,min
Pibsa-MEA	8	21.73 / 8.58	20.73 / 6.09	3.15 / 12.80
(in Mosspar-H)	14	18.87 / 6.81	14.79 / 4.20	2.78 / 11.20
Pibsa-IMIDE	8	18.79 / 8.38	12.97 / 5.23	2.81 / 6.24
(in Mosspar-H)	14	13.71 / 6.38	8.54 / 4.03	2.55 / 6.00
Pibsa-IMIDE	8	16.56 / 9.21	12.67 / 6.70	2.74 / 6.92
(in Shellsol)	14	13.78 / 6.26	8.50 / 3.74	2.55 / 5.06
Pibsa-UREA	8	17.02 / 8.04	13.60 / 4.87	4.87 / 8.01
(in Mosspar-H)	14	15.02 / 6.33	10.52 / 3.50	2.44 / 5.19
SMO	8	9.89 / 4.70	5.39 / 2.50	2.71 / 2.98
(in Mosspar-H)	14	7.88 / 3.50	4.69 / 1.70	2.63 / 2.34
Pibsa-MEA/SMO	8	18.79 / 6.91	13.26 / 3.70	2.32 / 5.42
(in Mosspar-H)	14	14.19 / 5.00	9.65 / 2.60	1.55 / 4.26

One can see that shearing, in all cases, leads to the remarkable decrease of the average droplet size and the narrowing of DSD. Addition of a low-molecular-weight surfactant (SMO) decreases the shear stability of emulsions, as it can be seen that it lowers the characteristic time θ and D_{crit} values. It is interesting to note that the mixture of SMO and Pibsa-MEA demonstrates a synergistic effect on the narrowing of the droplet size distribution, although using solely SMO is the most efficient way to reduce the droplet size.

It can be seen that a higher surfactant concentration provides a lower critical diameter – that is, the diameter below which droplet refinement does not take place – due to the increase of the probability of surfactant adsorption to the surface of droplets during emulsification (McClements, 2004, 2005). In terms of surfactant type, more or less the following trend for the critical diameter and characteristic time is seen:

Pibsa-MEA > Pibsa-IMIDE ≈ Pibsa-UREA > Pibsa-MEA/SMO > SMO

One could expect the higher concentration of a surfactant to lead to slower rupture of droplets, but this is not necessarily so, especially if considering the average droplet size.

The decrease of size distributions and droplet size has been presented in Figures 4.2 and 4.3 and has been studied before. Studies (by Djakovic *et al.*, 1987; Sanchez *et al.*, 2001; Oh *et al.*, 1993; Tornberg, 1978, 1980) utilising circulation mode emulsification have shown that changes in the drop size distribution and a decrease in mean drop size occur prior to reaching a steady state. The rate of achieving the steady state depends on the hydrodynamic conditions and on the emulsifier properties (concentration, kinetics of adsorption, etc.). This is because emulsion droplets increase in viscosity with the ongoing emulsification, which contributes to their ability to withstand shear stress, and this is an indication that emulsion droplets are less prone to fragmentation as emulsification is extended.

This phenomenon might also be better understood if one considers that deformation of emulsion droplets by shear stress is opposed by the Laplace pressure that aims to preserve the spherical shape. The Laplace pressure is inversely related to the radius of curvature of droplets and hence their size ($\Delta P = 2\sigma/R$ where σ is the interfacial tension and R is the radius of an un-deformed droplet). Therefore, it is likely that both an increase in viscosity of emulsion droplets and a decrease in their size, accompanied by prolonging the period of emulsification, present synergic resistance against movement to break up emulsion droplets (Yogita and Hongkee, 2000).

In summary, it could be observed from Table 4.1 that both the average droplet size and the width of size distributions decrease with an increase in time. The two models predict both the critical diameter and the width, as well the characteristic times at which there is no change in droplet size or width of distribution with increase in emulsification time, that is the mean droplet size and width of distribution decrease over time and level off to a final value with further mixing, resulting in no noticeable decrease in droplet size or distribution width reduction.

Instead of time, a more physically based argument can be used. This involves the energy consumption during mixing. It is observed from Table 4.1 that both mass mediam diameter (D_{50}) and width of the distribution decrease with increase in mixing time, but increasing the time of mixing is one way of increasing energy input into the system and the results shown in Figure 4.4 illustrate the findings (see Appendix D for all formulations).

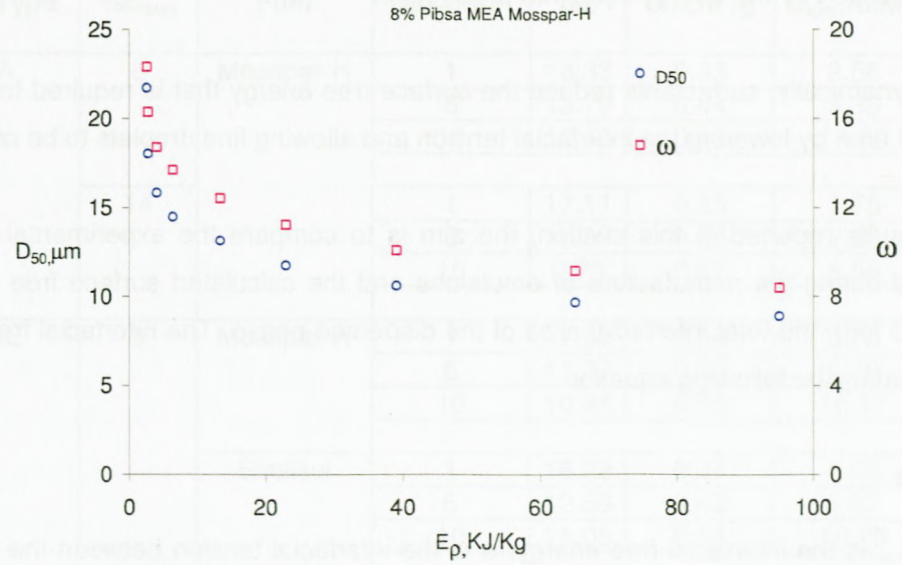

Figure 4.4: D_{50}, ω as a function of energy density, Pibsa-MEA in Mosspar-H

Figure 4.4 points out two important factors in the emulsification process which will be discussed in detail in sections 4.5 and 4.6:

- Effect of surfactant concentration
- Influence of energy input

It can be generally concluded that mean droplet size and width of distribution decrease with an increase in energy density and approach constant values for longer emulsification times.

4.3 Comparison of experimental and theoretical energy

Mechanical emulsion starts with a premix of the fluid containing surfactants. The emulsification process includes two steps. First, deformation and disruption of droplets which increase the specific surface area of the emulsion and, secondly, stabilisation of the newly formed interface by surfactants, for emulsions are thermodynamically unstable, droplets tend to coalesce. This is due to excess free energy associated with the surface of emulsion droplets. The excess surface energy arises as a result of the cohesive forces between the molecules of an individual liquid being greater than the adhesive forces between the liquids (Banker and Rhodes, 1979; Martin *et al.*, 1993). On dispersion, the interfacial area of the dispersed phase liquid increases

considerably compared to that of the continuous phase liquid. The dispersed droplet diameter is also conditioned by the energy input into the system.

Thermodynamically, surfactants reduce the surface free energy that is required to increase any interfacial area by lowering the interfacial tension and allowing fine droplets to be created easily.

In the results reported in this section, the aim is to compare the experimental energy (E_{exp}) measured during the manufacture of emulsions and the calculated surface free energy (E_{theo}) needed to form the total interfacial area of the dispersed phase. The interfacial free energy was determined by the following equation:

$$E_{theo} = \sigma A \qquad \textbf{Equation 2.4}$$

where E_{theo} is the interfacial free energy, σ is the interfacial tension between the oil phase and the dispersed phase measured from the Kruss K100 tensiometer and A is the total interfacial area of the dispersed phase obtained from the Malvern Mastersizer 2000 droplet size measurements. The specific surface area (SSA, m^2/g), defined as the total area of particles divided by the total weight, was calculated from particle size distribution. The calculation of this value was based on the assumption that the particles were both spherical and non-porous. The results are summarised in Table 4.3 for all formulations. It could be observed generally from Table 4.3 that the specific surface area (SSA) increases as the mixing time increases, for all formulations. This is to be expected, as the breakage of large droplets into smaller involves increasing the surface area through increasing the mixing time, which is an indirect way of increasing energy input.

NB: The emulsification times in Table 4.3 are chosen arbitrarily as an illustration

Table 4.3: Summary of results, comparison of E_{exp} (KJ/Kg) and E_{theo} (KJ/Kg)

Pibsa Type	$\%C_{surf}$	Fuel	t_{mixing},min	d_{32}	S.A,m^2/g	E_{exp},KJ/kg	E_{theo},KJ/kg
MEA	8	Mosspar-H	1	18.33	0.33	2.56	7.56×10^{-4}
			6	13.70	0.44	6.39	1.23×10^{-3}
			10	12.43	0.48	13.30	7.92×10^{-3}
	14		1	17.11	0.35	1.75	9.80×10^{-4}
			6	10.87	0.55	3.28	1.55×10^{-3}
			10	9.76	0.61	8.55	1.72×10^{-3}
IMIDE	8	Mosspar-H	1	17.52	0.34	3.26	3.42×10^{-4}
			6	11.37	0.53	9.78	5.27×10^{-4}
			10	10.44	0.58	16.17	5.7×10^{-4}
		Shellsol	1	16.22	0.37	1.46	4.07×10^{-4}
			6	12.68	0.49	5.82	5.40×10^{-4}
			10	11.05	0.54	10.28	5.97×10^{-4}
	14	Mosspar-H	1	12.94	0.47	1.21	4.69×10^{-4}
			6	8.64	0.69	6.44	6.94×10^{-4}
			10	7.83	0.77	12.49	7.66×10^{-4}
		Shellsol	1	13.03	0.46	0.18	5.06×10^{-4}
			6	8.33	0.72	5.46	7.92×10^{-4}
			10	7.58	0.79	11.03	8.71×10^{-4}
MEA/SMO	8	Mosspar-H	1	14.44	0.42	0.75	3.74×10^{-4}
			6	9.81	0.61	7.48	5.50×10^{-4}
			10	8.74	0.69	14.51	6.17×10^{-4}
	14		1	10.95	0.55	0.60	4.93×10^{-4}
			6	6.85	0.88	6.19	7.88×10^{-4}
			10	6.19	0.97	9.33	8.71×10^{-4}
UREA	8	Mosspar-H	1	15.34	0.39	1.82	1.45×10^{-3}
			6	11.49	0.52	6.10	1.93×10^{-3}
			10	10.36	0.57	11.15	2.14×10^{-3}
	14		1	13.92	0.43	1.28	1.59×10^{-3}
			6	8.84	0.68	3.60	2.51×10^{-3}
			10	7.91	7.42	7.42	2.80×10^{-3}

It can be observed from Table 4.3 that the energy spent to form the emulsion is larger than the actual droplet surface energy in the actual product. According to Fradette *et al.*, (2007), the reason for this is that most of the energy is actually lost as heat (thermal dissipation) or converted into momentum for phase contacting (hydrodynamic mixing). In practice, however, a lot of energy is lost during emulsification through heating, either because of viscous dissipation, for a mechanical energy supply, or through diffusion or convection for a chemical energy supply. Reduction of this high amount of lost energy is a real challenge in industrial production of emulsions. It should be noted that the lower theroretical energy than experimental one can also be due to some energy loss dissipated for droplet deformation before break-up occurrence. From a more fundamental point of view, the mixture obtained is in a metastable state; the properties of an emulsion therefore depend not only on the state of variables (temperature and composition), as in the case of a thermodynamic system, but also on the preparation method. For this reason, emulsification is of the utmost importance where different emulsification routes can be distinguished.

In conclusion: the calculation of the energy needed to increase the specific area of a collective droplet by a certain amount of area shows that very little energy is needed to increase the surface area, but very high energy must be used in the emulsification machine to achieve small droplets, since the comminution of large droplets into smaller ones involves additional shear forces, so that viscous resistance during agitation absorbs most of the energy (Othmer, 1999; Walstra, 1993) and excess energy is dissipated as heat and/or droplet deformation prior to break-up. One reason for this is that energy is needed to create flow in which forces can act to deform droplets (Brosel and Schubert, 1999).

4.4 Characterisation of droplet disruption using power law equation

For this section specifically, it was necessary to start from the same large droplet size for all formulations to follow up the refining process of all surfactants. The formulations used for this investigation were carried out in Mosspar-H and Shellsol only. Figure 4.5, below, presents the chosen droplet size with similar size distribution. The chosen droplet size (DS) was found to be13μm.

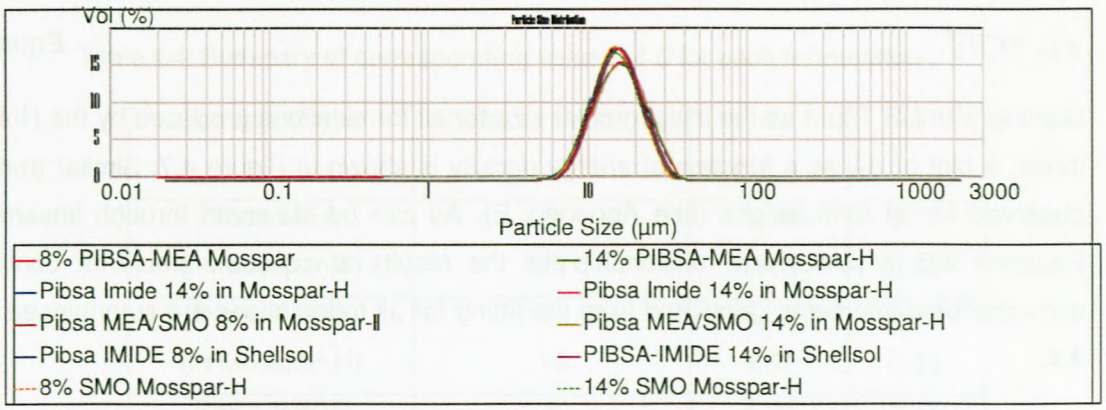

Figure 4.5: Histogram of drop size distribution of all formulations of DS 13µm

An evolution toward smaller droplets was also found, as can be deduced from drop size distribution (DSD) curves shown below in Figure 4.6.

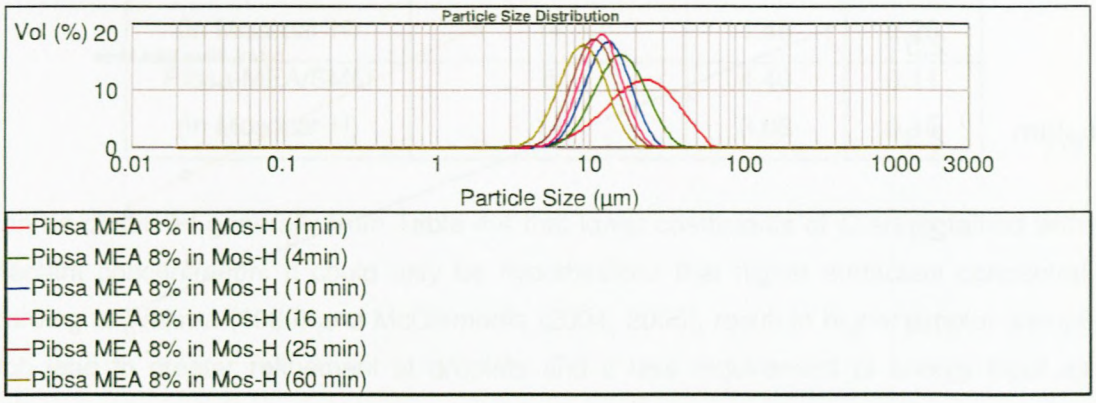

Figure 4.6: Evolution of droplet size for 8% Pibsa-MEA in Mosspar-H

In the emulsification devices that usually are employed, droplet disruption of a coarse emulsion premix is induced by various mechanisms. Shear forces in laminar flow and shear or inertial forces in turbulent flow are predominant in the case of rotor systems (Karbtsein, 1994; Stang, 1998). Depending on the respective predominant effects; droplet disruption (coefficient *C*) is influenced by several physical parameters, like the viscosity of the dispersed and continuous phase; interfacial tension; or density of the liquids (Walstra, 1993; Walstra and Smulders, 1997).

To achieve the result of droplet disruption, attention was paid particularly to the two coefficients, *C* and *b*. The power law equation was used and is formulated as:

$$d_{32} = CE_{\rho}^{-b}$$ **Equation 2.8**

Starting with DS 13µm as the initial droplet size for all formulations produced by the Hobart N50 mixer, a plot of d_{32} as a function of energy density is shown in Figure 4.7. Similar trends were observed for all formulations (see Appendix E). As can be observed through linearisation of Equation 2.8, a power law relationship fits the results at constant emulsifier content. The corresponding intercepts calculated from the fitting for all formulations are summarised in Table 4.4.

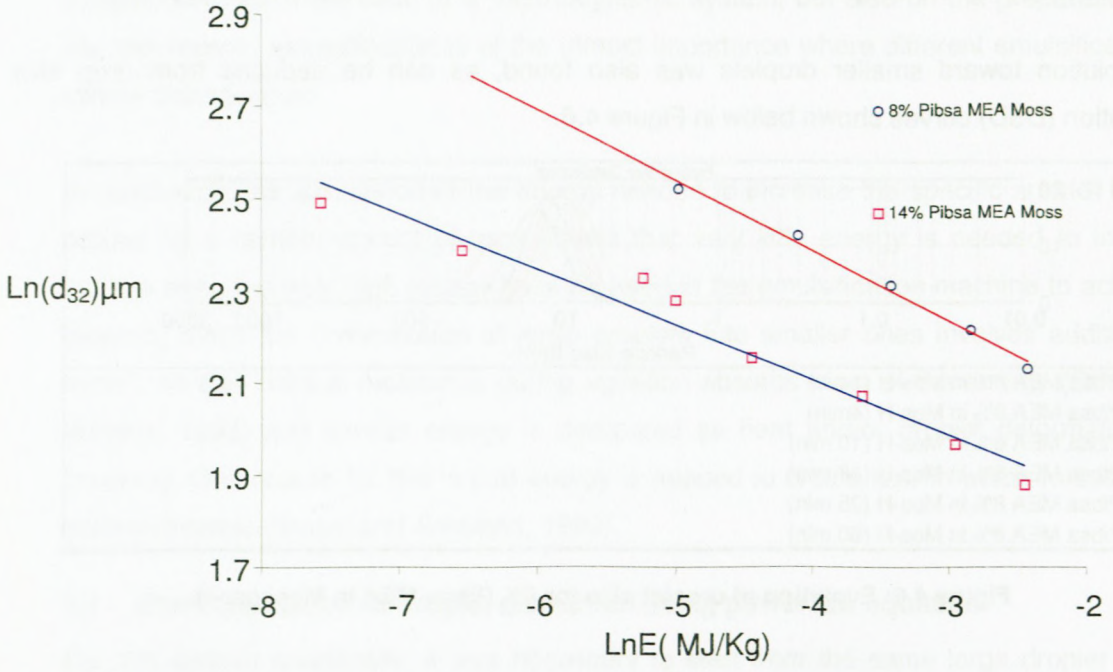

Figure 4.7: Degree of refinement as a function of energy density for Pibsa-MEA

Table 4.4: Summary of corresponding values of *C* for each formulation

Surfactant type	Surfactant conc, %	*C*	*b*
Pibsa-MEA	8	5.90	0.15
(in Mosspar-H)	14	5.10	0.13
Pibsa-IMIDE	8	5.83	0.13
(in Mosspar-H)	14	4.67	0.11
Pibsa-IMIDE	8	5.79	0.15
(in Shellsol)	14	3.97	0.14
Pibsa-UREA	8	5.71	0.16
(in Mosspar-H)	14	3.99	0.16
SMO	8	1.98	0.27
(in Mosspar-H)	14	1.45	0.26
Pibsa-MEA/SMO	8	4.40	0.11
(in Mosspar-H)	14	3.08	0.15

It can be observed generally from Table 4.4 that lower coefficients of *C* are obtained with high surfactant concentration. It could only be hypothesised that higher surfactant concentrations, according to Walstra (1983) and McClements (2004, 2005), result in higher droplet disruptions, which lead to greater refinement of droplets and a less requirement of energy input as this coefficient, *C*, which characterises droplet disruption, is influenced by several physical parameters, like viscosity of the dispersed and continuous phase, interfacial tension, or density of the liquids (Walstra, 1993; Walstra and Smulders, 1997). The *b* values obtained from these results are less than those reported in the literature ($b = 0.35$ for turbulent inertial forces and $b = 1$ for laminar shear or elongational flow). The difference between these results and results from literature could be due to different emulsion compositions and emulsification methods. The mixture (Pibsa-MEA/SMO) has a lower value of *C* than any formulation in the study. This was understood from studies by Ganguly *et al.*, (1992), specifically for this formulation (MEA/SMO). It is thought that, due to the small SMO molecules, there is a movement to the interface to lower the interfacial tension and facilitate droplet break-up (lower *C*), compared to other surfactants in both concentrations, with Urea and Imide having a better droplet disruption than MEA.

In summary: the lowest values of the coefficient *C* are observed when a higher amount of a low-molecular-weight surfactant has been used. It means that refining becomes easier in this case. The difference between the *b* values for Pibsa surfactants is not great, indicating that similar mechanisms are involved in the size reduction process.

The conclusions from the experimental results discussed above indicate the order of surfactants in relation to their shear stability. This order for the same oil is as follows:

Pibsa-MEA > Pibsa-IMIDE > Pibsa-UREA > Pibsa-MEA/SMO > SMO

Meanwhile, the difference between the first members of the row is not great and the noticeable decrease of the efficiency of stability under shear starts when the low-molecular-weight component SMO is added. The observed concentration dependence of the coefficient *C* possibly can be explained by the tendency of higher surfactant content to produce smaller droplets, as was supposed in (Walstra, 1983; McClements, 2004, 2005).

4.5 Effect of surfactant concentration on droplet size

The most widely used method for characterising the energy efficiency of an emulsification process consists of evaluating the relationship between sauter mean diameter (d_{32}) obtained after emulsification and the amount of energy supplied (McClements, 2004, 2005; Schubert and Engel, 2004; Walstra, 1983). This section investigates the effect of emulsifier concentration on the d_{32}, but from an energy point of view.

According to Walstra (1983), the surfactant has two roles: it lowers the interfacial tension, thereby facilitating drop break-up and it prevents (to a varying degree) re-coalescence. The addition of the surfactant to the aqueous (dispersed) phase leads to the reduction of the interfacial tension, which reduces the amount of energy necessary to produce small drops and also introduces a charge on the surface of the drops that prevents coalescence. During emulsification, a lot of energy is required to disperse one liquid into another as small droplets. The interfacial area is increased during this dispersion process. The droplet size of the internal dispersed phase of a w/o emulsion is determined by the energy consumption and interfacial tension. At low interfacial tension the dispersed droplets are easily deformable by stirring and break-up is possible even with low energy input.

A plot of d_{32} produced by the Hobart N50 mixer as a function of energy density (E_{ρ},) for an 8% and 14% surfactant concentration is shown in Figure 4.8 (see Appendix F for all formulations).

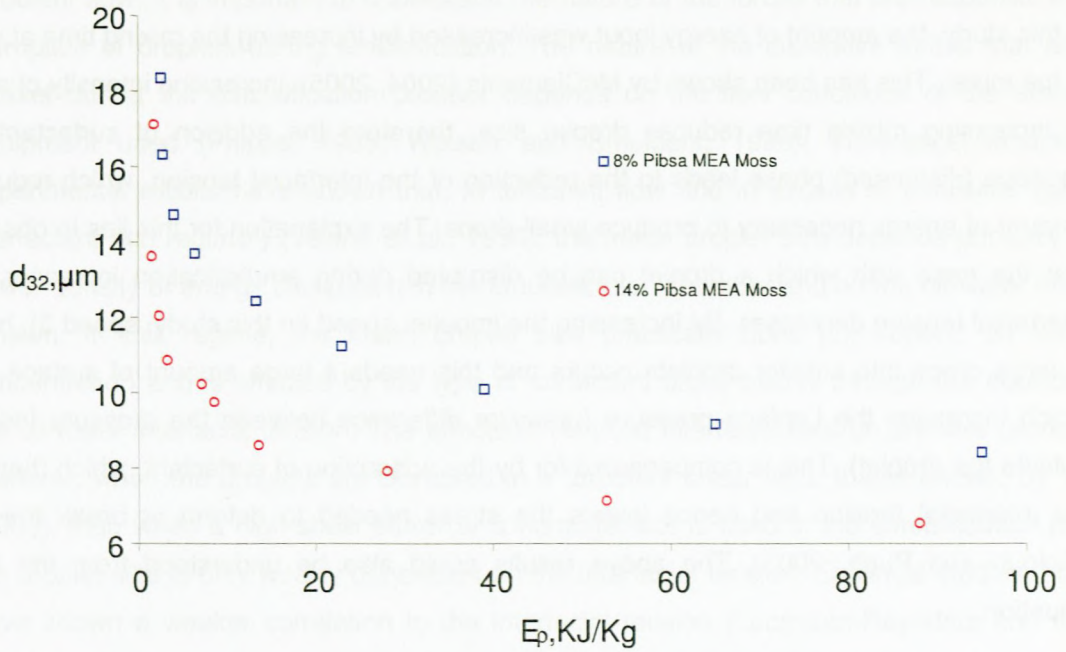

Figure 4.8: d_{32} as a function of energy density for Pibsa-Mea

It can be seen from Figure 4.8 that, firstly, the mean droplet size for both concentrations (8% and 14%) decreases exponentially with increase in energy input. This trend was observed for all samples manufactured. Secondly, for same energy input, the higher surfactant concentration (14%) needed less energy, while smaller droplet size was obtained than in the case of the low concentration (8%). This dependence was described by Karbstein and Schubert (1995) for different dispersing units and different dispersion zone geometries. According to Walstra (1983), more surfactant results in smaller droplets, hence a greater number of disruptions. The latter was understood from McClements (2004, 2005), who summarised the dependence on a number of characteristics of an emulsifier of the droplet size produced during emulsification:

- The ratio of emulsifier to the dispersed phase: - there has to be sufficient emulsifier to completely cover the new interfaces of the droplets formed.
- Probability that an emulsifier would be adsorbed to the surface of a droplet during an encounter between it and the droplet: - the greater the adsorption efficiency, the smaller the droplet size.

- Amount by which the emulsifier reduces the interfacial tension: - the greater the amount, the smaller the droplet size.

In this study, the amount of energy input was increased by increasing the mixing time at speed 3 of the mixer. This has been shown by McClements (2004, 2005): increasing intensity of agitation or increasing mixing time reduces droplet size, therefore the addition of surfactant to the aqueous (dispersed) phase leads to the reduction of the interfacial tension, which reduces the amount of energy necessary to produce small drops. The explanation for this lies in observation that the ease with which a droplet can be disrupted during emulsification increases as the interfacial tension decreases. By increasing the impeller speed (in this study, speed 3), break-up of large drops into smaller droplets occurs and this needs a large amount of surface energy, which increases the Laplace pressure (pressure difference between the pressure inside and outside the droplet). This is compensated for by the adsorption of surfactant, which then lowers the interfacial tension and hence lowers the stress needed to deform or break the droplet (Goloub and Pugh, 2003). The above results could also be understood from the Laplace equation:

$$p=\sigma\left(\frac{1}{R_1}+\frac{1}{R_2}\right). \qquad \textbf{Equation 2.5}$$

It can readily be inferred that the smaller the droplet size for a given system, the more energy input and/or surfactant is required (Walstra, 1983). The decrease in size with increasing energy is due to the intensity or duration of disruptive energy supplied during the emulsification process in which large masses of fluids are stretched and folded over by arranging for the viscosities of the phases to be more nearly equal and by the use of the correct emulsifier. Since the droplet size decreases with increasing energy input, the surface–volume ratio of the dispersed droplets is shifted to higher values. As a result, the number of molecules adsorbed on the surface increase, which results in smaller droplet size. Therefore the higher the energy density input, the smaller the droplets. Thus it is possible to produce droplets with smaller sizes by emulsification in the presence of surfactants which reduce the interfacial tension (Walstra, 1993b). The final drop size distribution of any emulsion results from the dynamic equilibrium between droplet disruption and coalescence, both favoured by intense agitation. The droplet size also depends strongly on the type of surfactant and it is for this reason that it is poorly correlated with σ, as this is measured under static conditions (Walstra, 1983).

All the explanations above assume that droplet break-up occurs under laminar conditions, though this assumption is not validated in this study; droplet break-up also occurs under turbulent flow. It is important to understand the nature of the forces that are responsible for the disruption of droplets during emulsification. The nature of the disruptive forces that act on a droplet during the emulsification process depends on the flow conditions of the emulsifying equipment used (Phipps, 1985; Walstra and Smulders, 1998). Theoretical analysis and experimental results have shown that, in turbulent flow and in excess of emulsifier (so-called "surfactant rich regime") (Taisne *et al.*, 1996), the mean droplet size depends primarily on the power density of energy dissipation in the emulsification chamber and on the oil-water interfacial tension. In this regime, the mean droplet size practically does not depend on surfactant concentration and is affected by the type of surfactant used, mainly through the equilibrium of the oil-water interfacial tension. The effects of reduced interfacial tension are less pronounced, however, when the droplets are disrupted in a turbulent shear field. It was shown, by Walstra (1983), that, when a high-shear stirrer or a homogeniser is used in the emulsification process, the droplet size is only weakly dependent on the interfacial tension. Empirical studies, however, have shown a weaker correlation to the interfacial tension (Lucassen-Reynders and Kuipers, 1992). Consequently, the reduction of interfacial tension is not sufficient to explain the success of many surfactants. In fact, kinetic effects occur that involve transportation of the surfactant to and within the interface and the surfactant is well known to influence the surface dilational modulus, which relates to the changed interfacial tension (resulting from a change in interfacial area). Generally, the dilational modulus is a complex quantity consisting of an elastic and a viscous term and is dependent on both the time scale of the process and the non-equilibrium conditions.

In summary: an increase in energy input generally produces a displacement toward smaller sizes, since the droplet disruption becomes predominant over coalescence although coalescence is also promoted (Sanchez *et al.*, 1998). As a consequence, there is an increase in the specific interface area, leading to a greater number of droplet interactions (Rahalkar, 1992).

In conclusion:

- To manufacture similar droplet size, lower energy input is required for higher surfactant concentrations.

4.6 Effect of surfactant type on droplet size

Investigation of the influence of kinetics on the emulsification process was followed by measuring d_{32} for all formulations as a function of time, as done by other workers like Goulob and Pugh (2003). The results are shown in Figures 4.9 and 4.10 for 8% and 14% respectively. It can be seen that the emulsification process during the first 10 minutes, approximately, was rather fast, resulting in a reduction of droplet size, but steady state was reached after 40 minutes, with droplet size remaining nearly constant. The origins of this kinetic effect on droplet size are discussed elsewhere (Groenewet *et al.*, 1994; Polat *et al.*, 1999).

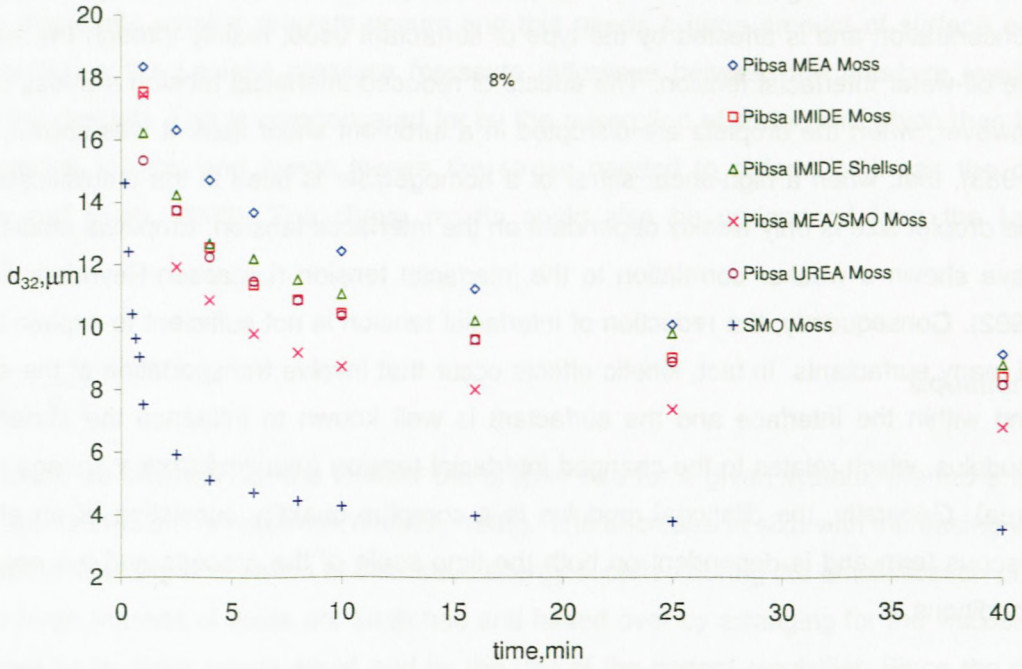

Figure 4.9: d_{32} as a function of time, 8%

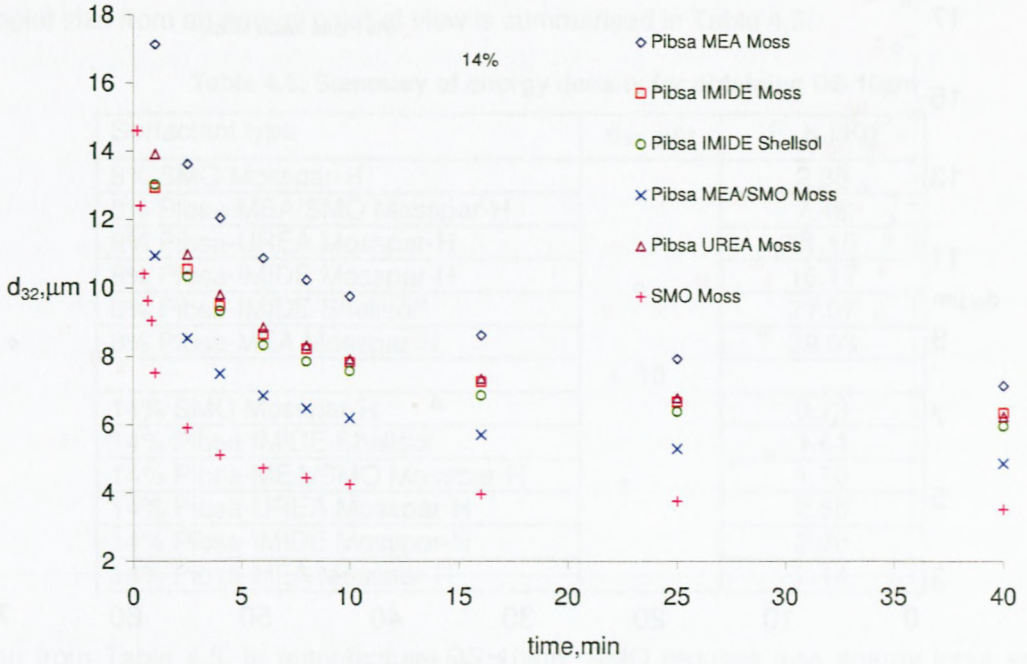

Figure 4.10: d_{32} as a function of time, 14%

It has been suggested that break-up occurs in the eddies in the boundary layer of the impeller, which consists of a relatively small volume in the tank. As a result, the total volume of emulsions has to pass through this zone before a steady state is reached. Inhomogeneities in the flow in this region would explain the range of emulsion droplet size distribution.

The above parameter (time) does not provide much information about the amount of energy consumed by each surfactant in the emulsification process. By presenting the above figures (4.9 and 4.10) as function of energy, however, Figures 4.11 and 4.12 are achieved.

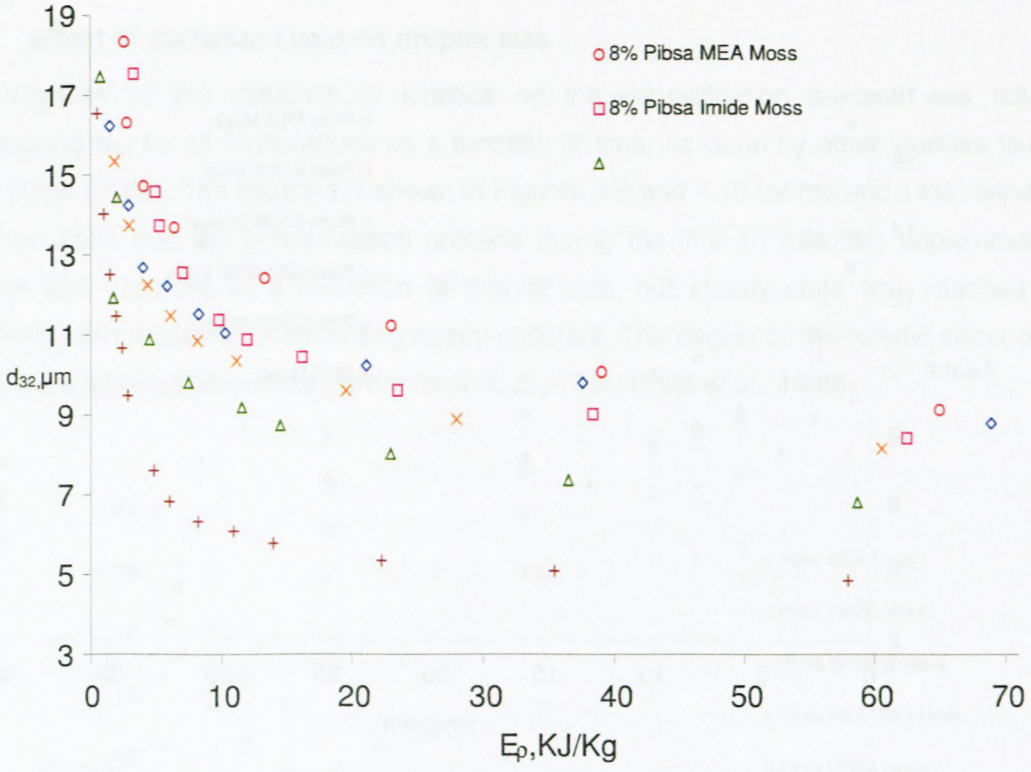

Figure 4.11: d_{32} as a function of Energy density, 8%

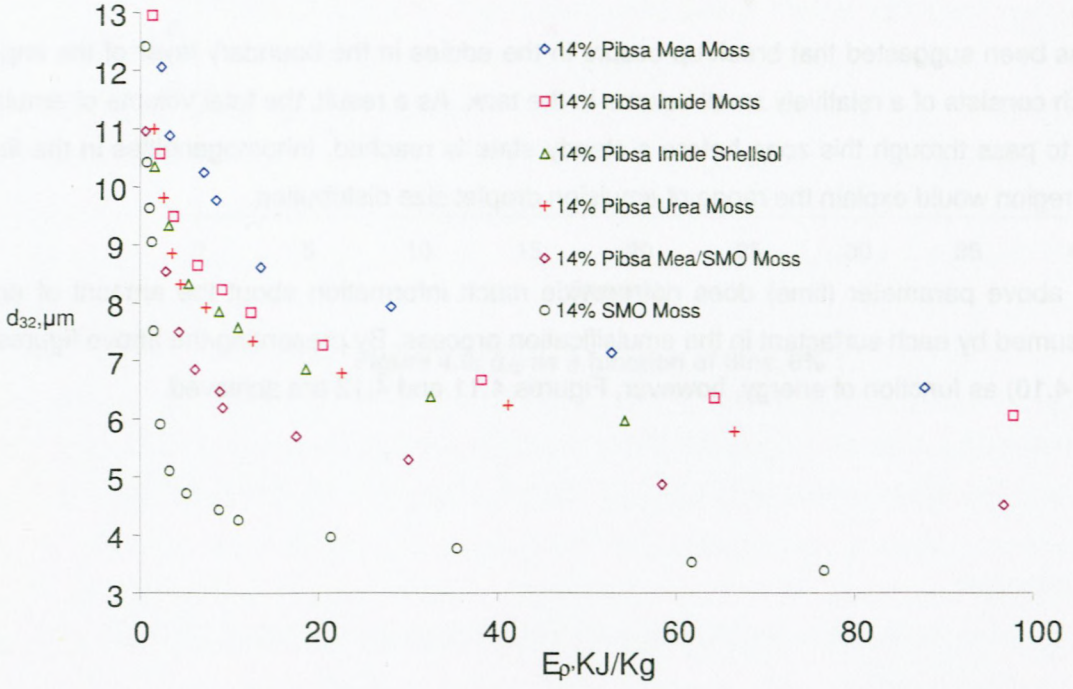

Figure 4.12: d_{32} as a function of energy density, 14%

Arbitrarily choosing, from Figures 4.11 and 4.12, 10μm, the energy input needed to manufacture this droplet size from an energy point of view is summarised in Table 4.5.

Table 4.5: Summary of energy density for obtaining DS 10μm

Surfactant type	d_{32}, μm	E_ρ,KJ/Kg
8% SMO Mosspar-H	10	2.38
8% Pibsa-MEA/SMO Mosspar-H		7.48
8% Pibsa-UREA Mosspar-H		11.15
8% Pibsa-IMIDE Mosspar-H		16.17
8% Pibsa-IMIDE Shellsol		21.07
8% Pibsa-MEA Mosspar-H		39.03
14% SMO Mosspar-H		0.79
14% Pibsa-IMIDE Shellsol		1.64
14% Pibsa-MEA/SMO Mosspar-H		1.70
14% Pibsa-UREA Mosspar-H		2.65
14% Pibsa-IMIDE Mosspar-H		2.20
14% Pibsa-MEA Mosspar-H		7.14

As seen from Table 4.5, to manufacture DS 10μm, SMO requires less energy input and the trend for both concentrations was as follows: *SMO < MEA/SMO < UREA < IMIDE < MEA.*

It is evident from both figures (4.11 and 4.12) that adsorption kinetics play a big role in covering the newly formed interface during the emulsification process. The results depicted in Figures 4.11 and 4.12 show that the rate at which an emulsifier adsorbs to an interface is one of the important factors determining its efficiency (Magdassi and Kamyshny, 1996; Walstra, 1996). It has been shown that adsorption rate depends on molecular characteristics of the emulsifier (e.g. size flexibility, conformation and interactions); the nature of the bulk liquid (e.g., viscosity, polarity); and the prevailing environmental conditions (e.g., temperature and flow profile).

SMO, having small molecular weight, moves to the interface quicker than any Pibsa derivatives (Pibsa-MEA, Pibsa-IMIDE and Pibsa-UREA) and the mixture (Pibsa-MEA/SMO). Ganguly *et al.*, (1992) have shown that interactions between polymeric surfactants, specifically Pibsa-MEA and SMO, show differences in strength towards electrolytes and that surfactant head groups in the two emulsifiers had moderate to strong hydrogen bonding tendencies, although the polar group in the polymeric emulsifier Pibsa-MEA could have a much stronger interaction compared to that of the corresponding group in the non-ionic surfactant SMO. It could be hypothesised from the latter that, in the mixture (8% and 14%, Pibsa-MEA/SMO), the SMO moves to the interface

faster, due to its size and molecular weight, than Pibsa-MEA. But after some time, Pibsa-MEA replaces SMO as it forms stronger interactions, even at low electrolyte concentrations that could be "masking" any further changes due to possible bulk hydrogen bonding effects which are entirely concentration-dependent. SMO fills the space in between the Pibsa-MEA head groups.

The above results could also be looked at from the point view of micelles. Different surfactants form different structures of micelles and the role of micelles have been shown to solubilise and transport through the aqueous phase which has a significant effect on the physicochemical properties of emulsions and can lead to time-dependent changes in droplet concentration, size distribution and composition (McClements and Dungan, 1993; Weiss *et al.*, 1996). As monomers are transported to the newly formed interface, the equilibrium condition between monomers and micelles is disturbed, which forces existing micelles to break up to provide additional monomers to the surface. Very stable micelles are not able to augment the flux necessary to stabilise the newly created interface and therefore emulsification will be less. However, if the micelles are relatively unstable, their disintegration supplies the depleted monomers and lower dynamic surface tensions are obtained. It may be that the rate of dissociation of the individual molecules from a micelle is rate determinant in some cases. On the other hand, it cannot be ruled out that micelles as such collide with the droplet, considering the strong forces in flow (Walstra, 1993). According to Windhab *et al.*, (2005) the emulsifier adsorption has to be considered in the context of four different steps:

- Emulsifier de-micellation in the bulk fluid
- Diffusive/convective transport to the interface
- Interfacial adsorption
- Structural changes at the interface

It was observed that, for the same energy input, different surfactants of the same concentration (Figures 4.11 and 4.12) resulted in different mean droplet sizes. It was proven by Goloub and Pugh (2003) that, at concentrations above the *cmc*, the droplet size is no longer concentration dependent. In this surfactant concentration region, both the mean droplet size and the size distribution vary considerably with the type of surfactant head.

To summarise: the evolution of the drop size distribution in an agitated emulsion depends on many variables related to emulsification conditions (equipment, duration, temperature, etc.) and to the nature and concentration of the emulsifier (kinetics of adsorption, interfacial tension, etc.), which, in turn, determines the drop-drop interaction and the barrier to coalescence. In fact, both

processes are promoted by intense agitation during emulsion formation (Walstra, 1983), so the outcome of emulsification depends mainly on four different types of factors:

- Hydrodynamic conditions in the mixing device
- Viscosity ratio of the two phases
- Volume fraction of oil and water phases
- Type and concentration of emulsifier used

4.7 Influence of energy input on rheological properties

In this section of the study, rheological properties of highly concentrated explosive water in oil emulsions are discussed. This is done from an energy input point of view. The rheological properties discussed involve the following:

- Effect of energy input on yield stress.
- Effect of energy on elastic modulus, as well and elasticity droplet size effect.

4.7.1 Effect of energy input on yield stress

To tackle this task, samples manufactured were measured on the MCR 300 using a plate-plate geometry shear-controlled rate-controlled deformation over a range of 200 to $10^{-4}s^{-1}$ at 30°C. Figure 4.13 represents a typical flow curve (FC).

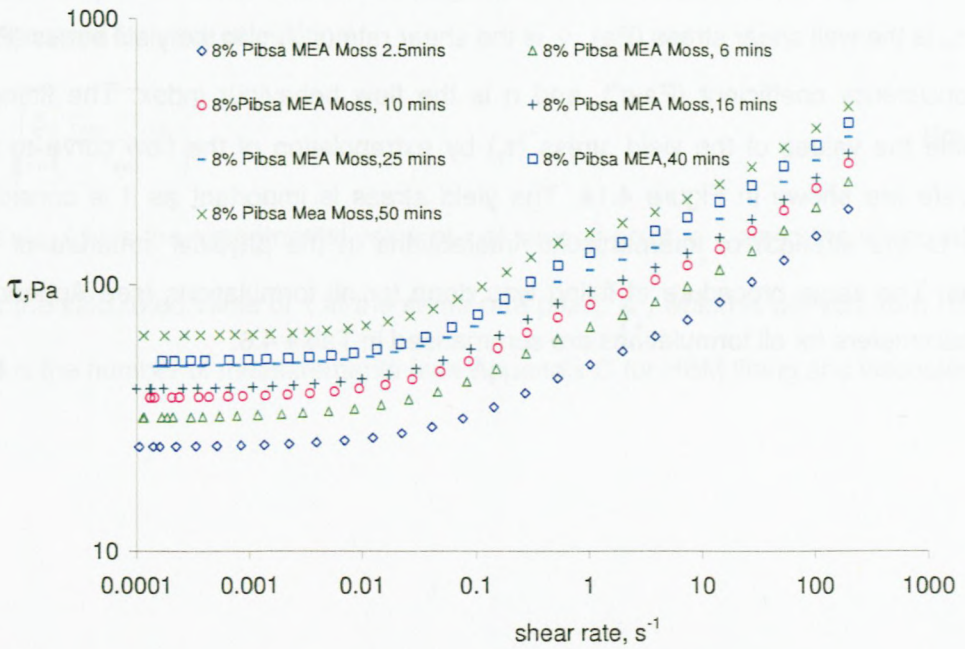

Figure 4.13: Flow curve of 8% Pibsa-MEA

It can be seen from Figure 4.13 and all formulations studied that, with increasing mixing time, the FC shifts to higher shear stress. The flow behaviour of the emulsion under investigation can be defined as yield pseudoplastic behaviour: (i) below the yield stress, the deformations of the particles are insufficient to allow flow in a global movement and elastic behaviour consequently prevails; (ii) above the yield stress, the deformations are sufficient to induce a flow which is characterised by the predominance of viscous effects. The close-packed configuration of highly concentrated emulsions and the profound hydrodynamic interaction between neighbouring droplets induce mechanical interference between the droplets, thus prohibiting their free movement. In such systems, extensive aggregation of the dispersed phase droplets occurs, which results in a stable, weak gel-like, particular network (Jager-Lezer *et al.*, 1998; Partal *et al.*, 1997). So, the emulsion is composed of a network of thin films, and its properties determined by mechanical properties of the oil film network, which, in turn, is characterised by a yield stress and plateau modulus.

The flow curves from the emulsification process were modelled, using the Herschel-Bulkley model to describe all the flow curves (shear stress as a function of shear rate) obtained. The Herschel-Bulkey model takes the form of:

$$\tau_w = \tau_y + K.\dot{\gamma}^n \qquad \textbf{Equation 3.12}$$

where τ_w is the wall shear stress (Pa), $\dot{\gamma}$ is the shear rate (s^{-1}), τ_y is the yield stress (Pa), K is the fluid consistency coefficient ($Pa.s^n$), and n is the flow behaviour index. The fittings used to determine the values of the yield stress (τ_y) by extrapolation of the flow curve to the 0.0001 shear rate are shown in Figure 4.14. The yield stress is important as it is considered to be related to the strength of interparticular interactions in the physical structure of multiphase systems. The same procedure of fitting was done for all formulations (see Appendix G). The fitting parameters for all formulations are summarised in Table 4.6.

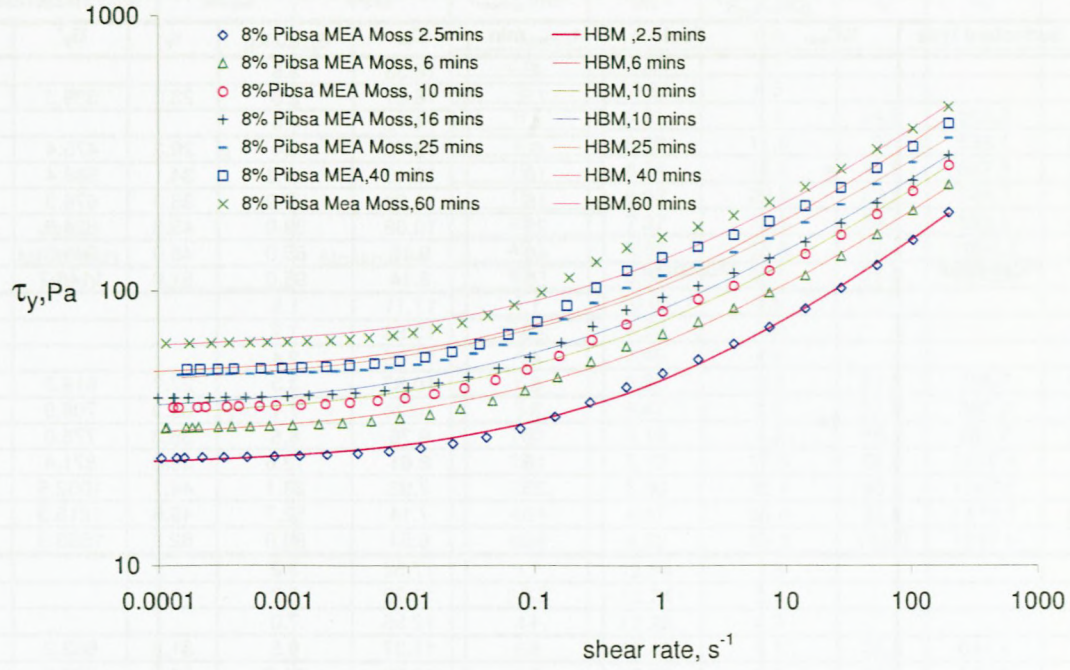

Figure 4.14: Approximation of flow curve by HBM

The standard procedure for the calculation of the mean square root error in any approximation was used. This procedure takes into account the results of measurements of τ in all the experimental points. In this case, an average error, E, was calculated, using:

Equation used for error calculation:

$$E = \frac{1}{N}\sqrt{\sum_{n=1}^{N}\left(\frac{\tau_{exp} - \tau_{calc}}{\tau_{exp}}\right)^2} \qquad \textbf{Equation 3.13}$$

where τ_{exp} ($\dot{\gamma}$) is the experimental value of τ at several point, $\dot{\gamma}_n$, along the shear rate scale;$\tau_{cal,n}$ ($\dot{\gamma}$) is the calculated value of τ at the same rate point, $\dot{\gamma}_n$, which is derived from HBM equation and N is the number of measurements (see Appendix G for HBM fitting and viscoelastic graphs).

Table 4.6: Summary of yield stress and plateau modulus for all formulations

Surfactant type	%C_{surf}	Fuel	t_{mixing},min	D_{32}	E_p,KJ/Kg	τ_y	G_p'	Error
Pibsa-MEA	8	Mosspar-H	1	18.33	2.6			
			2.5	16.31	2.8	23.3	339.3	0.005
			4	14.72	4.0			
			6	13.70	6.4	29.3	475.4	0.006
			10	12.43	13.3	34.1	588.4	0.008
			16	11.23	22.9	36.3	676.3	0.009
			25	10.08	39.0	43.6	824.8	0.01
			40	9.15	65.0	48.0	949.5	0.01
			50	8.14	95.0	51.9	1146.7	0.01
	14		1	17.11	1.5			
			2.5	13.63	1.7			
			4	12.05	2.4			
			6	10.87	3.3	27.7	619.3	0.01
			8	10.24	7.1	33.3	706.9	0.01
			10	9.76	8.6	36.8	776.0	0.01
			16	8.61	13.6	39.6	871.4	0.01
			25	7.93	28.1	44.1	1002.6	0.01
			40	7.14	52.7	49.6	1215.3	0.009
			60	6.54	88.0	62.3	1563.3	0.01
Pibsa-IMIDE	8	Mosspar-H	1	17.52	3.2			
			2.5	13.72	5.2			
			4	12.55	7.0			
			6	11.37	9.8	51.2	663.2	0.004
			8	10.88	11.9	54.5	693.8	0.004
			10	10.44	16.2	58.4	765.0	0.005
			16	9.61	23.4	62.1	838.9	0.005
			25	9.02	38.3	82.2	1019.8	0.004
			40	8.43	62.5	87.0	1117.9	0.005
			60	7.76	93.9	110.7	1333.2	0.005
	14		1	12.94	1.3			
			2.5	10.56	2.2			
			4	9.48	3.7			
			6	8.64	6.4	62.1	780.9	0.004
			8	8.22	9.2	72.5	858.1	0.004
			10	7.83	12.5	74.4	904.9	0.004
			16	7.26	20.2	77.3	1076.1	0.005
			25	6.66	38.2	86.8	1195.5	0.005
			40	6.35	64.3	100.2	1399.0	0.005
			60	6.06	97.8	102.7	1544.87	0.006
	8	Shellsol	1	16.22	1.5			
			2.5	14.23	2.9			
			4	12.68	4.0			
			6	12.22	5.8	49.2	558.6	0.005
			8	11.53	8.3	63.5	572.2	0.0009
			10	11.05	10.3	66.9	602.8	0.0008
			16	10.23	21.1	76.7	755.4	0.002
			25	9.80	37.6	86.1	896.6	0.002
			40	8.81	68.9	96.6	1067.2	0.004
	14		1	13.03	0.2			
			2.5	10.34	1.6	49.6	527.3	0.002
			4	9.33	3.2			
			6	8.33	5.5	66.0	744.9	0.008
			8	7.85	8.9	79.7	810.9	0.003
			10	7.58	11.0	85.8	866.9	0.003
			16	6.86	18.6	107.9	1062.9	0.005
			25	6.38	32.6	124.1	1187.2	0.003
			40	5.96	54.2	136.0	1425.8	0.006

Surfactant type	%C_{surf}	Fuel	t_{mixing},min	d_{32}	E_p,KJ/Kg	τ_y	G_p'	Error
Pibsa-MEA/SMO (10:1)	8	Mosspar-H	1	14.44	0.8			
			2.5	11.92	1.7			
			4	10.88	4.5			
			6	9.81	7.5	24.0	550.9	0.02
			8	9.19	11.6	37	598.1	0.007
			10	8.74	14.5	47.5	697.8	0.006
			16	8.02	22.9	52.8	746.7	0.007
			25	7.37	36.5	59.8	885.5	0.008
			40	6.82	58.8	73.4	1056.3	0.009
			60	6.36	85.9	75.0	1245.8	0.01
	14		1	10.95	0.6			
			2.5	8.53	2.9			
			4	7.49	4.4			
			6	6.85	6.2	51.5	796.7	0.009
			8	6.47	9.0	57.8	880.2	0.006
			10	6.19	9.3	66.4	933.7	0.006
			16	5.70	17.6	68.0	1050.4	0.01
			25	5.30	30.1	80.8	1197.6	0.008
			40	4.87	58.4	93.0	1372.5	0.008
			60	4.52	96.8	104.5	1597.9	0.007
Pibsa-UREA	8	Mosspar-H	1	15.34	1.8			
			2.5	13.74	2.9			
			4	12.25	4.3			
			6	11.49	6.1	25.8	644.4	0.02
			8	10.86	8.2	35.7	672.9	0.01
			10	10.36	11.2	36.9	673.0	0.01
			16	9.61	19.5	50.6	882.0	0.009
			25	8.89	28.0	52.4	985.4	0.02
			40	8.18	60.6	64.3	1144.1	0.01
			60	7.55	96.3	89.4	1375.4	0.01
	14		1	13.92	1.3			
			2.5	10.98	1.5			
			4	9.80	2.6			
			6	8.84	3.6	38.3	762.9	0.01
			8	8.31	4.6	53.6	891.2	0.008
			10	7.91	7.4	57.8	954.2	0.008
			16	7.34	12.7	59.5	1058.8	0.009
			25	6.78	22.6	86.4	1270.9	0.007
			40	6.23	41.2	88.0	1447.6	0.007
			60	5.78	66.6	97.7	1628.2	0.007
SMO	8	Mosspar-H	1	9.48	2.8			
			2.5	7.61	4.8			
			4	6.84	6.0	27.0	466.4	0.01
			6	6.33	8.2	41	658.4	0.008
			8	6.01	10.9	44.6	615.1	0.005
			10	5.77	14.0	51.2	676.8	0.005
			16	5.35	22.2	63.6	806.2	0.005
			25	5.09	35.4	70.4	876.9	0.005
			40	4.85	58.0	83.8	1037.3	0.005
			50	4.68	71.2	93.3	1100.4	0.005
	14		1	7.51	1.5			
			2.5	5.91	2.3			
			4	5.10	3.3	42.6	622.9	0.005
			6	4.72	5.2	53.9	695.3	0.005
			8	4.44	8.9	57.0	761.9	0.005
			10	4.26	11.1	61.0	813.5	0.006
			16	3.96	21.4	67.7	923.3	0.007
			25	3.77	35.5	76.8	1062.8	0.007
			40	3.53	61.8	102.7	1213.3	0.006
			50	3.39	76.6	114.2	1318.1	0.006

The refinement of droplets influences the rheology of emulsions because rheological properties depend on the droplet size (Malkin *et al.*, 2004). The evolution of yield stress with increasing energy input is quite evident (Figures 2.12 and 4.15). The effect of the increase of the yield stress of emulsions along with the increase of energy consumption has been described by Brummer (2006).

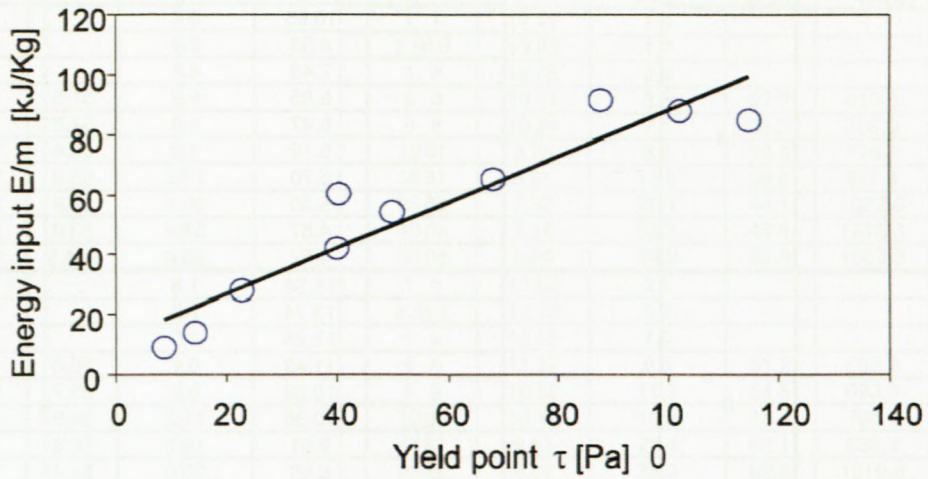

Figure 2.12: Influence of energy input on yield stress (Adapted from Brummer, 2006)

In order to compare the results with work by Brummer (2006), it was necessary to plot energy input as a function of yield stress, but not vice versa. The results for emulsions under study are presented in Figure 4.15. It can be seen that the results show an exponential increase of yield stress, as opposed to the linear relationship found by Brummer (2006). The system studied by Brummer (2006) was a water in oil emulsion. Similar results were found for all formulations studied in this work (see Appendix H for all formulations).

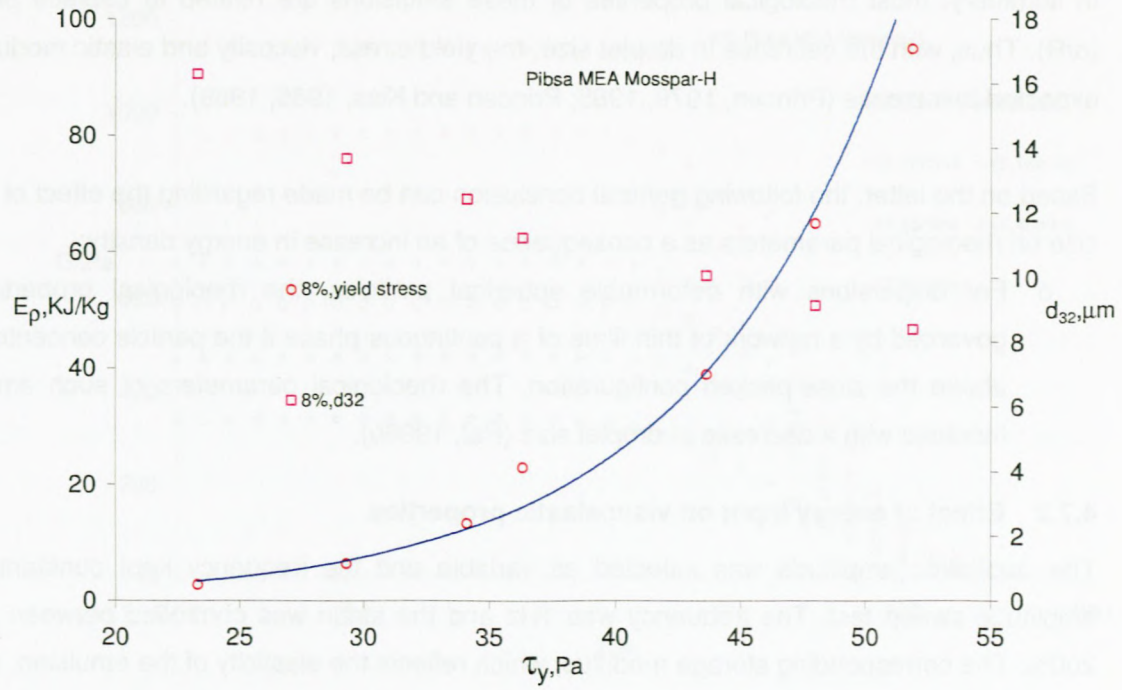

Figure 4.15: Influence of energy input on yield stress

The reasons for the discrepancy could be related to the type of emulsion used (not as highly concentrated as in this study), as well to the difference in the averaging procedure for polydispersed samples and the type of equipment used for preparing the emulsions. However, regardless whether the increase is linear or not, the yield stress increased with increase in energy input. This increase, according to Brummer (2006), is due to the internal structure which increases with increasing energy input. The increase cannot be explained, either by the increase in the phase volume, ϕ, or by synergistic effects of ingredients that approach each other. Since the droplet size decreases with increasing energy, the surface-volume ratio of the dispersed droplets is shifted to higher values, resulting in an interparticulate interaction for a constant phase volume ratio. To cement the latter observation of increasing yield stress, a number of publications have mentioned the fact that the concentrated liquid-liquid dispersions have peculiar mechanical and rheological properties when the volume fraction of the dispersed phase exceeds about 0.74 and the dispersed units are no longer spherical: a high degree of crowding results in the elastic behaviour at small deformations; a yield stress; and a shear rate-dependent viscosity when the yield stress is exceeded (Princen, 1986; Mason *et al.*, 1996).

In summary: most rheological properties of these emulsions are related to Laplace pressure (σ/R). Thus, with the decrease in droplet size, the yield stress, viscosity and elastic modulus are expected to increase (Princen, 1979, 1985; Princen and Kiss, 1986, 1989).

Based on the latter, the following general conclusion can be made regarding the effect of droplet size on rheological parameters as a consequence of an increase in energy density:

- For dispersions with deformable spherical particles, the rheological properties are governed by a network of thin films of a continuous phase if the particle concentration is above the close-packed configuration. The rheological parameters of such emulsions increase with a decrease in droplet size (Pal, 1996b).

4.7.2 Effect of energy input on viscoelastic properties

The oscillation amplitude was selected as variable and the frequency kept constant in the amplitude sweep test. The frequency was 1Hz and the strain was controlled between 0.01 to 200%. The corresponding storage modulus, which reflects the elasticity of the emulsion, and the loss modulus, which reflects the dissipation, were measured as a function of strain. Figures 4.16 and 4.17 show the evolution of storage (G') and loss (G") moduli according to the increase of strain amplitude with different mixing times. It can be observed that all curves shift to higher levels of storage and loss moduli respectively, as the mixing time increases. The plateau values of the storage modulus were taken from the linear region of the graph by extrapolation of the curve to zero deformation. These plateau modulus (G'_p) values were then plotted as a function of energy density and compared to some findings of researchers like Romero *et al.*, (2008). The results of G_p' for all formulations are summarised in Table 4.6.

Figure 4.16: Influence of emulsification time on storage moduli

Figure 4.17: Influence of emulsification time on loss moduli

For the material, the elastic modulus G' is greater than the viscous modulus G" over the entire range of applied strain, indicating the predominantly elastic behaviour of the material with G'/G">>10 in all cases, at low-test strains. As can be seen, the storage modulus is independent of strain amplitude up to some critical deformation (approximately 10 %), a zone of constant response (plateau region), indicating an unaltered structure not disturbed by shear. It is related only to the equilibrium microscopic structure, forces, and inherent dissipation of fluctuations (Bird *et al.*, 1987). In this linear region, the particles were crowded and could not move freely past one another: this defined the elastic domain. Then, at higher deformations, the values of the storage modulus decreased with a deformation increase, the applied strain being sufficient to allow the particles to move past one another and inducing a transition to the viscous domain. Above the critical shear stress value, emulsion lost its viscoelasticity and became a fluid. This stress value is known as yield stress. The peak in loss modulus also confirmed and elucidated the transition from elastic to viscous region. From an empirical point of view, the existence of a loss modulus maximum means a transition phenomenon in most cases, whatever its nature. From a micro-structural point of view, this peak probably means that the dissipation energy is maximal when the droplets are deformed and flattened enough to allow movement despite the crowding (Jager-Lezer *et al.*, 1998; Ponton *et al.*, 2001).

The length of the plateau of elastic modulus is an indication of the structure flexibility to deformation and drop of modulus is related to a break-down of solid structure.

By plotting G_p' from Table 4.6, together with the sauter mean diameter as a function of energy density, Figure 4.18 is achieved (see Appendix I for all formulations). As can be seen, an increase in energy input was followed by an exponential decrease of the sauter mean diameter for both concentrations, but with power law increase in the elastic modulus. The higher concentration of surfactant was observed to have higher elastic modulus due to the effect of droplet size on rheological properties, as described by Malkin *et al.*, (2004). An increase in energy input did not produce any change in the shape of the mechanical spectrum, but led to an increase in both G' and G".

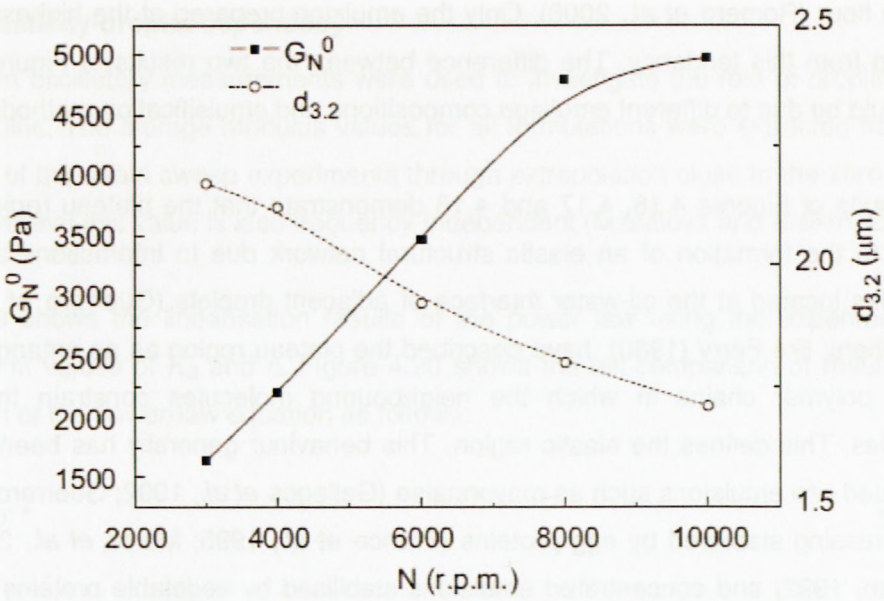

Figure 2.1: Evolution of plateau modulus (Adapted from Romero *et al.*, 2008)

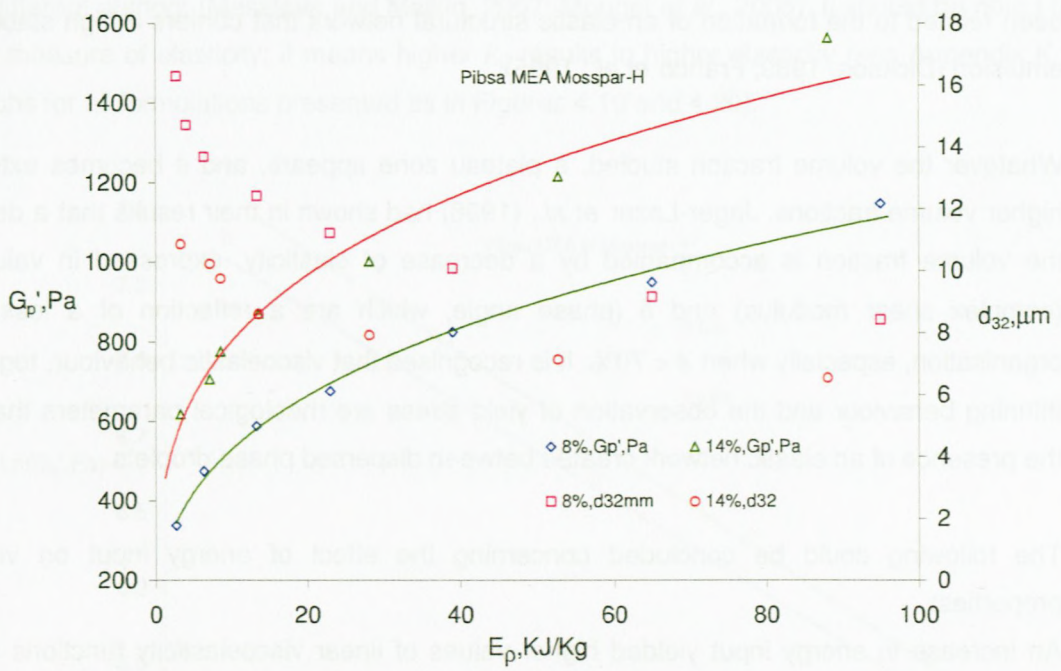

Figure 4.18: Evolution of the storage modulus and sauter mean diameter as a function of energy density

An almost linear relationship between plateau modulus (from frequency sweep) and agitation speed was established for highly concentrated oil in water (o/w) emulsions stabilised with

crayfish flour (Romero *et al.*, 2008). Only the emulsion prepared at the highest agitation speed deviated from this tendency. The difference between the two results of Figure 2.1 and Figure 4.18 could be due to different emulsion compositions and emulsification methods.

The results of Figures 4.16, 4.17 and 4.18 demonstrate that the plateau region of G' may be related to the formation of an elastic structural network due to interactions among emulsifier molecules located at the oil-water interface of adjacent droplets (Guerrero *et al.*, 1998). Other researchers, like Ferry (1980), have described the plateau region as an entanglement networks among polymer chains in which the neighbouring molecules constrain the movement of molecules. This defines the elastic region. This behaviour generally has been found for highly flocculated o/w emulsions such as mayonnaise (Gallegos *et al.*, 1992; Guerrero and Ball, 1994), salad dressing stabilised by egg proteins (Franco *et al.*, 1995; Moros *et al.*, 2003; Munoz and Sherman, 1992) and concentrated emulsions stabilised by vegetable proteins (Bengoechea *et al.*, 2006; Franco *et al.*, 1998, 2000; Raymundo *et al.*, 2002). The occurrence of a well-developed plateau region, where a very low frequency dependence for G' can be observed, has been related to the formation of an elastic structural network that confers a high stability to the emulsion (Dickson; 1989; Franco *et al.*, 1995).

Whatever the volume fraction studied, a plateau zone appears, and it becomes extended for higher volume fractions. Jager-Lezer *et al.*, (1998) had shown in their results that a decrease in the volume fraction is accompanied by a decrease of elasticity, expressed in values of G* (complex shear modulus) and δ (phase angle, which are a reflection of a less compact organisation, especially when $\phi < 70\%$. It is recognised that viscoelastic behaviour, together with thinning behaviour and the observation of yield stress are rheological parameters that indicate the presence of an elastic network created between dispersed phase droplets.

The following could be concluded concerning the effect of energy input on viscoelastic properties:
An increase in energy input yielded higher values of linear viscoelasticity functions and small droplet size, as has been found generally in the literature on emulsion rheology. This behaviour leads to an enhancement of the elastic net work, as well as an increase in emulsion stability.

4.7.2.1 Elasticity-droplet dependecy

Results from oscillatory measurements were used to investigate the role of droplet size on the shear modulus. The storage modulus values for all formulations were extracted from the linear region part of the strain sweep experiments through extrapolation close to the zero strain value. It was shown that this value is also frequency-independent (Masalova and Malkin, 2007).

Figure 4.19 shows the linearisation results of the power law using the experimental data to obtain best fit values of K_G and n. Figure 4.20 shows the full comparison of results with n = 2 linearisation of the power-law equation as follows:

$$G = k_G D^{-n} \qquad \textbf{Equation 2.2}$$

In this equation, if $n = 1$, it means that rheological properties follow the Princen model (Princen and Kiss, 1989), while $n = 2$ is the case that experimentally and semi-empirically was explained by different authors (Masalova and Malkin, 2007; Mougel *et al.*, 2006). It should be noted that k_G is a measure of elasticity; it means higher k_G results in higher elasticity (see Appendix K for all graphs for all formulations presented as in Figures 4.19 and 4.20).

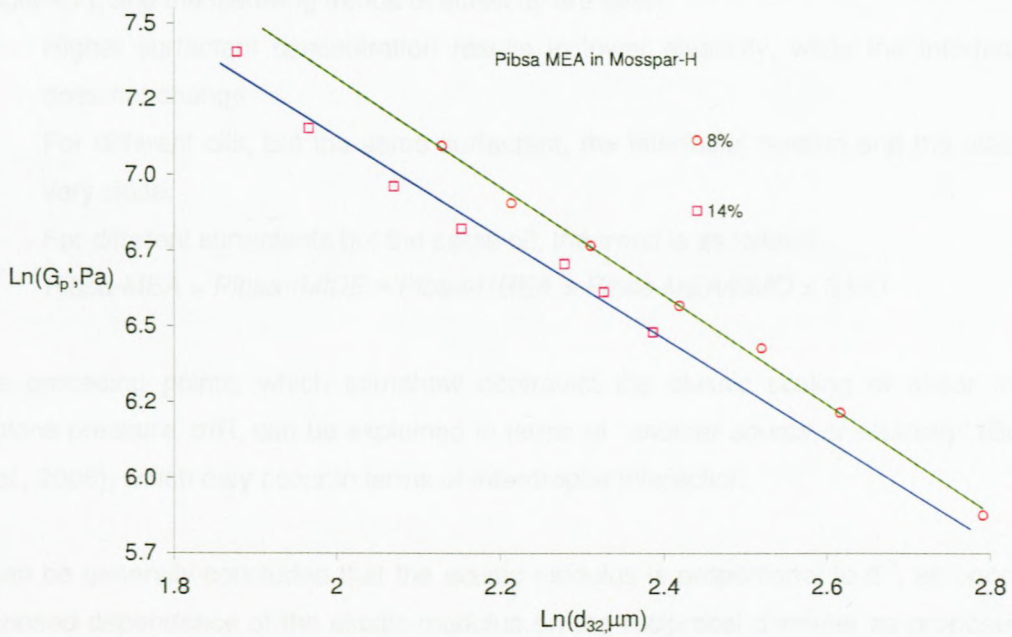

Figure 4.19: Linearisation results of equation 2.2 for Pibsa-MEA

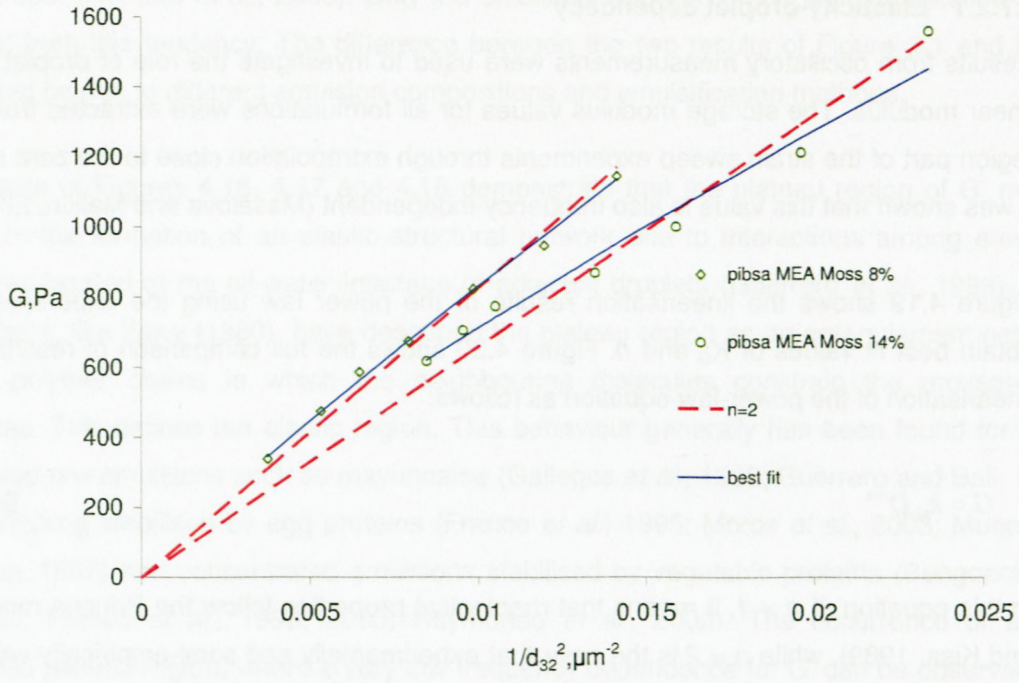

Figure 4.20: Dependence of elasticity on the droplet size with $n = 2$

The fitting parameters from Equation 2.2 (k_G and n) and K_G value (when $n = 2$) are summarised in Table 4.7.

Table 4.7: Summary of fitting parameters from empirical Equation 2.2

Surfactant type	Surfactant conc,%	Continuous phase	n	k_G (KPa.m^n)	k_G for n=2 (KPa.m^2)
Pibsa-MEA	8	Mosspar-H	1.80	52.1	83.0
	14		1.67	33.7	66.1
Pibsa-IMIDE	8		1.85	60.0	81.0
	14		1.89	45.3	56.1
	8	Shellsol	2.19	126.8	81.1
	14		1.93	43.6	50.0
Pibsa-UREA	8	Mosspar-H	1.89	62.2	78.2
	14		1.76	36.2	57.1
SMO	8		2.25	35.2	23.4
	14		1.87	12.6	15.1
Pibsa-MEA/SMO	8		1.81	33.9	49.5
	14		1.64	18.6	33.8

In order to compare the elasticity of samples in which only the surfactant is different, we can compare the results of k_G. To do this comparison more analogically, the $n = 2$ fittings are chosen (Table 4.7), and the following trends of elasticity are seen:

- Higher surfactant concentration results in lower elasticity, while the interfacial tension does not change
- For different oils, but the same surfactant, the interfacial tension and the elasticities are very close.
- For different surfactants but the same oil, the trend is as follows:
  Pibsa-MEA > Pibsa-IMIDE ≈ Pibsa-UREA > Pibsa-MEA/SMO > SMO

The preceding points, which somehow contradict the classic scaling of shear modulus by Laplace pressure, σ/R, can be explained in terms of "*another source of elasticity*" (Bengoechea *et al.*, 2006), which may occur in terms of interdroplet interaction.

It can be generally concluded that the elastic modulus is proportional to d^{-2}, as opposed to the proposed dependence of the elastic modulus on the reciprocal diameter as proposed by some theoretical models (Princen and Kiss, 1986; Babak *et al.*, 2001; Pal, 2002) and observed by several for other emulsions (Aronson and Petko, 1993; Pons *et al.*, 1992b; Langenfield *et al.*,

1999) and does not correspond to findings by Malkin *et al.* (2004) of $G \propto d^{-2}$. According to Malkin *et al.*, (2004), the reasons for the discrepancy of the experimental results may be related to the type of emulsion used (emulsions not as highly concentrated as in this study), as well as to the difference in the averaging procedure for polydispersed samples.

4.8 Capillary number and viscosity ratio for explosive concentrated emulsions

Many industrial processes involve the dispersion of immiscible liquid/liquid systems, the final morphology resulting from the mixing process, which influences the mechanical and other properties of the product.

Despite the widespread use of emulsions, the fundamental understanding is limited to the rupture of a single droplet of viscosity, η_d, suspended in a fluid having a viscosity η_e. For droplet deformation to occur, the viscous stress of the external phase, $\eta_e\dot{\gamma}$, must overcome the characteristic Laplace σ/R, where R is the droplet radius neglecting the role of η_d (Taylor, 1934). For rupturing to occur, the capillary number, defined as the ratio of the shear stress to the Laplace pressure, must exceed a critical value of order unity, which implies that the droplet has been elongated by the viscous shear before rupturing. A complete theoretical description of the droplet deformation and bursting between these two regimes is complicated and depends on the capillary number, viscosity ratio and the type and history of shear flow (Rallison, 1984).

To calculate the capillary number and viscosity ratio, the following equations were used:

$$Ca = \frac{\eta_e \dot{\gamma}_{Ave,hob} R}{\sigma_{eq}}$$ **Equation 3.11**

where ηe is the emulsion viscosity found by using the average Hobart shear rate, $\dot{\gamma}_{Ave,hob}$ (380s^{-1}), R is the droplet radius ($D_{50}/2$) and σ_{eq} is measured from the Kruss K100 tensiometer.

$$\lambda = \frac{\eta_d}{\eta_e}$$ **Equation 3.12**

NB: No emulsion breakage was observed during the measurements at 70°C.

The results of the calculations of capillary number and viscosity ratio are summarised in Table 4.8.

Table 4.8: Results of calculations of capillary number and viscosity ratio

Surfactant type	%C_{surf}	Fuel	t_{mixing},min	D_{50},μm	η_e	$\lambda = \eta_d/\eta_e$	*Ca*
Pibsa-MEA	8	Mosspar-H	1	21.63	0.16	0.26	0.23
			2.5	18.04	0.24	0.17	0.29
			4	15.84	0.33	0.12	0.35
	14		1	18.87	0.30	0.14	0.38
			2.5	14.42	0.55	0.075	0.54
			4	12.60	0.63	0.065	0.54
Pibsa-IMIDE	8	Mosspar-H	1	18.79	0.19	0.22	0.68
			2.5	14.39	0.25	0.16	0.68
			4	13.16	0.28	0.15	0.70
	14		1	13.71	0.39	0.11	1.00
			2.5	11.03	0.45	0.091	0.94
			4	9.85	0.46	0.089	0.86
	8	Shellsol	1	17.56	0.16	0.26	0.26
			2.5	15.28	0.24	0.17	0.63
			4	13.40	0.30	0.14	0.69
	14		1	13.78	0.14	0.29	0.33
			2.5	10.79	0.58	0.071	1.10
			4	9.73	0.67	0.061	1.10
Pibsa-MEA/SMO (10:1)	8	Mosspar-H	0.5	18.79	0.13	0.32	0.52
			1	15.32	0.27	0.15	0.87
			2.5	12.46	0.47	0.087	1.20
			4	11.28	0.57	0.072	1.40
	14		0.5	14.19	0.49	0.084	1.50
			1	11.47	0.57	0.072	1.40
			2.5	8.84	0.74	0.055	1.40
			4	7.75	0.84	0.049	1.40
Pibsa-UREA	8	Mosspar-H	1	17.02	0.36	0.11	0.31
			2.5	14.78	0.48	0.085	0.36
			4	12.98	0.55	0.075	0.37
	14		1	15.02	0.52	0.079	0.40
			2.5	11.50	0.70	0.059	0.41
			4	10.25	0.78	0.053	0.41

One of the most important issues in determining drop size distributions in blends is to find critical flow conditions that reflect the boundaries between the occurrence of a stable drop shape and drop break-up. These conditions are often given in terms of a critical capillary number as a function of the viscosity ratio, $Ca_{crit}(\lambda)$, known as the Grace curve. The capillary number and viscosity ratio values were plotted from Table 4.8 as a function of viscosity ratio for all formulations excluding SMO. These are shown in Figure 4.21.

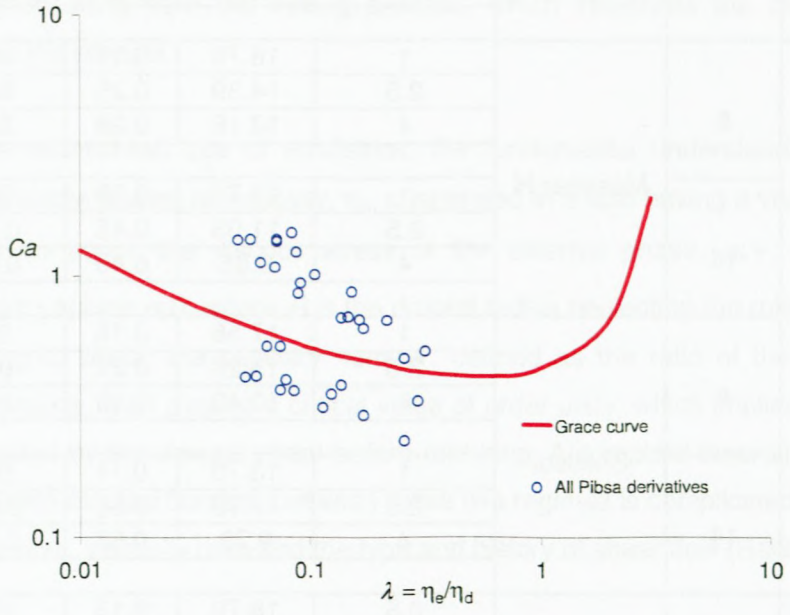

Figure 4.21: Capillary number and viscosity ratio of explosive emulsions

The purpose of the results shown in Figure 4.21 was to calculate the capillary number and viscosity ratio and to put all the data points on the master curve. Jansen *et al.* (2001) took similar approaches. It can be seen that some experimental points lie above the boundary curve, i.e. they correspond to the instability zone where shearing can break-up droplets. This is exactly what the experimental results show. Several data points lie very close to the boundary curve. Meanwhile, it is necessary to take into account that experimental points have been calculated using averaged values of processing values. It shows that some material is deformed under more severe conditions corresponding to the zone above the critical curve and some not. The latter can be understood from the work by DeRoussel *et al.*, (2001) and Janssen and Meijer (1995) on dynamics of liquid-liquid mixing. They showed that material passes through cycles of alternating 'strong' and 'weak' zones. The strong zone represents regions of the mixer in which

stretching and break-up during mixing occurs. The weak zone represents the regions of the mixer where coalescence and break-up at rest occurs, though no coalescence was observed in the study as all the surfactants that were used were beyond critical micelle concentrations (*cmc*). The results shown in Figure 4.21 highlight the findings of Jansen *et al.*, (2001) and Loewenberg and Hinch (1996). Jansen *et al.*, (2001) worked on concentrated emulsions with a dispersed phase volume fraction from 0 to 70% and showed that, with an increase in the volume fraction of the dispersed phase, the 'curves' shifted downwards (lower critical capillary number) confirming that break-up, indeed, is easier in concentrated emulsions. Similar findings by Loewenberg and Hinch (1996) showed that drops deform more and orient more into the flow direction as the dispersed phase volume is increased and droplet break-up occurs at a slightly lower capillary number in more concentrated emulsions. As a result of the high internal phase ratio of highly concentrated emulsions, their viscosities are enormously increased. In such a case the viscous emulsion itself acts as the continuous phase for rupturing the drops. As a result, the rupturing of drops in concentrated emulsions is boosted. This leads to the formation of fine drops.

The explosive emulsion under study has a volume fraction of about 85%, clearly beyond that used by Jansen *et al.*, (2001), and supports their findings (Jansen *et al.*, 2001; Loewenberg and Hinch, 1996). From Figure 4.21, it can be concluded that the Grace curve is a good estimate for the system under study.

4.9 SUMMARY

This chapter has outlined the important results found through the experiments conducted for the current study. The study focused on assessing the evolution of droplet size and droplet size distribution with prolonged mixing time. From these, corresponding critical parameters were determined from proposed models:

- o critical diameter (D_{crit}).
- o critical width of droplet size distribution (ω_{crit}).
- o critical time at which D_{crit} and ω_{crit} are obtained.

The characterisation of droplet disruption for Mosspar-H formulations was done by starting with the same droplet size for all formulations and for droplet disruption; the characterisation was done using the famous power-law equation from which the coefficient *C* was used as the main coefficient to compare formulations in terms of efficiency in droplet disruption. The work also focused on the effect of surfactant concentrations on droplet size when applying the same energy input into the system, as well as the effect of surfactant type on droplet size. The effect of

energy input on some rheological properties was investigated. The rheological properties included the yield stress and plateau modulus from oscillatory measurements of storage and loss moduli. The aim was to correlate the yield stress and plateau modulus with energy density specifically. The relation of the elasticity-droplet size effect was also presented. Finally, the capillary number as a function of the viscosity ratio was plotted on the master curve known as the Grace curve to evaluate whether it is a good estimate for the system under study, following the methodology developed by Jansen *et al.*, (2001).

CHAPTER 5

SUMMARY AND CONCLUSIONS

5.1 INTRODUCTION

The literature review, the experimental method, the analysis of results and the discussion and evaluation of results have been presented. In this chapter, the conclusions arrived at through this research will be presented and recommendations proposed.

5.2 SUMMARY

Emulsification is usually referred to as the dispersion of one liquid, such as fuel oil, into another, immiscible, liquid such as water. This requires energy input and a surfactant.

The subject that is investigated in this research is a highly concentrated emulsion of the waterinoil type used as liquid explosive. The water phase of the particular emulsion (concentration approximately 94wt%) investigated, consisted of a supersaturated aqueous solution of nitrate salts, with water comprising less than 20% of it by mass. The properties of this emulsion explosive system were presented in Chapter 2.

The material utilised in the study involved two concentrations of surfactants, five surfactants, two fuels and an aqueous solution of ammonium nitrate (AN). In the making of the emulsion samples, energy density (KJ/Kg) was measured for all formulations to determine its influence on width of size distribution, mean droplet size (D_{50}), sauter mean diameter (d_{32}) and the influence of surfactant type on droplet size. Power law and exponential models were used to determine the critical width of size distribution, critical time and critical diameter and droplet disruption characterisation. The study compared the experimental energy input into making emulsions with energy needed to increase the interfacial area and also focused on the influence of energy density on rheological properties including yield stress, shear modulus and elastic modulus – droplet size dependency. Capillary numbers and viscosity ratios for all Pibsa surfactant formulations were calculated and plotted on the Grace curve to confirm whether the master curve is a good/not so good estimate for the system under study.

From the analysis of the results, it was found that the droplet size and droplet size distributions for all formulations decreased with increased mixing time, though remaining Gaussian.

Exponential models were applied to follow up the evolution of droplet size and droplet size distributions. It was established from the models that a higher surfactant concentration resulted in a smaller critical droplet size and critical width of size distributions. The study also focused on the effect of the surfactant's concentration. It was found that a higher surfactant concentration resulted in smaller droplet sizes and that less energy was consumed. The study also investigated the effect of type of surfactant. It was observed that different formulations with the same surfactant concentration all required a different energy input to manufacture droplets of similar size. This was attributed to different adsorption kinetics of the surfactants under study. Calculations involving the comparison of the experimental energy input into the emulsification process with the theoretical energy needed to expand the interfacial area were investigated. It was found that the energy spent to form emulsions was larger than the droplet surface energy in the actual product. This was attributed, in accordance with Fredette *et al.*, (2007), to the dissipation of a large amount of energy as heat and the creation of flow. Droplet disruption was investigated using the power law equation. It was found that the *b* values were close, indicating alike mechanism in droplet refinement. The coefficient *C* was shown to depend on the surfactant concentration. It decreased with the increase of the surfactant concentration and a trend for using different surfactants but the same oil was established. The rheological parameters, namely the yield stress and the plateau of shear modulus, were found to be sensitive to droplet size. Both parameters shifted to higher values when droplet size was decreased by increasing the mixing time. The aim was to correlate these parameters with energy input. The results indicated that the yield stress increased exponentially with an increase in energy input. The plateau of shear modulus increased in a power law format with the increase in energy input. The empirical equation formulated by Malkin *et al.*, (2004) ($G = K_G d^n$) was used to study the elasticity-droplet size dependency. It was found that $n = 2$ was a good approximation in all cases, as it was found by Malkin *et al.*, (2004) and Masalova and Malkin (2007). To compare the elasticity coefficient, $K_{G,(n=2)}$ fittings were chosen. It was established that a higher surfactant concentration results in lower elasticity and a trend using different formulations with same oil was observed. Calculations of capillary numbers and viscosity ratios were made and plotted. It was found that the droplet refinement occurs at high values of the capillary number lying above or close to the stability curve. Some data points lie below the stability curve, indicating that shear rate is not constant and some material are sheared more severely than the others in the mixer.

5.3 CONCLUDING REMARKS

- Highly concentrated emulsions are unstable under shearing. Depending on the duration of shearing, the average droplet size decreases and droplet size becomes narrower, though remaining Gaussian. The average droplet size, as well as the width of the size distribution, approaches some limit which is found by a proposed fitting equation. Both critical width of distribution and droplet diameter were found to be lower for higher surfactant concentrations.

- The kinetics of the emulsification process was followed by measuring d_{32} for all surfactants with the same concentration as a function of energy input. It was found that, to manufacture similar droplet sizes, the trend for surfactants needing less energy input in descending order was:

  Pibsa-MEA > Pibsa-IMIDE >Pibsa-UREA > Pibsa-MEA/SMO > SMO.

  The observed trend was mainly attributed to adsorption kinetics of surfactants and interfacial tension, though Walstra (1983) proved that droplet size was weakly dependent on the interfacial tension.

- Comparison between experimental and theoretical energy was made. It was established that experimentally determined energy was greater than the theoretical energy. This was due to high energy used in the emulsification machine to achieve small droplets, since comminution of large droplets into smaller ones involves additional shear forces so that viscous resistance during agitation absorbs most of the energy (Othmer, 1999; Walstra, 1993) and excess energy is dissipated as heat. One reason was that energy is needed to create the flow in which forces can act to deform droplets (Brosel and Schubert, 1999).

  It was established that an increase of the surfactant concentration leads to a decrease in energy consumption and smaller droplets. According to Walstra (1983), high concentrations of surfactant results in smaller droplets, hence a greater number of disruptions. McClements (2004, 2005) similarly postulated that the higher the amount of surfactant, the greater the probability that an emulsifier would be adsorbed to the surface of a droplet during an encounter between it and the droplet – the greater the adsorption efficiency, the smaller the droplet size.

- Droplet disruption efficiency was investigated using the power law equation. The order for the same oil was found to follow the order:
  Pibsa-MEA >Pibsa-IMIDE >Pibsa-UREA > Pibsa-MEA/SMO > SMO

  Meanwhile, the difference between the first members of the row is not great and the noticeable decrease of the efficiency of stability under shear starts when the low-molecular-weight component SMO is used. It was found that lower values of droplet disruption coefficient, *C*, were observed for higher surfactant concentrations. This meant that the refining of droplets became easier. The observed concentration of coefficient *C* can possibly be explained by the tendency of a higher surfactant content to produce smaller droplets, as was shown by Walstra (1983) and McClements (2004, 2005).

- Results from oscillatory measurements were used to investigate the role of droplet size on the shear modulus. It was found that $n = 2$ remains a very good approximation in all cases, as was found and discussed by Malkin *et al.*, (2004). The results of k_G were compared to compare the elasticity of samples in which only the surfactant was different. To do this comparison more analogically, the $n = 2$ fittings were chosen and the following trends of elasticity were seen:

- A higher surfactant concentration results in lower elasticity, while the interfacial tension does not change.
- For different oils, but same surfactant, the interfacial tension and the elasticities are very close.
- For different surfactants, but the same oil, the trend is as follows:
  Pibsa-MEA > Pibsa-IMIDE ≈ Pibsa-UREA > Pibsa-MEA/SMO > SMO

  The preceding points, which somehow contradict the classic scaling of shear modulus by Laplace pressure, σ/R, can be explained in terms of "*another source of elasticity*" (Bengoechea *et al.*, 2006) which may be due to the interdroplet interaction.

- The refinement of droplets influences the rheology of emulsions, because rheological properties depend on the droplet size Malkin *et al.*, (2004). It was found, from the results that have been presented (section 4.7), that yield stress and elastic modulus increased with an increase in energy input. The rheological properties of these emulsions are related to Laplace pressure (σ/R). Thus, the yield stress, viscosity and elastic modulus

are expected to increase with the decrease in droplet size (Princen, 1979, 1985; Princen and Kiss, 1986, 1989).

- The refinement of droplets by shearing was possible because the capillary number of this process lies above or close the critical values, with some data points below. This points out that there are strong and weak zones or regions of mixing in a batch mixing chamber as the shear rate is not constant (DeRoussel *et al.*, 2001). The strong zone represents the regions of the mixer in which stretching and break-up during flow occurs and the weak zone represents the regions of the mixer where coalescence and break-up at rest occurs.

5.4 FUTURE RESEARCH RECOMMENDATIONS

A number of areas have been identified as possible future research initiatives, as a consequence of this study:

- Preparation of emulsions with different volume fractions of the dispersed phase, with the objective of determining the capillary number as a function of the viscosity ratio of the dispersed phase to the emulsion. This could prove/disprove the observed results obtained by Jansen *et al.*, in, 2001, namely that lower capillary numbers are observed and break-up of droplets becomes easier with an increase in the dispersed volume fraction.
- Preparation of emulsions with different emulsifying equipment, with the objective of comparing the energy input into the emulsification process, evolution of droplet size and droplet size distribution.
- Preparation of emulsions with different volume fractions of the dispersed phase, with the objective of investigating this effect on elasticity-droplet size dependency.

BIBLIOGRAPHY

Acrivos, A., Lo T.S. 1978. Deformation and break up of a single drop in an extensional flow. *J. Fluid Mech*, 86:641-672.

Adamson, A.W. 1976. Physical chemistry of surface. 3rd., Wiley & Sons, Inc, New York.

Aris, R. 1962. Vectors, tensors and the basic equations of fluid mechanics Prentice-Hall, Englewood Cliffs, NJ.

Aronson, M.P., Petko, F.M. 1993. Highly concentrated water in oil emulsions: Influence of electrolyte on their properties and stability. *J colloid interface Sci*, 159:134 -149.

Babak, V.G., Langfield, A., Fa, N., Stebe, M.J. 2001. Rheological properties of highly concentrated fluorinated emulsions. *Prog Colloid Polym Sci*, 118:216 -220.

Bampfield, H., Cooper, J. 1988. Emulsions Explosives, Part 7 in "*Encyclopedia of emulsion technology*", vol3, Marcel Dekker, Ink. NY.

Banker, G.S., Rhodes, T. 1979. *Modern Pharmaceutics*. New York: Marcel Dekker, 239-256.

Barnes, H.A. 1999. The yield stress- a review or "παυτα" – everything flows?. *J Non Newtonian Fluid Mech*, 81:133-178.

Barthes – Biesel, D., Acrivos, A. 1973. Deformation and burst of a viscous drop in general shear flows. *J Fluid Mechs*, 61:1-21.

Barnea, E., Mizrahi, J. 1973. A general approach to the fluid dynamics of particulate systems, Part1: General correlation for fluidization and sedimentation in solids multiparticle system. *J Chem Eng*, 5:171-189.

Barry, B.W. 1975. Viscoelastic properties of concentrated emulsions. *Adv coll Interface*, 5:37-75.

Bazhlekov, I.B., Anderson, P. D., Meijer, H.E.H. 2006. Numerical investigation of the effect of insoluble surfactants on drop deformation and breakup in simple shear flow. *Journal of Colloid and Interface Science*,298:369-394.

Becher, P. 1965. *Emulsions: theory and practice*. 2nd ed. Reinhold, New York.

Benali, L. 1993. Rheological and granulometrical studies of a cutting oil emulsion. I. The effect of oil concentration. *J colloid interface Sci*, 156:454 -461.

Benita, S., Benoit, J.P., Puieux, F., Thies, C. 1984. Characterization of drug-loaded ploy (*d,l*-lactide) microspheres. *J Pharm Sci*, 73:721-1724.

Bengoechea, C., Cordobes, F., Guerrero, A. 2006. Rheology and microstructure of gluten and soya based o/w emulsions. *Rheologica Acta*,46:13-21.

Bentley, B.J., Leal, L.G. 1986. An experimental investigation of drop deformation and breakup in steady, two-dimensional linear flows. *Journal of Fluid Mechanics*, 167:241-283.

Bibette, J. 1992. Stability of thin film in concentrated emulsions.*Langmuir*, 8:3178-3182.

Binet, R., Cloutier, J.A.R., Edmonds, C.A.F, Holden, N.W., Mcnickol M.A. 1982. US Patent 4,357,184.(Patent).

Bird, R.B., Armstrong, R.C., Hassager, O. 1987. *Dynamic Liquids.* Willey, New York.

Bird, R.B., Stewart, W.E., Lightfoot, E.N. 2007. *Transport Phenomena.* John Wiley and Sons, New York.

Boisdron-Celle, M., Menei, P.H., Beoit, J.P. 1995. Preparation and Characterization of 5-fluorouracil-loaded microparticles as biodegradable anticancer drug carriers. *J Pharm Pharmacol*, 47:108-114.

Bohr, N. 1909. Determination of the Surface-Tension of Water by the Method of Jet Vibration. *Phil Trans Roy Soc* Ser A, 209:281-317.

Briscoe, B.J., Lawrence, C.J., Mietus, W.G.P. 1999. A review of immiscible fluid mixing. *Adv. Colloid Interface Sci*, 81:1–17

Brosel, S., Schubert, H. 1999. Investigation on role of surfactants in mechanical using a high pressure homogenizer with an orifice valve. *Chemical Engineering and Processing*, 38:533-540.

Brummer, R. 2006. *Rheology Essentials of Cosmetic and Food emulsions.*, Springer, Berlin, Heidelberg., New York, 166.

Cameron, I.R., Cooper, J.1978.British Patent, 2518,065. (Patent).

Changzhi, L, Liejin, G. 2007. Experimental Study of Drop Deformation and Breakup in SimpleShear Flows. *Chin. J. Chern. Eng,* 15(1):1-5.

Chin, H.B., Han, C.D. 1979. Studies on Droplet Deformation and Breakup. I. Droplet Deformation in Extensional Flow. *Journal of Rheology*, 23:557-590.

Christov, N.C., Ganchev, D.N., Vassileva, N.D., Denkov, N.D., Danov, K.D., Kralchevsky, P.A. 2002. Capillary mechanisms in membrane emulsification: Oil-in-water emulsions stabilized by Tween 20 and milk proteins. *Colloids and Surfaces A: Physicochemical and Engineering Aspects*, 209:83.

Coulaloglou, C.A., Tavlarides, L.L. 1977. Description of interaction processes in agitated liquid-liquid dispersions. *Chem Eng.Sci*, 32:1289.

Cross, M.M. 1965. Rheology of non Newtonian fluids: a new flow equation for pseudoplastic systems. *J coll Sci*, 20:417 – 437.

Curle, N., Davies, H.J. 1968. *Modern Fluid Dynamics*, Vol. 1 Incompressible Flow ., D Van Nostrand, London.

Damodaran, S. 1990. Interfaces, protein films and foams, in *Advances in food and Nutrition* Research, Vol 34,Kinsella J.E., Ed., Academic Press, San Diego.

Damodaran, S. 1996. *Amino acids. peptides and proteins, in Food chemistry*,3rd ed., Fennema O.R., Ed., Mercel Dekker,NY.

DeBruijin R.A., 1989. Deformation and break up of drops in Simple Shear flow, Ph.D. thesis. Eindhoven University of Technology, Eindhoven, the Netherlands.

DeBruijin, R.A. 1993. Tip Streaming of drops.*Chem.Eng.Sci*,48:277.

DeRoussel, P., Khakhar, D.V., Ottino, J.M. 2001. Mixing of viscous immiscible liquids. Part 2: Over emulsification interpretation and use. *Chemical Engineering Science*, 56:5531-5537.

DeRoussel, P., Khakhar, D.V., Ottino, J.M. 2001. Mixing of viscous immiscible liquids. Part 1: Computational models for strong-weak and continuous flow systems. *Chemial Engineering Science*, 56:5511-5529.

Dickson E. 1989. Food colloids-an overview. *Colloid surface*, 42:91-204.

Dickinson, E and Stainsby, G. 1988. Emulsion stability, in Advances in food emulsions and Foams, Dickinson, E and Stainsby, G., Eds. Elsevier Applied Science, London, chap.1.

Djakovic, L., Dokic, P., Radivojevic, P., Sefer, I., Sovilj, V. 1987. Action of emulsifiers during homogenization of o/w emulsions. *J Colloid Polym. Sci*, 265:993.

Dukhin, S.S., Krietchamer, G., Miller, R. 1995. *Dynamics of adsorption at liquid interfaces: Theory, Experiment and Application*, Elsevier, Amsterdam.

Drumright-Clarke, M.A., Renardy, Y. 2004. The effect of insoluble surfactant at dilute concentration on drop breakup under shear with inertia. *Physics of fluids*, 16:14-21.

Eggleton, C.D., Stebe, K.J. 1998. An Adsorption–Desorption-Controlled Surfactant on a Deforming Droplet. *Journal of Colloid and Interface Science*, 208:68-80.

Eggleton, C.D., Pawar, Y., Stebe, K.J. 1999. Insoluble surfactants on a drop in an extensional flow: a generalization of the stagnated surface limit to deforming interfaces. *Journal of Fluid Mechanics*,385:79-99.

Fellows, P. 1988. *Food processing Technology: Principles and Practice*, VCH Publishers, Weinheim, Germany.

Ferry J.D.1980. *Viscoelastic properties of polymers*, Wiley, New York.

Franco, J.M., Guerrero, A., Gallegos, C. 1995. Rheology and Processing of salad dressing emulsions. *Rheo Acta*, 34:513-524.

Franco, J.M., Rymundo, A., Sousa, I., Gallegos, C. 1998. Influence of processing variables on the rheological and textural properties of lupin protein stabilized emulsions. *Journal of Agricultural food chemistry*, 46:3109-3115.

Franco, J.M., Partal, P., Gallegos, C., Ruiz, D., Conde, B. 2000. Influence of pH and protein thermal treatment on the rheology of pea protein stabilized emulsions. *J of the American oil of chemists Society*, 77:975-983.

Fradette, L., Brocart, B., Tanguy, P.A. 2007. Comparison of Mixing Technologies for the Production of Concentrated Emulsions. *Chemical Engineering Research and Design*, 85:1553-1560.

Gallegos, C., Berjano, M., Choplin L. 1992. Linear viscoelstic behavoiur of commercial and model mayonnaise. *J Rheo*, 36:465-478.

Ganguly, S., Krishna Mohan, V., Jyothi Bhasu, V.C., Mathews, E., Adiseshiah, K.S., Kumar, A.S. 1992. Surfactant-electrolyte interactions in concentrated emulsions: FT-IR spectroscopic and low-temperature differential scanning calorimetric studies. *J Colloid and Surfaces*, 65:243-256.

Goloub, T., Pugh, J. 2003. The role of the surfactant head group in the emulsification process: single surfactant systems. *Journal of Colloid and Interface Science*, 257:337-343.

Gopal, E.S.R. 1968. Principles of emulsions formation, in *Emulsion Science*, Sherman P., Ed Academic Press, London, chap.1.

Grace H. P. 1982. Dispersion phenomena in high viscosity immiscible fluid systems and applications of static mixers as dispersion devices in such systems.*Chem Eng. Commun*,14:225-277.

Grace H.P. 1971. Dispersion phenomena in high viscosity immiscible fluid systems and applications of static mixers as dispersion devices in such systems., *Eng. Found., Res. Conf. Mixing 3rd, Andover, N .H.* Republished in 1932 in *Chem Eng Commun*,14:113.

Groeneweg, F., Van Dieren, F., Agterof, W. G. M. 1994. Droplet break-up in a stirred water-in-oil emulsion in the presence of emulsifiers. *J Colloids and surfaces*,91:207-214.

Guerrero, A., Ball, H. 1994. Effect of spray dried or reduced cholesterol yolk and temperature on the linear viscoelastic properties of mayonnaise. *J of Texture Studies*, 25:363-381.

Guerrero, A., Partal, P., Gallegos, C. 1998. Linear viscoelasticity of sucrose ester stabilized oil in water emulsions. *J Rheo*, 42:1375-1388.

Ha, J.W., Yang, S.M. 1999. Breakup of a Multiple Emulsion Drop in a Uniform Electric Field. *Journal of Colloid and Interface Science*, 213:92–100

Hiemenz, P.C., Rajagopalan R., 1997., *Principles of Colloid and Surface Chemistry*, 3rd ed., Marcel Dekker, New York, NY.

Hinch, E.J., Acrivos, 1979. A., Steady long slender droplets in a simple shear flow. *J. Fluid Mech*, 98:302-328.

Hu, Y., Lips, A. 2003. Transient and steady state three dimensional drop shapes and dimensions under planar extensional flow. *Journal of Rheology*, 47: 349-369.

Hubbard A.T, 2002. Encyclopaedia of Surface and Colloid Science, CRC Press 3152–3154.

Ikeda, Y., Inoae, A., Tanabe, Y., Airki, T.1983.US Patent ,4,386,977.(Patent).

Israelachvili, J.N. 1992. *Intermolecular and Surface Forces*. Academic press, London.

Jackson, N.E., Tucker, C.L. 2003. A model for large deformation of ellipsoid droplet with interfacial tension. *J Rheo*, 47:659-682.

Jager Lezer, N., Tranchant, J.F., Alard, V., Vu, C., Tchoreloff, P.C., Grossiord, J.L. 1998. Rheological analysis of highly concentrated w/o emulsions. *Rheo Acta*, 37:129 -138.

Jansen, K.M.B., Agterof, W.G. M., Mellema, J. 2001. Droplet breakup in concentrated emulsions. *Journal of Rheology*, 45:227-236.

Janssen, J.J.M., Boon, A., Janssen, W.G.M. 1994. Droplet break up in simple shear flow in the presence of emulsifiers. *Coll Surfaces*,91:141-148.

Janssen, J.M.H., Meijer, H.E.H. 1995. Dynamics of liquid-liquid mixing: a two-zone model. *Polym. Eng. Sci*, 35:1766-1780.

Jeyanthi, R., Mehta, RC., Thanoo, B.C., Deluca, P.P. 1997. Effect of processing parameters on the properties peptide containing PLGA microspheres. *J Microencapsulation*, 14:163-174.

Jurlaanse, A.C., DeBruijn, D.W., Out, D.J.P.1990. *Manupulation of product structure of food emulsions via processing and composition*, in W. E. L. Spiess and Schubert H (Eds), Engineering and food, Vol 1,Physical Properties and Processing control, Elsivier Science Publishers, Barking.

Kabalnov, A., Weers, J. 1996. Macroemulsion stability: The orientated wedge theory revisted. *Langmuir*, 12:276.

Kandori, K. 1995. Applications of microporous glass membranes: Membrane emulsification, in Food processing: Recent Developments, Gaonkar, A.G., Ed. Elsevier Science,Amsterdam.

Karbstein, H. 1994. Untersuchungen zum Herstellen und Stabilisieren vonO¨ l-in-Wasser-Emulsionen. Thesis, Universita¨t Karlsruhe (TH).

Karbstein, H., Schubert, H. 1995. Development in the continuous mechanical production of oil in water macro emulsions. *Chemical Engineering and Processing*, 34:205-211.

Kawakatsu, T., Kikuchi Y., Nakajima M. 1997. Regular-sized cell creation in micro channel emulsification by visual micro processing method. *Journal of the American Oil Chemists Society*, 74:317.

Kawakatsu,T., Trägardh G.; Trägardh C.H., Nakajima M., Oda N., Yonemoto T. 2001. The effect of hydrophobicity of microchannels and components in water and oil phases on droplet formation in micro-channel water-in-oil emulsification. *Colloids and Surfaces A: Physicochemical and Engineering Aspects*, 179:29.

Khakhar, D. V., Ottino, J. M. 1986. A note on the linear vector model of Olbricht, Rallison, and Leal as applied to the breakup of slender axisymmetric drops. *Journal of non-newtonian fluid mechanics*, 21:127-131.

Khakhar, D. V., Ottino, J. M. 1987. Breakup of liquid threads in linear flows. *International journal of multiphase flow*, 13:71-86.

Knops, Y.M.M., Slot, J.J.M., Elemans P.H.M., Bulters, M.J.H. 2001. Simultaneous breakup of multiple viscous threads surrounded by viscous liquid *AIChE Journal*, 47(8):1740-1745.

Kobayashi, I., Nakajima, M., Mukataka, S. 2003. Preparation characteristics of oil-in-water emulsions using differently charged surfactants in straight-through micro channel emulsification. *Colloids and Surfaces A: Physicochemical and Engineering Aspects.*, 229:33.

Koglin, B., Pawlowski, J., Schnoring H. 1981. Kontinuierliches Emulgieren mit Rotor/Stator- Maschinen EinfluB der volumenbezogenen Dispergierleistung und der Verweilzeit auf die Emulsionsfeinheit.*Chem Ing Tchn*, 53:641-647

Kozicki, W., Kuang, P.Q. 1993. Prediction of Lower/Upper Limiting Viscosities. *Canadian J of Chem Eng*, 71:329 – 331.

Kretzchmar, G., Miller, R. 1995. *Dynamics of adsorption at liquid interfaces: Theory, Experiment, Application*, studies in interfaces series, edited by D. Mobius and Miller R. Elsevier, Amsterdam.

Kruijt-Stegeman, Y.W., van de Vosse, F.N., Meijer, H.E.H. 2004. Droplet behavior in the presence of insoluble surfactants. *Physics of Fluids*, 16:2785-2796.

Lacroix, C., Aressy, M., Carreau, P.J. 1997. Linear viscoelasic behaviour of molten polymer blends: a comparative study of lierne and Lee and Parks models. *Rheo Acta*, 36:416-428.

Langenfield, A., Schmitt, V., Stebe, M.J. 1999. Rheological behaviour of fluorinated highly concentrated reverse emulsions with temperature. *J Colloid Interface Sci*, 218:522 – 528.

Levich, V.G. 1962. Physicochemical Hydrodynamics. Prentice Hall, Englewood Cliffs

Ostwald.W.1910.Kolloid Z.6:103; 7:64.

Lissant, K.J.1966. The geometry of high internal phase ratio emulsions. *J .colloid interface Sci*, 22:462 – 468.

Lissant, K.J.1970. Geometry of emulsions. *J. Soc. Cosmet Chem*, 21:141-154.

Lissant, K.J., Mayhan, K.G.1973. A study of medium and high internal phase ratio water/polymer emulsions. *J .colloid interface Sci*, 42:201 – 208.

Lissant, K.J., Peace, B.W.1974. Wu S.H. Mayhan K.G. Structure of high internal phase ratio water/polymer emulsions. *J .colloid interface Sci,* 42:416 – 423.

LI, X., Pozrikidis, C.1997. The effect of surfactants on drop deformation and on the rheology of dilute emulsions in Stokes flow. *Journal of Fluid Mechanics*,341:167-194.

Loewenberg, M., Hinch E.J. 1996. Numerical simulation of a concentrated suspension in shearflow. *J Fluid Mech*, 321:395-419.

Loewenberg, M., 1998. Numerical Simulation of Concentrated Emulsion Flows. *Journal of Fluids Engineering*,120:824-832.

Lucassen – Reyanders, E.H., Kuijpers, K.A. 1992. The role of interfacial properties in emulsification. *Colloids and surfaces*,65:175.

Maffettone, P. L., Minale, M. 1998. Equation of change for ellipsoidal drops in viscous flow. *Journal of Non-Newtonian Fluid Mechanics* , 78:227-241.

Magdassi, S., Kamyshny, A. 1966. Surface Activity and functional properties of proteins, *in surface Activity of proteins: Chemical and Physicochemical Modifications*, Magdassi S., Ed., Marcel Dekker, NY, chap.1.

Malkin, A. YA., Masalova, I., Slatter, P., Wilson, K. 2004. Effect of droplet size on the rheological properties of super concentrated water in oil emulsion. *Rheo.Acta*, 43:584 - 591.

Malkin, A.Y.1994. *Rheology Fundamentals.* Chem Tac Publishing,Canada.

Malmsten, M. 2003. Ellipsometry and Reflectrometry for studying protein adsorption in *Biopolymers at interfaces* 2nd ed., Malmsten M., Ed., Marcel Dekker. New York, NY, p 539.

Martin, A., Swarbrick, J., Cammarata, N. 1993. Physical Pharmacy ,fourth edition, Philadelphia, Pennsylvania: Lee & Febiger,371-490.

Masalova, I., Malkin, A.Y., Slatter, P. 2003b. Effect of droplet size on the rheological properties of super-concentrated emulsions. Proc. First Annual Rheology Conference Guimaraes (Portugal).

Masalova, I., Malkin, A.Y. 2007. A new mechanism of aging of highly concentrated emulsions: Correlation between crystallization and plasticity.*Colloid J*, 69:198 – 202.

Mason, T. G., Bibette J. 1996. Emulsification in viscoselastic media. *Phys. rev. lett*, 77:3481-3484.

Mason, T.G. 1999. New fundamental concepts in emulsion rhreology. Current Opinion in *Colloid and Interface Sci.*, 4:231-238

McClements, D.J. 2004. *Food emulsions. Principles, Practices and techniques*, Boca Raton, USA:CRC Press.

McClements, D.J. 2005. *Food emulsions. Principles, Practices and techniques*, Boca Raton, USA:CRC Press.

McClements, D.J., Fairley, P. 1992. Frequency scanning ultrasonic pulse echo reflectometer. *Ultrasonics*, 30:403-405.

McClements, D.J., Dungan, S.R. 1993. Factors That Affect the Rate of Oil Exchange between Oil-in-Water Emulsion Droplets Stabilized by a Nonionic Surfactant: Droplet Size, Surfactant Concentration, and Ionic Strength. *J. Phys. Chem*, 97:7304-7308.

Mezger, T.G. 2002. The rheology handbook: for users of rotational and oscillatory rheometry, Hannover, Germany: Viencentz Verlag 29.

Mijnlieff, P.F., Ditmarsch, R. 1965. Rate of Micelle Formation of Sodium Alkyl Sulphates inwater *Nature*, 208:889.

Miller, R., Kretzschmar, G. 1991. Adsorption kinetics of surfactants at fluid interfaces. *Adv Colloid Interface Sci*, 37:97-121

Milliken, W.J., Leal L.G. 1991. Deformation and breakup of viscoelastic drops in planar extensional flows. *J. Non Newtonian Fluid Mech*,40:355-379.

Milliken, W.J., Stone, H.A., Leal, L.G. 1993. The effect of surfactant on the transient motion of Newtonian drops. *Physics of Fluids* A: Fluid Dynamics, 5:69-79.

Milliken , W.J., Leal, L.G. 1994. The Influence of Surfactant on the Deformation and Breakup of a Viscous Drop - The Effect of Surfactant Solubility. *Journal of Colloid and Interface Science*,166:275-285.

Mittal, K.L. 1975. Colloid Dispersions and Micellar Behavoir, ACS Symposium Series. No 9, Ch4.

Moros, J.E., Cordobes, F., Franco, J.M., Gallegos, C. 2003. Enhancement of gel strength by application of thermal treatments in highly flocculated emulsions. *Food Hydrocolloids*, 17:199-206.

Mougel, J., Alvarez, O., Baravian, C, Caton, F., Marchal P., Stébé, M.J., Choplin, L. 2006. Aging of an unstable w/o gel emulsion with a nonionic surfactant. *Rheologica Acta*, 45:555-560

Munoz, J., Sherman, P. 1992. Dynamic viscoelastic properties of some commercial salad dressings *of Texture Studies*, 21:411-426.

Mukerjee, P., Bunsenges, B. 1978. Formation and Some Properties of Micelles. *Phys. Chem*, 82:931.

Mu, Y., Lyddiatt, A., Pacek, A.W. 2005. Manufacture by water/oil emulsification of porous agarose beads: Effect of processing conditions on mean particle size, size distribution and mechanical properties. *Chemical engineering and processing*, 44:157-1166.

Myers D. 1992. *Surfactant Science and Technology*, 2nd Ed., VCH , New York.

Narsimhan, G., Goel, P. 2001. Drop coalescence during emulsion formation in a high pressure homogenizer for tetradecane in water emulsion stabilized by sodium dodecyl sulfate. *J Colloid Interface Sci*, 238:420.

Nienow, A.W., Break-up. 2002.Coalescence and Catastrophic phase inversion in turbulent contactors. *Proceedings of the 3rd World Congress of emulsions*, Lyon, France.

Nippon oils and Fats K.K.1980Japanese Patent,55/57,995 (Patent).

Nixon, J. Beerbower, A. 1969. Amer. Chem. Soc. Div. Petrol. Chem. Prepr . 14 (1):49-62.

Norde, W. 2003. Colloid and Interfaces in life sciences, Marcel Dekker, New York, NY.

Oh, S.G., Jobalia, M., Shah, D.O. 1993. The effect of micellar lifetime on the droplet size in emulsions. *J Colloid Interface Sci*, 155: 511.

Östberg, G., Bergenstähl, B., Huldén, M. 1995. Influence of emulsifier on the formation of alkyd emulsions; *Colloids and Surfaces A: Physicochemical and Engineering Aspects,* 94:161-171.

Ostobo, Y., Prud'homme, R.K. 1994a. Rheology of oil in water emulsions. *Rheo Acta*, 33:29 -37.

Othmer, K.1994. Encyclopedia of Chemical Technology, 4th , Vol 9, Wiley, New York, 393-413.

Pal, R. 1990. On the flow characteristics of highly concentrated oil in water emulsions. *J Chem Eng*, 43:53-57.

Pal, R., Yushua, Y., Masliyah, J. 1991. Rheology of highly concentrated oil in water emulsions with added solids. *J Chem Eng*, 46:985-994.

Pal, R. 1996b. Effect of droplet size on the rheology of emulsions. *AIChe, J* 42:3181-3190.

Pal, R. 1999. Anomalous wall effects in parallel plate torsional flow of highly concentrated emulsions. *ASME FED,* 249:137- 150.

Pal, R. 2002. Novel shear modulus equations for concentrated emulsions of two immiscible elastic liquids with interfacial tension. *J. Non Newtonian Fluid Mech*, 105:21-33.

Partal, P., Guerrero, A., Berjano, M., Gallegos, C. 1997. Influence of concentration and temperature on the flow behavoiur of oil in water emulsions stabilized by sucrose pulmitate. *JAOCS*, 74:1203 – 1212.

Pawar, Y., Stebe, K.J.1996. Marangoni effects on drop deformation in an extensional flow: The role of surfactant physical chemistry. I. Insoluble surfactants. *Physics of Fluids*,8:1738.

Phipps, L.W. 1985. *The high Pressure Dairy Homogenizer*, The National Institute for Research in Dairying, Reading, England.

Polat, H., Polat, M., Chander, S. 1999. Kinetics of oil dispersion in the absence and presence of block copolymers. *AIChe. Eng*,45:1866 -1874.

Poncelet, De Smet B., Neufeld, R.J. 1989. Control of mean diameter and size distribution during formulation of microcapsules with cellulose nitrate membranes. *Enzyme Micro Technol*,11:29-37.

Pons, R., Solans, C., Stebe, M.J., Erra, P., Ravey J.C. 1992. Stabilibility and rheological properties of gel emulsions. *Progr. colloid Polymer Sci*,89:110-113.

Pons, R., Solans, C., Tadros, T.F. 1995. Rheological behavoiur of highly concentrated oil in water emulsions (o/w) emulsions. *Langmuir*,11:1966-1971.

Ponton, A., Clement, P., Grossiord, J.L. 2001. Collaboration of Princen's theory to cosmetic concentrated water in oil emulsions. *J Rheo,* 45:521-526.

Princen, H.M., 1979. Highly concentrated emulsions: I. Cylindrical Systems. *J Colloid and Interface Sci*, 71:55-66.

Princen, H.M., Aranson, M.P., Moser J.C.1980. Highly concentrated emulsions: II. Real Systems. The effect of film thickness and contact angle on the volume fraction in creamed emulsions. *J Colloid and interface Sci,* 75:246-271.

Princen, H.M. 1983. Rheology of foams and highly concentrated suspensions. I. Elastic properties and yield stress of a cylindrical model system. *J Colloid & Interface Sci*, 91:160-175.

Princen, H.M. 1985. Rheology of foams and highly concentrated suspensions. II Experimental study of the yield stress and wall effects for concentrated oil-in-water emulsions. *J Colloid & Interface Sci*, 105:150-171.

Princen, H.M., Kiss, A.D. 1986. Rheology of foams and highly concentrated emulsions. III. Static shear modulus. *J coll and Inter Sci*, 112:427-437.

Princen, H.M., Kiss, A.D.1989. Rheology of foams and highly concentrated emulsions. IV. An experimental study of the shear viscosity and yield stress of concentrated emulsions. *J coll and Inter Sci*, 128:176-187.

Rallison, J M. 1980. Note on the time-dependent deformation of a viscous drop which is almost spherical. *Journal of Fluid Mechanics,* 98:625-633.

Rallison, J.M. 1984. The deformation of small viscous drops and bubbles in shear flows. Ann Rev Fluid Mech, 16:45-66

Rayleigh, L. 1879. On the Capillary Phenomena of Jets. *Proc Royal. Soc Lond*, 29:71-97.

Rayleigh, L. 1882. On an instrument capable of measuring the intensity of aerial vibrations. *Phil. Mag*,14:186-187.

Raymundo, A., Franco, J.M., Empis, J., Sousa, I. 2002. Optimization of the composition of the low fat o/w emulsions stabilized by white lupin protein. *J of the American oil of chemists Society,* 79:783-790.

Reinelt, D.A., Kraynik, A.M. 1993. Large elastic deformations of three dimensional foams and highly concentrated water in oil emulsions (gel emulsions).*J colloid interface Sci*,159:460-470.

Renardy, Y.Y., Renardy, M., Cristini, V. 2002a. A new volume-of-fluid formulation for surfactants and simulations of drop deformation under shear at a low viscosity ratio. *Eur. J Mech. B/Fluids*, 21:49-59.

Romero, A., Cordobes, F., Puppo, M.C., Guerrero, A., Bengoechea, C. 2008. Rheology and droplet size distribution of emulsions stabilized by crayfish flour. *J Food Hydrocolloids*, 22:1033–1043.

Rumscheidt F.D., Mason S.G. 1961. Particle motion in sheared suspensions. XII., deformation and burst of fluid drops in shear and hyperbolic flow. *J. Colloid Sci*,16:238–261.

Rumscheidt F.D., Mason S.G. 1962. Break-up of stationary liquid threads. *J Colloid Sci*, 17:260–269.

Rusli, D., Shahinas, B., Ibrahim, A. 2007. Effect of molecular weight on the droplet size and rheolgical properties of liquid natural rubber emulsion. *Malaysian Polymer Journal*, 2:29-38.

Sanchez, M.C., Berjano, M., Brito, E., Guerrero, A., Gallegos, C. 1998. Evolution of the microstructure and rheology of o/w emulsions during the emulsification process. *Canadian Journal of Chemical Engineering*, 76:479-485.

Sanchez, M.C., Berjano, M., Guerrero, A., Gallegos, C. 2001. Emulsification rheokinetics of nonionic surfactant-stabilized oil in oil in water emulsions. *Langmuir*, 17:5410.

Sanchez, A., Vila-Jatta J.L. 1993. Development of biodegradable microspheres and nanospheres for controlled release of cyclosporine A. *Int J Pharm*,99:263-273.

Schmitt, V., Leal-Calderon, F., Bibette, J. 2003. Preparation of monodisperse particles and emulsions by controlled shear. *Journal Topics in current chemistry*, 227:195-215.

Schubert, H., Armbruster, H. 1992. Principles of formation and stability of emulsions. *International Chemical Engineering*, 32:14–28.

Schubert, H., Ax, K., Behrend, O.2003. Product engineering of dispersed systems. *Trends in Food Science and Technology*,14:9-16.

Schubert, H., Lambrich, U. 2003. Membrane emulsification, in *Proceedings of the 34th Thematic Meeting, Membrane Emulsification-the Quest for the Perfect Membrane*, Wageningen, the Netherlands.

Schubert, H., Engel, R. 2004. Product and formulation engineering of emulsions. *Trans IChem E, Part A. Chemical Engineering Research and Design*,82:1137-1143.

Schubert, H., Karbstein H. 1994. Mechanical emulsification. In Yano, T., Matsuno, R., Nakamura K (Eds), Developments in food engineering . Proc. 6th Int. Congr. Eng Food (ICEF6) (Vol2), Chiba, Japan,23 May 1993. London: Blackie Academic and Professional.

Schwartz, L.W., Princen, H.M. 1987. A theory of extensional viscosity for flowing foams and concentrated emulsions. *Journal of colloid and interface science*,118:210-211.

Schröder, V., Schubert, H. 1999. Production of emulsions using microporous ceramic membranes. *Colloids and Surfaces A: Physicochemical and Engineering Aspects*, 152:103.

Stang, M., Karbstein, H. 1994. Adsorption kinetics of emulsifiers at oil water interfaces and their effect on mechanical emulsification. *Chemical Engineering and Processing*, 33:307.

Stang, M., 1998., Zerkleinern und Stabilisieren von Tropfen beim mechanischen Emulgieren. Thesis, Universita¨t Karlsruhe (TH).

Stang M., Schuchmann H., Schubert H. 2001. Emulsification in high pressure Homogenizers. *Engineering and life Science*,1(4):151-157.

Strawbridge, K.B., Ray, E., Hallet, F.R., Tosh, S.M., Dalgleish, D.G. 1995. Measurement of the particle size distribution in the milk in homogenized by microfluidizer-Estimation of populations of particles with radii less than 100nm.*J of colloid and Interface Science*, 171:392.

Stone H.A. 1990. A simple derivation of the time dependent convective - diffusion equation for surfactant transport along deforming interface. *Phys Fluids*, A2:111-112.

Stone, H.A., Leal L.G. 1990. The effects of surfactants on drop deformation and breakup. *J Fluid Mech*, 220:161-186.

Stone, H. A. 1994. Dynamics of Drop Deformation and Breakup in Viscous Fluids. *Annual Review of Fluid Mechanics*, 26:65-102.

Sugiura, S., Nakajima, M., Yamamoto, K., Iwamoto, S., Oda, T., Satake, M., Seki, M. 2004. Preparation characteristics of water-in-oil-in-water multiple emulsions using micro channel emulsification. *Journal of Colloid and Interface Science*, 270:221.

Suzuki, K., Hayakawa, K., Hagura, Y. 1999. Preparation of high concentration O/W and W/O Emulsions by the membrane phase inversion emulsification method. *Food Science and Technology Research*, 5:234.

Tadros, T.F., Hopkinson, A. 1990. Use of viscoelastic measurements for investigating the stability/flocculation of concentrated emulsions. *Faraday discuss. chem Soc*, 90:41-45.

Tadros, T.F. 1994. Fundamentals principles of emulsions rheology and their applications. Colloid and surface A, *Physical and Engineering aspects*, 91:39-55.

Tadros, T.F. 2004. Application of rheology for assessment and prediction of the long-term physical stability of emulsions. *Advances in Colloid and Interface Science*,109:227-258.

Tai, H., Sergienko, A., Silverstein, M. S. 2001. Organic-inorganic networks in foams from high internal phase emulsion polymerizations. *Polymer*, 42:4473-4482.

Taisne, L., Walstra, P., Cabane, B. 1996. Transfer of oil between emulsion droplets. *J. Colloid Interface Sci*, 184:378-390.

Taylor, G.I. 1932. The viscosity of a uid containing small drops of another Fluid. *Proc. Roy. Soc. London Ser. A*, 138:41-48.

Taylor, G.I. 1934. The formation of emulsions in definable field of flow, *Proc Royal. Soc. Lond. Ser A*, 146:501- 523.

Tjahjadi, M., Stone, H.A., Ottino, J.M. 1992. Satellite and Subsatellite formation in capillary break up. *J Fluid Mech*,243:297-317.

Tomotika, S. 1935. On the Instability of a Cylindrical Thread of a Viscous Liquid Surrounded by Another Viscous Fluid. *Proceedings of the Royal Society of London. Series A, Mathematical and Physical Sciences*,150:322-337.

Tomotika, S. 1936. Breaking up of a Drop of Viscous Liquid Immersed in Another Viscous Fluid Which is Extending at a Uniform Rate. *Proceedings of the Royal Society of London. Series A, Mathematical and Physical Sciences*,153:302-318.

Tornberg, E. 1978. Functional characterization of protein stabilised emulsions:emulsifying behavoiur of proteins in a valve homogeniser. *J Sci.Food Agric*, 29:867.

Tornberg, E. 1980. Functional characterization of protein stabilised emulsions:emulsifying behavoiur of proteins in a valve homogeniser. *J Food Sci*,46:1662.

Ultracki, L.A. 1980. The rheology of Basic Emulsion Explosives, ERL Report no EL.0812, Catergory B.

Vanoene, H. 1972. Modes of dispersion of viscoelastic fluids in flow. *J. Colloid Interface Sci*, 40:448–467.

Van den Tempel. 1960. The function of stabilizers during emulsification. *Proc.3rd Int. Congr. Surface Activity. Cologne, 2*:573-579.

Van de Ven T.G.M. 1989. Basic concepts of fluid dynamics and colloidal forces in colloidal hydrodynamics., Academic press., San Diego.

Vladisavljevic, G.T., Schubert, H. 2003a. Preparation of emulsions with a narrow particle size distribution using microporous *a*-aluminia membranes. *Journal of Dispersion Science and Technology*, 24:811.

Vladisavljevic, G.T., Schubert H. 2003b. Influence of process parameters on droplet size distribution in SPG membrane emulsification and stability of prepared emulsion droplets. *Journal of Membrane Science*, 225:15.

Vlahovska, P.M., Loewenberg, M., Blawzdziewicz, J. 2005. Deformation of a surfactant-covered drop in a linear flow. *Physics of Fluids*, 17:103.

Wade C.G.1978.US Patent, 4,110,134 (Patent).

Walstra, P. 1983. Formation of emulsions, in *Encyclopedia of Emulsion Technology*, Vo1, Becher, P., (Ed), Marcel Dekker, New York.

Walstra, P. 1993. Principles of emulsion formation. *Chemical Engineering Science*, 48:333.

Walstra, P. 1996a. Emulsion stability, in *Encyclopedia of Emulsion Technology*, Vol 4, Becher P., Ed., Marcel Dekker, New York, Chap.1.

Walstra, P. 1996b. Disperse systems: Basic considerations, in food Chemistry, 3rd ed, Fennema,O.R.,Ed., Marcel Dekker, New York,1996b.Chap.3.

Walstra P., Smulder P.E.A. 1997. Emulsion Making emulsions and foams., An overview. In Dickson E and Bergenstahl (Eds), *Food colloids*, Cambridge: The Royal Society of Chemistry.

Walstra P., Smulder P.E.A., 1998. Emulsion Formation. In B.P. Binks(Ed), *Modern aspects of emulsion science*. Cambridge, Reino Unido: The Royal Society of Chemistry.

Walstra, P., Guerts, T.J., Noonment, A., Jellema, A., Van Boekel.,1999. M.A.J.S. *Dairy Technology*; Marcel Decker: New York.

Ward, A.F.H., Tordai, L. 1946. Time-dependence of boundary tensions of solutions J. *Chem. Phys*, 14:453.

Waxman, A M. 1984. Dynamics of a couple-stress fluid membrane. *Studies in Applied. Mathematics*, 70:63-86.

Weiss, J., McClements, D.J., Coupland, J.N. 1996. Solubilization of Hydrocarbon Emulsion Droplets Suspended in Nonionic Surfactant Micelle Solutions. *Journal of Physical Chemistry*, 100:1066.

Wieringa, J.A., Vandieren, F., Janssen, J.J., Agterof, W.G .1996. Droplet Breakup Mechanisms During Emulsification in Colloid Mills at High Dispersed Phase Volume Fractions. *Trans. Inst. Chem. Eng.*, Part A, 74A:554-561.

Willemse I, 1991; Statistical Methods and Financial Calculations, Cape Town, Juta.

Williams, A., Janssen, J.J.M., Prins, A. 1997. Behaviour of droplets in simple shear flow in the presence of a protein emulsifier Colloids and Surfaces A: *Physicochemical and Engineering Aspects*,125:189-200.

Windhab, E.J., Dressler, M., Feigl, K., Fischer, P. 2005. Megias-Alguacil D., Emulsion processing from single drop formation to design of complex processes and products. *J .Chemical engineering Science*, 60:2101-2113.

Witschi, C., Doelker, E. 1998. Influence of the microencapsulation method and peptide loading on poly(lactic acid) and poly(lactic-co-glycolic acid) degradation during in vitro testing. *J controlled Release*, 51:327-341.

Yogita, B., Hongkee, S. 2000. Dynamic changes in size distribution of emulsion droplets during Ethyl Acetate-Based Micro encapsulation process. *AAPS PharmSciTech*, 1:1.

Yorke, W.J., Binet, R., Lee, M.C., Bampfield, H.A.1983.US Patent,4,404,050 (Patent).

APPENDIX A.

Gauss fitting

PIBSA MEA Mosspar-H

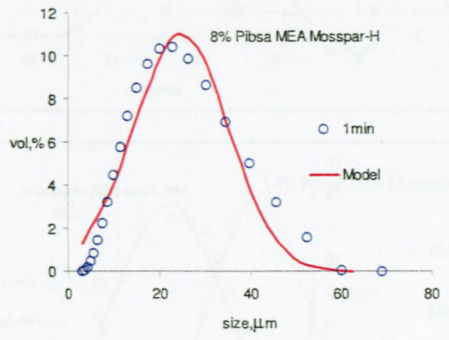

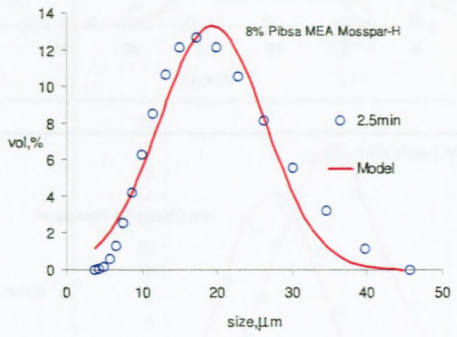

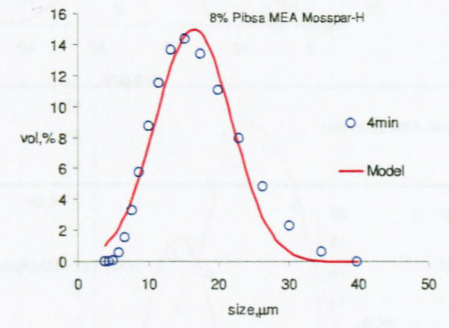

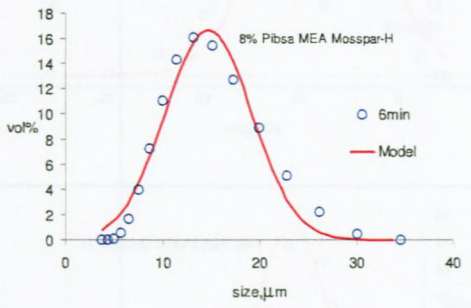

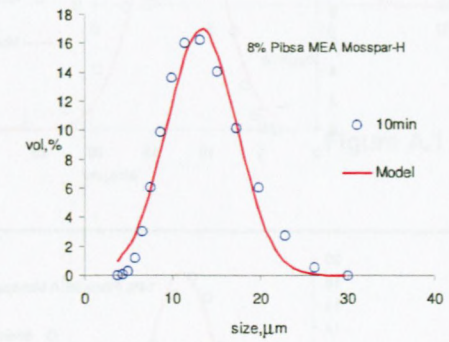

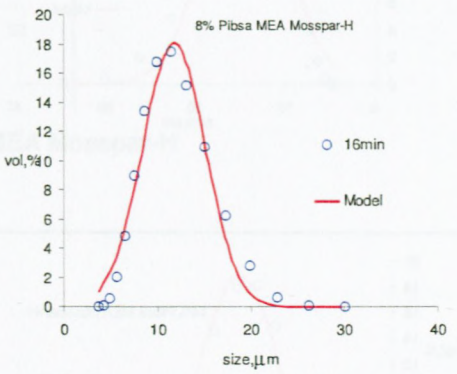

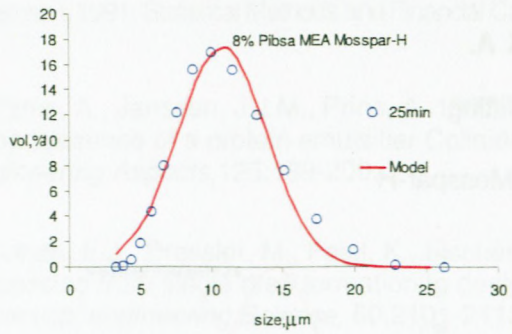
8% Pibsa MEA Mosspar-H
25min
Model
vol,%
size,µm

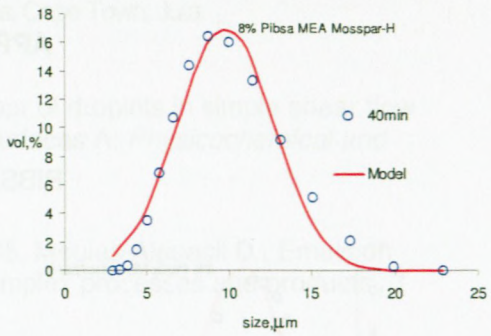
8% Pibsa MEA Mosspar-H
40min
Model
vol,%
size,µm

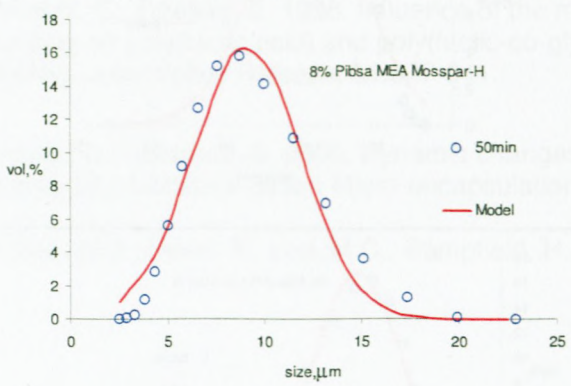
8% Pibsa MEA Mosspar-H
50min
Model
vol,%
size,µm

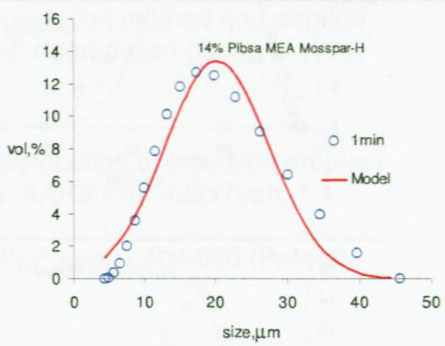
14% Pibsa MEA Mosspar-H
1min
Model
vol,%
size,µm

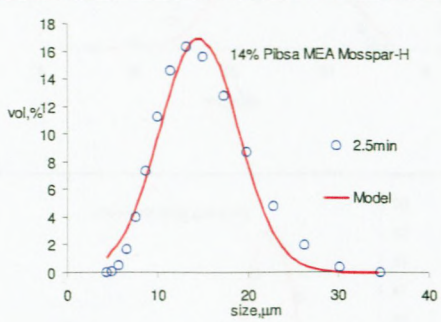
14% Pibsa MEA Mosspar-H
2.5min
Model
vol,%
size,µm

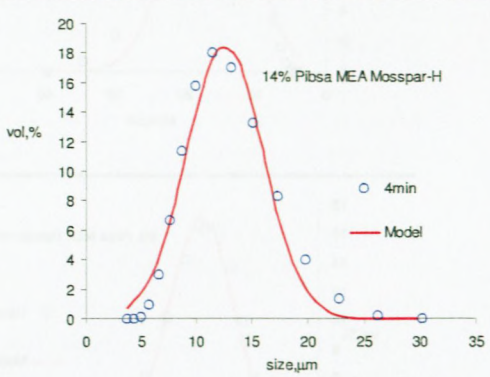
14% Pibsa MEA Mosspar-H
4min
Model
vol,%
size,µm

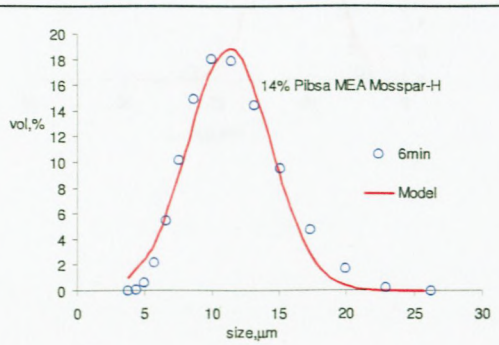
14% Pibsa MEA Mosspar-H
6min
Model
vol,%
size,µm

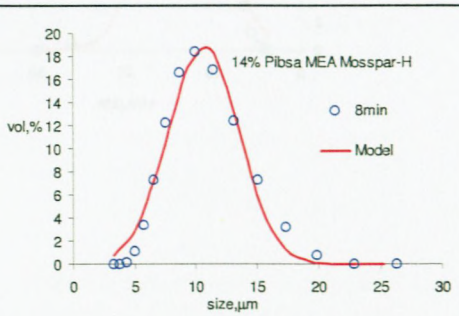
14% Pibsa MEA Mosspar-H
8min
Model
vol,%
size,µm

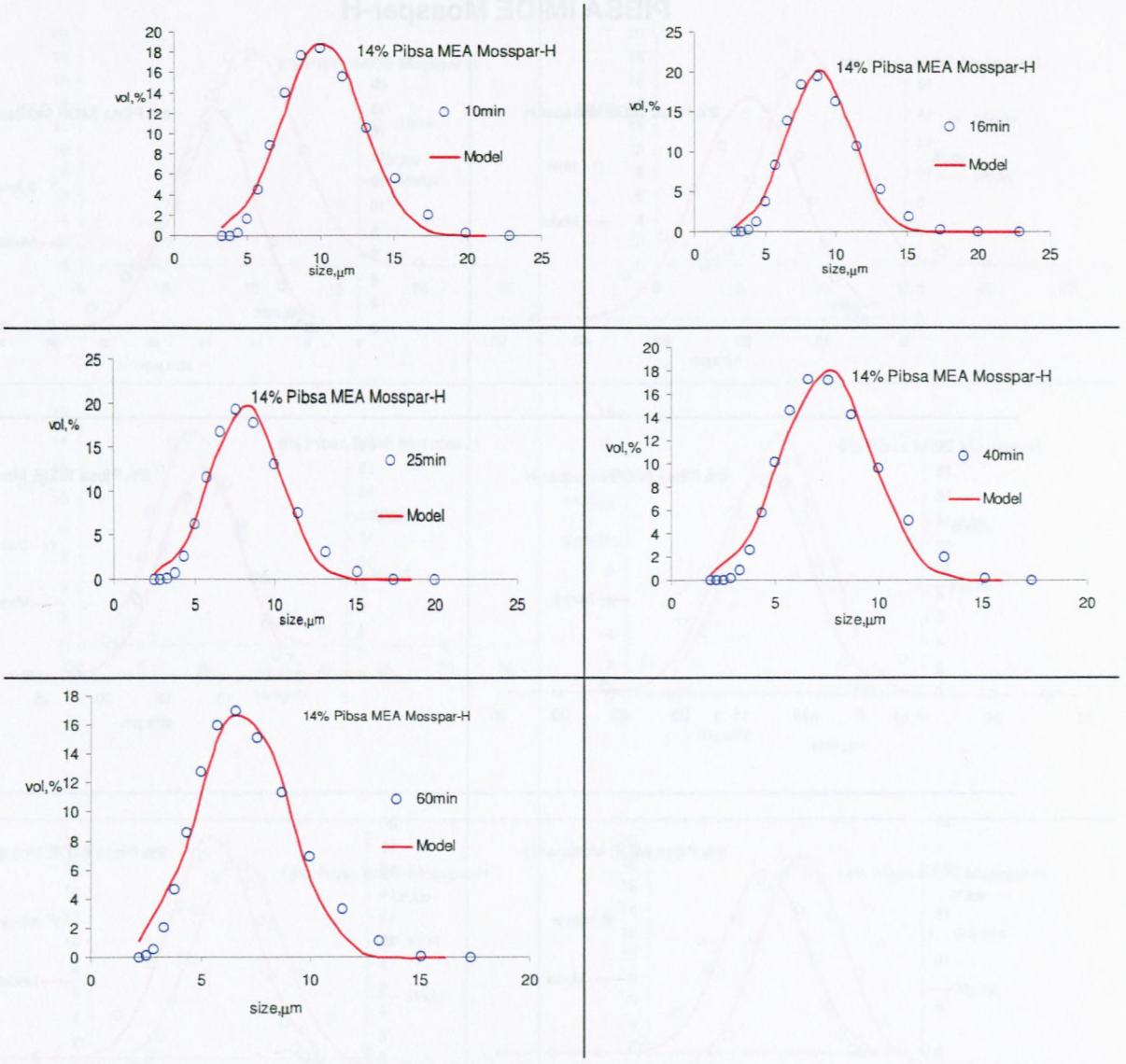

Figure A.1 Pibsa MEA Mosspar-H

PIBSA IMIDE Mosspar-H

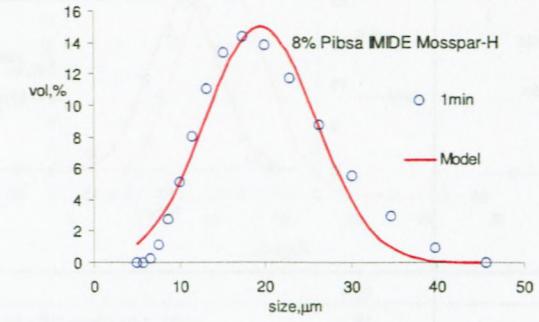

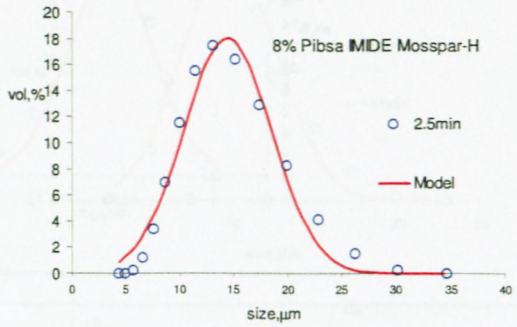

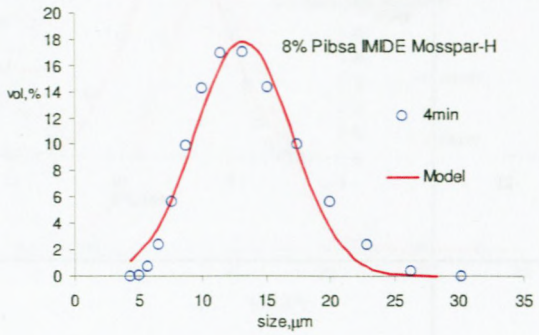

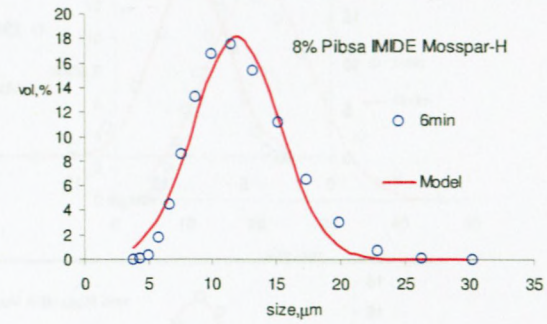

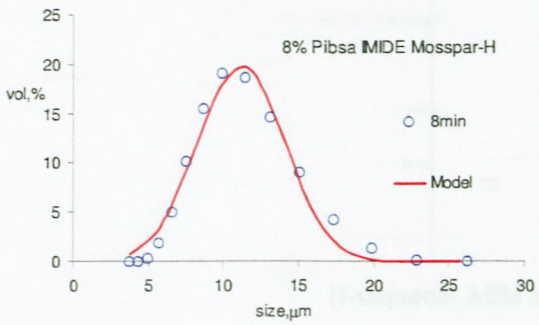

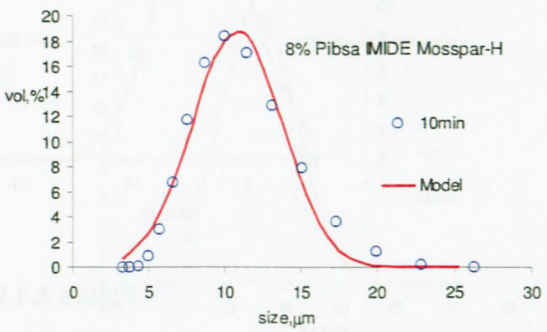

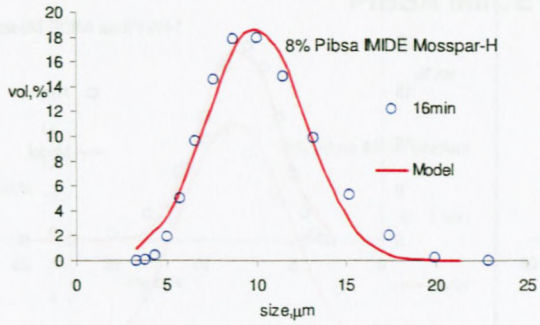
8% Pibsa IMIDE Mosspar-H
16min
Model
vol,%
size,µm

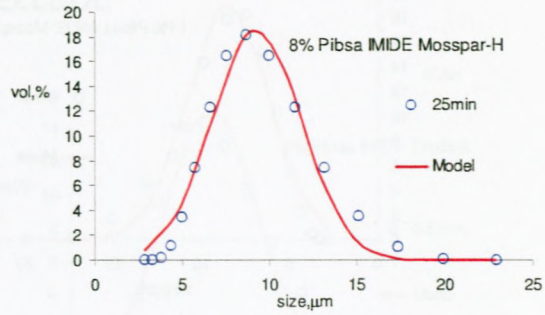
8% Pibsa IMIDE Mosspar-H
25min
Model
vol,%
size,µm

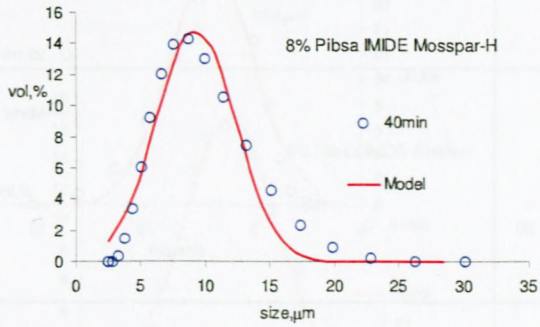
8% Pibsa IMIDE Mosspar-H
40min
Model
vol,%
size,µm

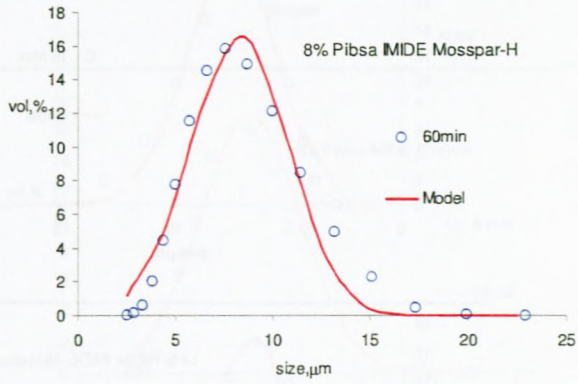
8% Pibsa IMIDE Mosspar-H
60min
Model
vol,%
size,µm

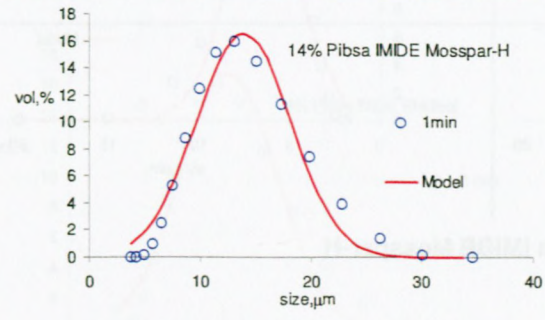
14% Pibsa IMIDE Mosspar-H
1min
Model
vol,%
size,µm

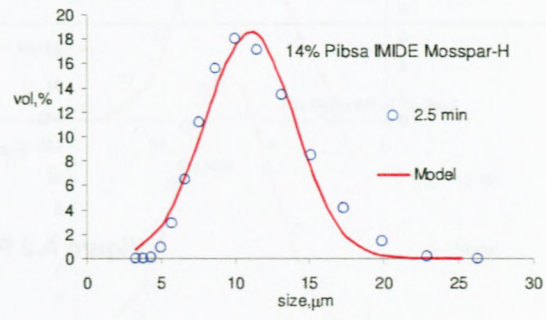
14% Pibsa IMIDE Mosspar-H
2.5 min
Model
vol,%
size,µm

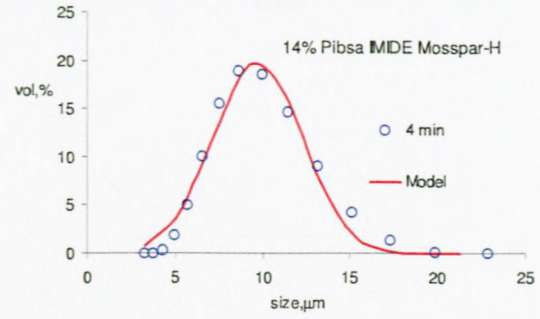
14% Pibsa IMIDE Mosspar-H
4 min
Model
vol,%
size,µm

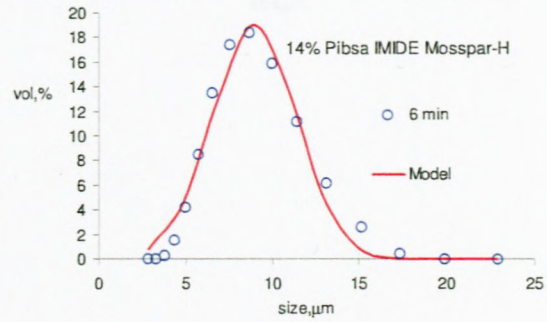
14% Pibsa IMIDE Mosspar-H
6 min
Model
vol,%
size,µm

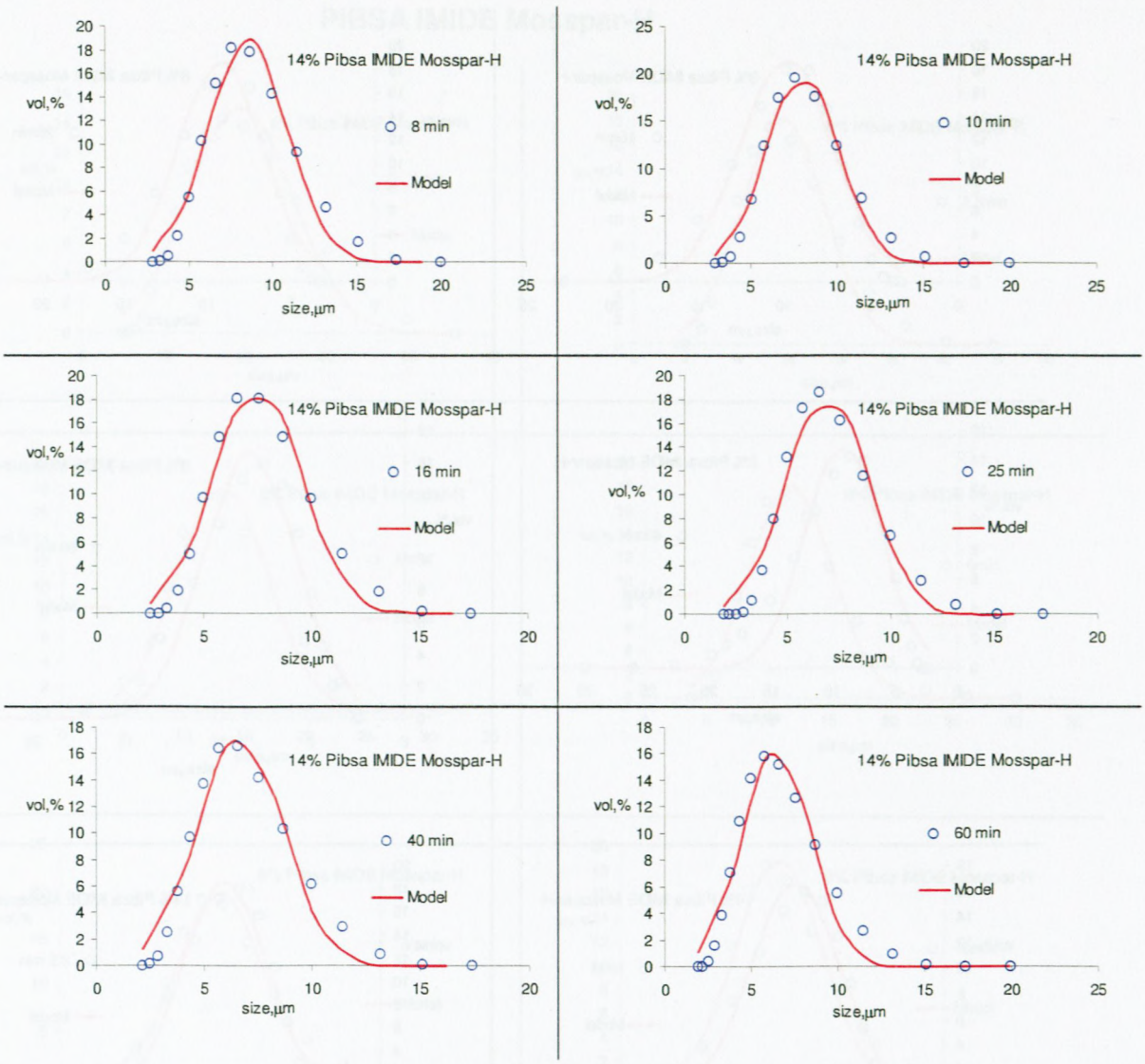

Figure A.2 Pibsa IMIDE Mosspar-H

PIBSA IMIDE SHELLSOL

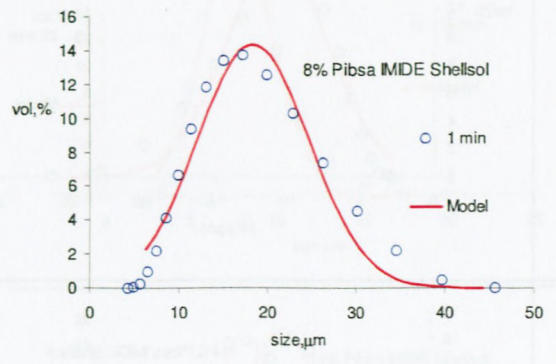

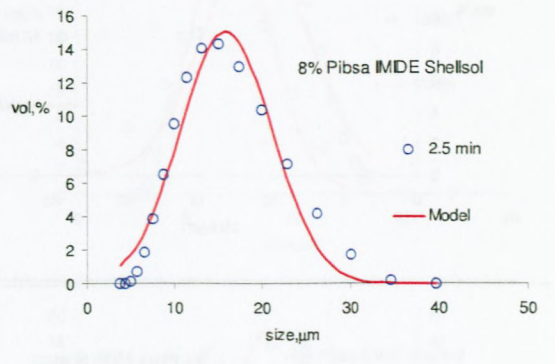

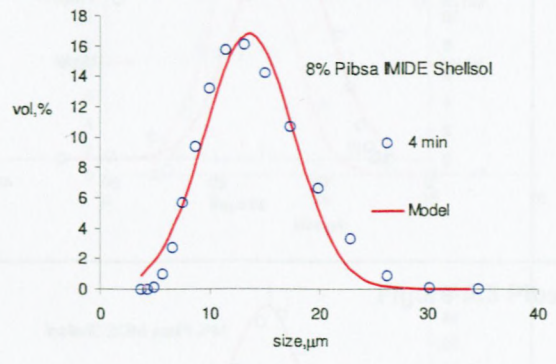

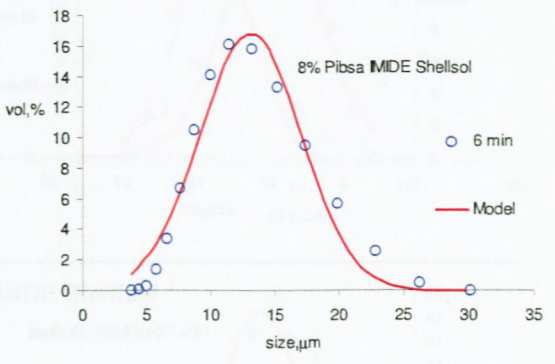

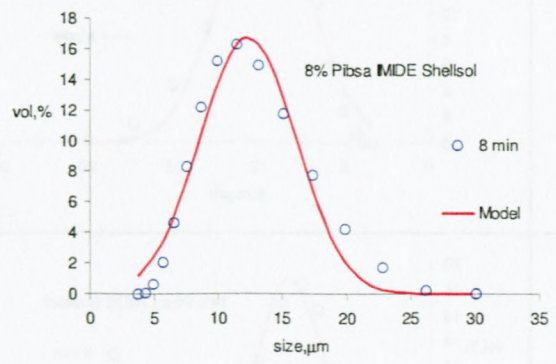

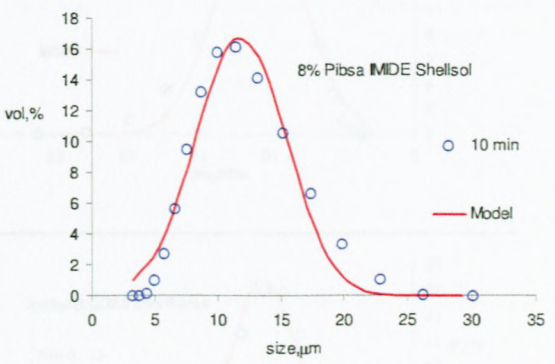

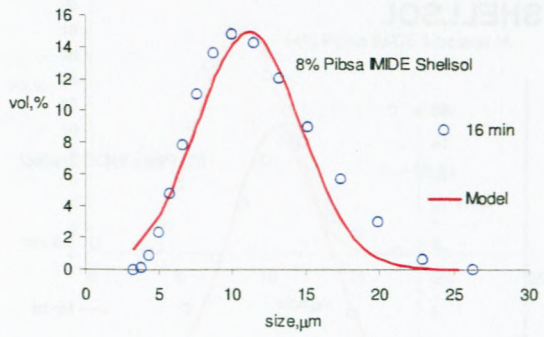
8% Pibsa IMIDE Shellsol
16 min
Model
vol,%
size,µm

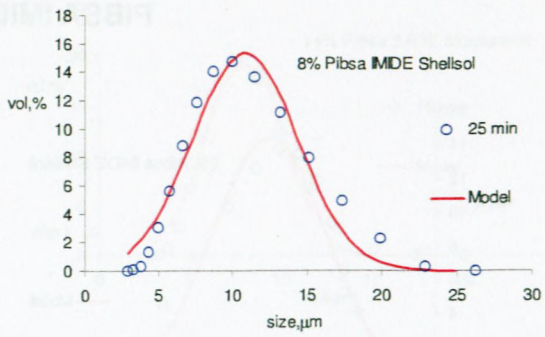
8% Pibsa IMIDE Shellsol
25 min
Model
vol,%
size,µm

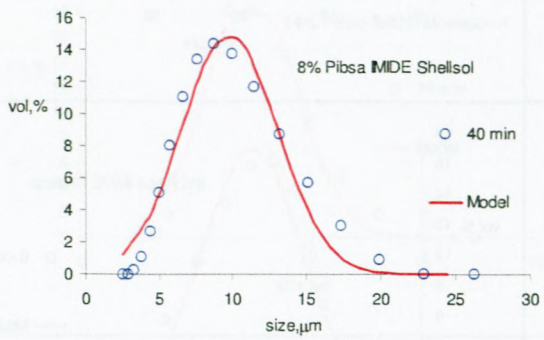
8% Pibsa IMIDE Shellsol
40 min
Model
vol,%
size,µm

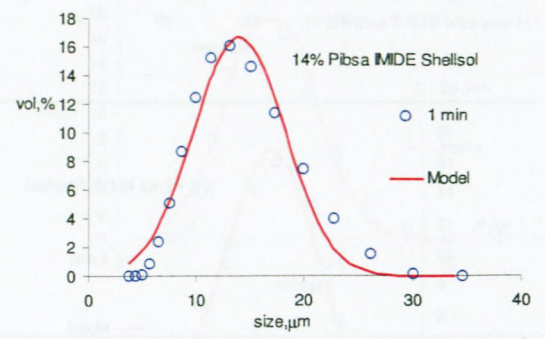
14% Pibsa IMIDE Shellsol
1 min
Model
vol,%
size,µm

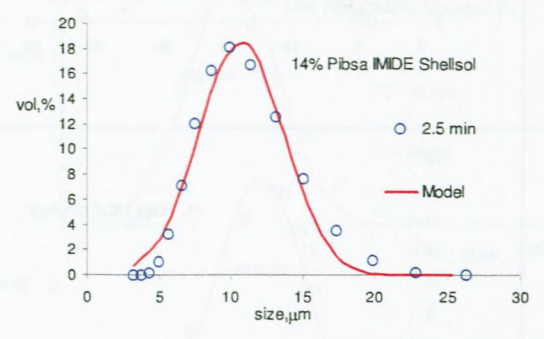
14% Pibsa IMIDE Shellsol
2.5 min
Model
vol,%
size,µm

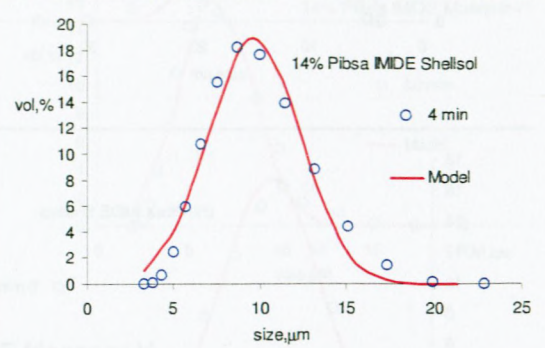
14% Pibsa IMIDE Shellsol
4 min
Model
vol,%
size,µm

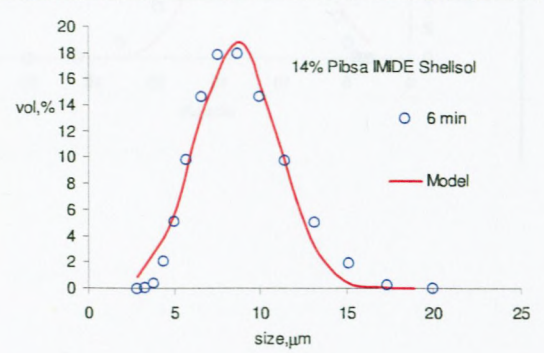
14% Pibsa IMIDE Shellsol
6 min
Model
vol,%
size,µm

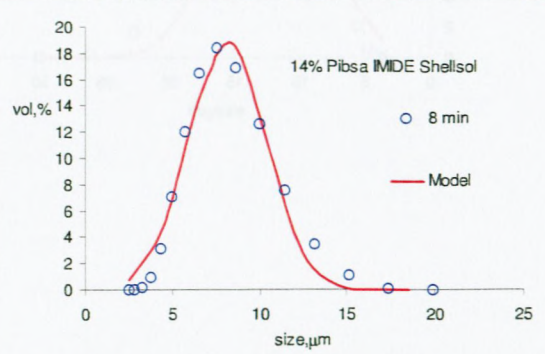
14% Pibsa IMIDE Shellsol
8 min
Model
vol,%
size,µm

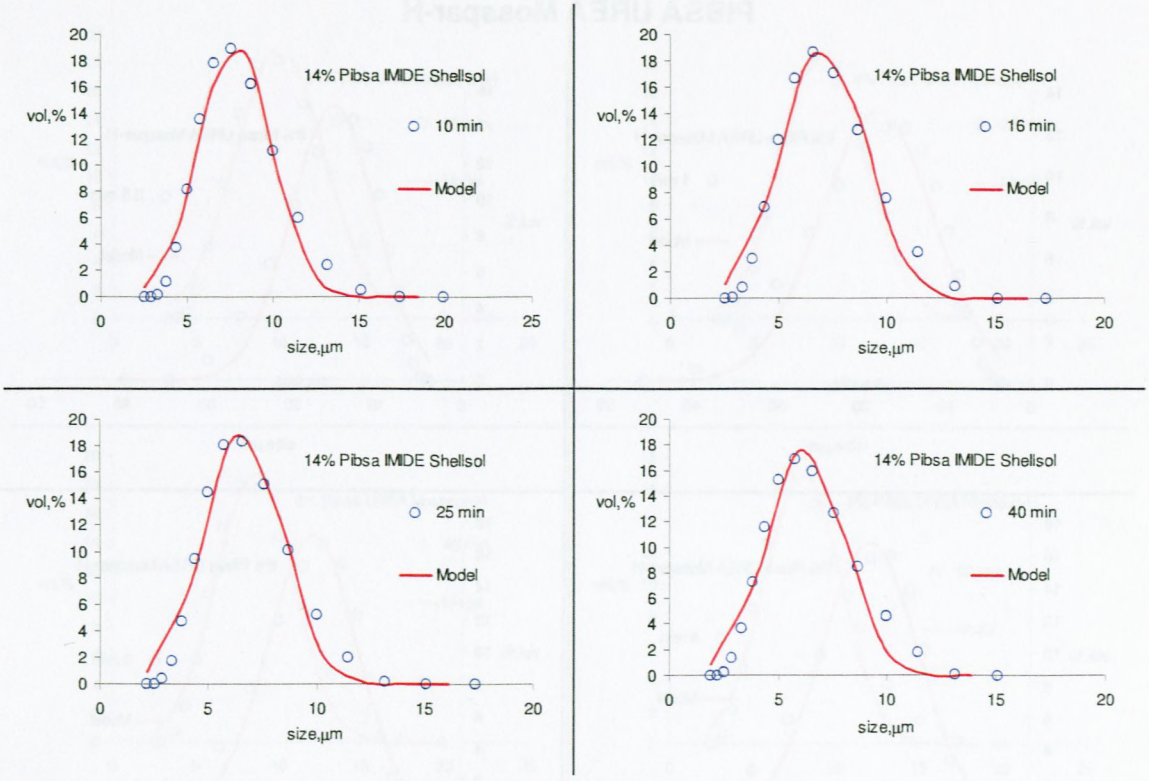

Figure A.3 Pibsa IMIDE Shellsol

PIBSA UREA Mosspar-H

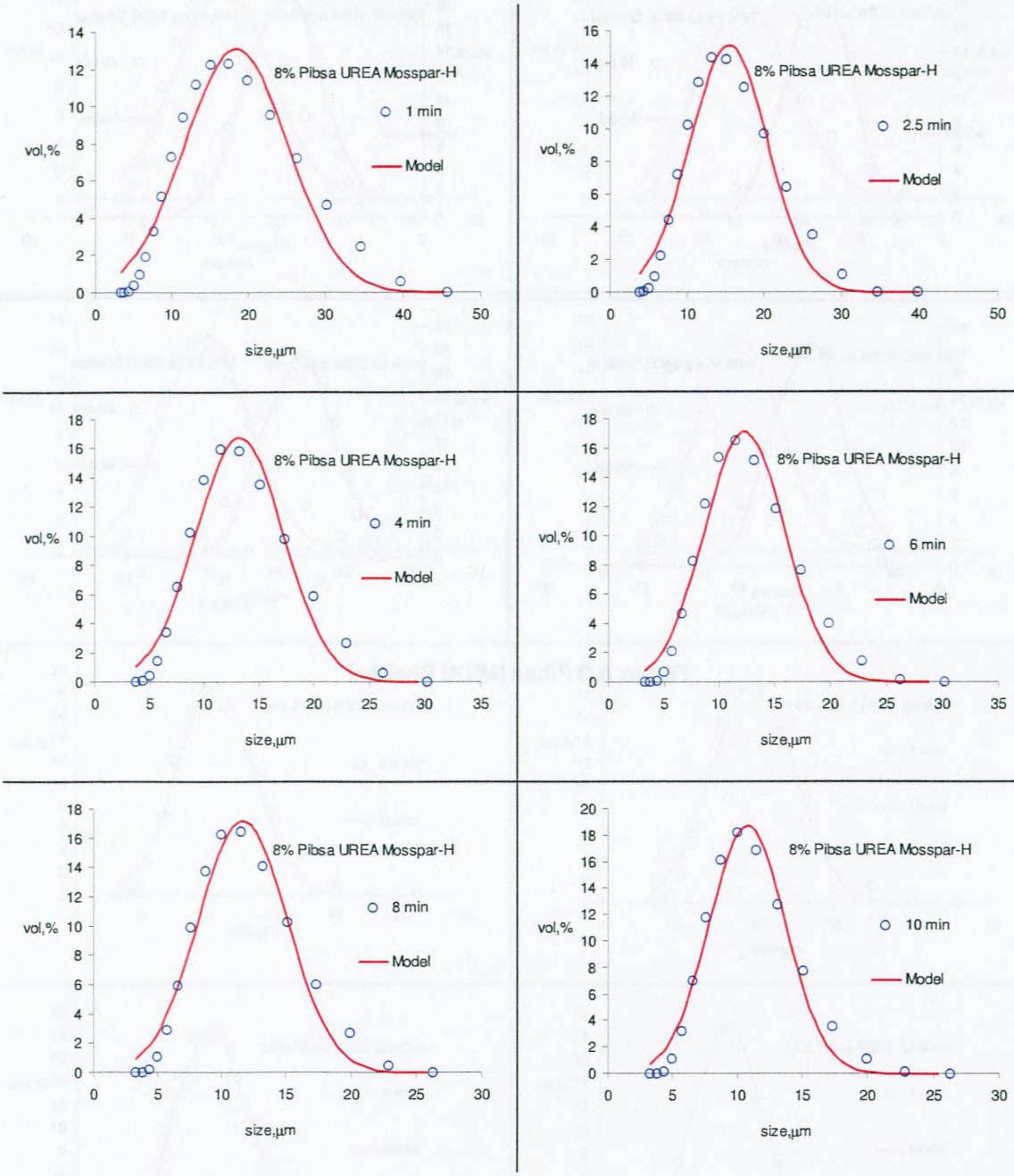

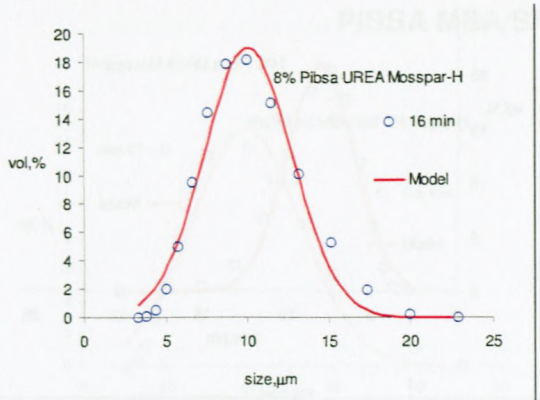
8% Pibsa UREA Mosspar-H
16 min
Model
vol,%
size,µm

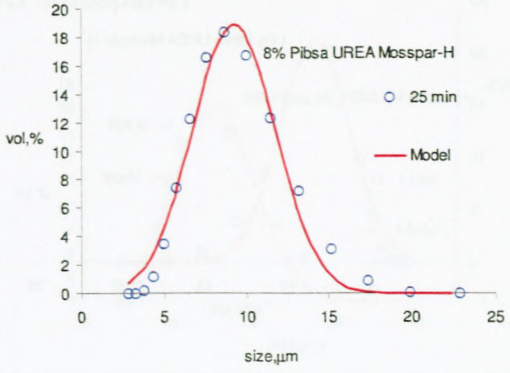
8% Pibsa UREA Mosspar-H
25 min
Model
vol,%
size,µm

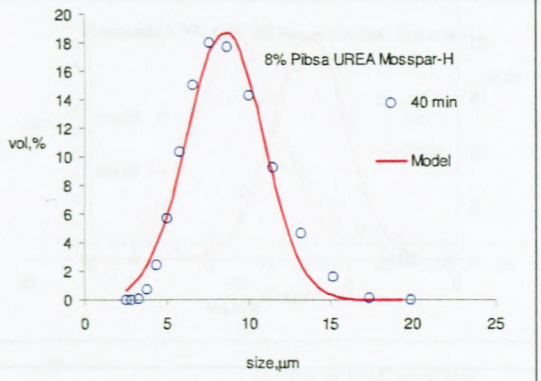
8% Pibsa UREA Mosspar-H
40 min
Model
vol,%
size,µm

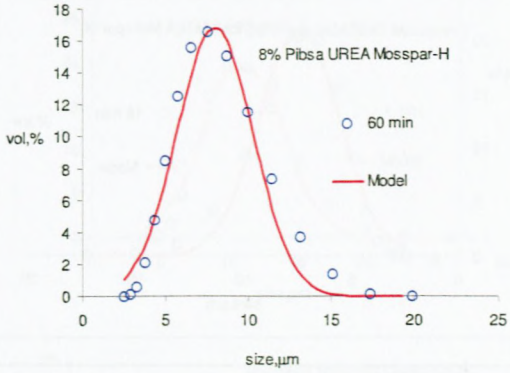
8% Pibsa UREA Mosspar-H
60 min
Model
vol,%
size,µm

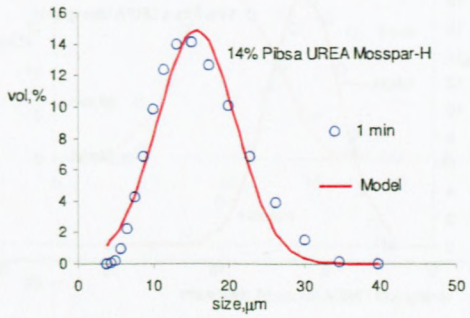
14% Pibsa UREA Mosspar-H
1 min
Model
vol,%
size,µm

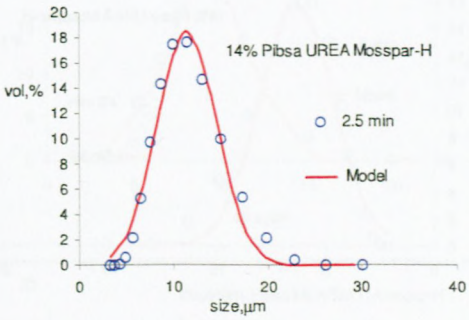
14% Pibsa UREA Mosspar-H
2.5 min
Model
vol,%
size,µm

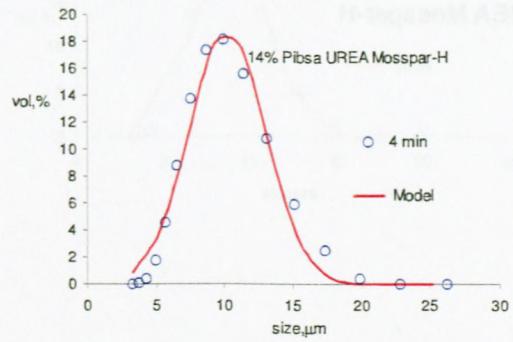
14% Pibsa UREA Mosspar-H
4 min
Model
vol,%
size,µm

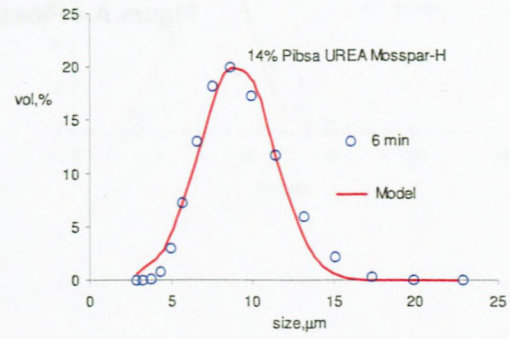
14% Pibsa UREA Mosspar-H
6 min
Model
vol,%
size,µm

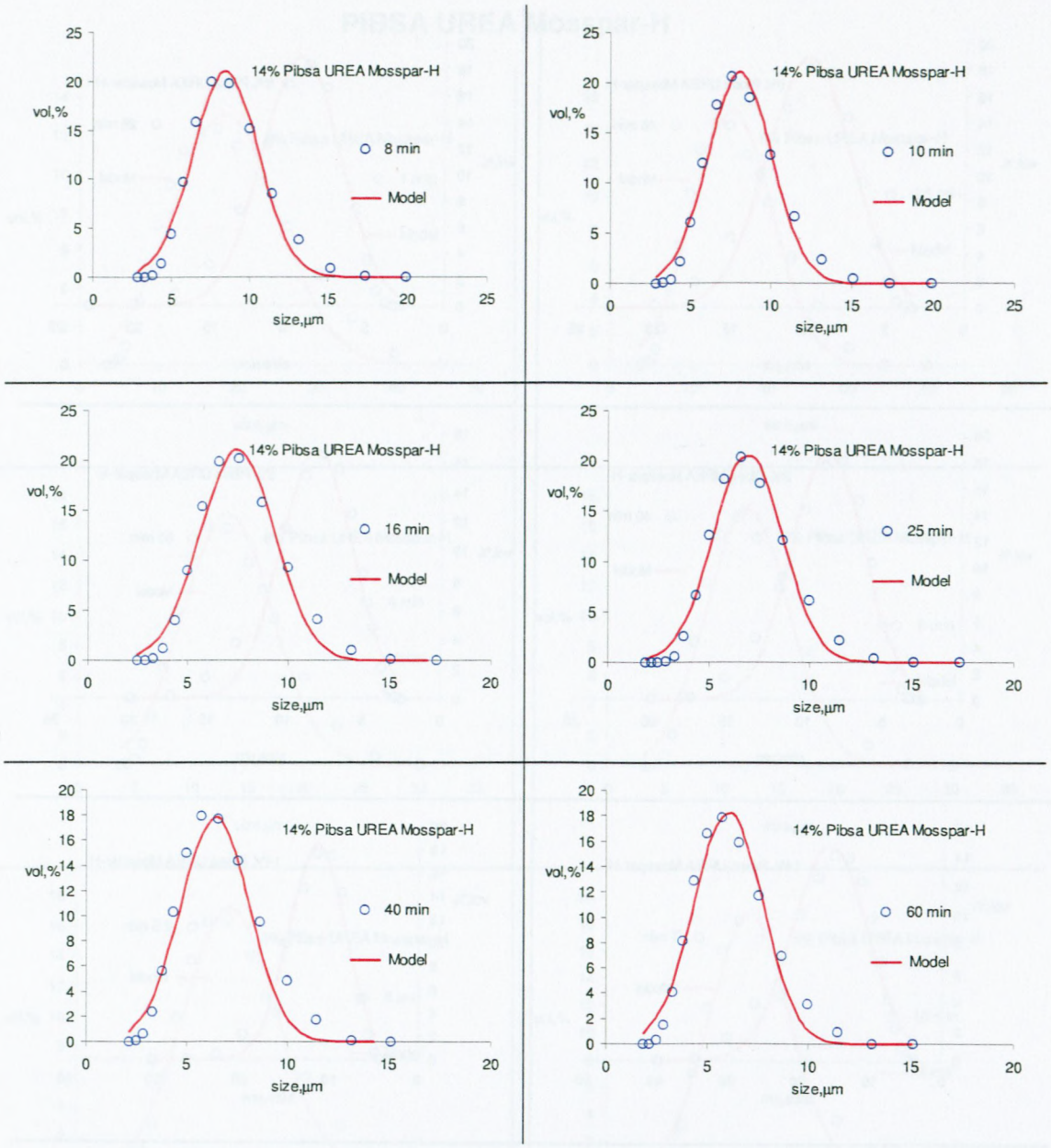

Figure A.4 Pibsa UREA Mosspar-H

PIBSA MEA/SMO Mosspar-H

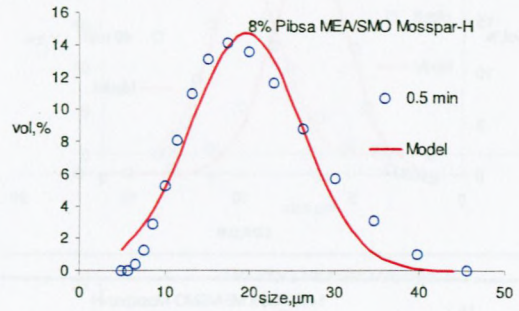

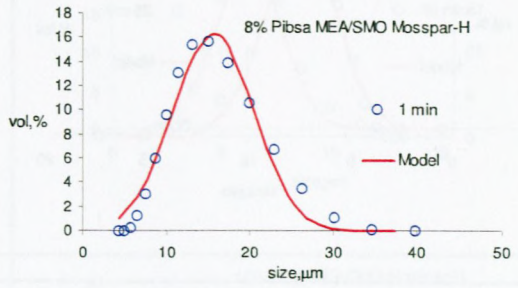

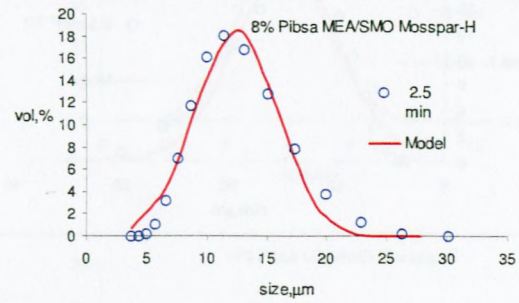

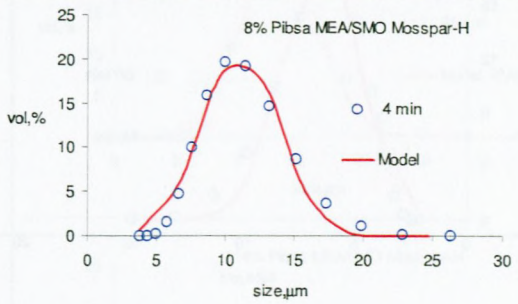

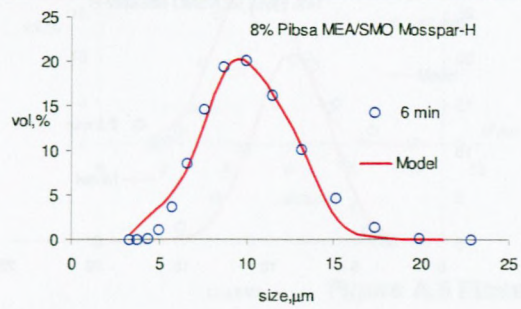

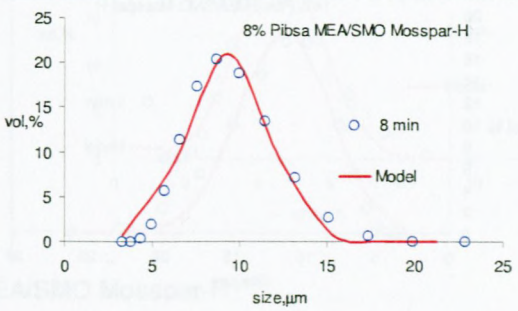

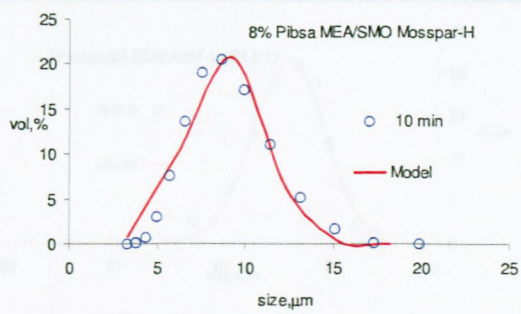

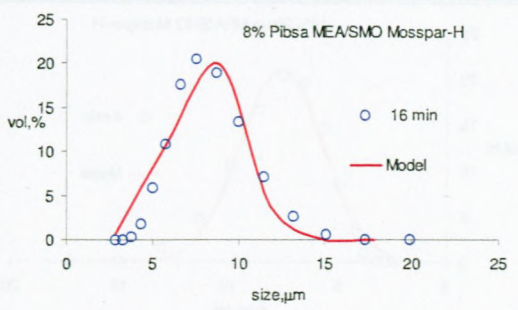

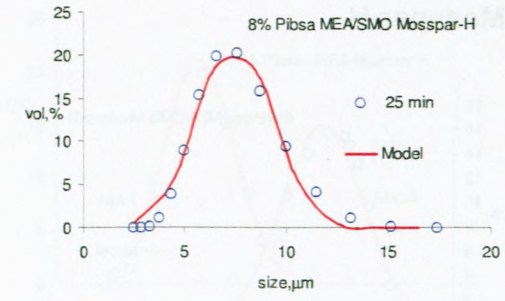
8% Pibsa MEA/SMO Mosspar-H
25 min
Model
vol,%
size,µm

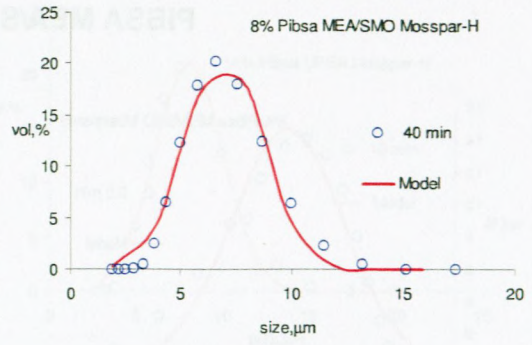
8% Pibsa MEA/SMO Mosspar-H
40 min
Model
vol,%
size,µm

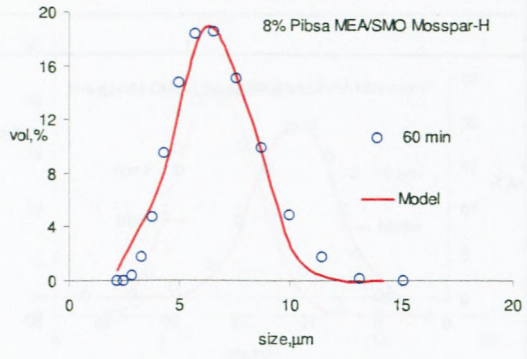
8% Pibsa MEA/SMO Mosspar-H
60 min
Model
vol,%
size,µm

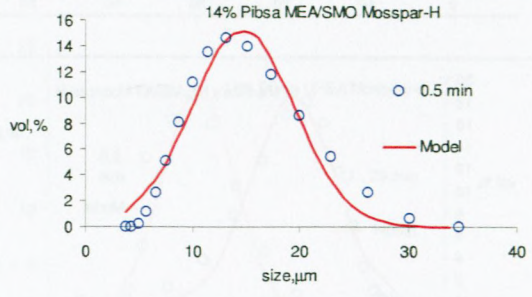
14% Pibsa MEA/SMO Mosspar-H
0.5 min
Model
vol,%
size,µm

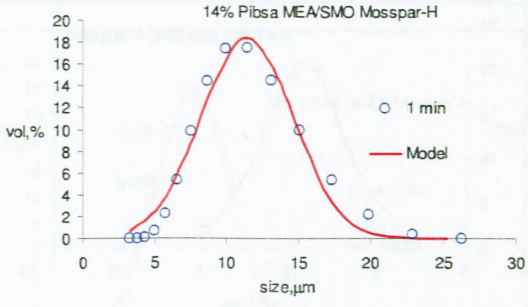
14% Pibsa MEA/SMO Mosspar-H
1 min
Model
vol,%
size,µm

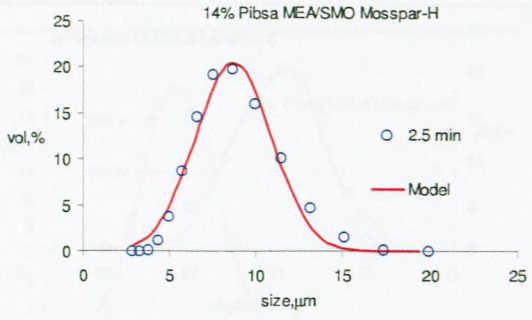
14% Pibsa MEA/SMO Mosspar-H
2.5 min
Model
vol,%
size,µm

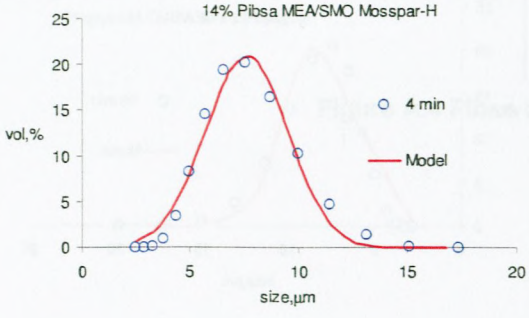
14% Pibsa MEA/SMO Mosspar-H
4 min
Model
vol,%
size,µm

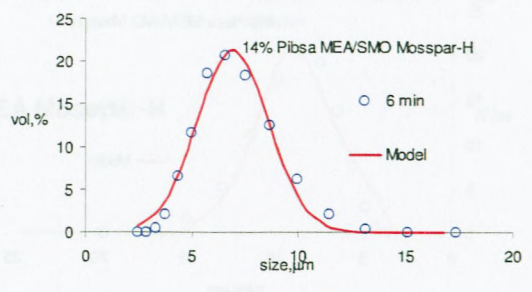
14% Pibsa MEA/SMO Mosspar-H
6 min
Model
vol,%
size,µm

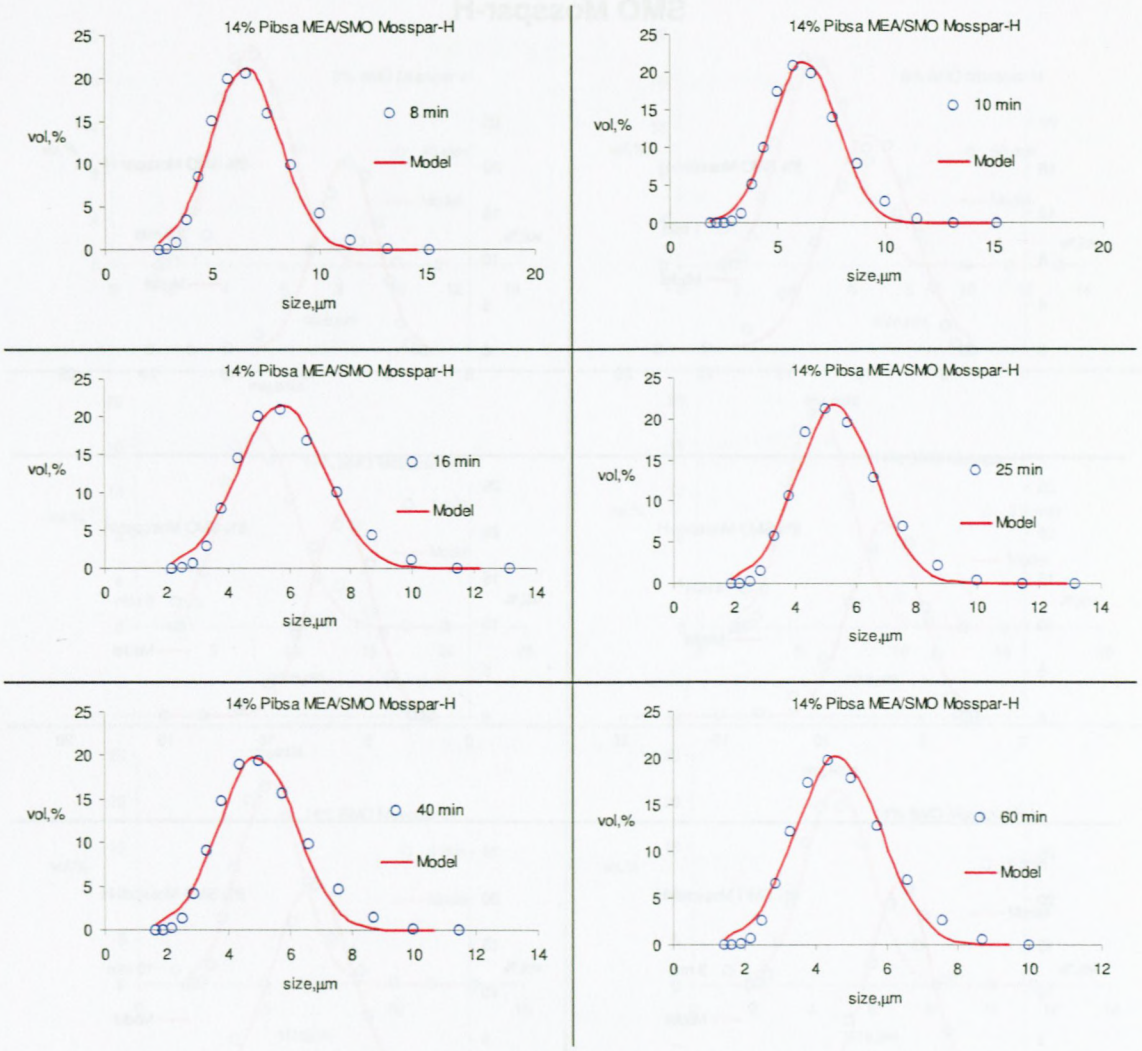

Figure A.5 Pibsa MEA/SMO Mosspar-H

SMO Mosspar-H

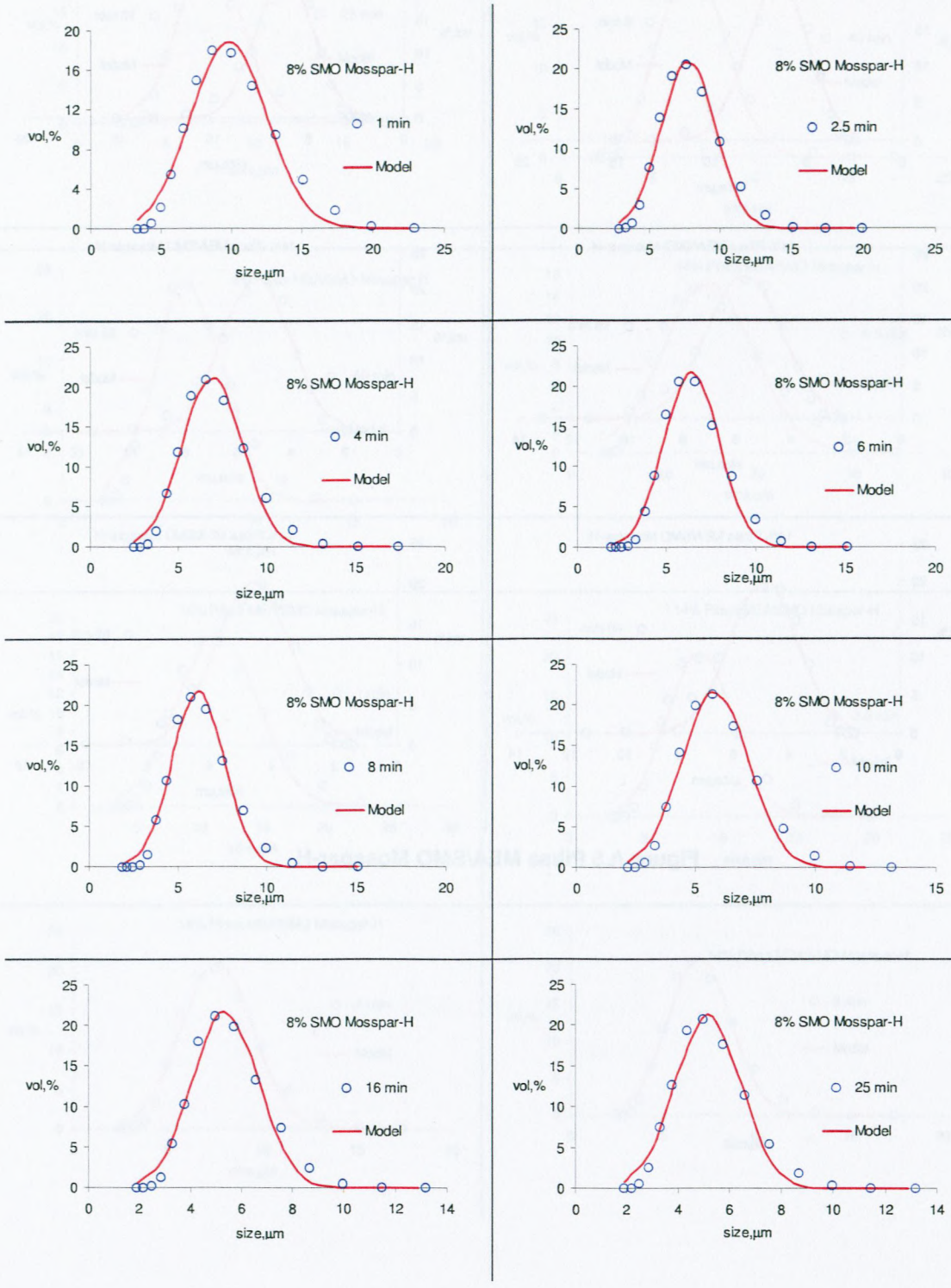

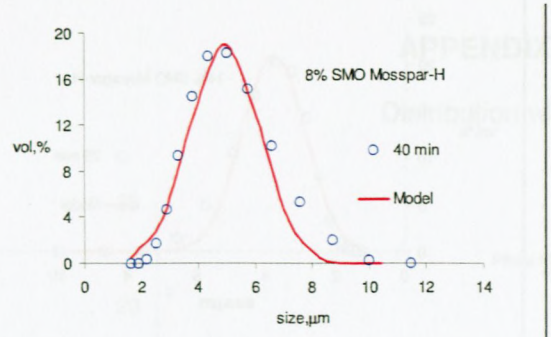
8% SMO Mosspar-H
40 min
Model
vol,%
size,µm

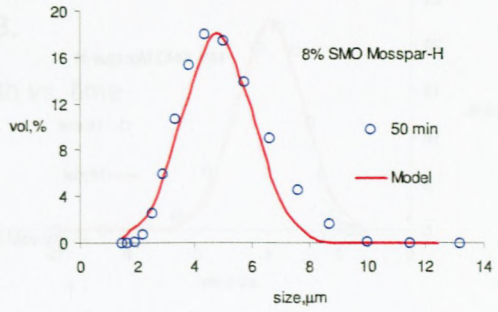
8% SMO Mosspar-H
50 min
Model
vol,%
size,µm

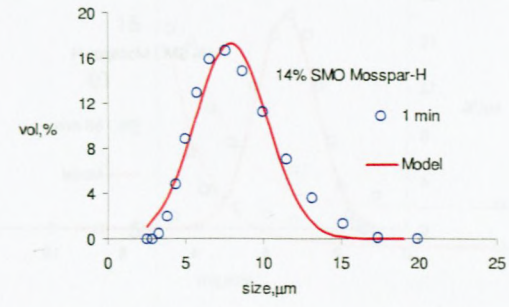
14% SMO Mosspar-H
1 min
Model
vol,%
size,µm

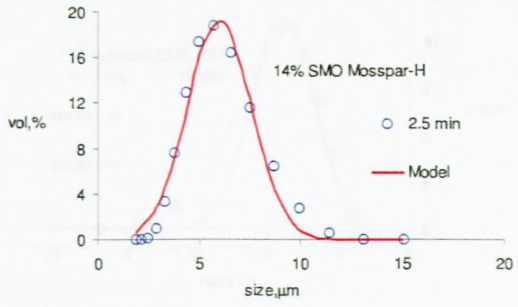
14% SMO Mosspar-H
2.5 min
Model
vol,%
size,µm

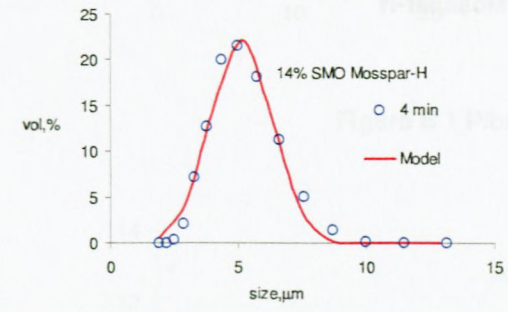
14% SMO Mosspar-H
4 min
Model
vol,%
size,µm

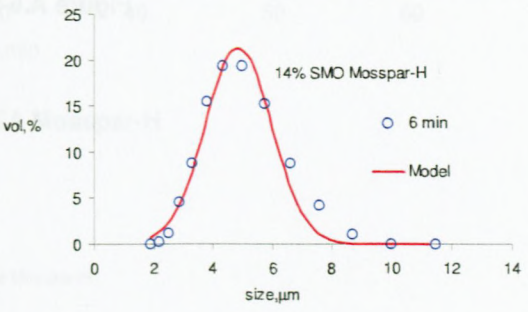
14% SMO Mosspar-H
6 min
Model
vol,%
size,µm

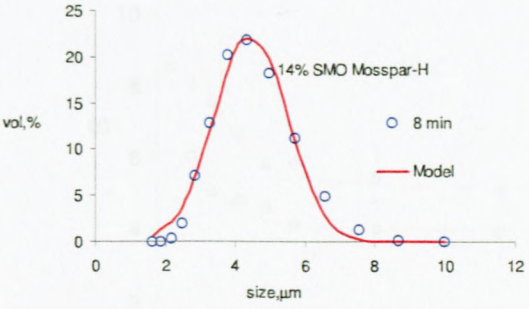
14% SMO Mosspar-H
8 min
Model
vol,%
size,µm

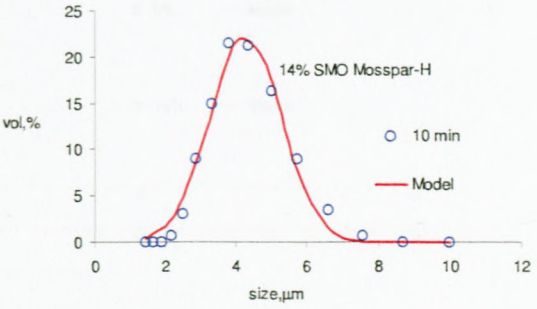
14% SMO Mosspar-H
10 min
Model
vol,%
size,µm

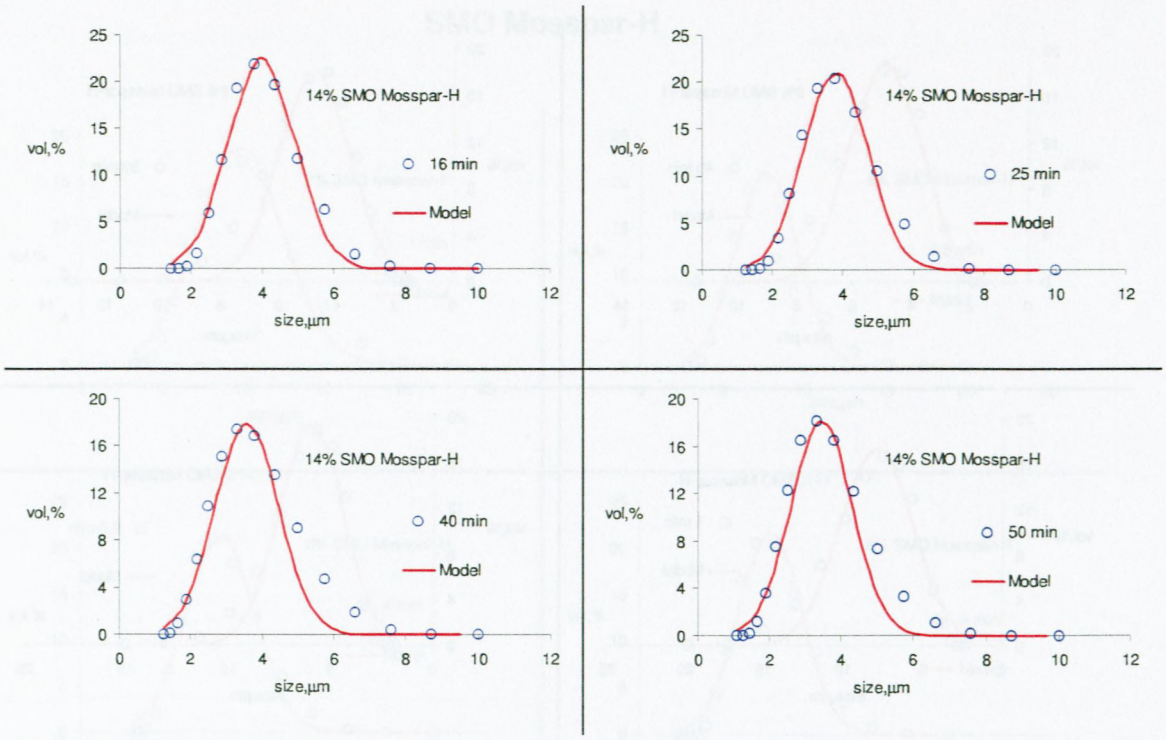

Figure A.6 SMO Mosspar-H

APPENDIX B.

Distribution width vs. time

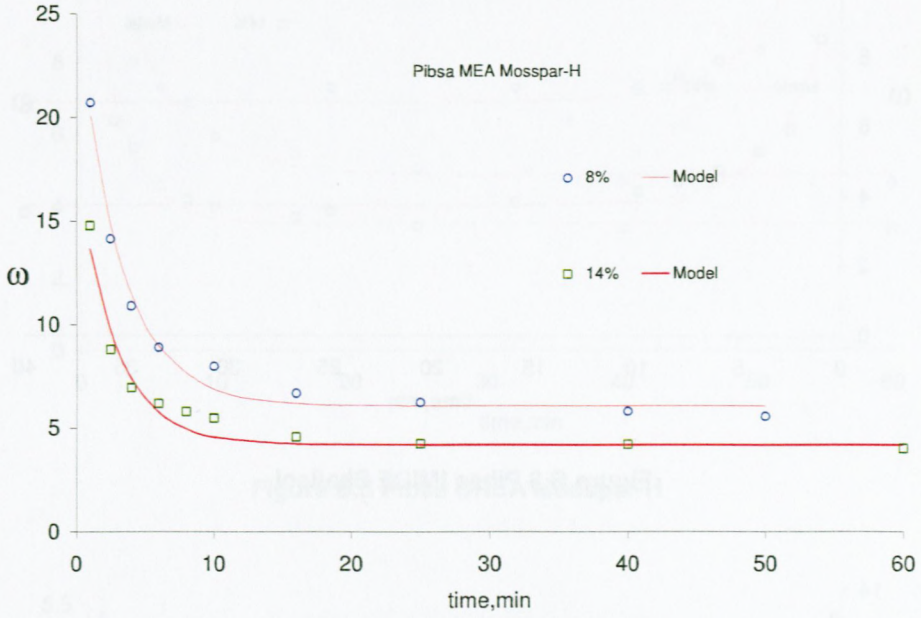

Figure B.1 Pibsa MEA Mosspar-H

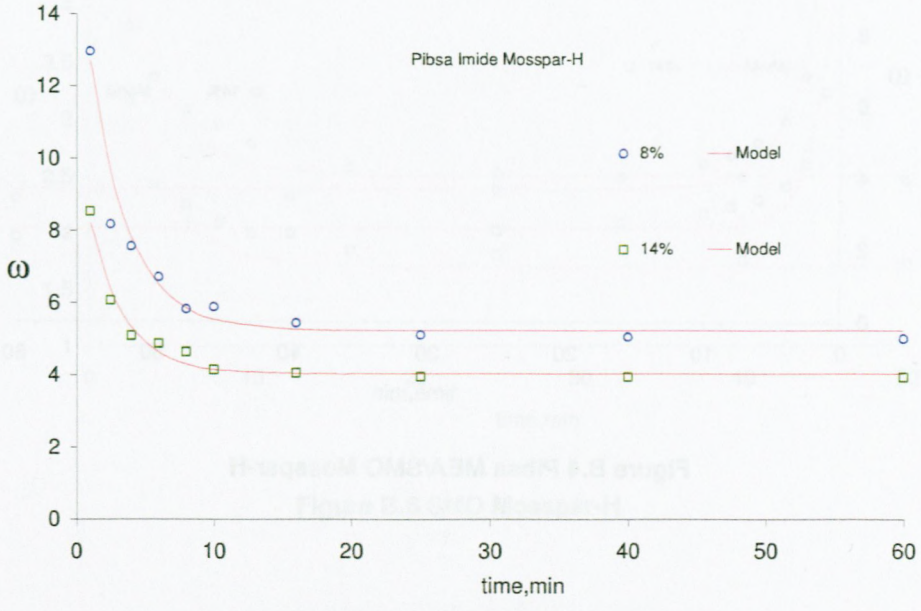

Figure B.2 Pibsa IMIDE Mosspar-H

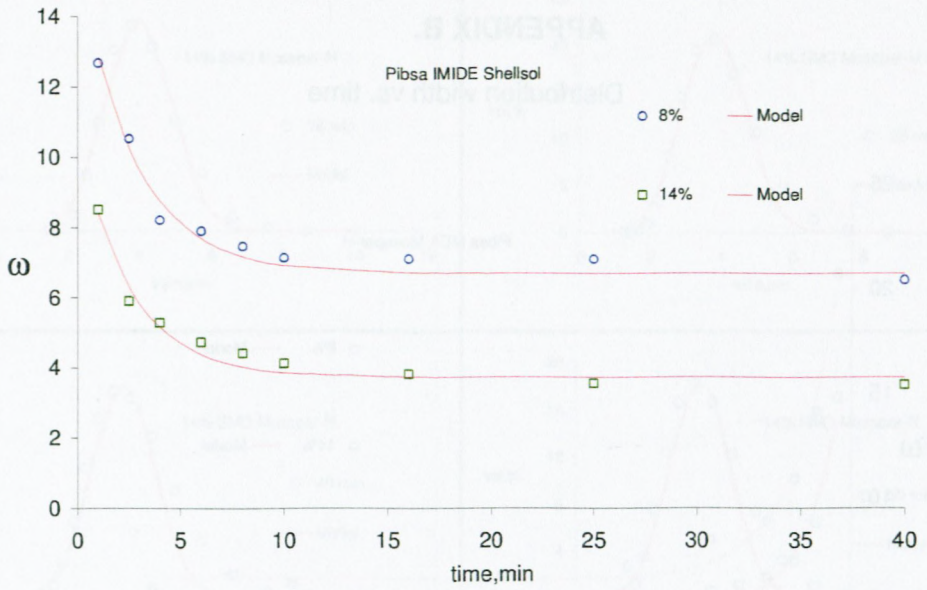

Figure B.3 Pibsa IMIDE Shellsol

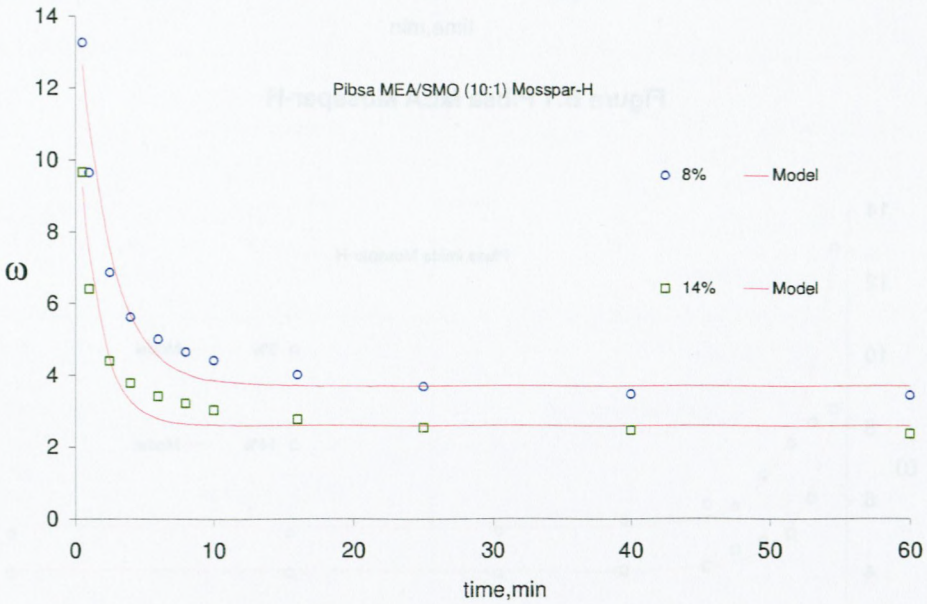

Figure B.4 Pibsa MEA/SMO Mosspar-H

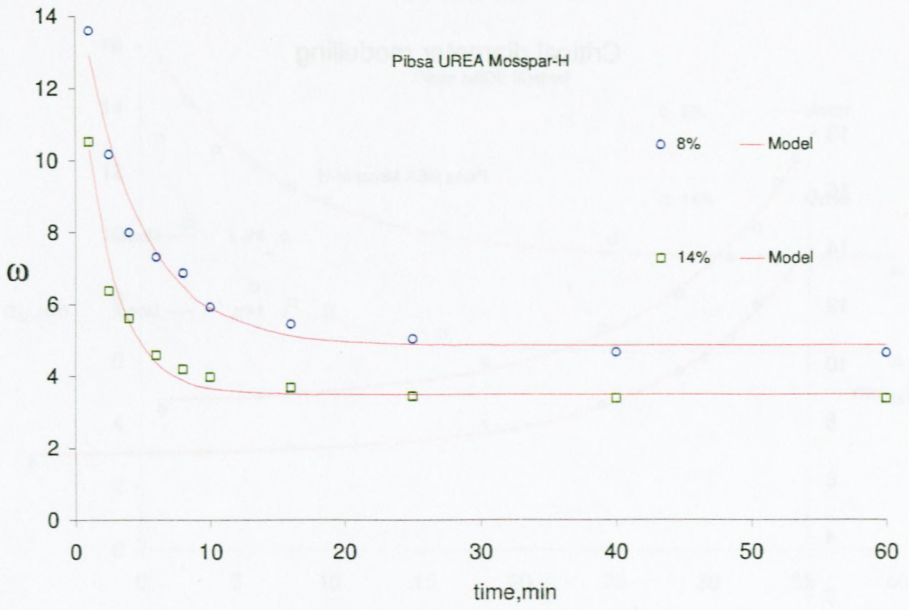

Figure B.5 Pibsa UREA Mosspar-H

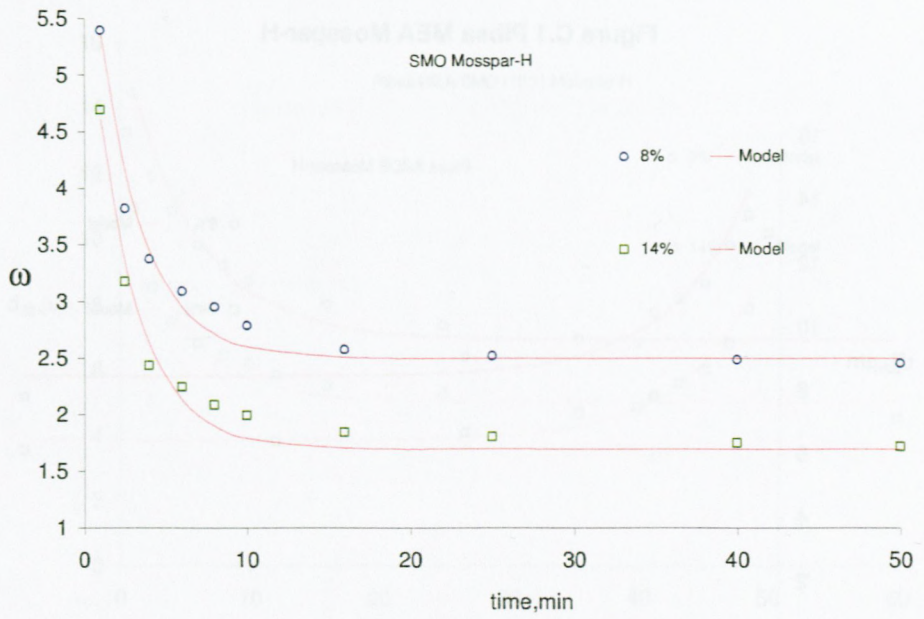

Figure B.6 SMO Mosspar-H

APPENDIX C.

Critical diameter modelling

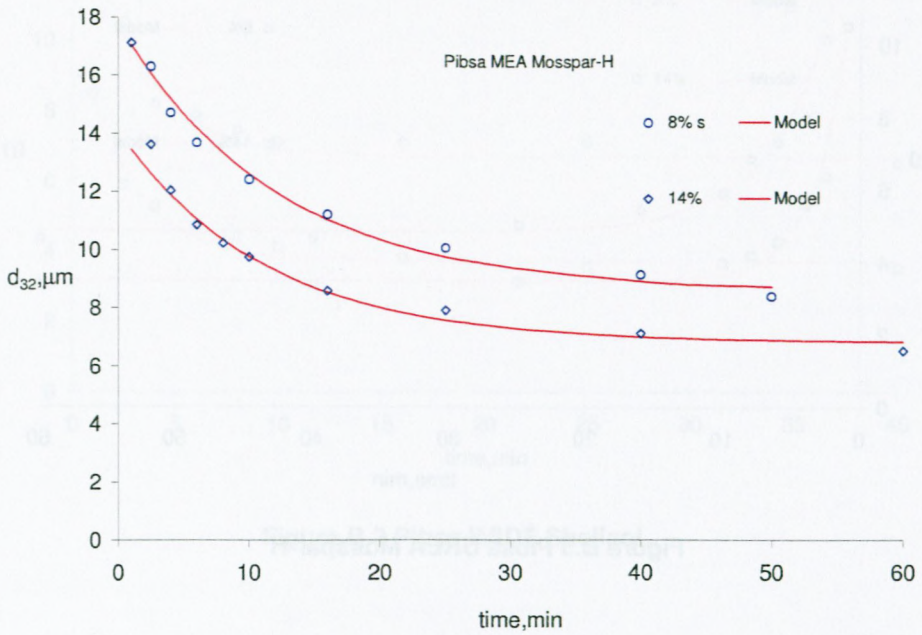

Figure C.1 Pibsa MEA Mosspar-H

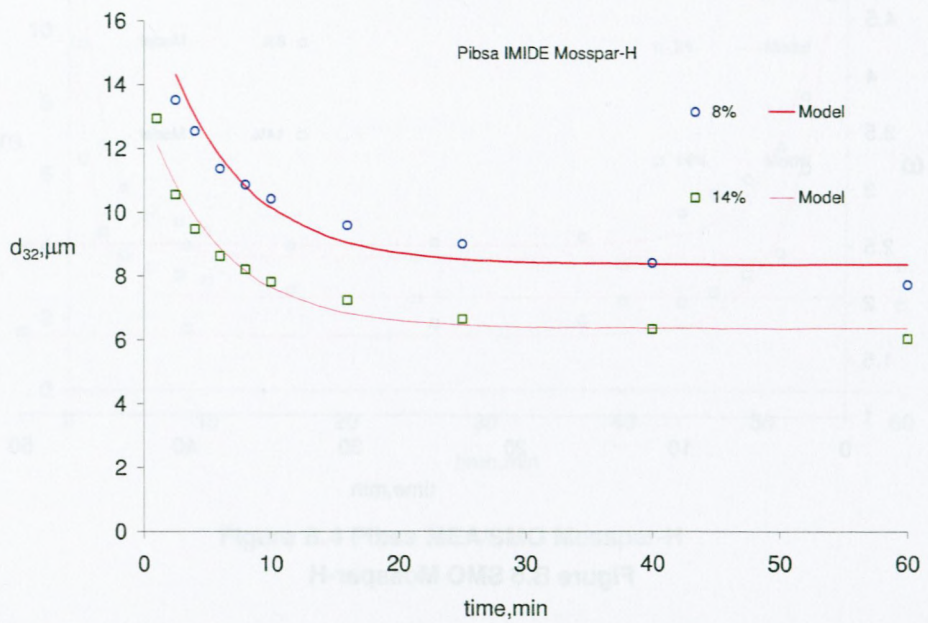

Figure C.2 Pibsa IMIDE Mosppar-H

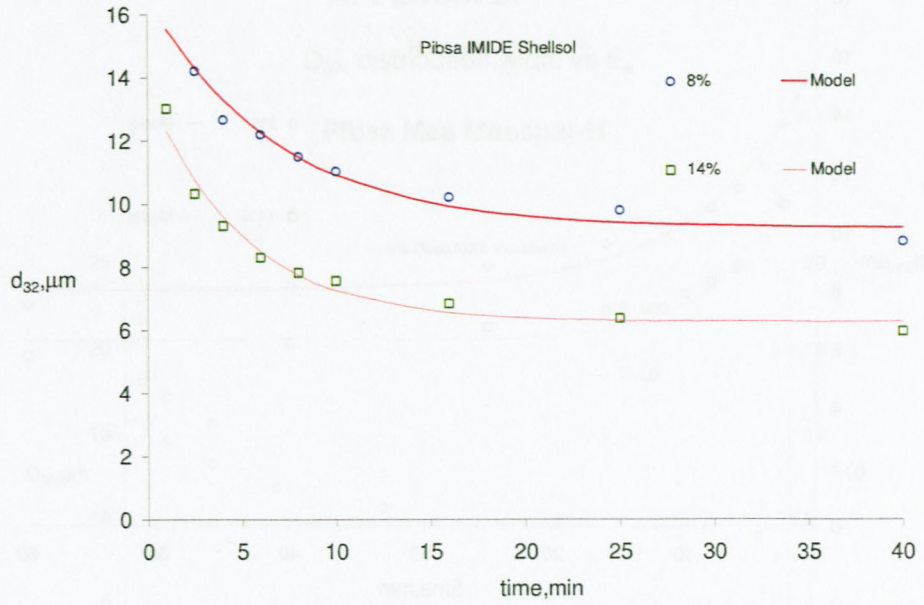

Figure C.3 Pibsa IMIDE Shellsol

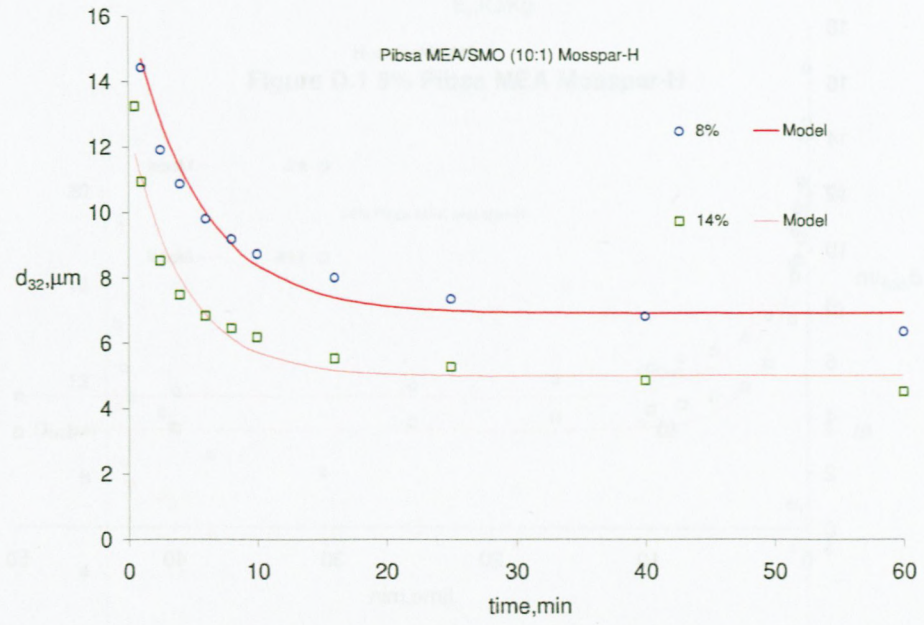

Figure C.4 Pibsa MEA/SMO Mosspar-H

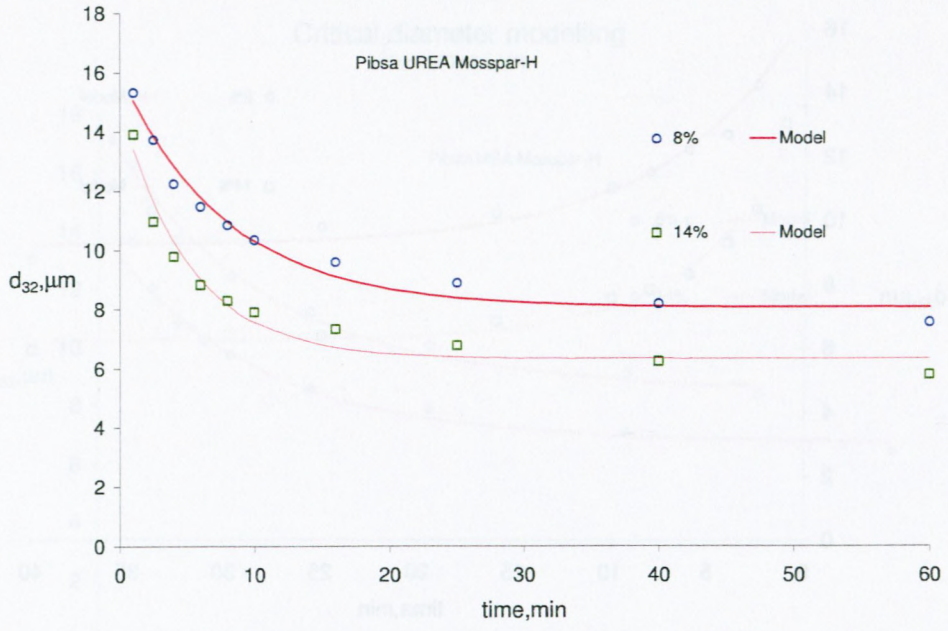

Figure C.5 Pibsa UREA Mosspar-H

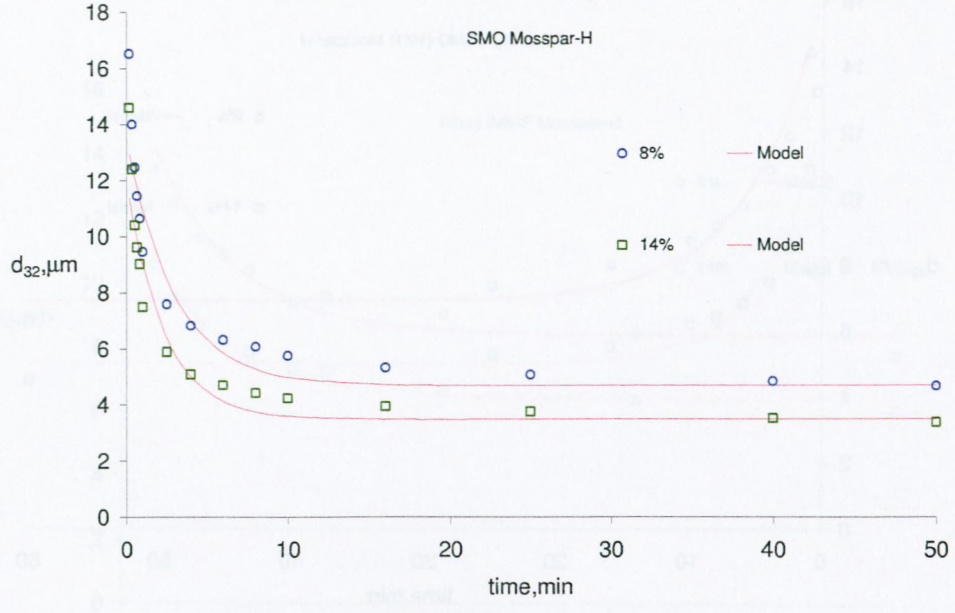

Figure C.6 SMO Mosspar-H

APPENDIX D.

D_{50}, distribution width vs E_ρ

Pibsa Mea Mosspar-H

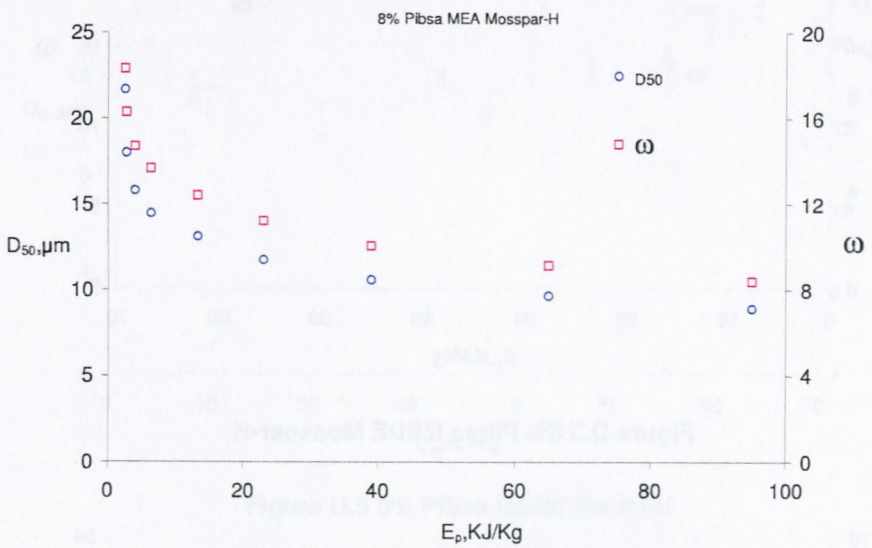

Figure D.1 8% Pibsa MEA Mosspar-H

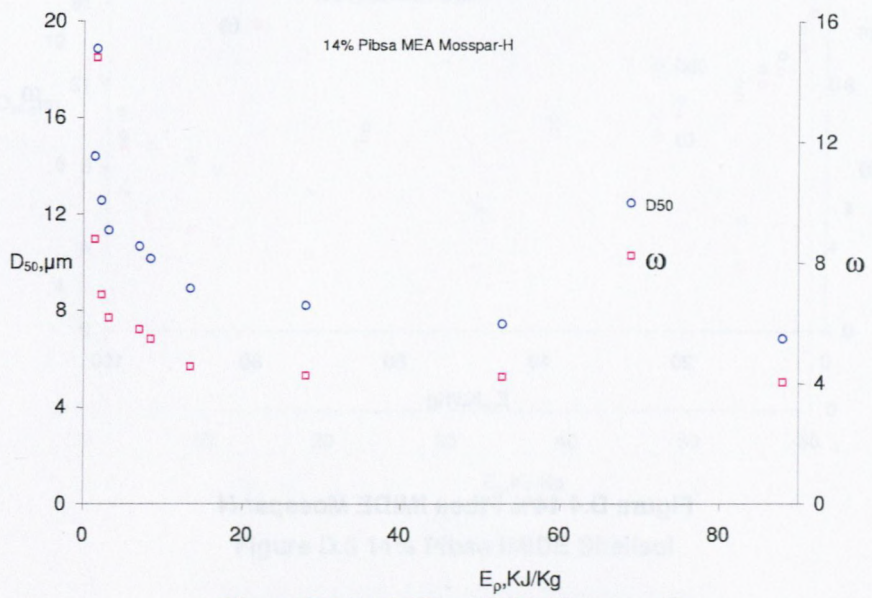

Figure D.2 14% Pibsa MEA Mosspar-H

Pibsa Imide Mosspar-H

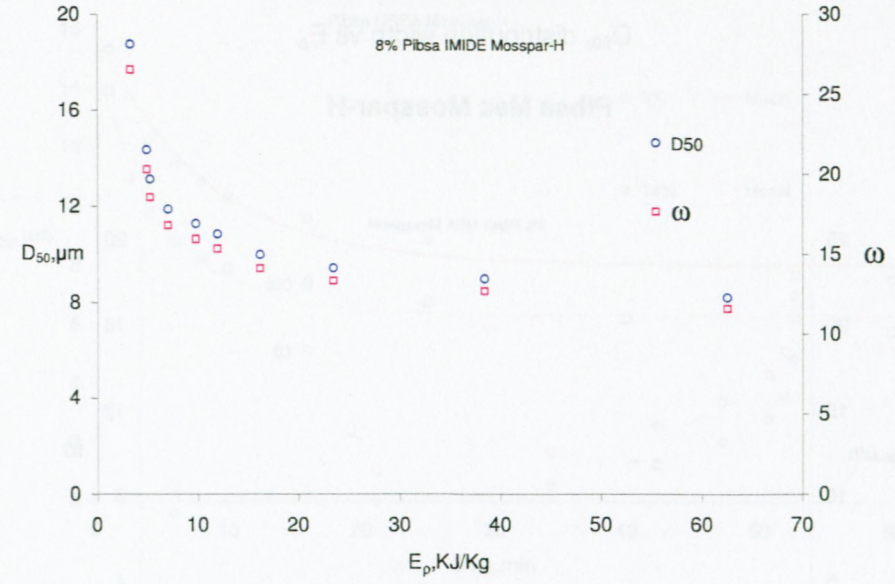

Figure D.3 8% Pibsa IMIDE Mosspar-H

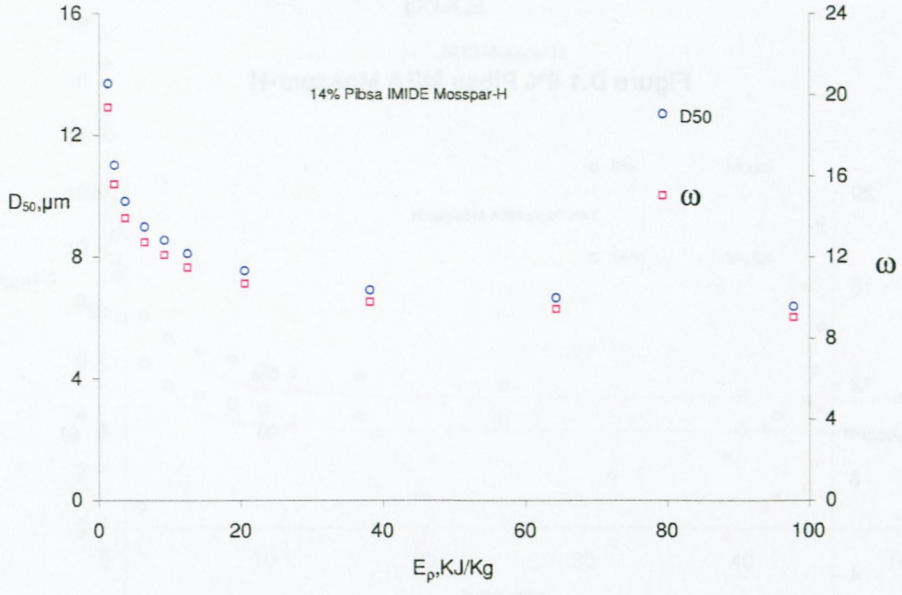

Figure D.4 14% Pibsa IMIDE Mosspar-H

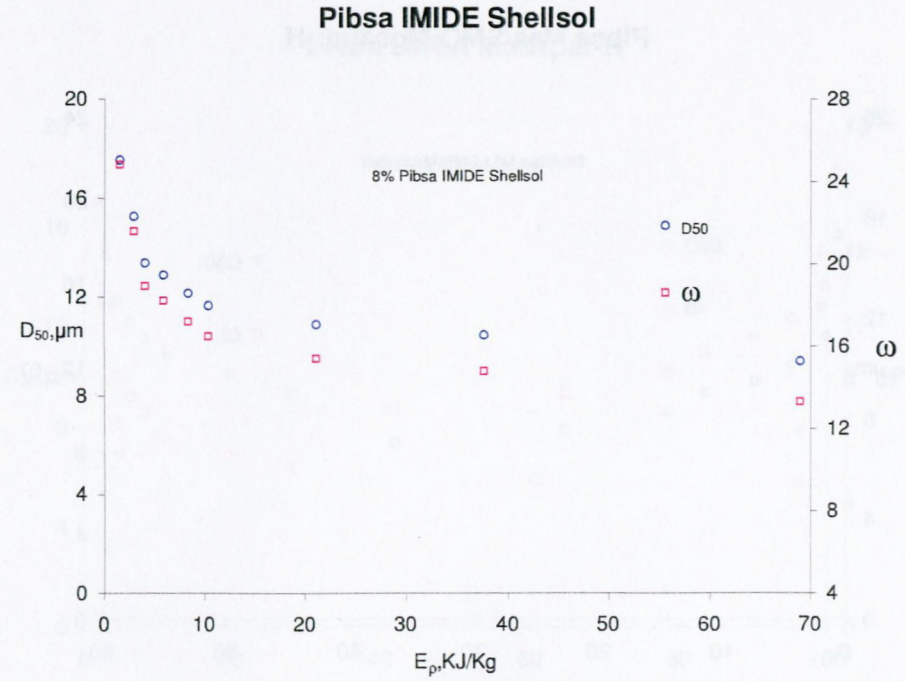

Figure D.5 8% Pibsa IMIDE Shellsol

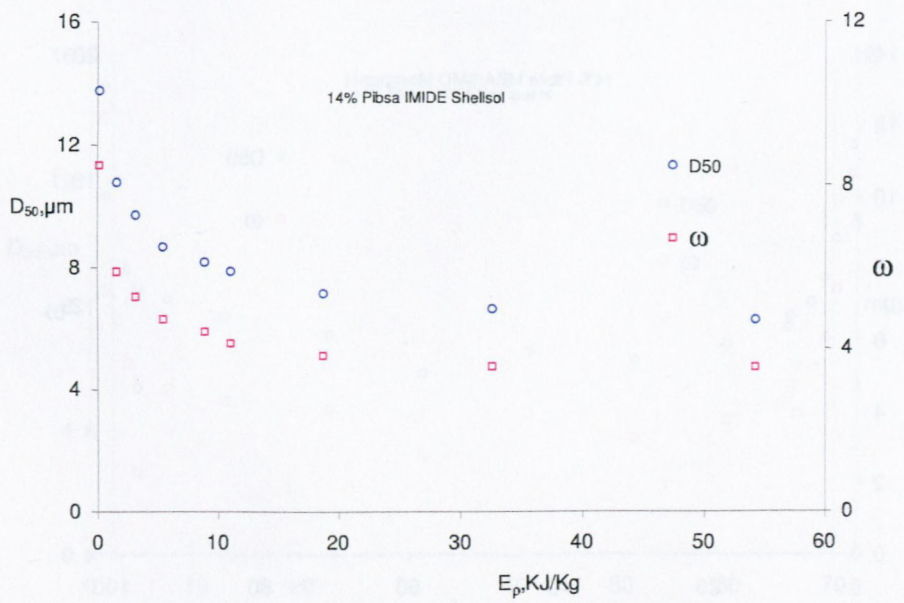

Figure D.6 14% Pibsa IMIDE Shellsol

Pibsa Mea/SMO Mosspar-H

Figure D.7 8% Pibsa MEA/SMO Mosspar-H

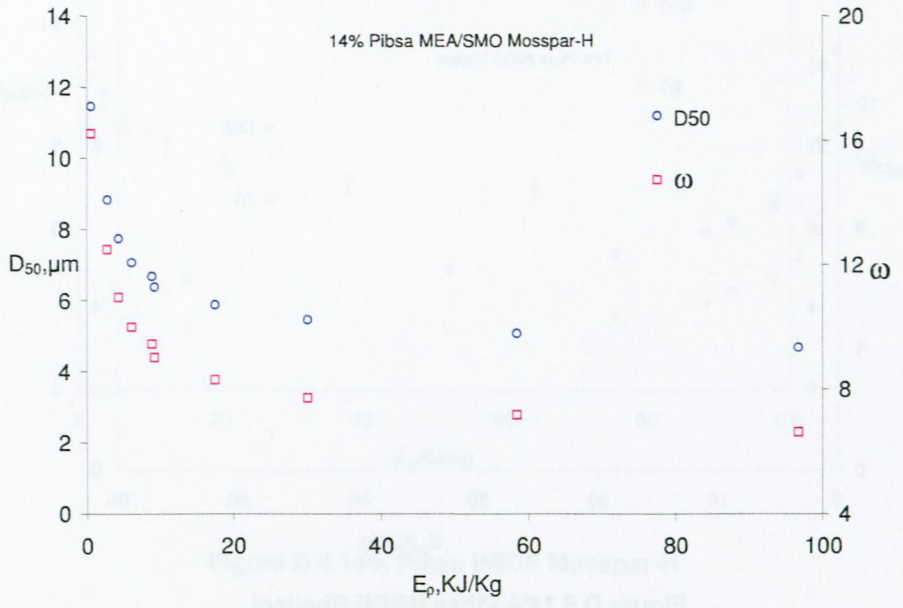

Figure D.8 14% Pibsa MEA/SMO Mosspar-H

Pibsa UREA Mosspar-H

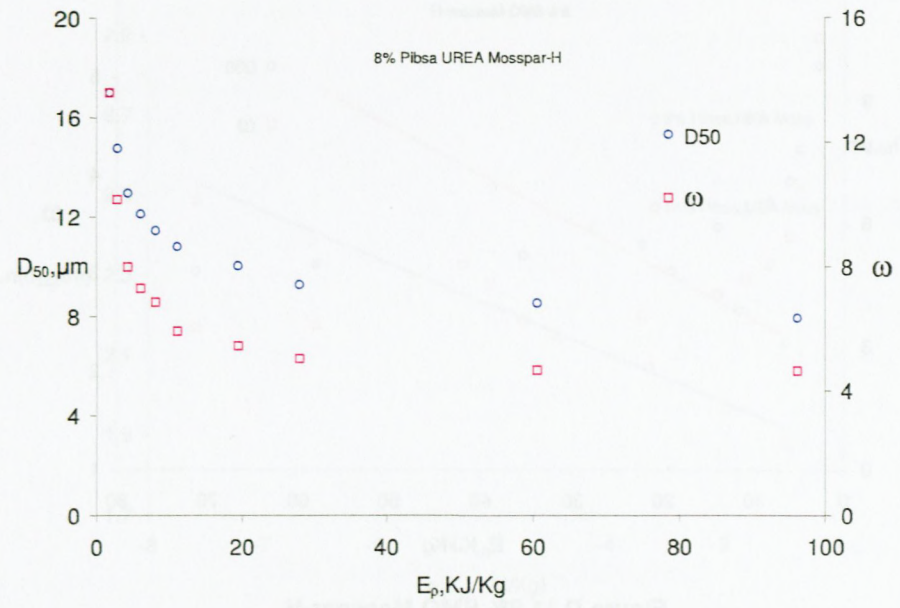

Figure D.9 8% Pibsa UREA Mosspar-H

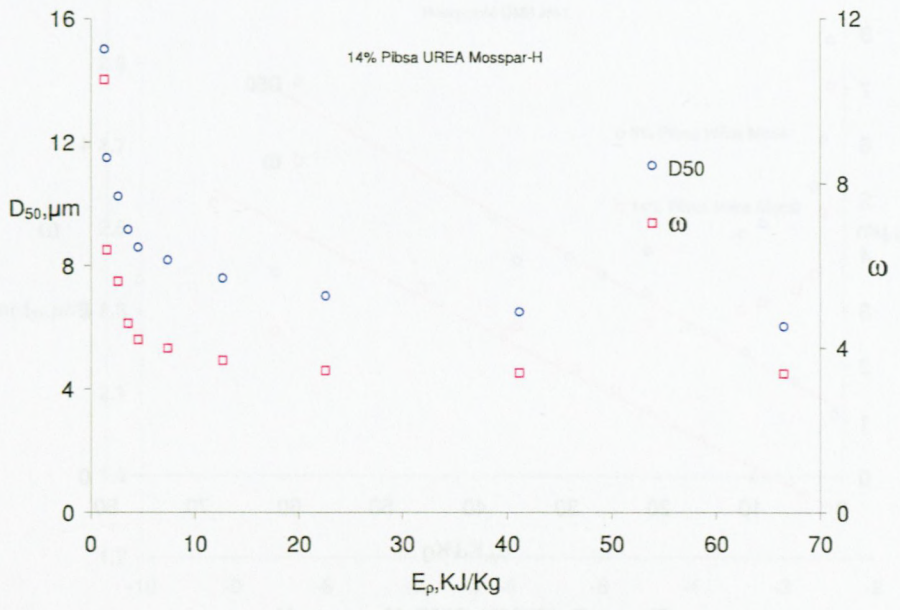

Figure D.10 14% Pibsa UREA Mosspar-H

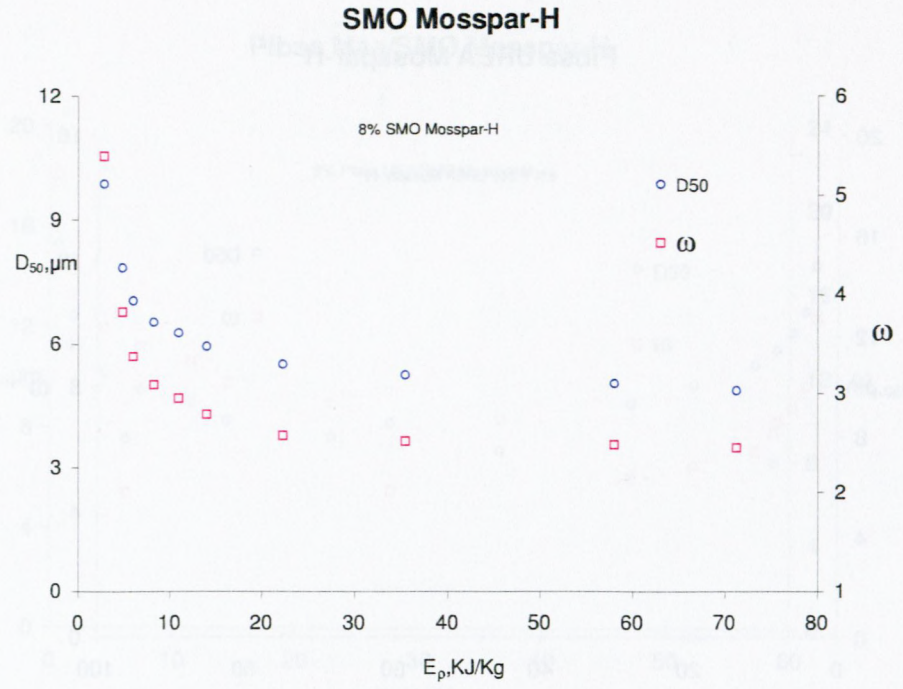

Figure D.11 8% SMO Mosspar-H

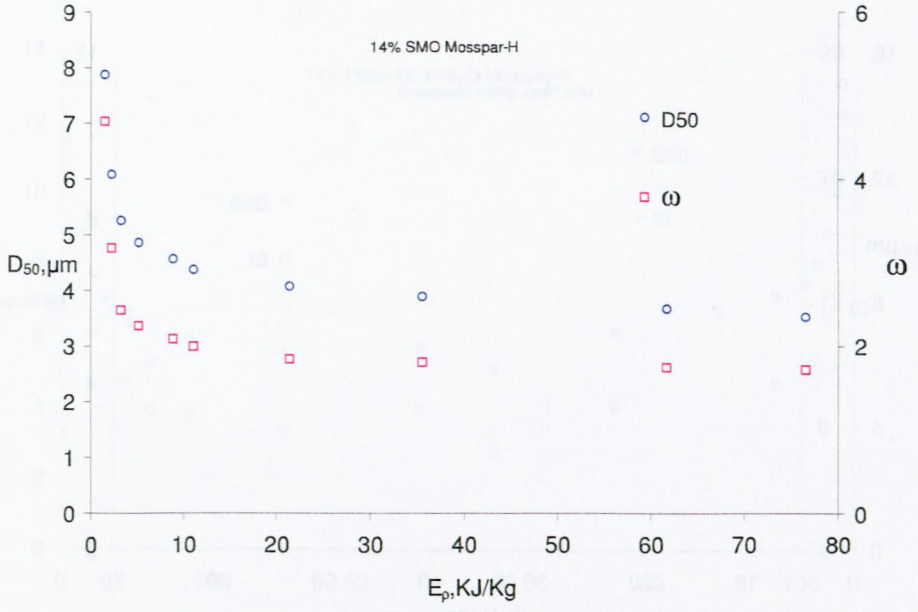

Figure D.12 14% SMO Mosspar-H

APPENDIX E.

Power law fitting

Pibsa MEA Mosspar-H

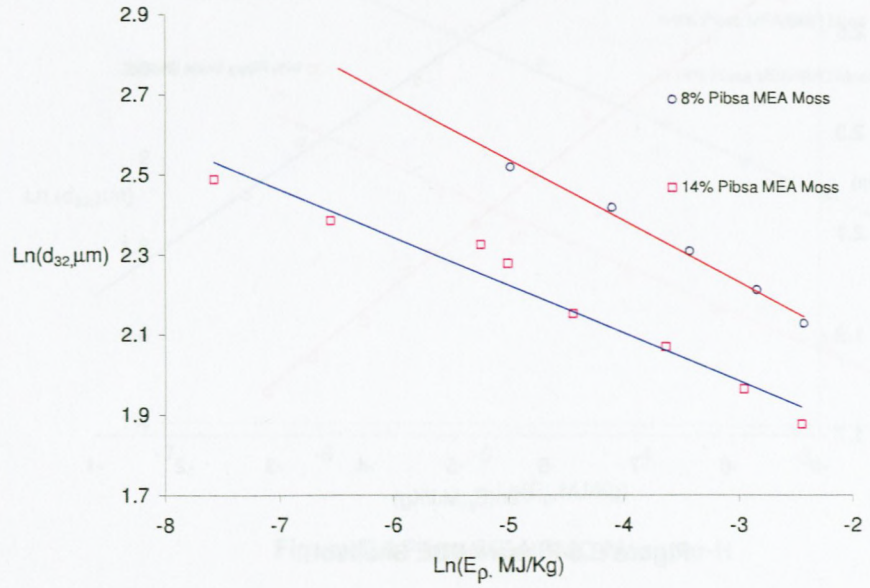

Figure E.1 Pibsa MEA Mosspar-H

Pibsa Imide Mosspar-H

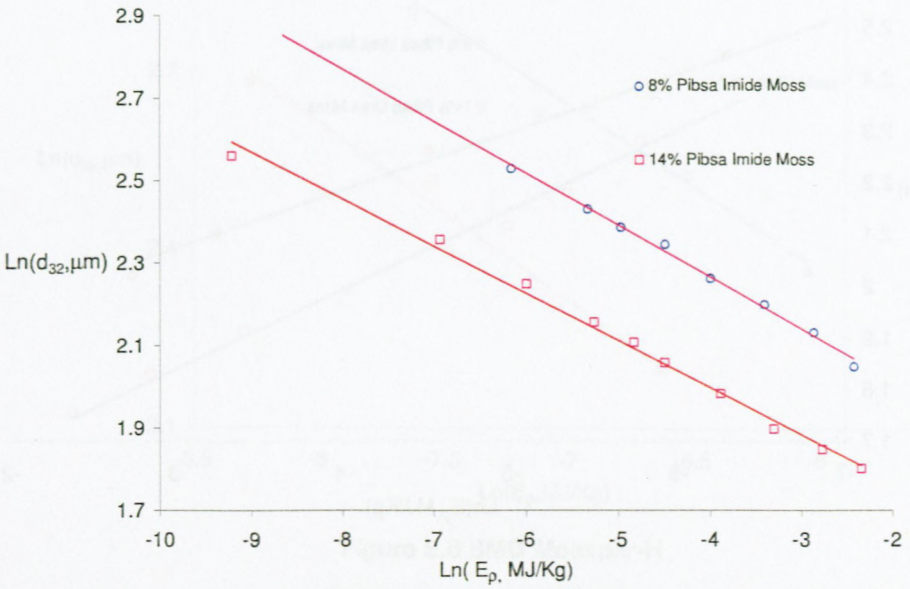

Figure E.2 Pibsa IMIDE Mosspar-H

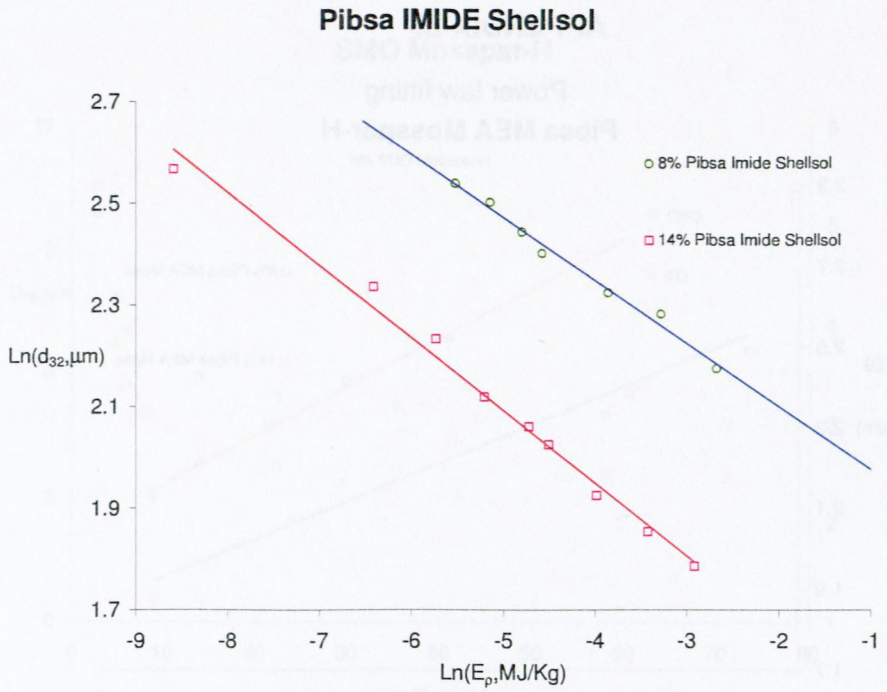

Figure E.3 Pibsa IMIDE Shellsol

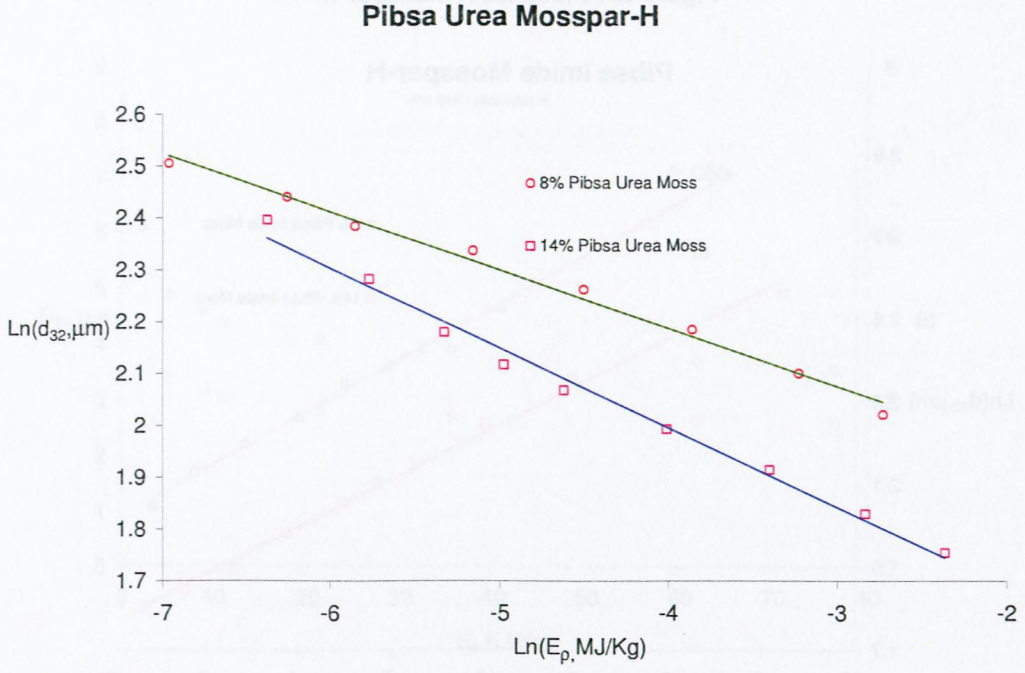

Figure E.4 Pibsa UREA Mosspar-H

Pibsa MEA/SMO Mosspar-H

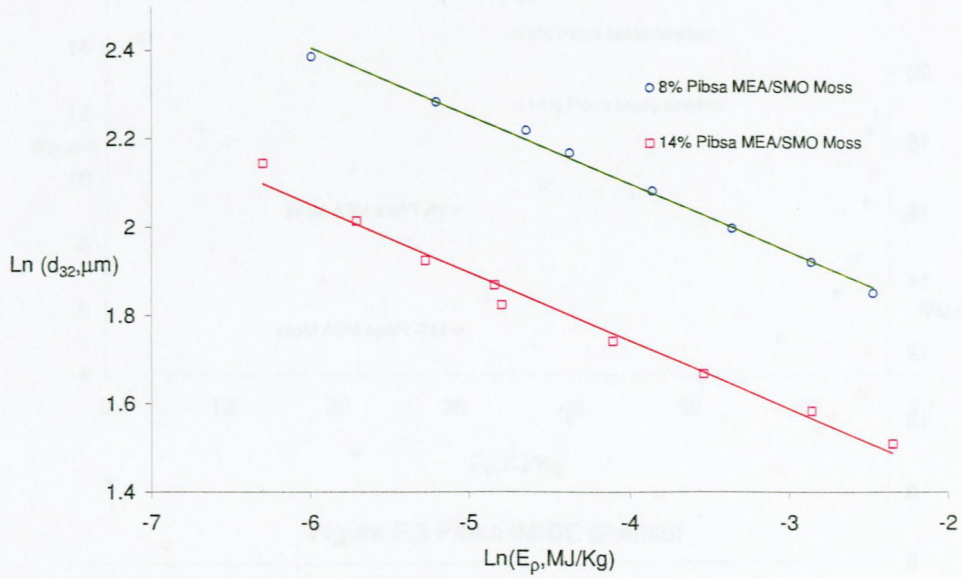

Figure E.5 Pibsa MEA/SMO Mosspar-H

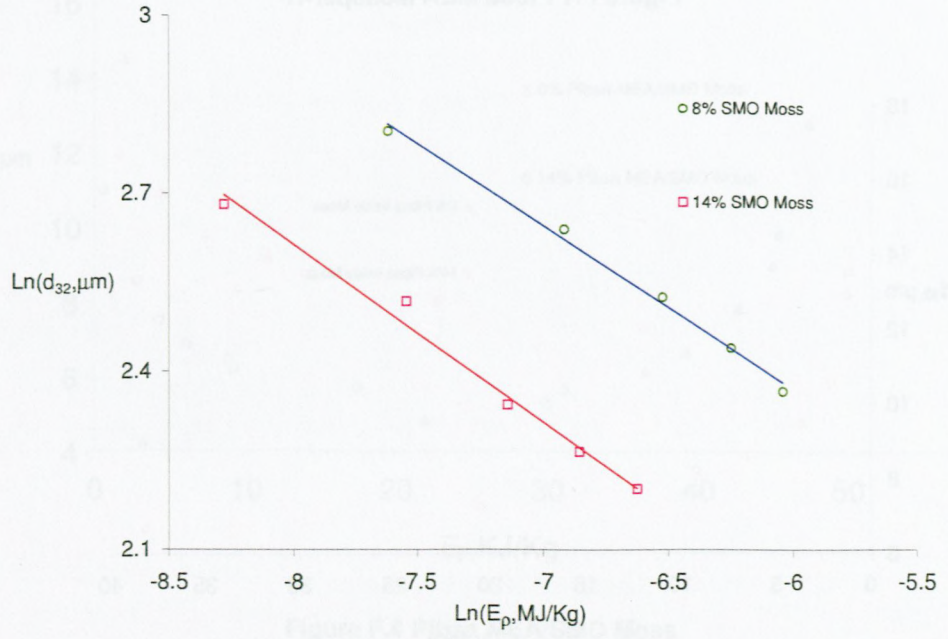

Figure E.6 SMO Mosspar-H

APPENDIX F.

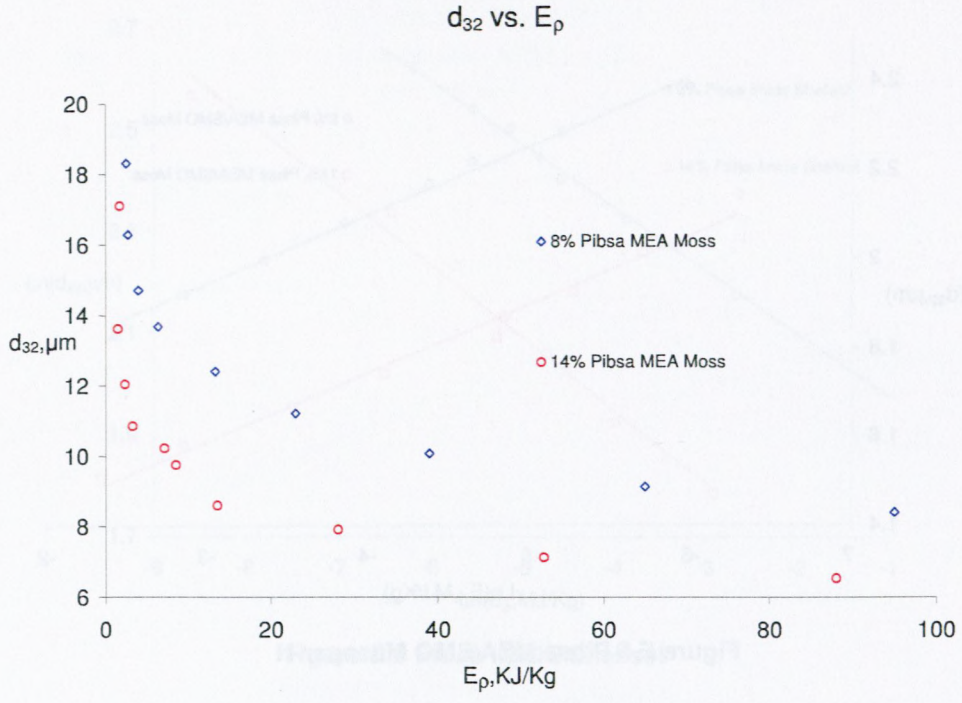

Figure F.1 Pibsa MEA Mosspar-H

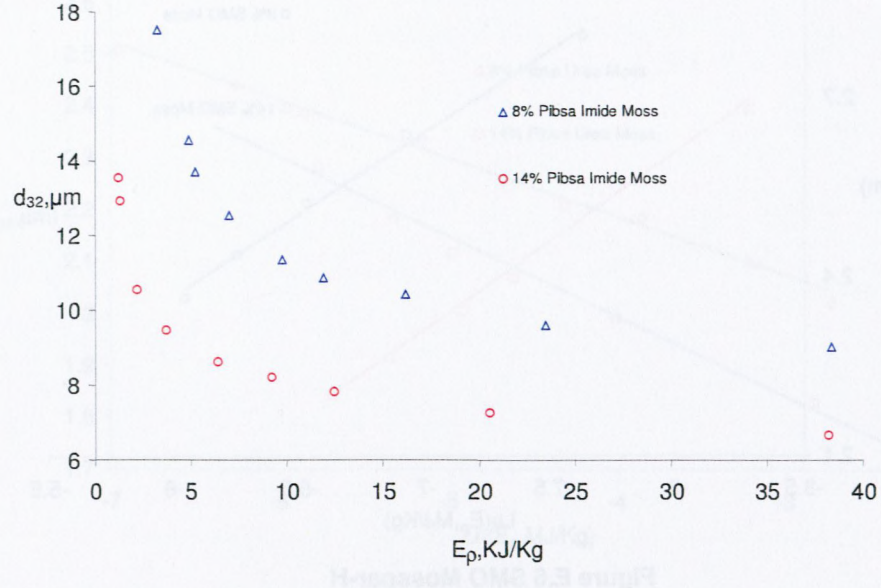

Figure F.2 Pibsa IMIDE Mosspar-H

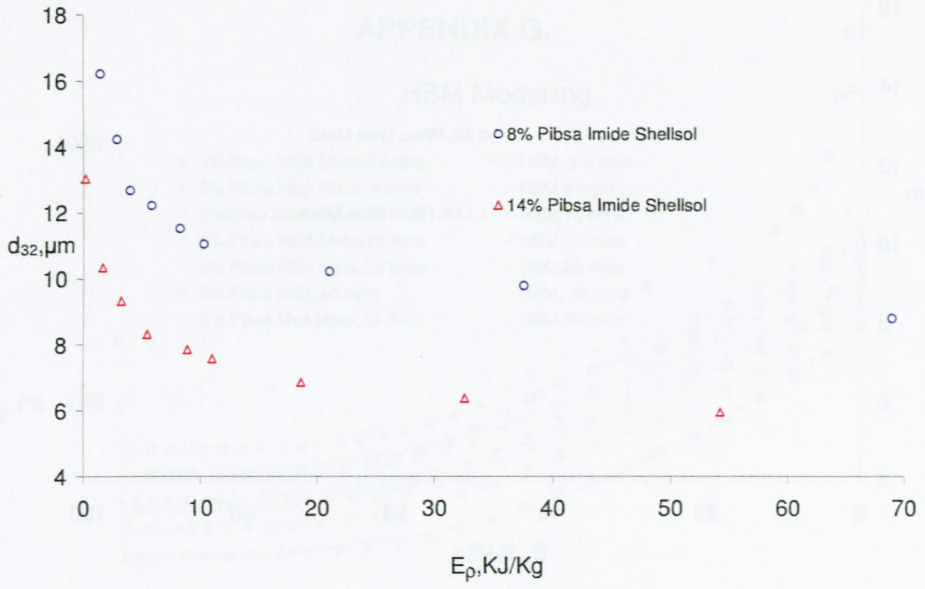

Figure F.3 Pibsa IMIDE Shellsol

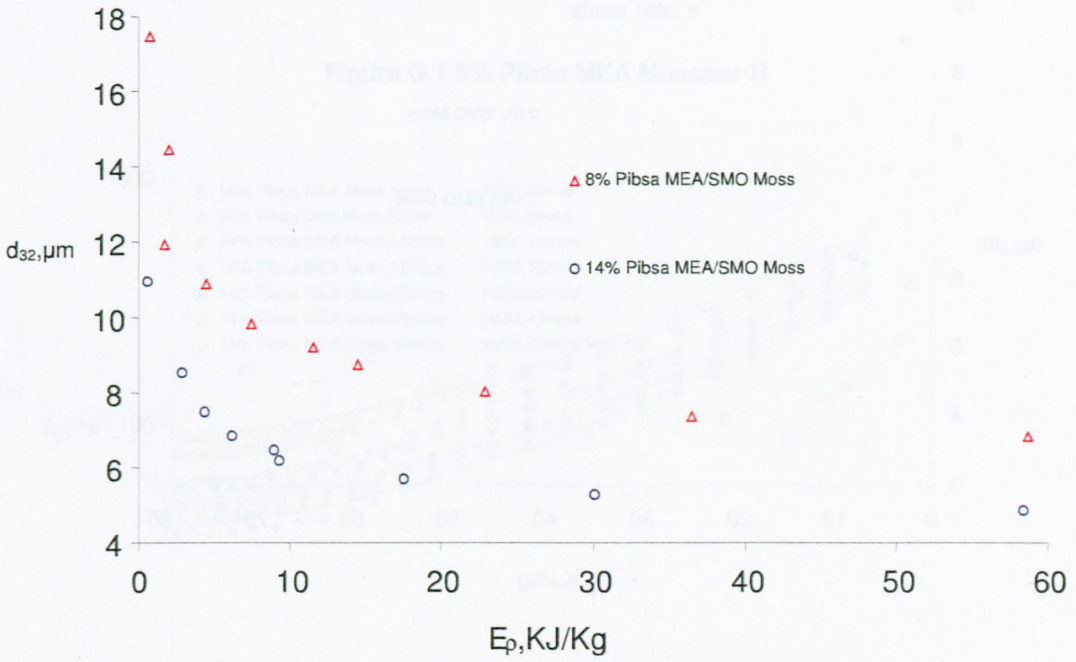

Figure F.4 Pibsa MEA/SMO Moss

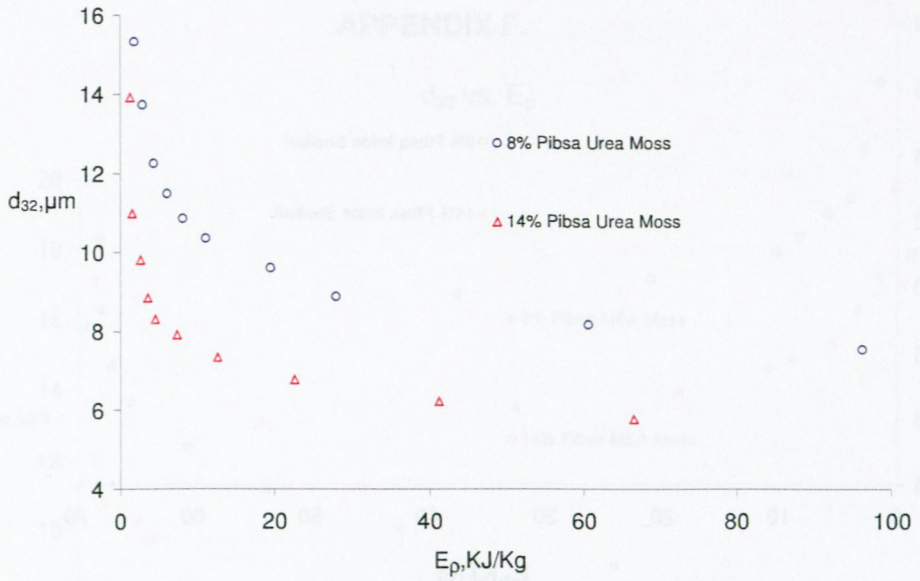

Figure F.5 Pibsa UREA Mosspar-H

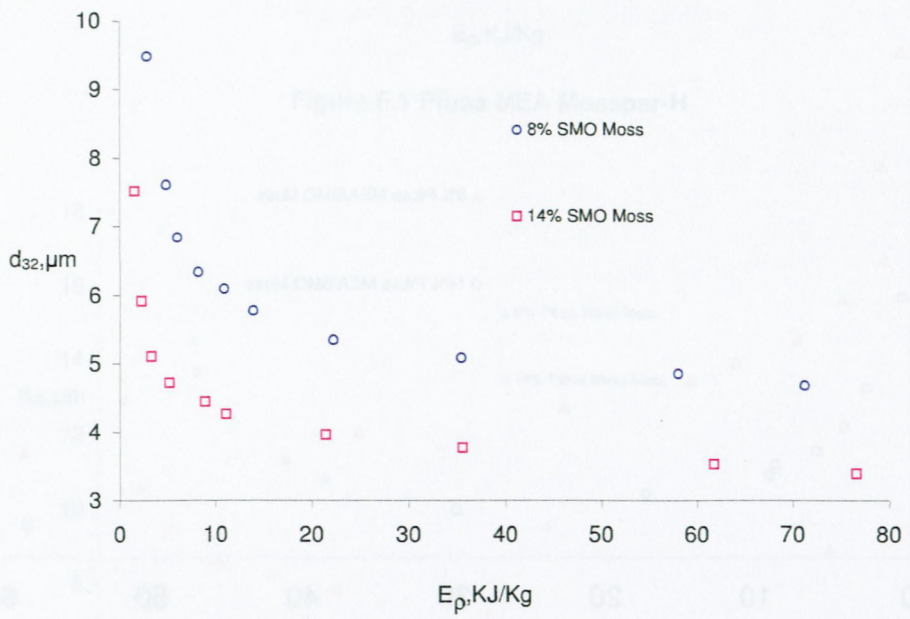

Figure F.6 SMO Mosspar-H

APPENDIX G.

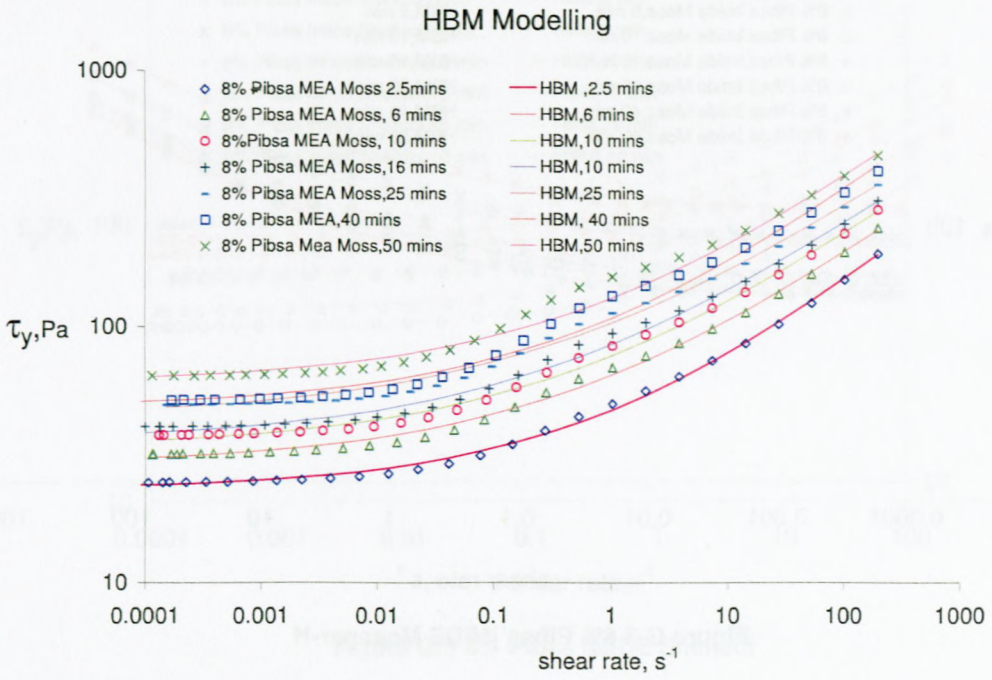

Figure G.1 8% Pibsa MEA Mosspar-H

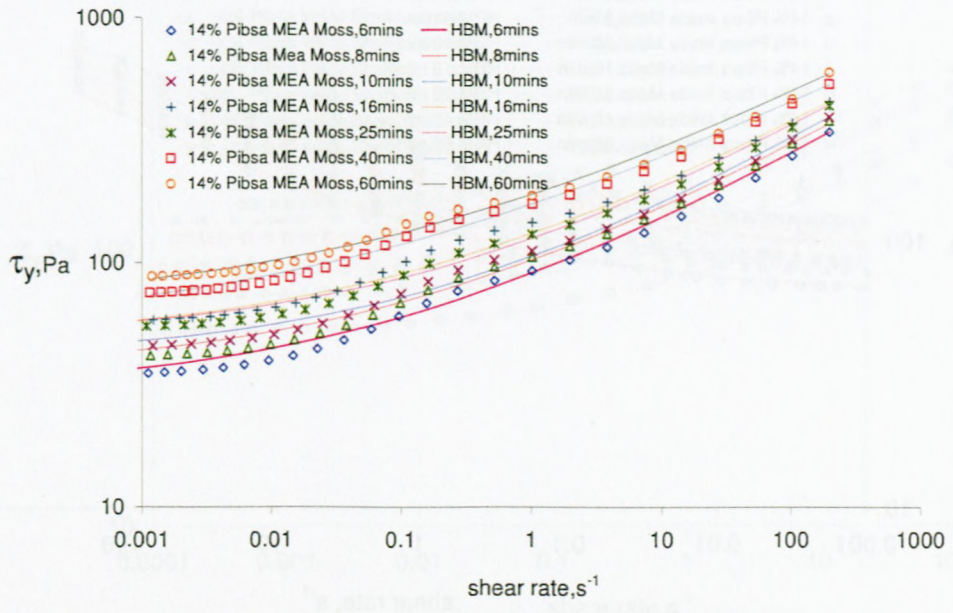

Figure G.2 14% Pibsa MEA Mosspar-H

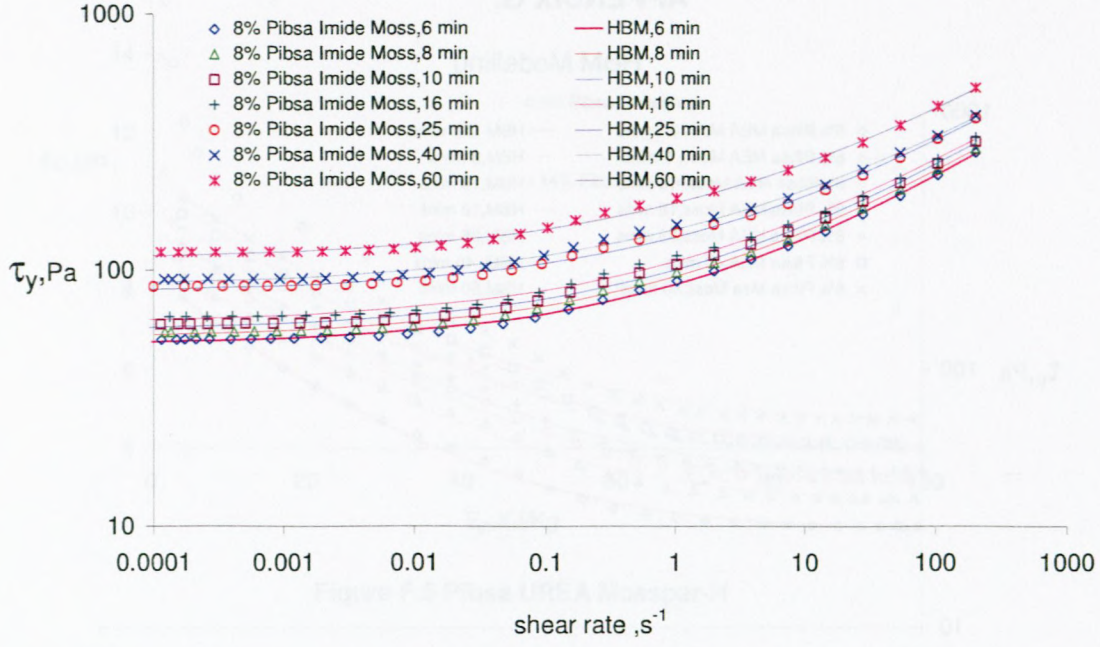

Figure G.3 8% Pibsa IMIDE Mosspar-H

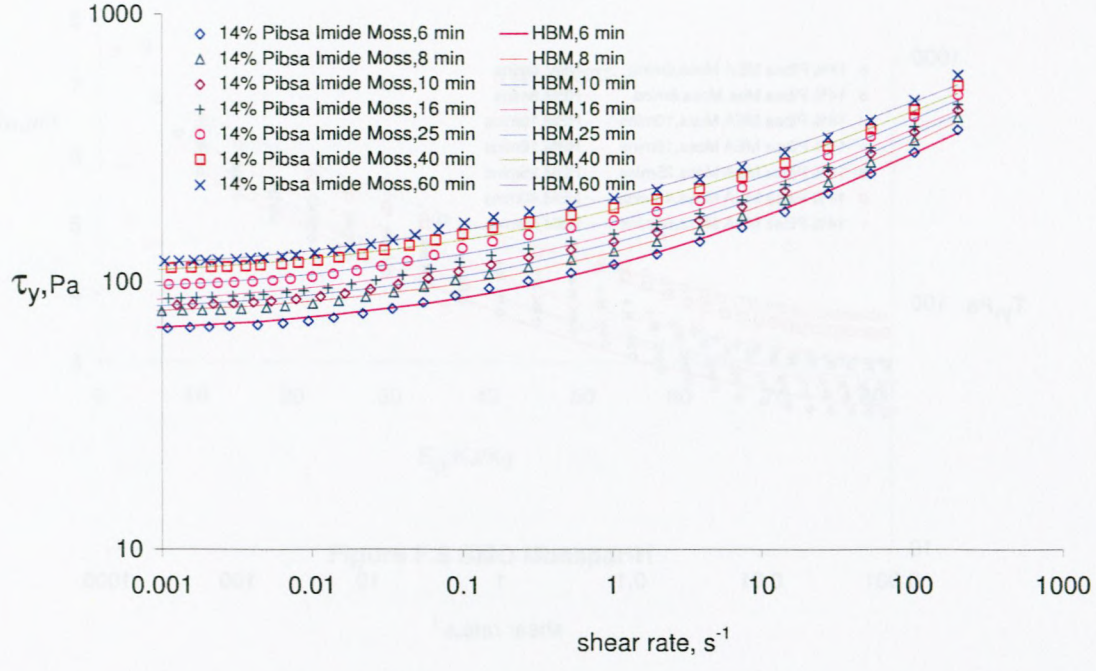

Figure G.4 14% Pibsa IMIDE Mosspar-H

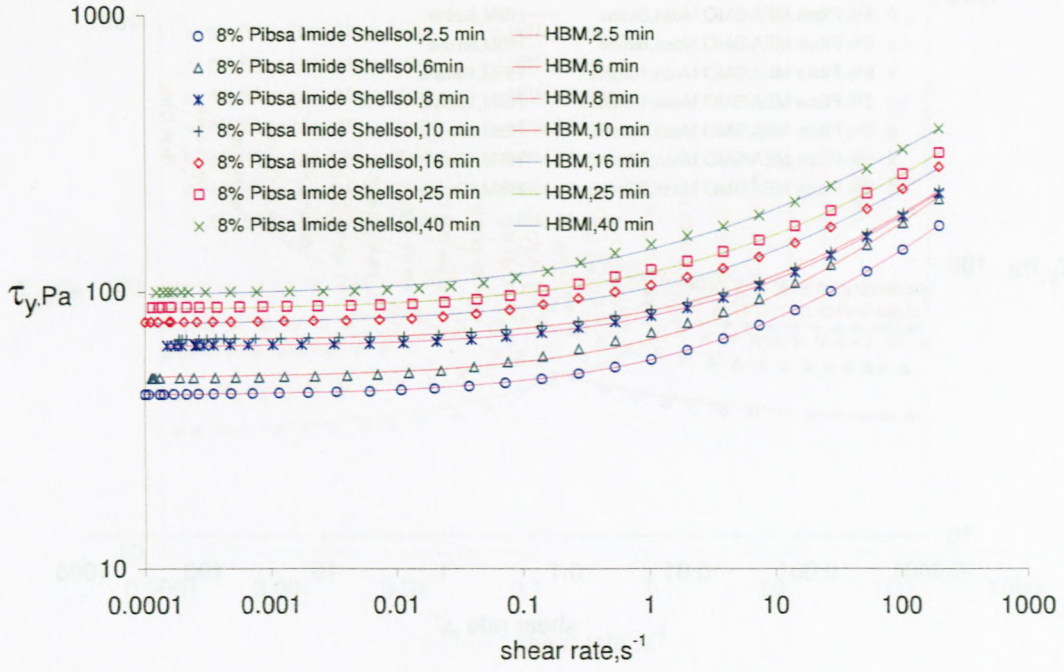

Figure G.5 8% Pibsa IMIDE Shellsol

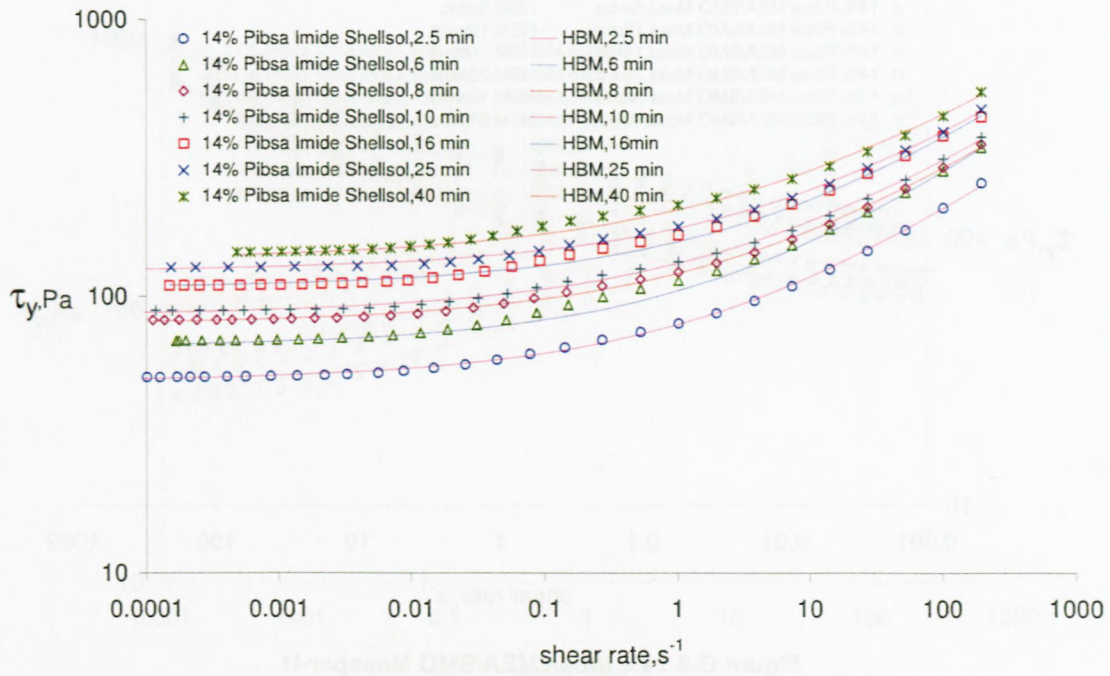

Figure G.6 14% Pibsa IMIDE Shellsol

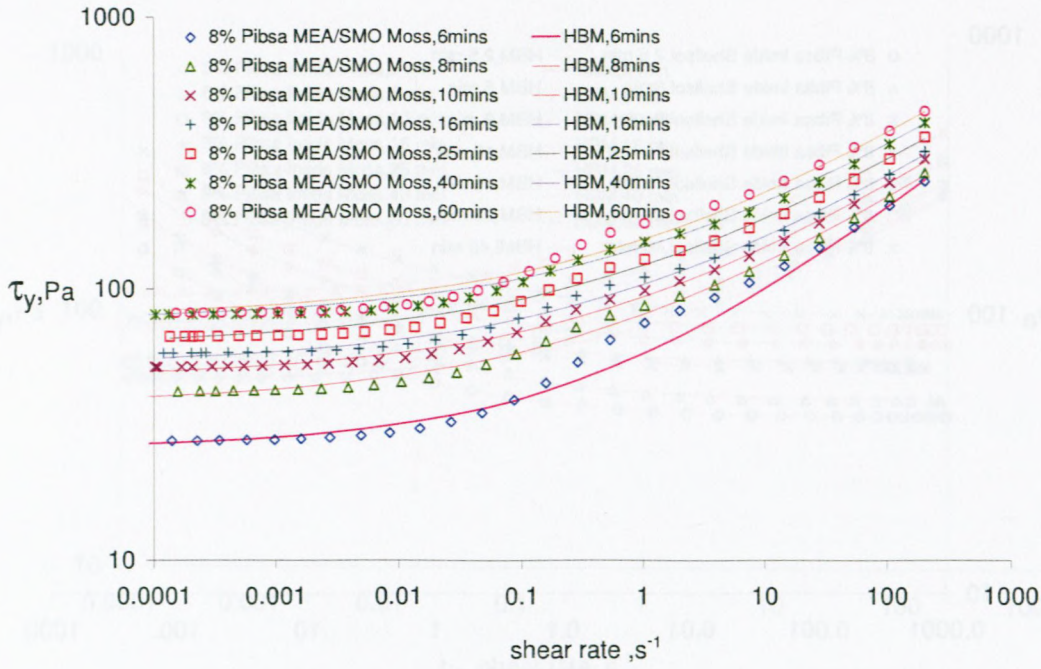

Figure G.7 8% Pibsa MEA/SMO Mosspar-H

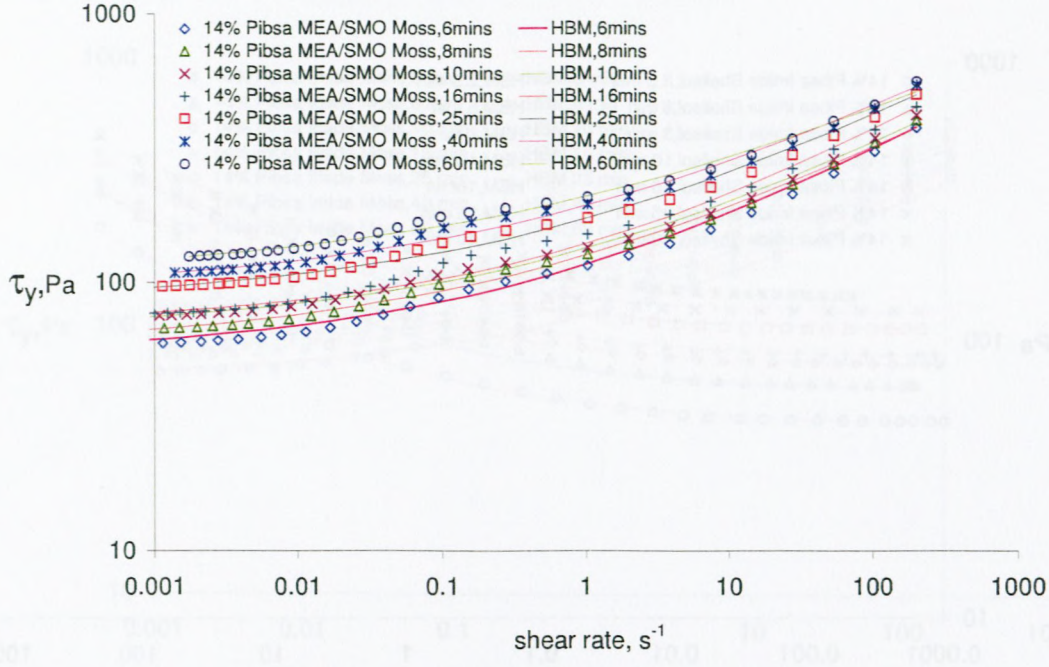

Figure G.8 14% Pibsa MEA/SMO Mosspar-H

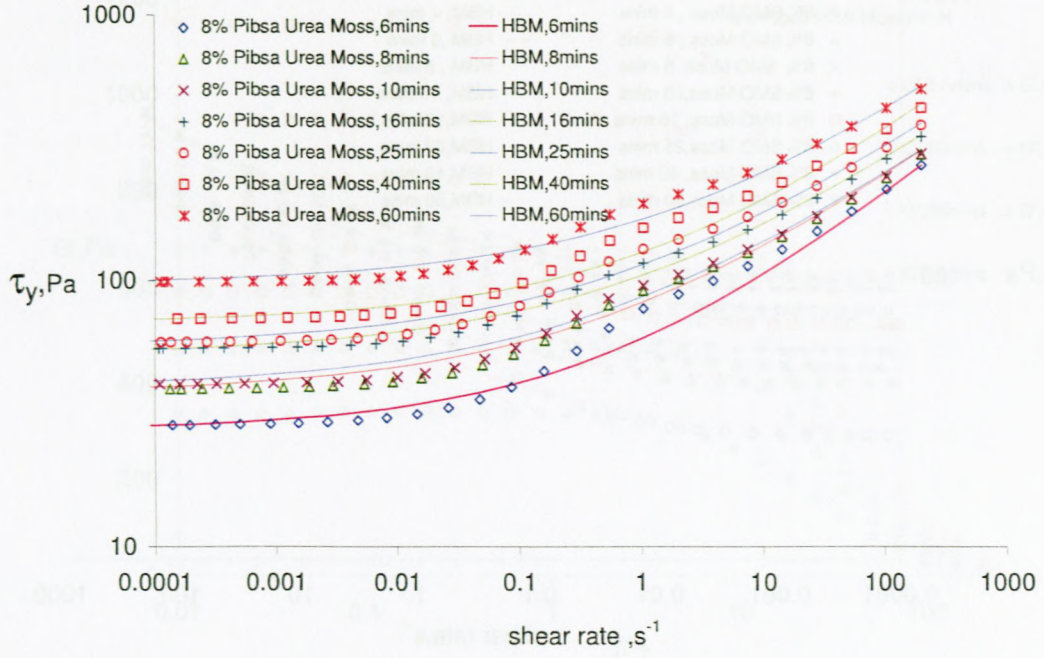

Figure G.9 8% Pibsa UREA Mosspar-H

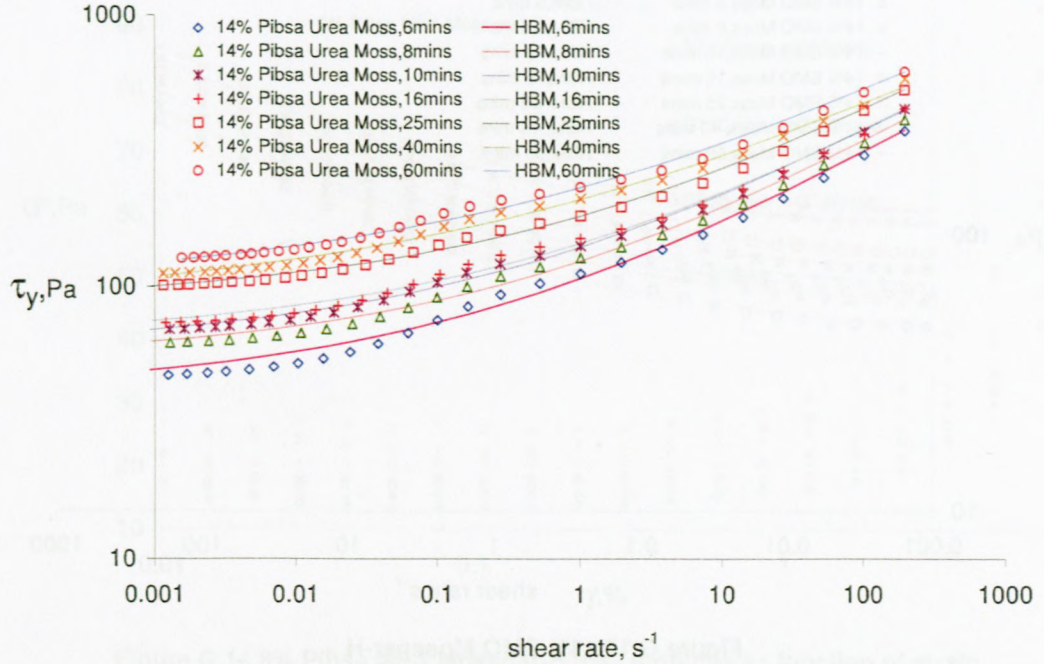

Figure G.10 14% Pibsa MEA/SMO Mosspar-H

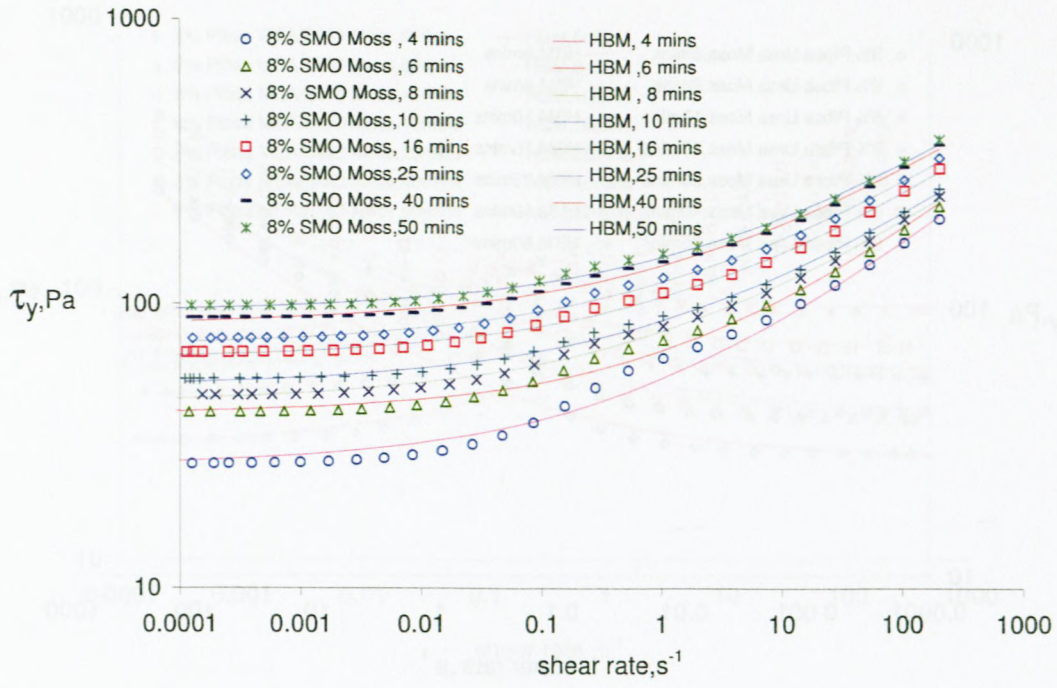

Figure G.11 8% SMO Mosspar-H

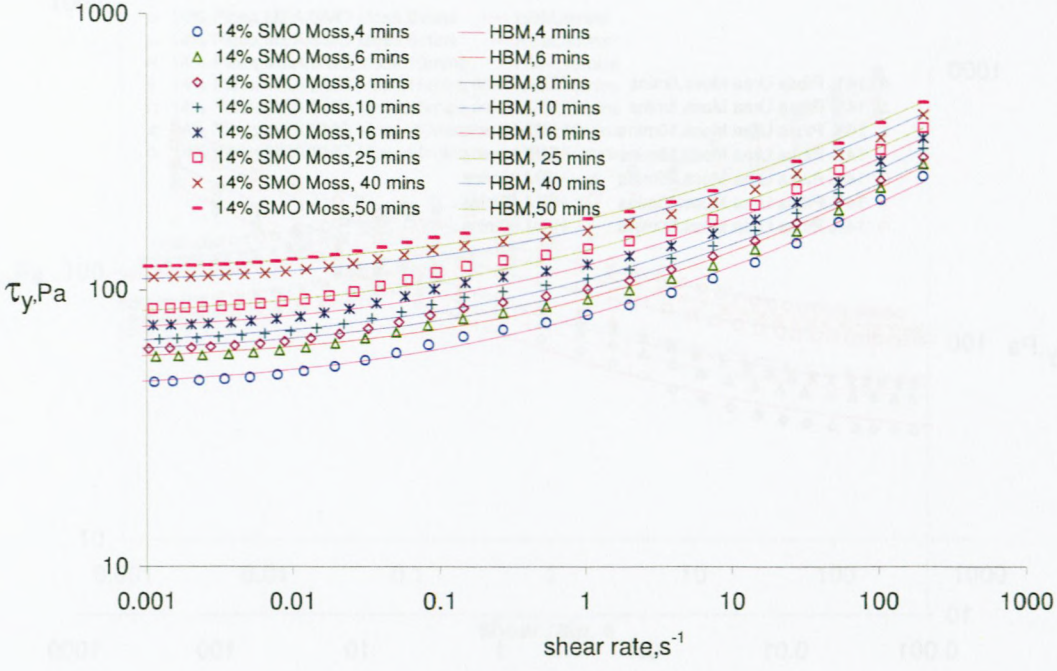

Figure G.12 14% SMO Mosspar-H

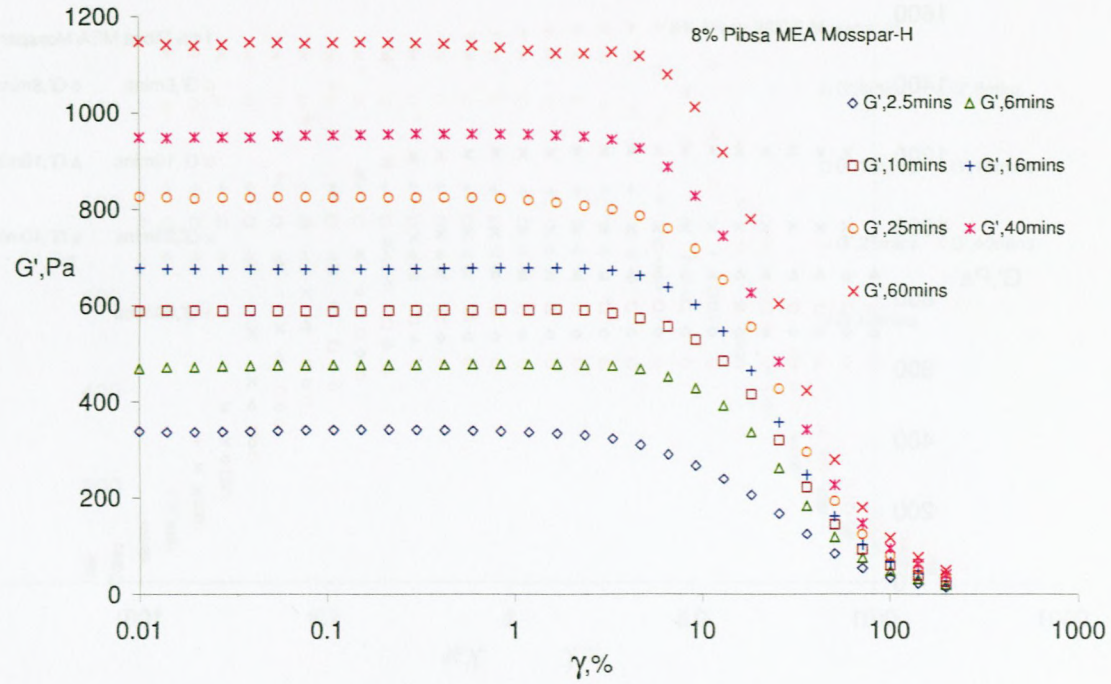

Figure G.13 8% Pibsa MEA Mosspar-H storage modulus as function of strain

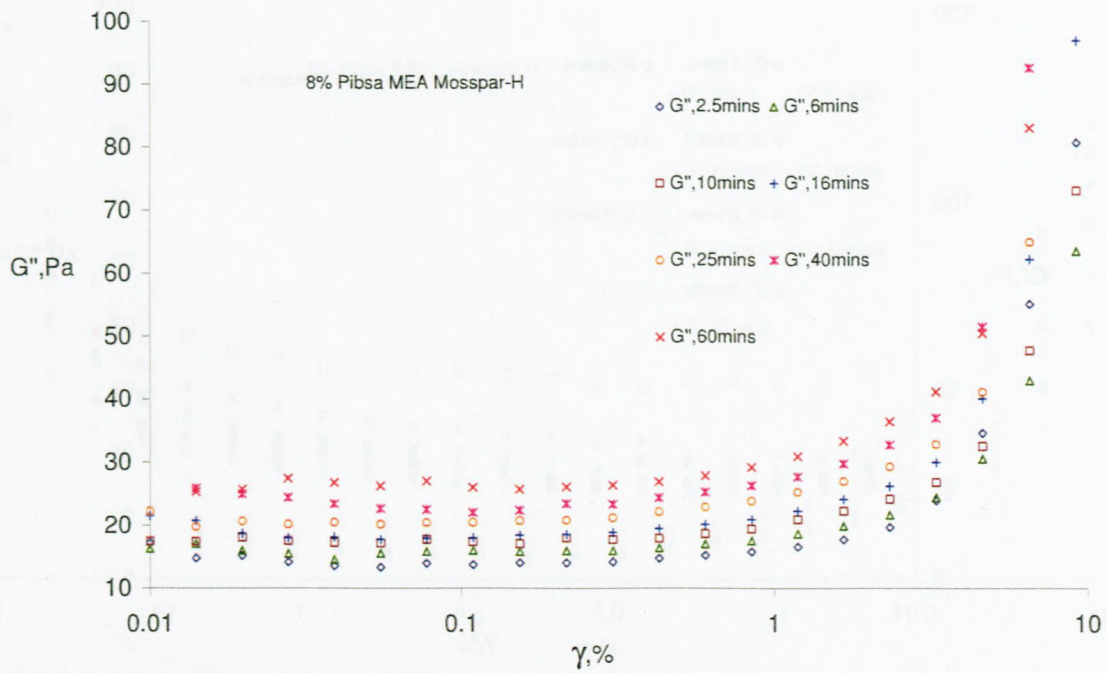

Figure G.14 8% Pibsa MEA Mosspar-H loss modulus as function of strain

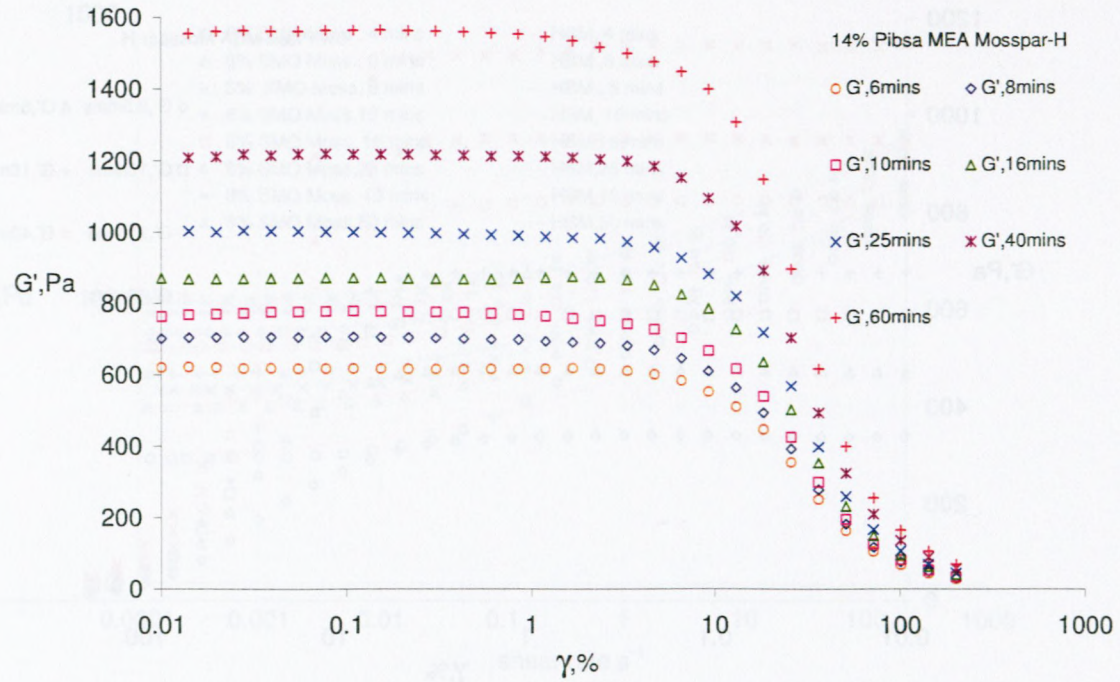

Figure G.15 14% Pibsa MEA Mosspar-H storage modulus as function of strain

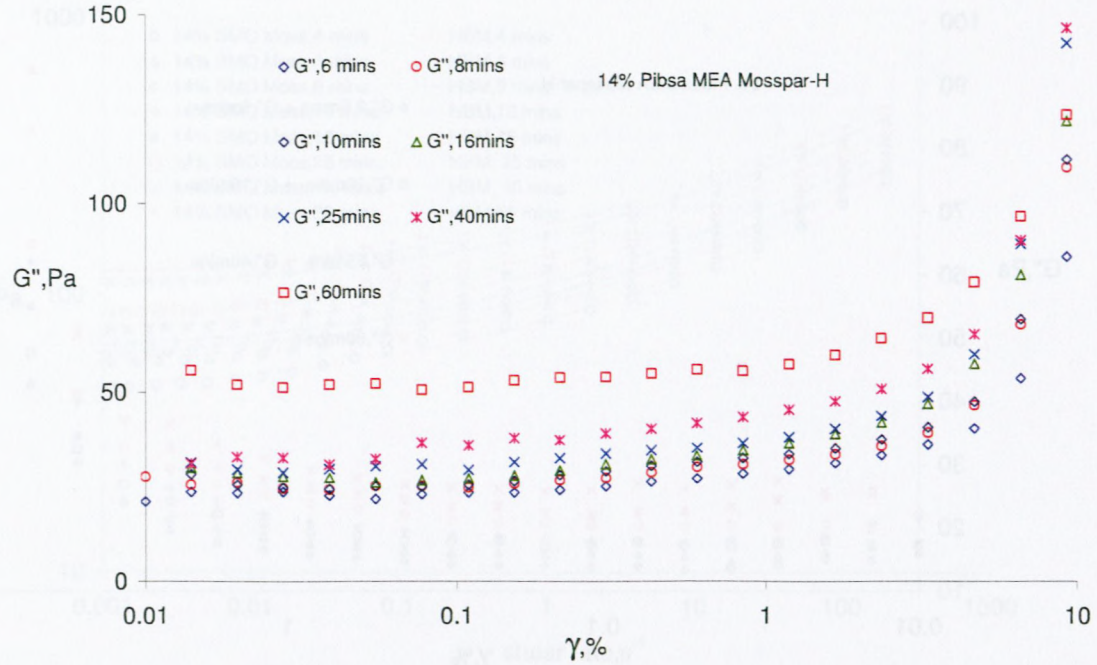

Figure G.16 14% Pibsa MEA Mosspar-H loss modulus as function of strain

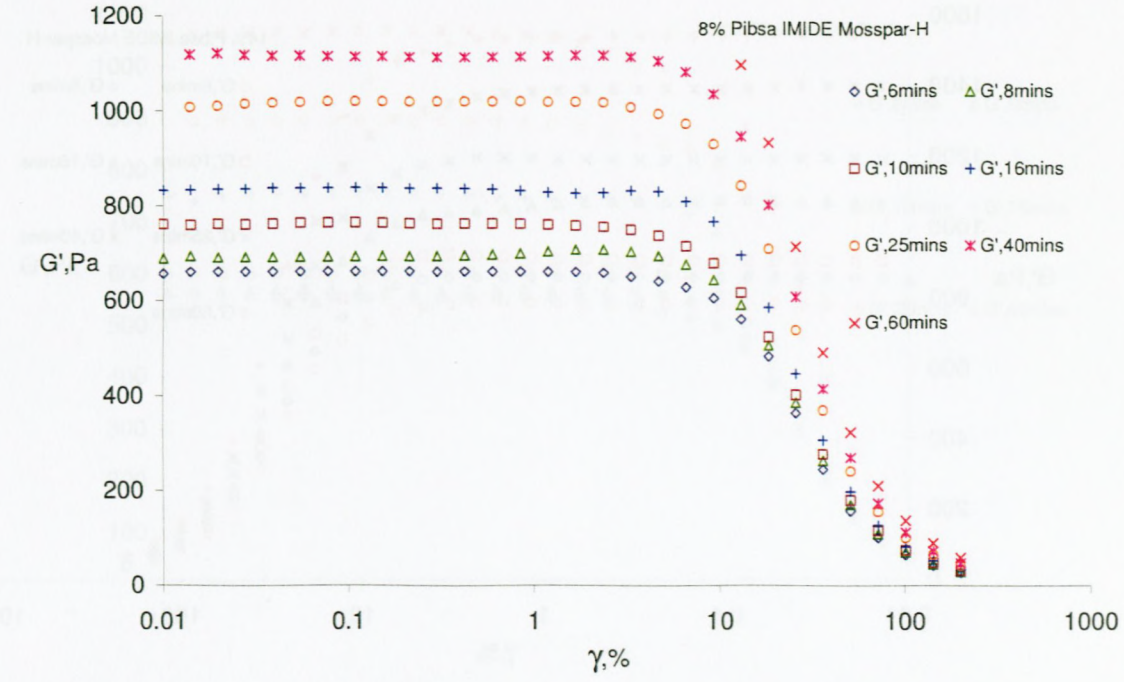

Figure G.17 8% Pibsa IMIDE Mosspar-H storage modulus as function of strain

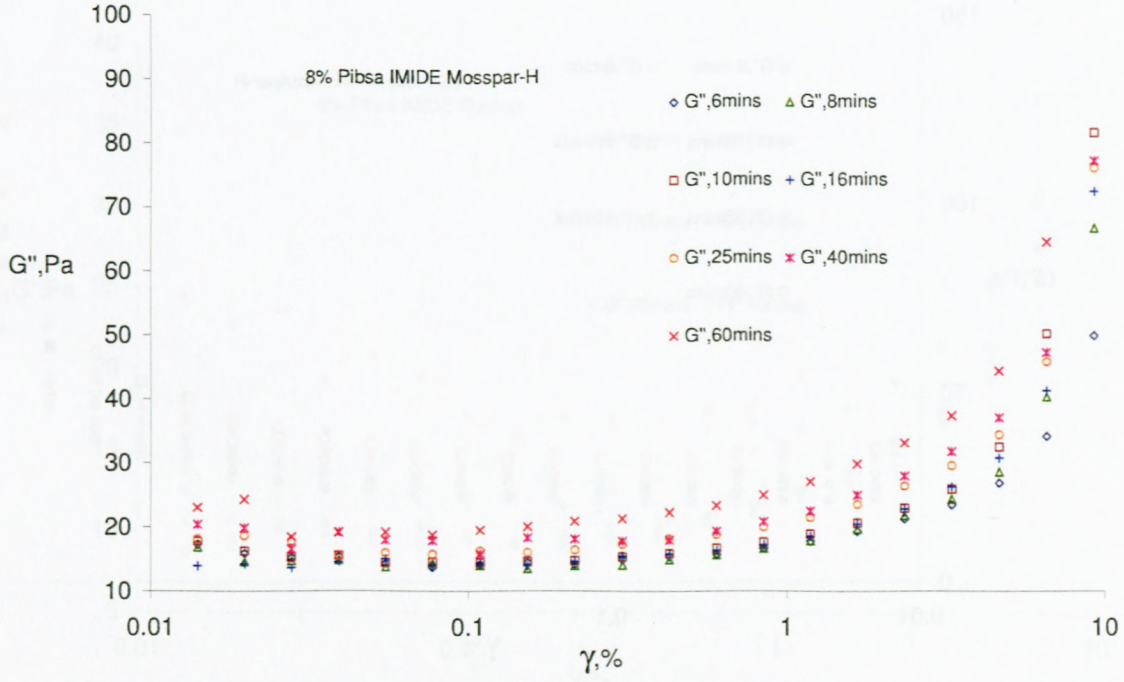

Figure G.18 8% Pibsa IMIDE Mosspar-H loss modulus as function of strain

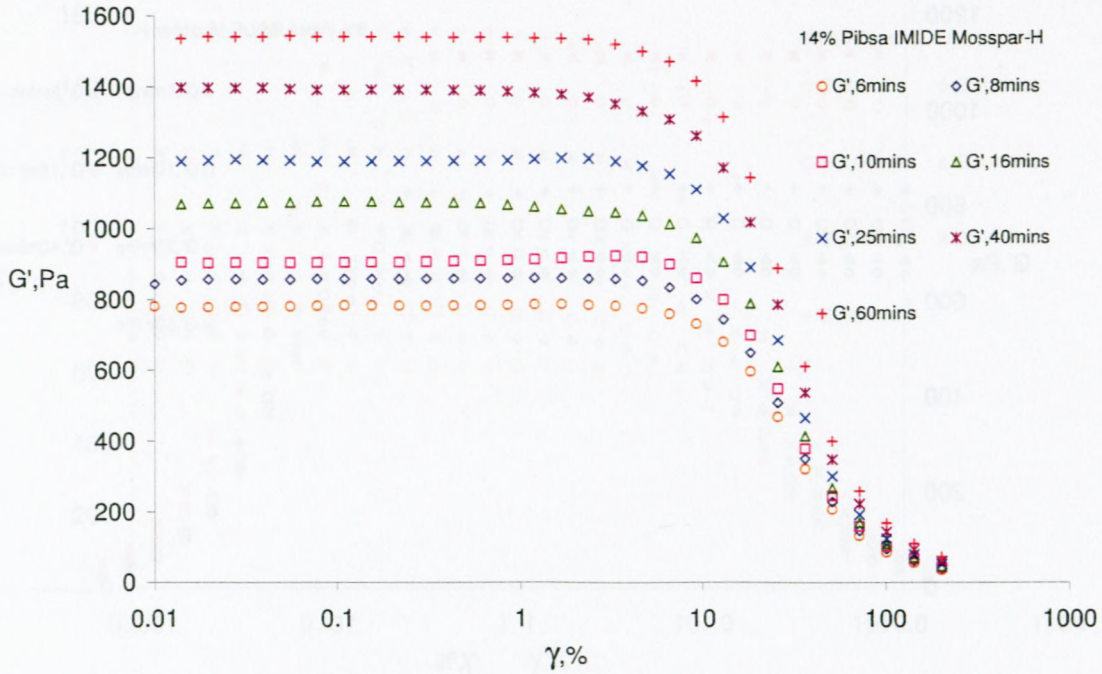

Figure G.19 14% Pibsa IMIDE Mosspar-H storage modulus as function of strain

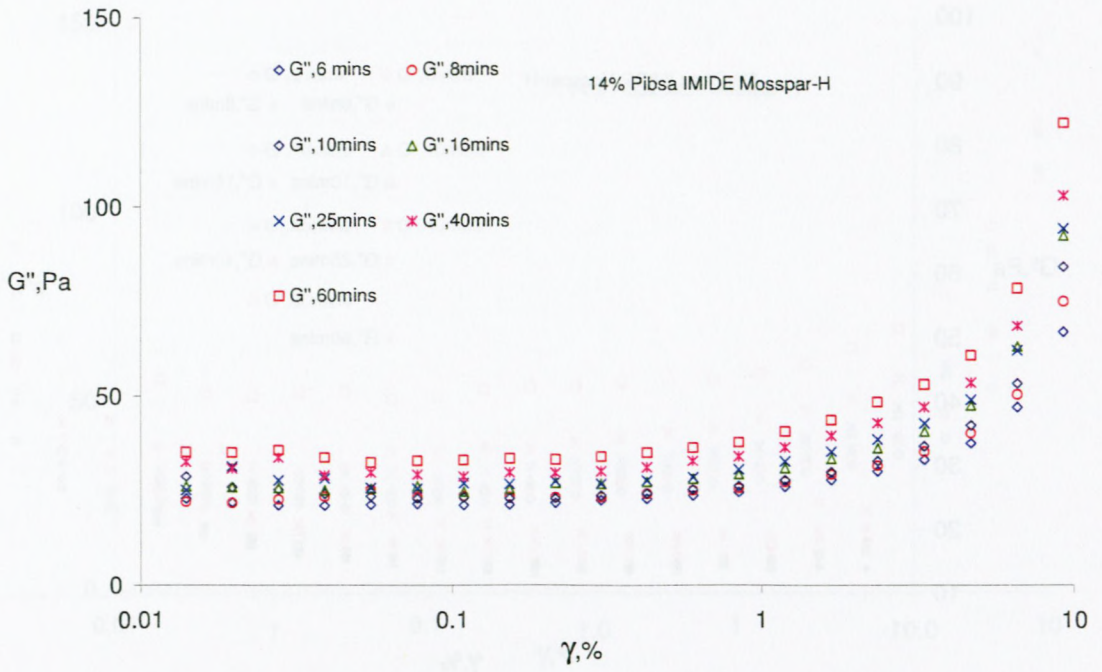

Figure G.20 14% Pibsa IMIDE Mosspar-H loss modulus as function of strain

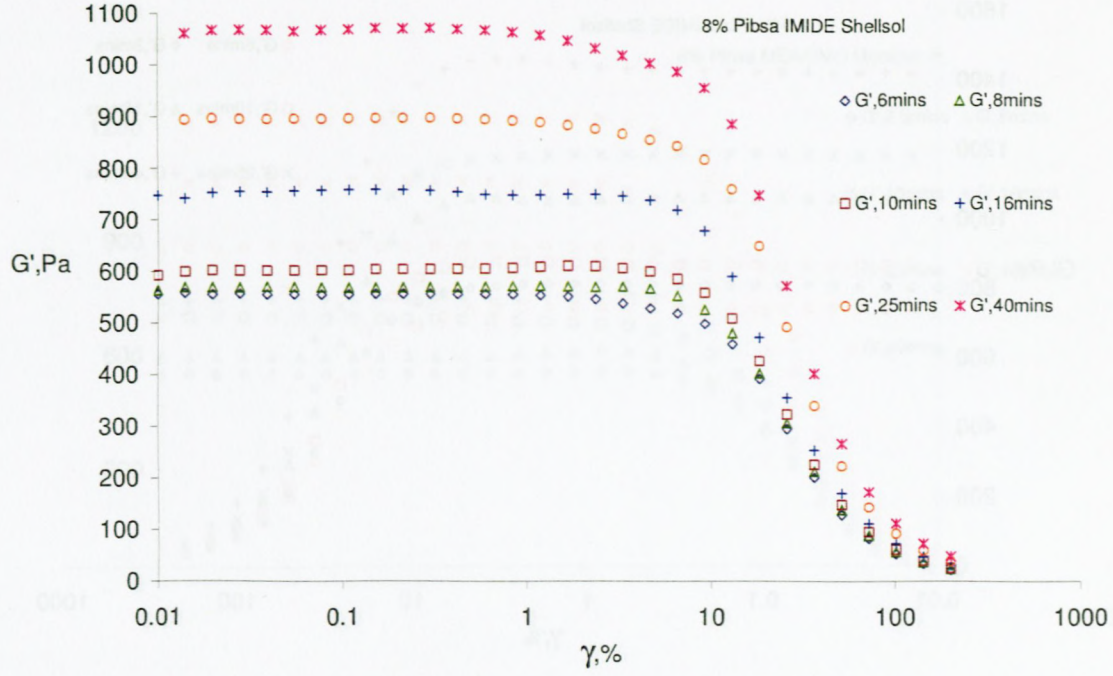

Figure G.21 8% Pibsa IMIDE Shellsol storage modulus as function of strain

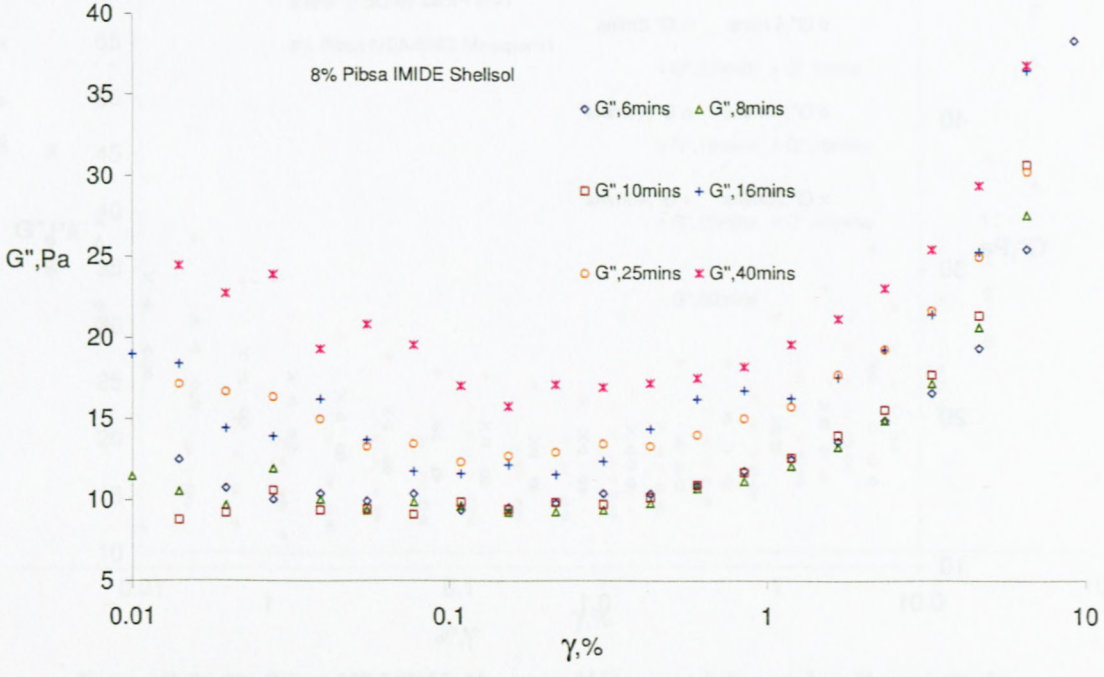

Figure G.22 8% Pibsa IMIDE Shellsol loss modulus as function of strain

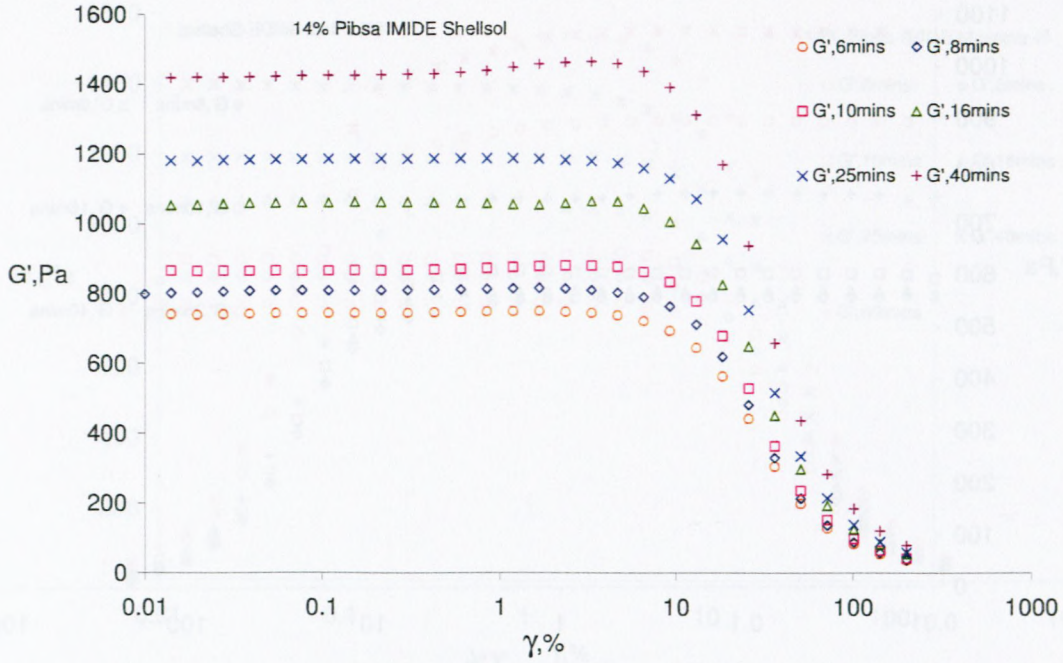

Figure G.23 14% Pibsa IMIDE Shellsol storage modulus as function of strain

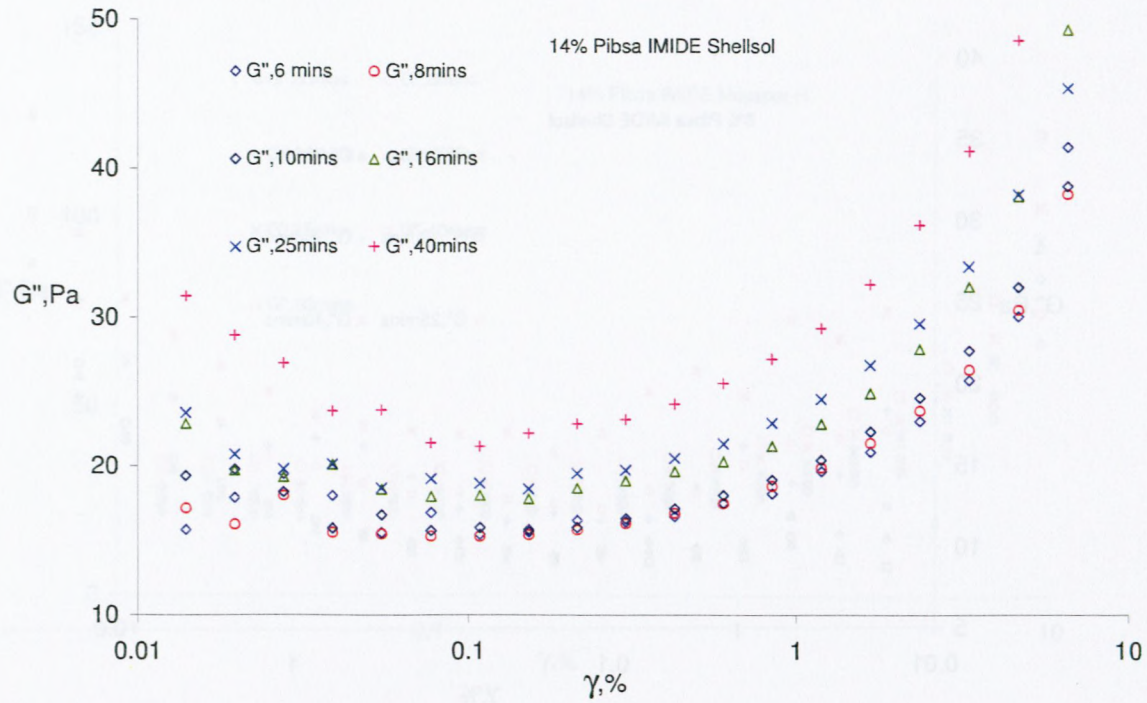

Figure G.24 14% Pibsa IMIDE Shellsol loss modulus as function of strain

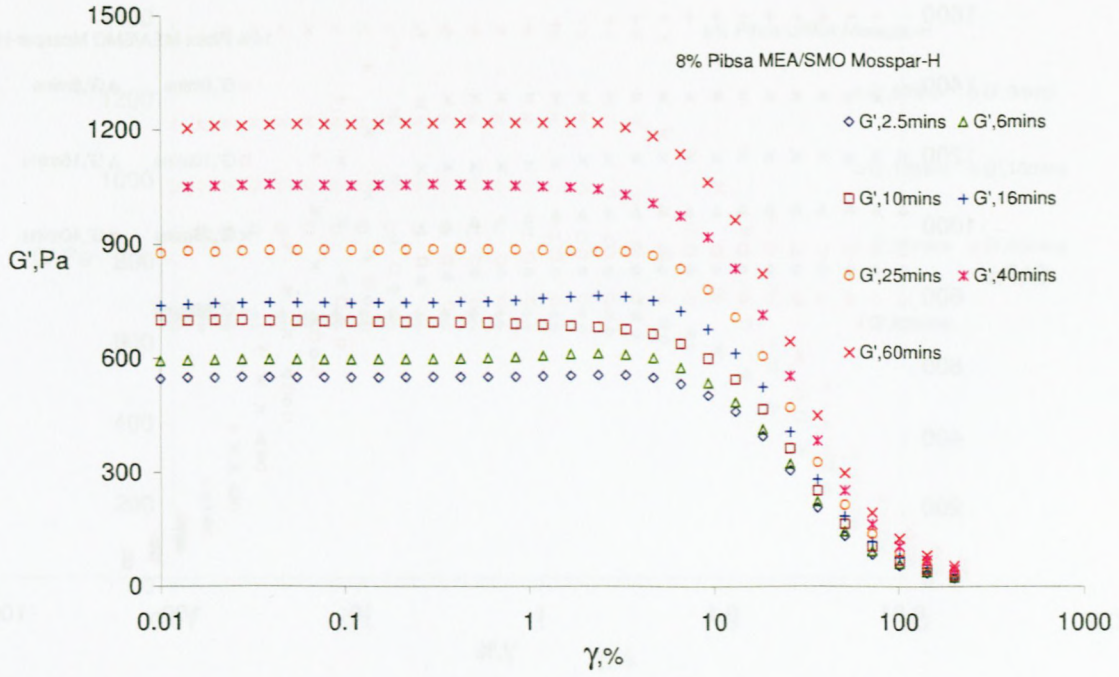

Figure G.25 8% Pibsa MEA/SMO Mosspar-H storage modulus as function of strain

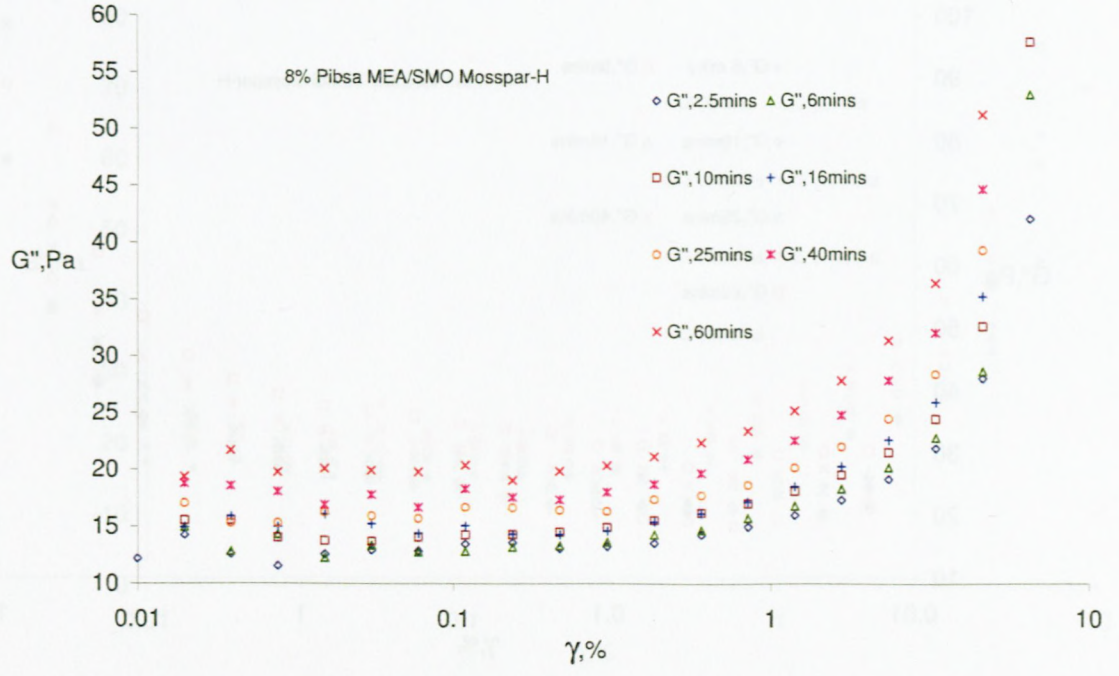

Figure G.26 8% Pibsa MEA/SMO Mosspar-H loss modulus as function of strain

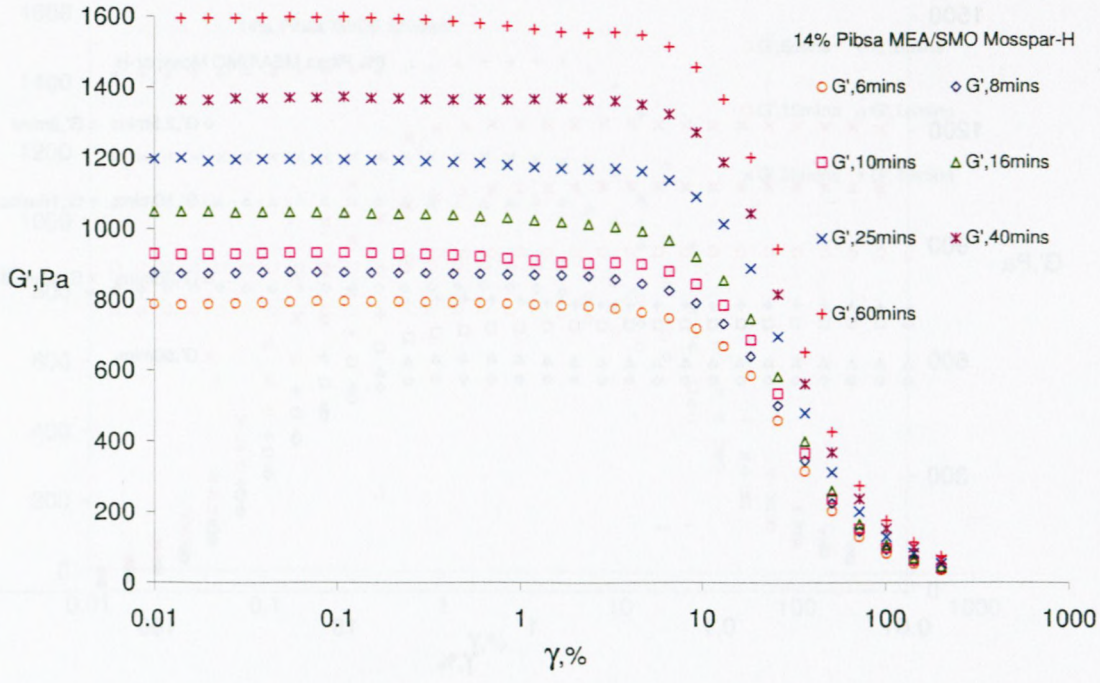

Figure G.27 14% Pibsa MEA/SMO Mosspar-H storage modulus as function of strain

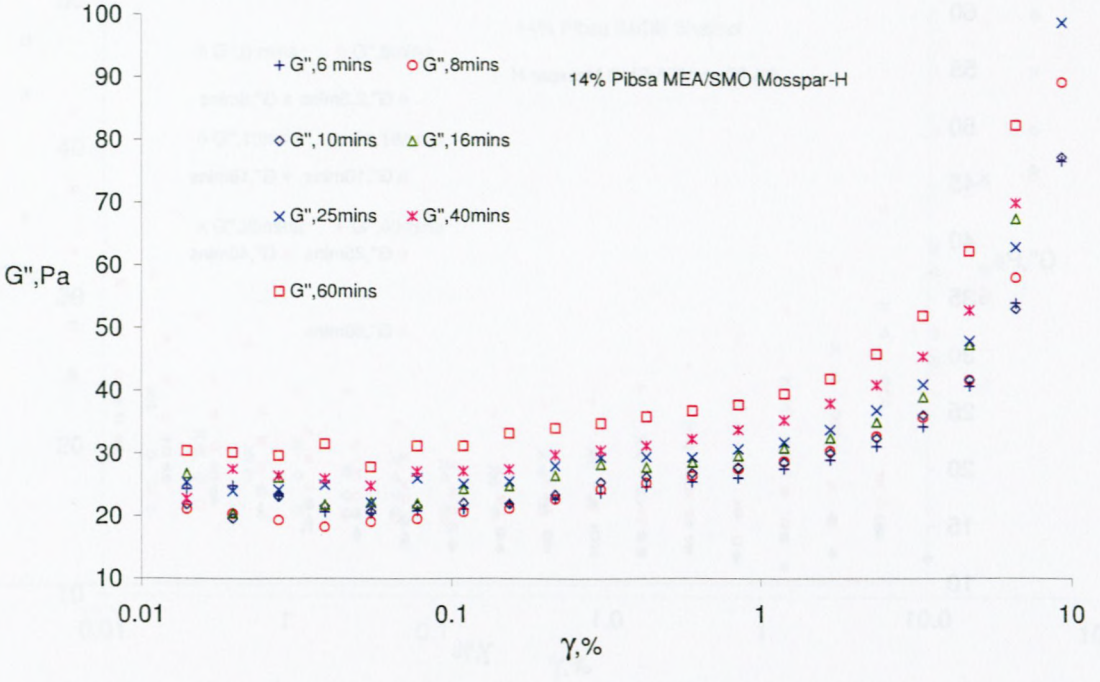

Figure G.28 14% Pibsa MEA/SMO Mosspar-H loss modulus as function of strain

Figure G.29 8% Pibsa UREA Mosspar-H storage modulus as function of strain

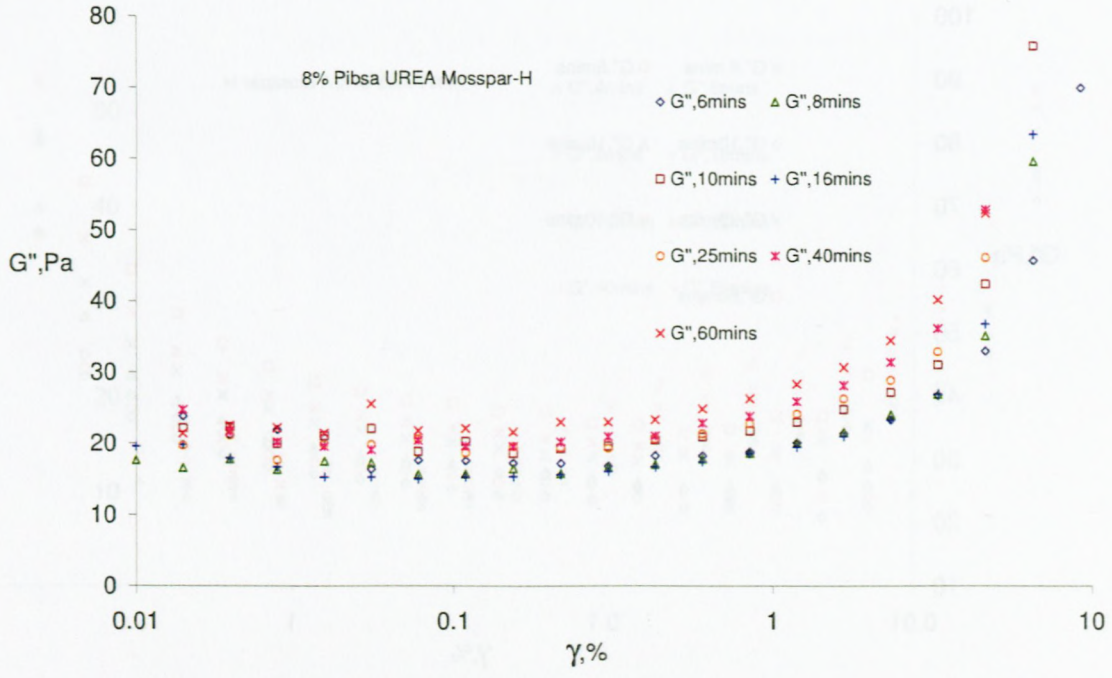

Figure G.30 8% Pibsa UREA Mosspar-H loss modulus as function of strain

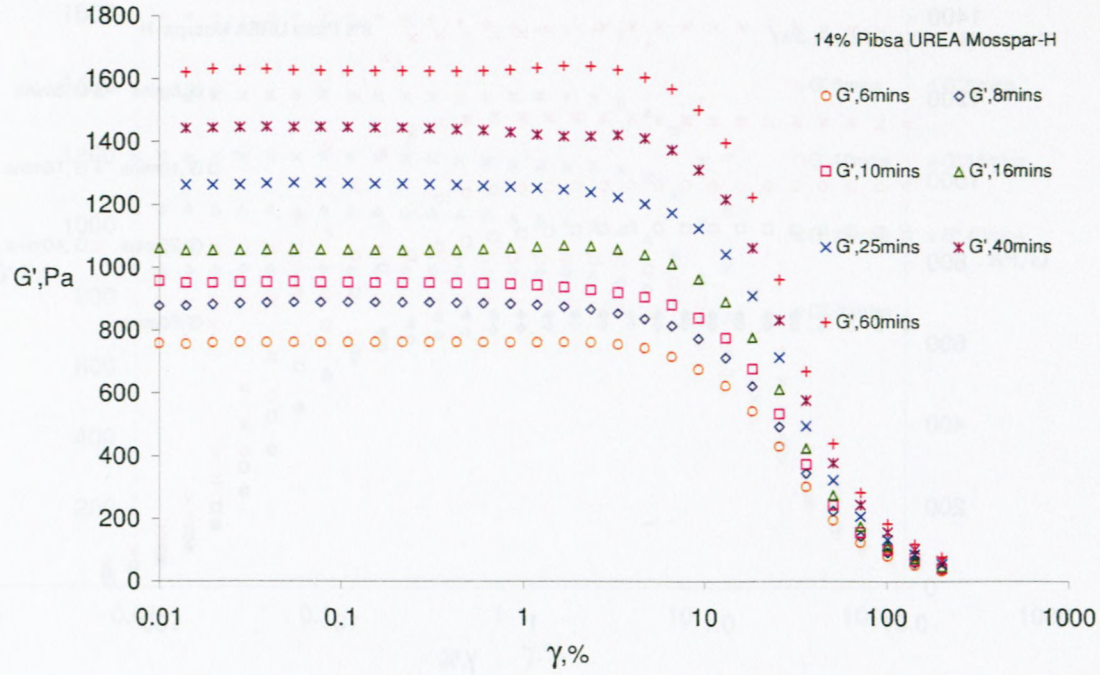

Figure G.31 14% Pibsa UREA Mosspar-H storage modulus as function of strain

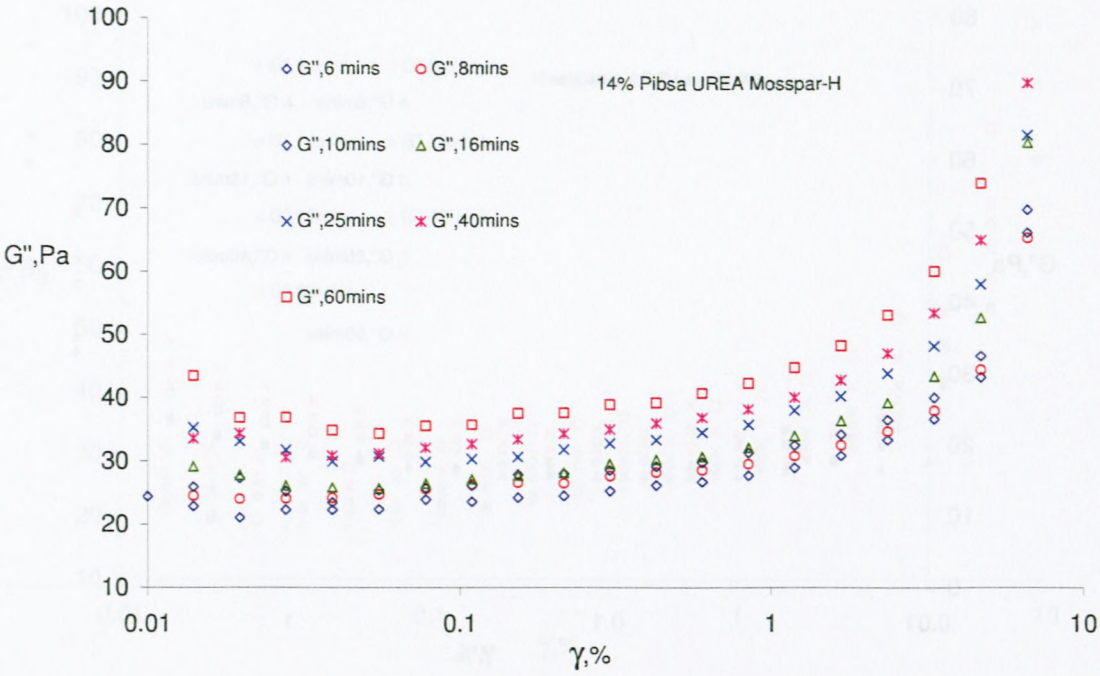

Figure G.32 14% Pibsa UREA Mosspar-H loss modulus as function of strain

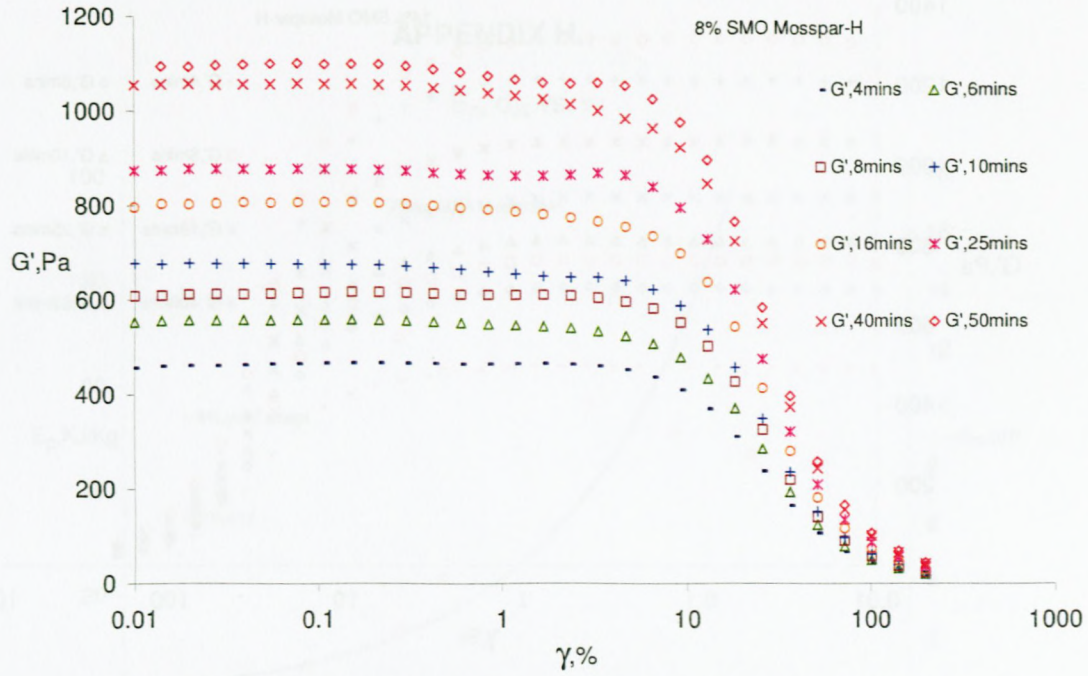

Figure G. 33 8% SMO Mosspar-H storage modulus as function of strain

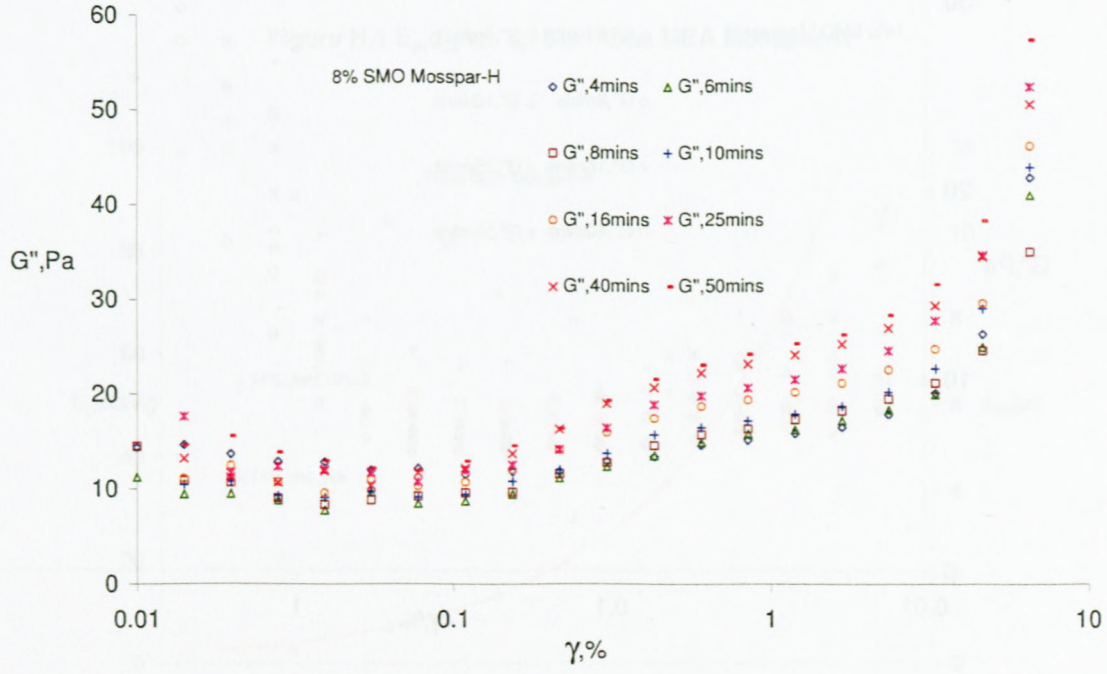

Figure G. 34 8% SMO Mosspar-H loss modulus as function of strain

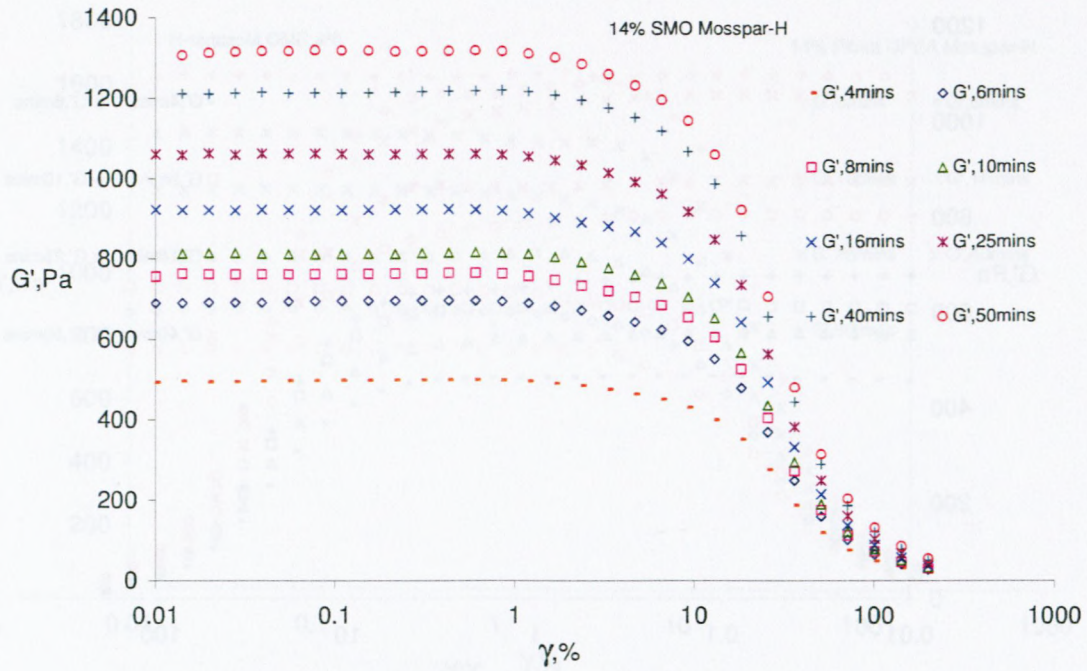

Figure G.35 14% SMO Mosspar-H storage modulus as function of strain

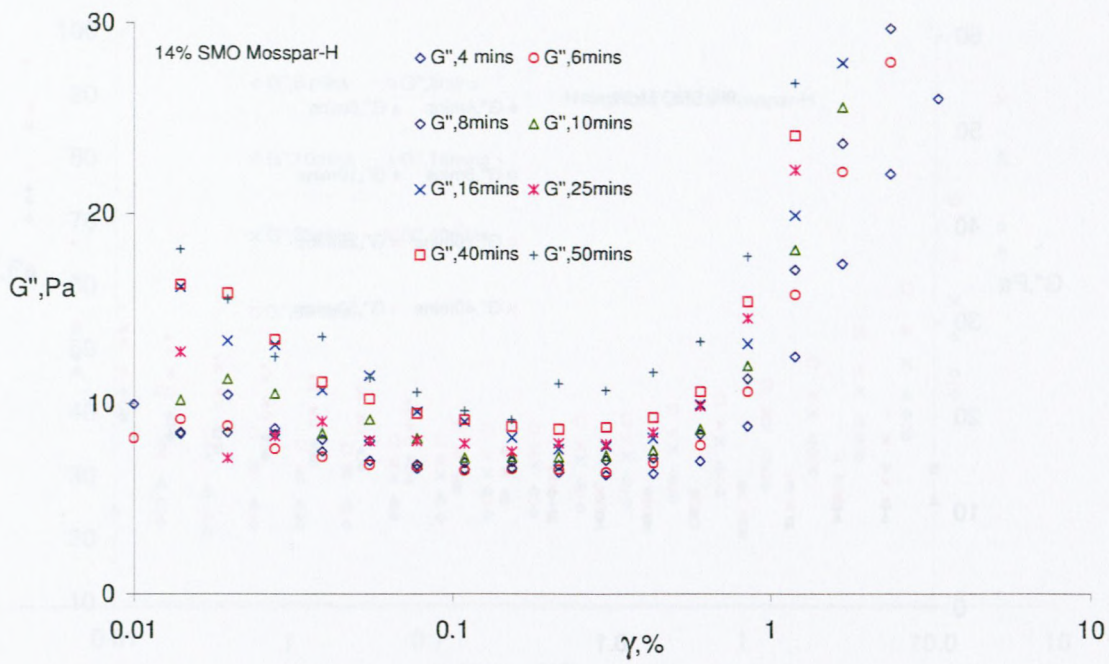

Figure G.36 14% SMO Mosspar-H loss modulus as function of strain

APPENDIX H.

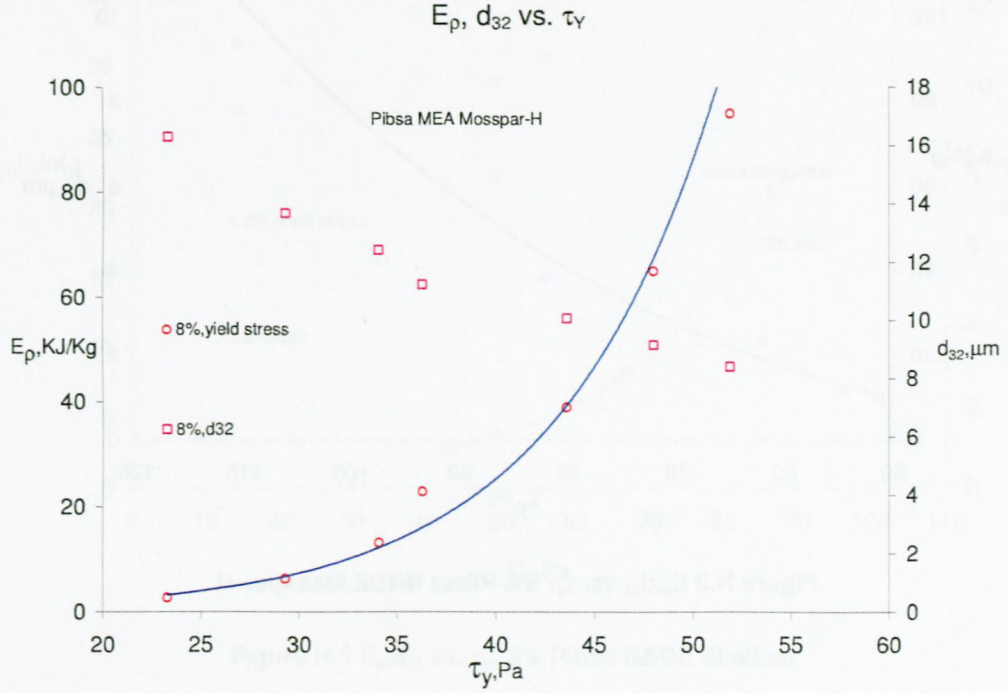

Figure H.1 E_ρ,d_{32} vs. τ_y: 8% Pibsa MEA Mosspar-H

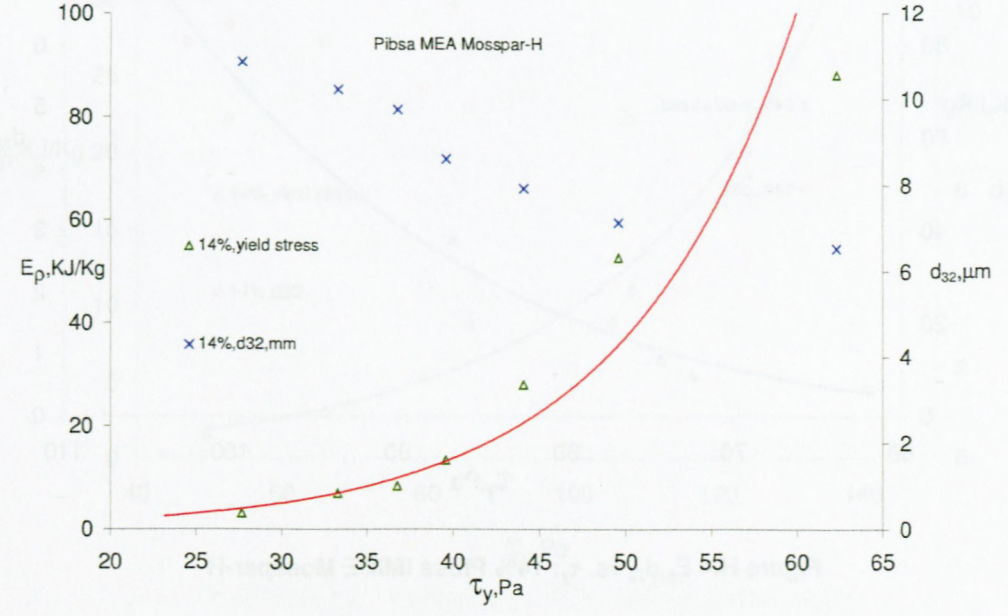

Figure H.2 E_ρ,d_{32} vs. τ_y 14% Pibsa MEA Mosspar-H

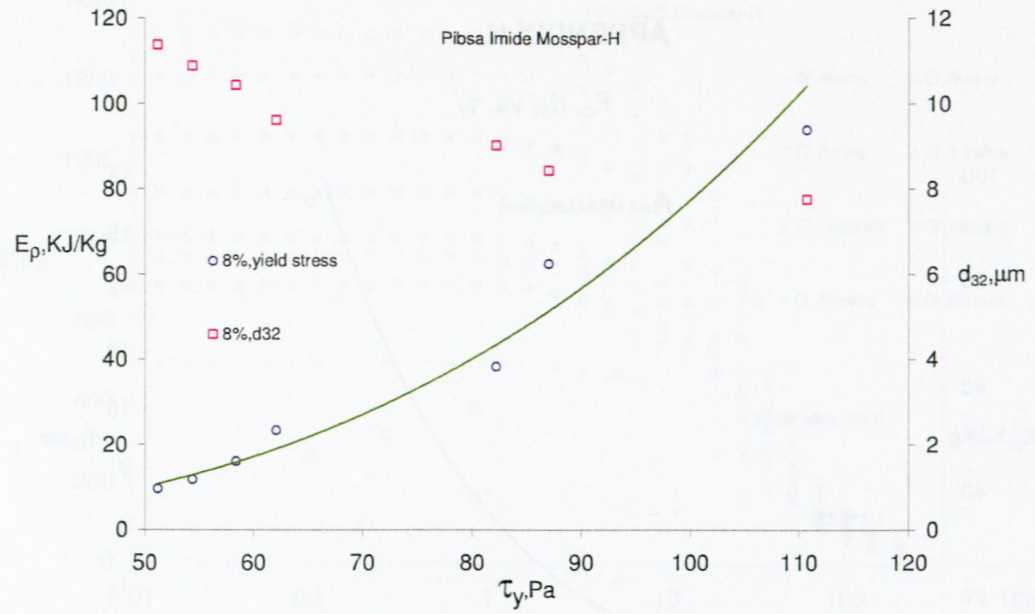

Figure H.3 E_ρ,d_{32} vs. τ_y: 8% Pibsa IMIDE Mosspar-H

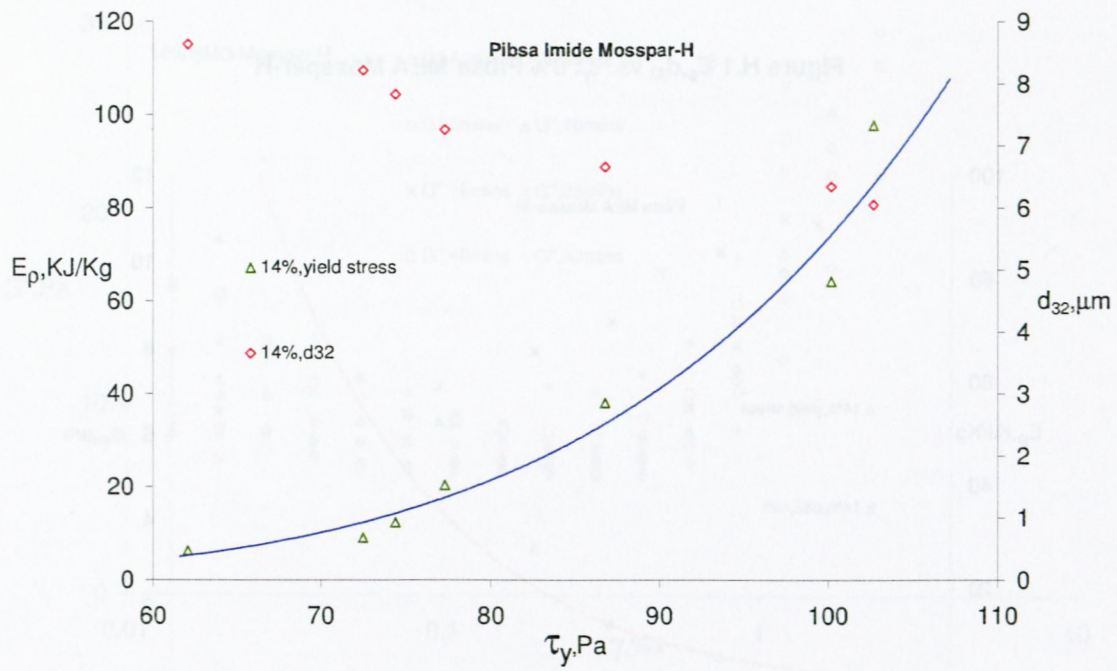

Figure H.4 E_ρ,d_{32} vs. τ_y: 14% Pibsa IMIDE Mosspar-H

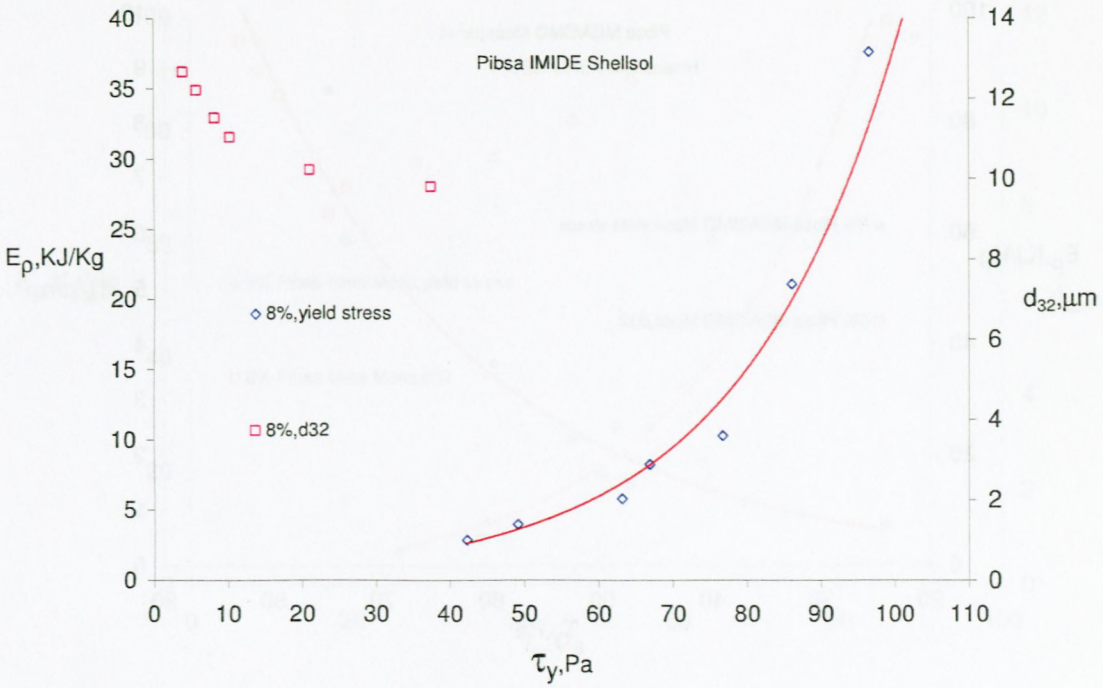

Figure H.5 E_ρ,d_{32} vs. τ_y: 8% Pibsa IMIDE Shellsol

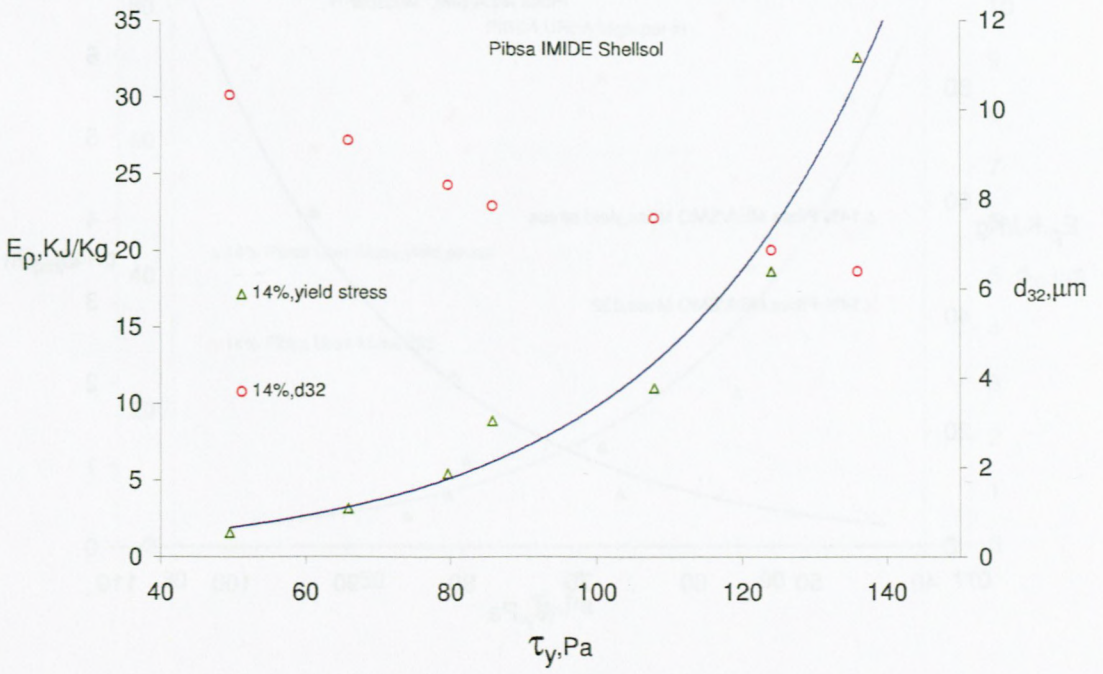

Figure H.6 E_ρ,d_{32} vs. τ_y: 14% Pibsa IMIDE Shellsol

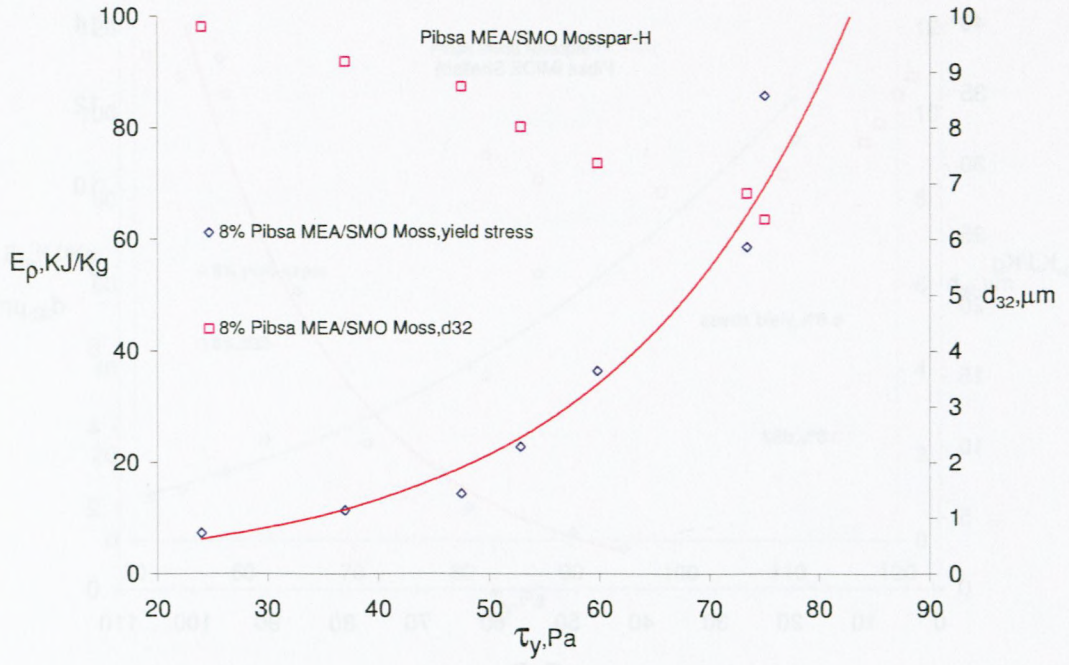

Figure H.7 E_ρ,d_{32} vs. τ_y: 8% Pibsa MEA/SMO Mosspar-H

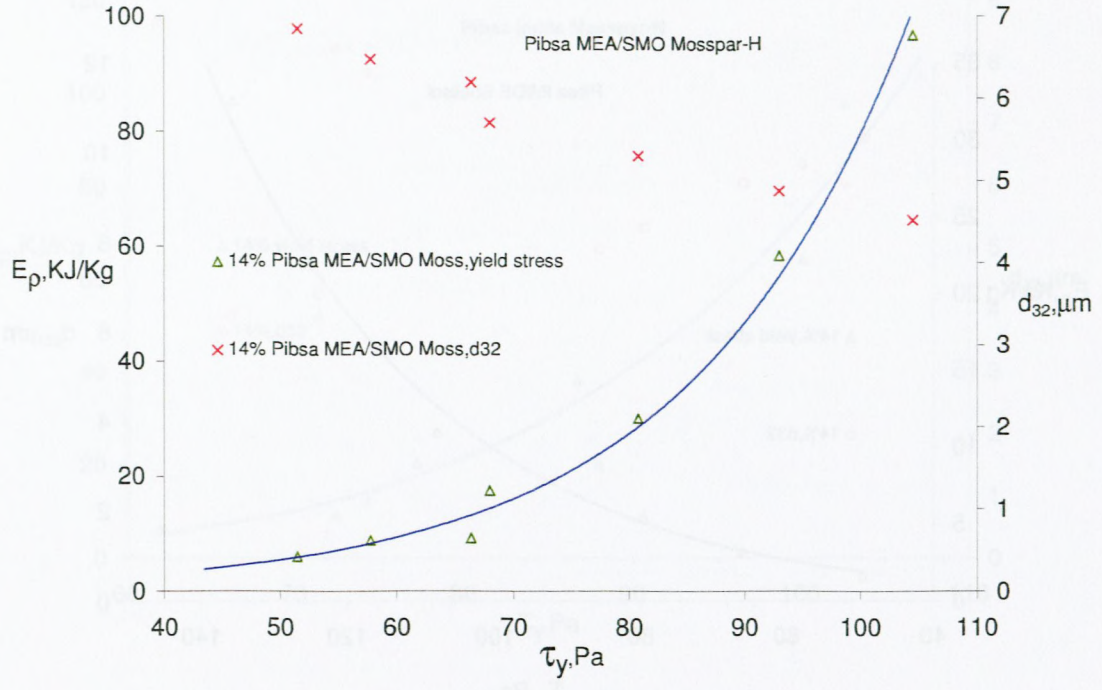

Figure H.8 E_ρ,d_{32} vs. τ_y: 14% Pibsa MEA/SMO Mosspar-H

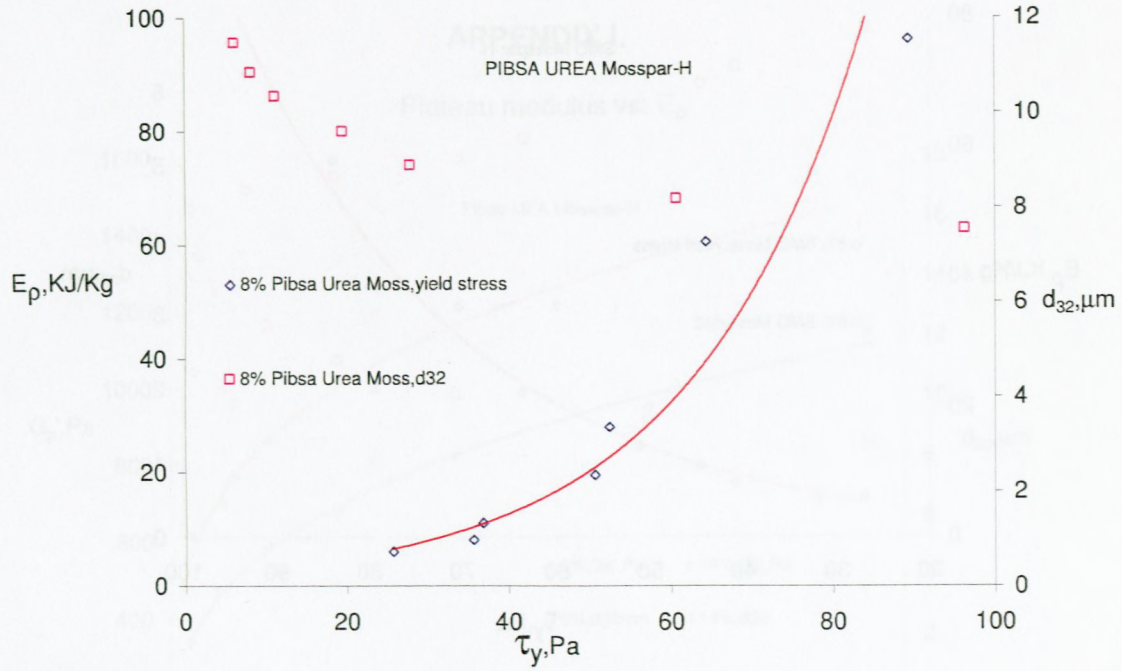

Figure H. 9 E_p,d_{32} vs. τ_y: 8% Pibsa UREA Mosspar-H

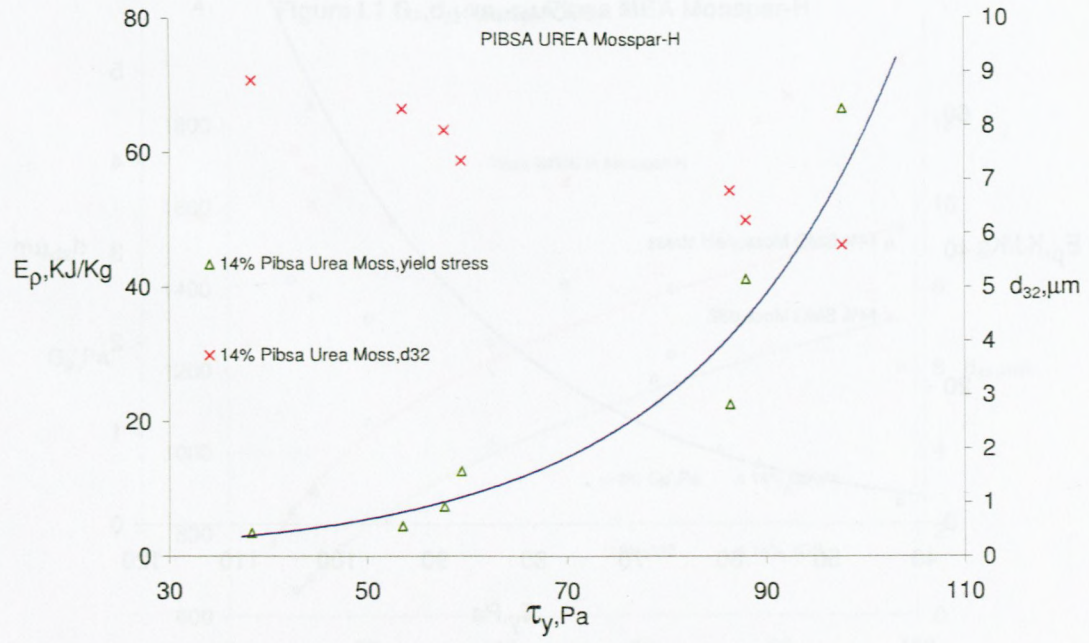

Figure H.10 E_p,d_{32} vs. τ_y: 14% Pibsa UREA Mosspar-H

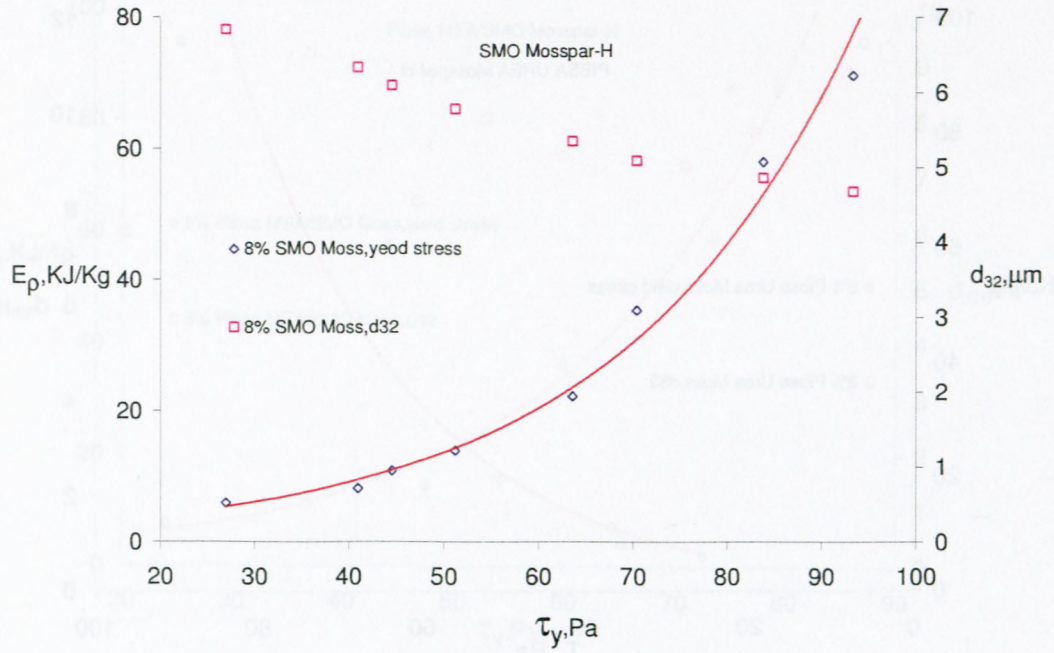

Figure H.11 E_ρ,d_{32} vs. τ_y: 8% Pibsa SMO Mosspar-H

Figure H.12 E_ρ,d_{32} vs. τ_y: 14% Pibsa SMO Mosspar-H

APPENDIX I.

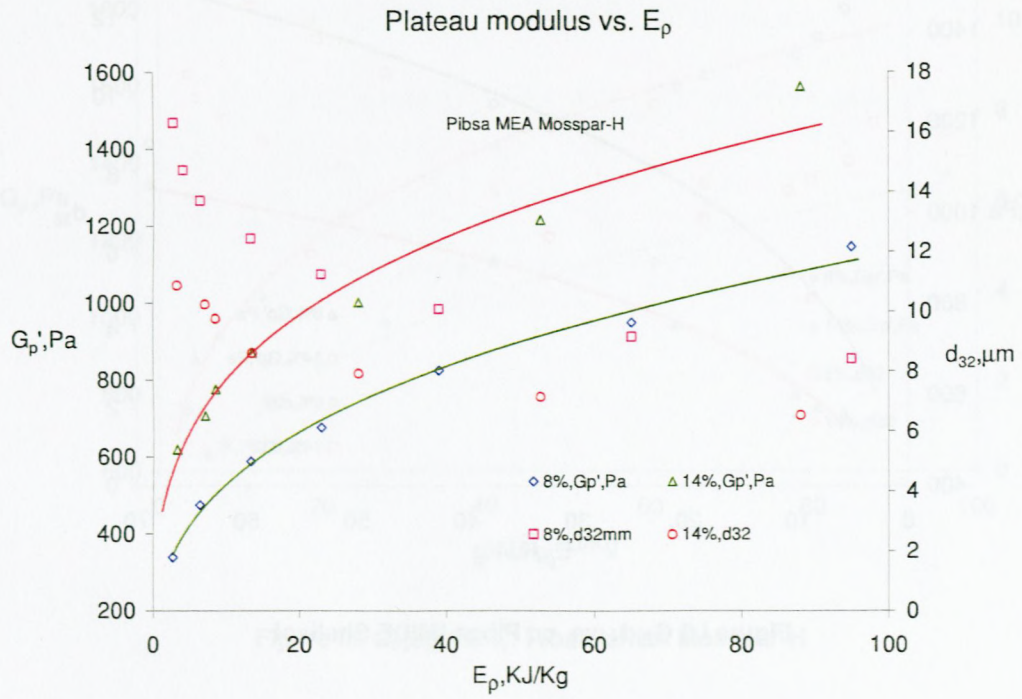

Figure I.1 G_P,d_{32} vs. τ_y: Pibsa MEA Mosspar-H

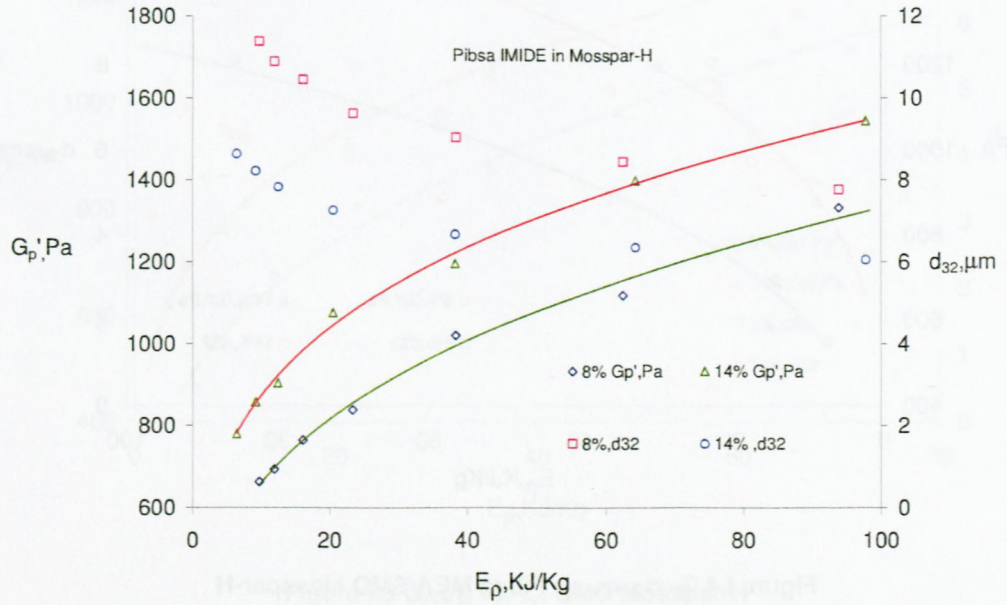

Figure I. 2 G_P,d_{32} vs. τ_y: Pibsa IMIDE Mosspar-H

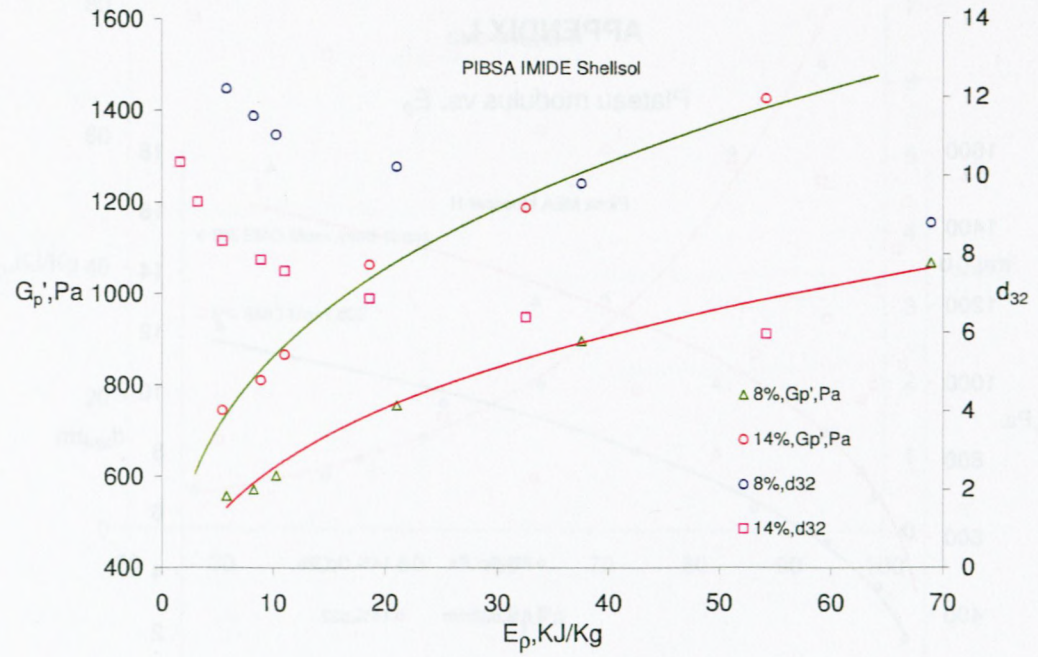

Figure I.3 G_P,d_{32} vs. τ_y: Pibsa IMIDE Shellsol

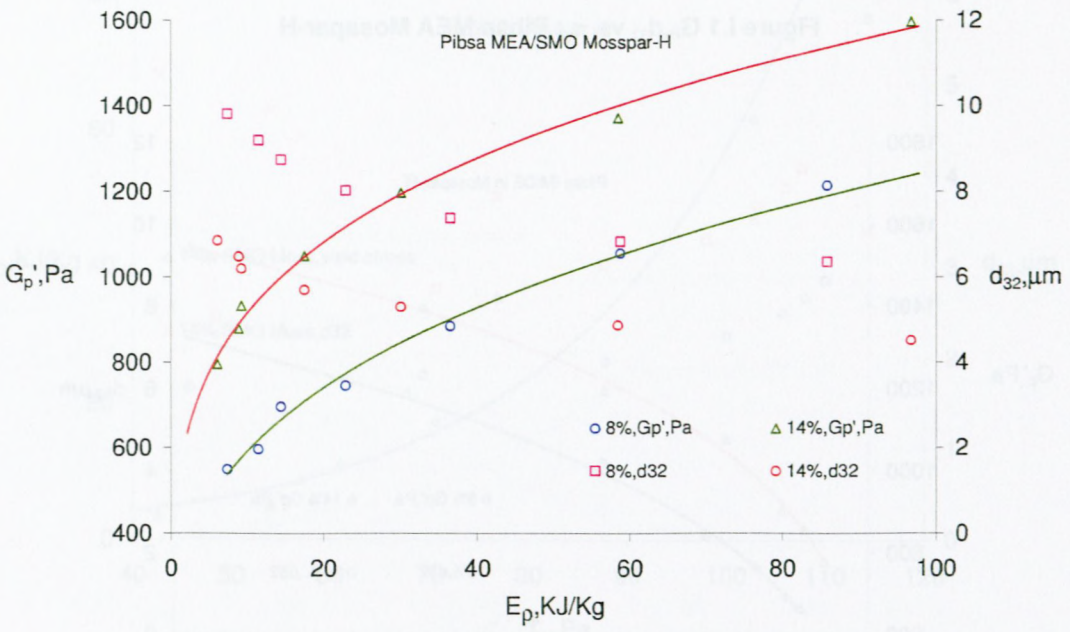

Figure I.4 G_P,d_{32} vs. τ_y: Pibsa MEA/SMO Mosspar-H

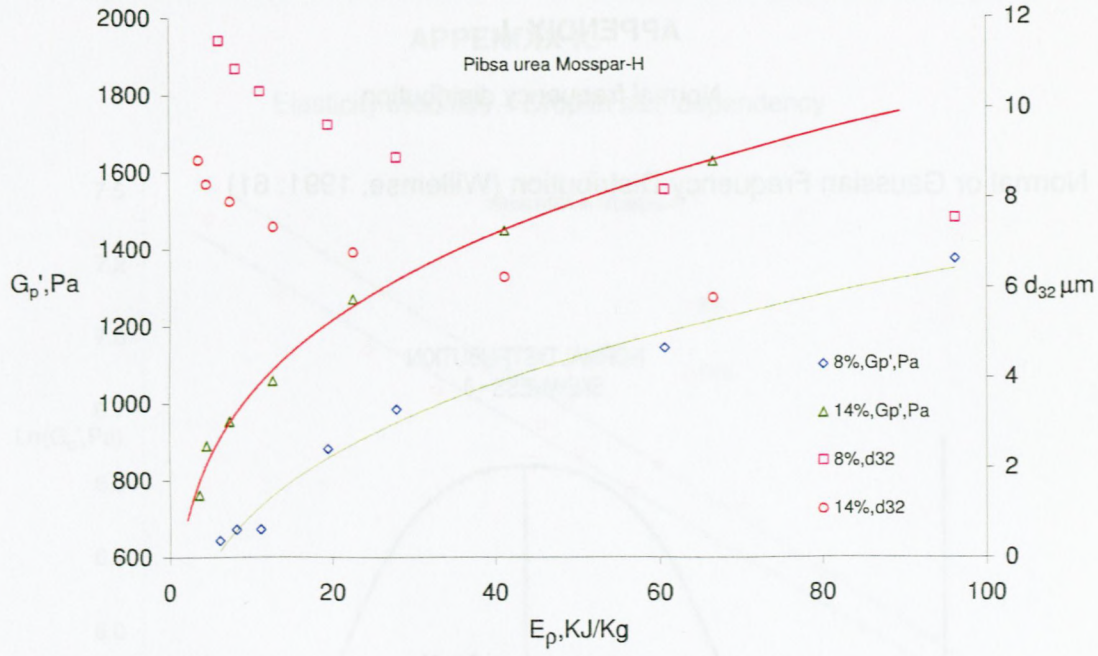

Figure I.5 G_P,d_{32} vs. τ_y: Pibsa UREA Mosspar-H

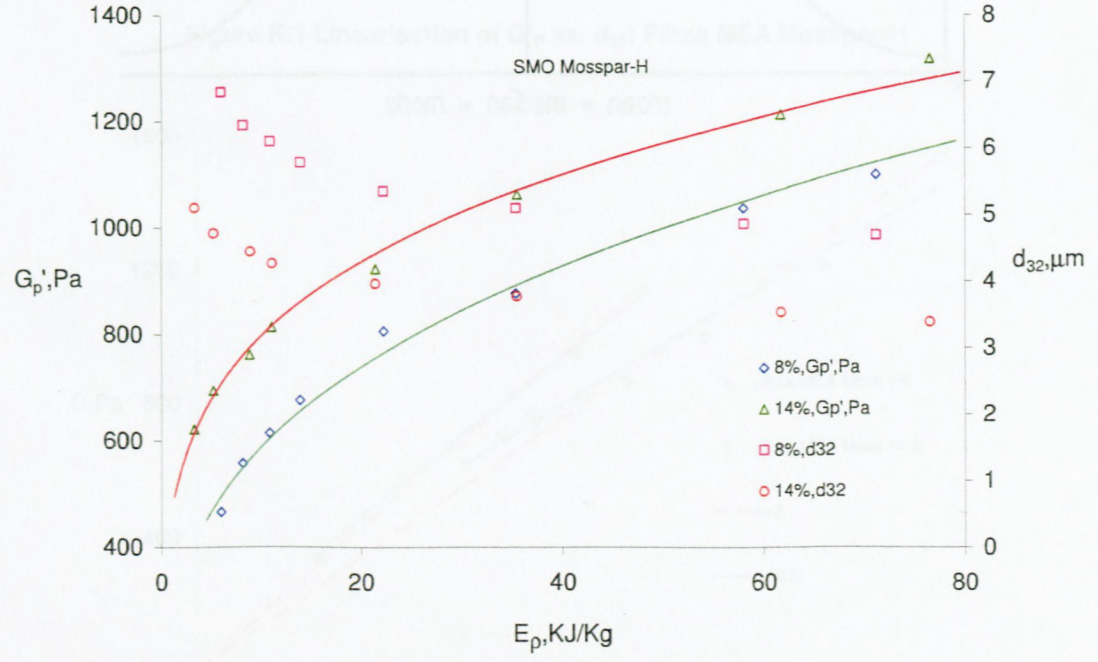

Figure I.6 G_P,d_{32} vs. τ_y: SMO Mosspar-H

APPENDIX J.

Normal frequency distribution

Normal or Gaussian Frequency Distribution (Willemse, 1991: 61)

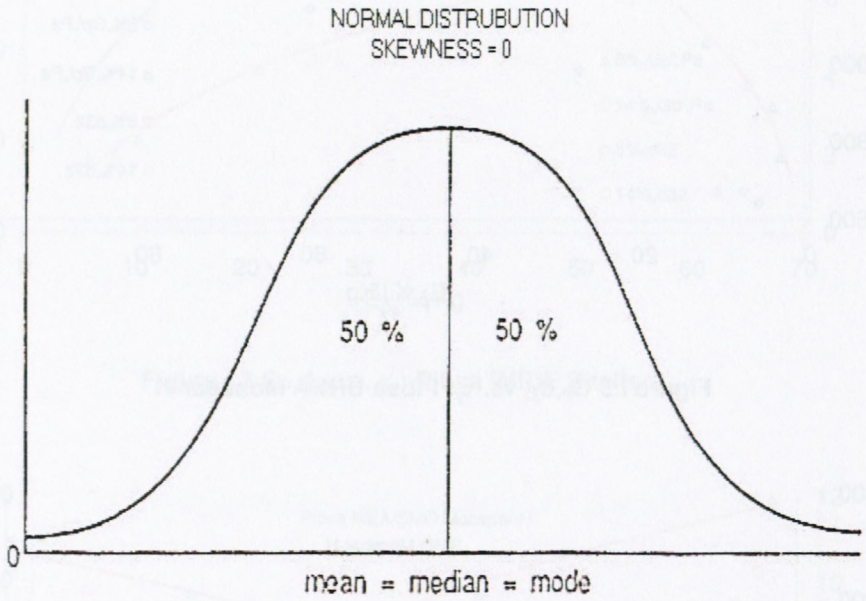

APPENDIX K.

Elasticity modulus – Droplet size dependency

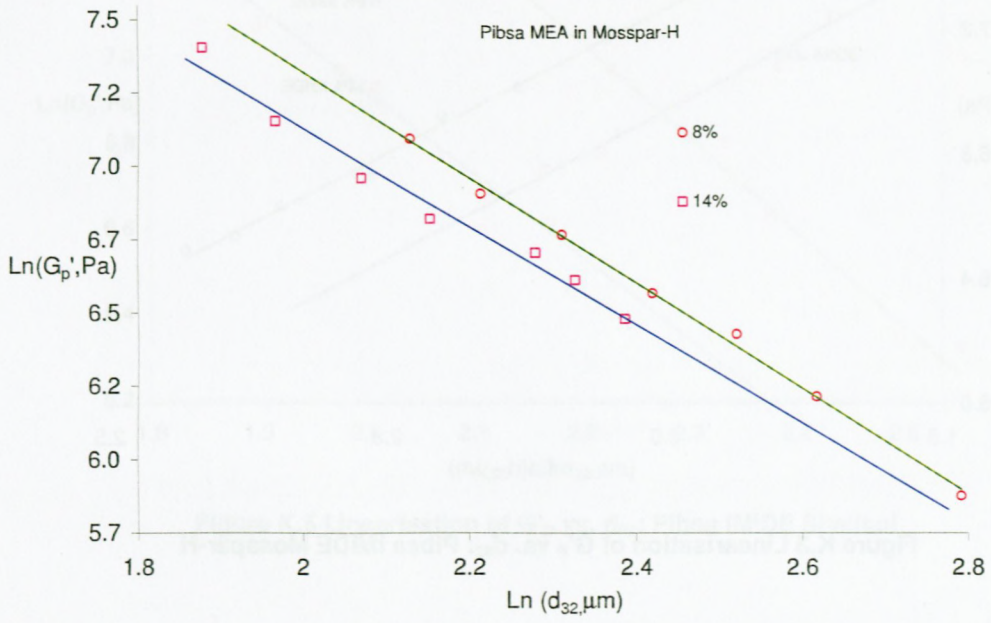

Figure K.1 Linearisation of G'_P vs. d_{32}: Pibsa MEA Mosspar-H

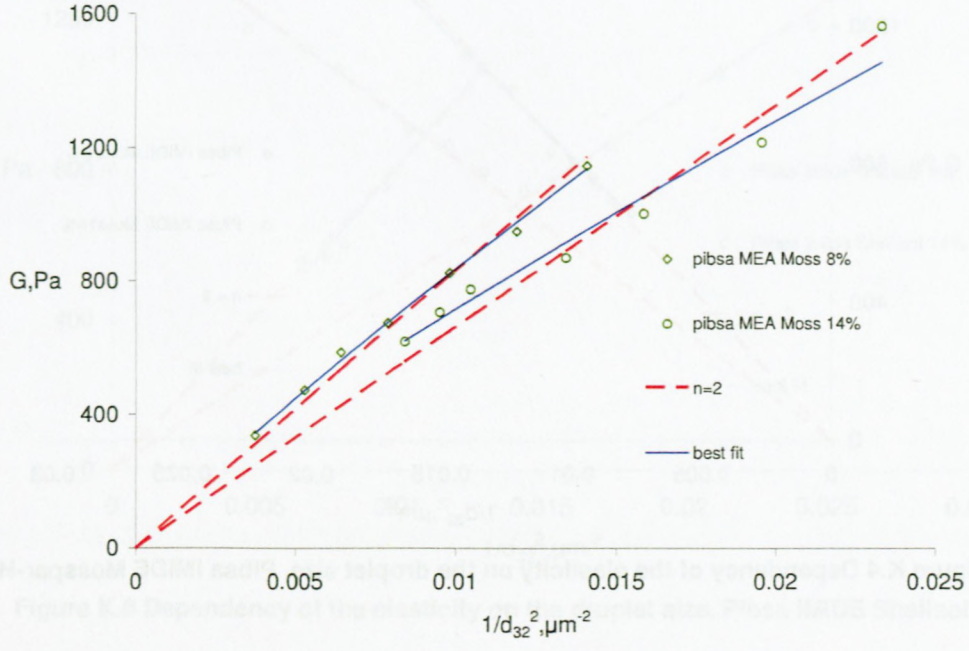

Figure K.2 Dependency of the elasticity on the droplet size, Pibsa MEA Mosspar-H

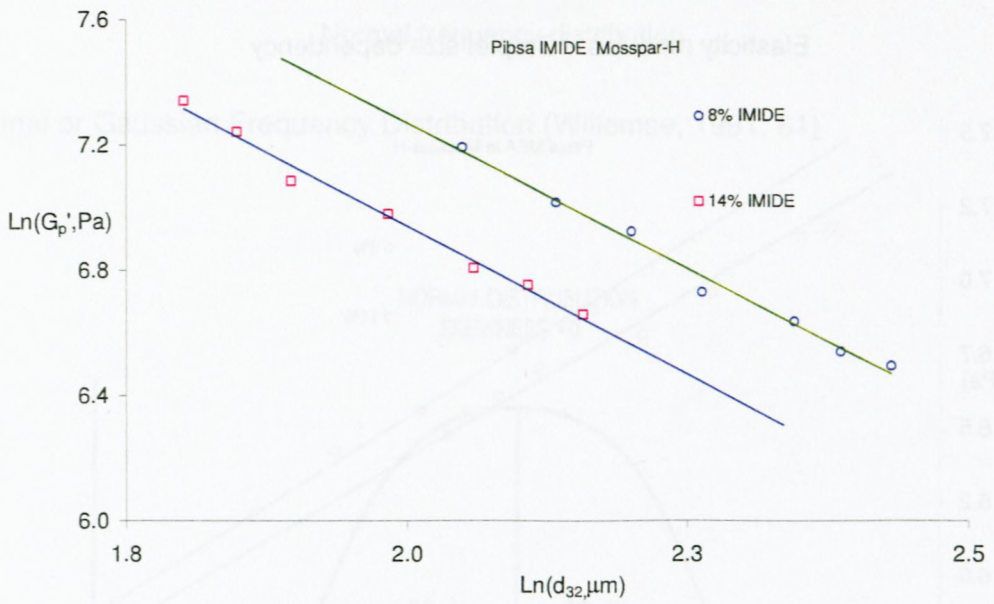

Figure K.3 Linearisation of G'_P vs. d_{32}: Pibsa IMIDE Mosspar-H

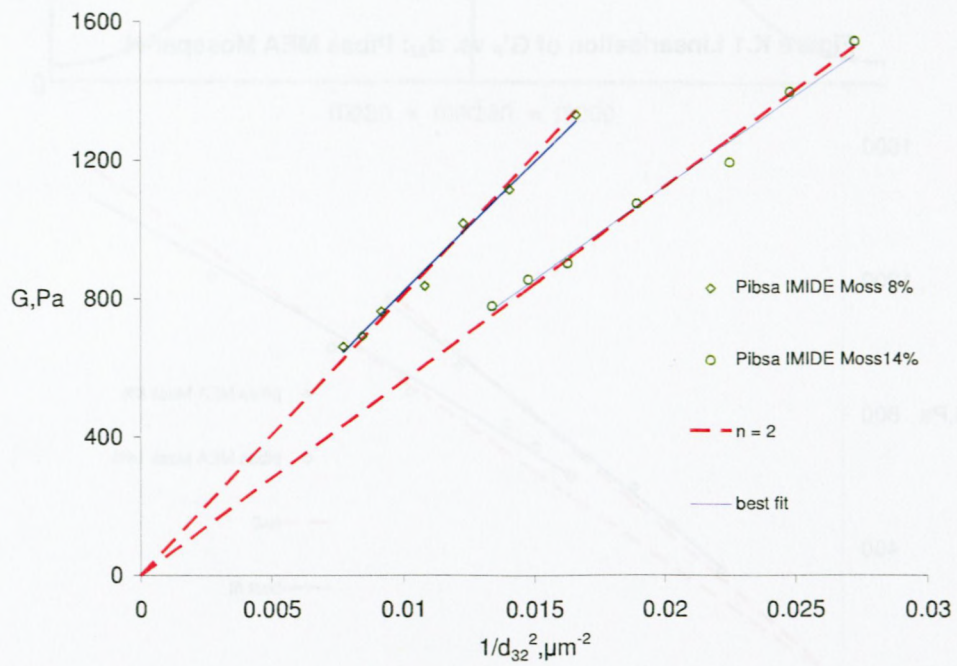

Figure K.4 Dependency of the elasticity on the droplet size, Pibsa IMIDE Mosspar-H

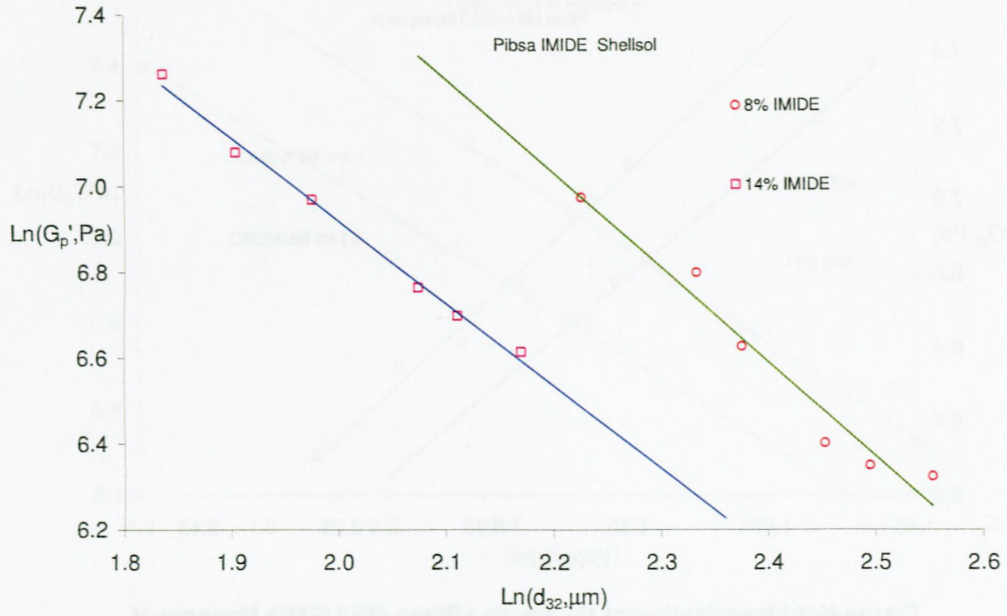

Figure K.5 Linearisation of G'_P vs. d_{32}: Pibsa IMIDE Shellsol

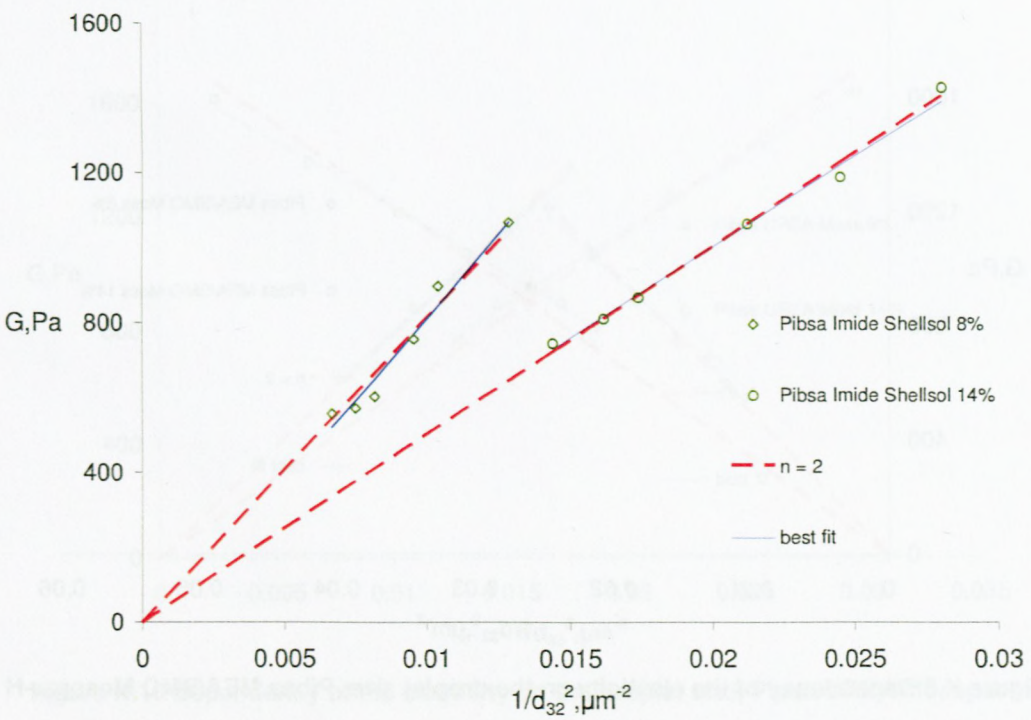

Figure K.6 Dependency of the elasticity on the droplet size, Pibsa IMIDE Shellsol

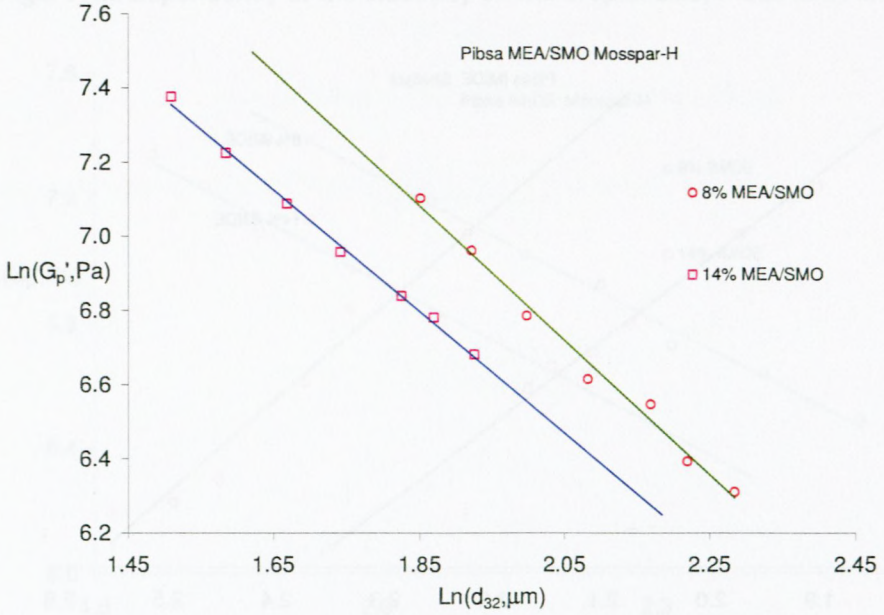

Figure K.7 Linearisation of G'_P vs. d_{32}: Pibsa MEA/SMO Mosspar-H

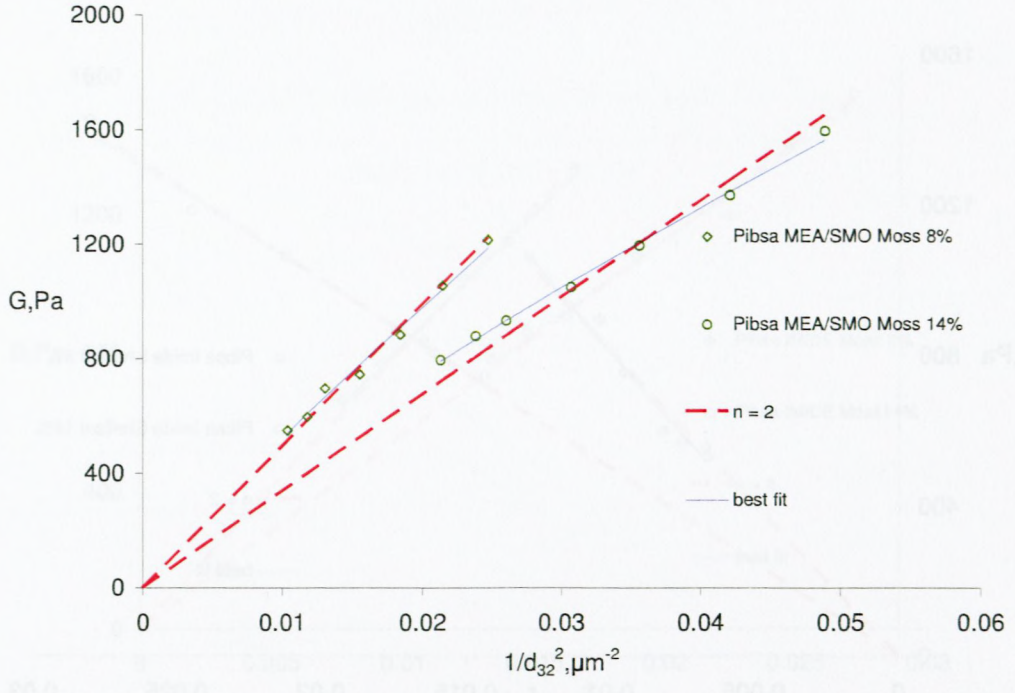

Figure K.8 Dependency of the elasticity on the droplet size, Pibsa MEA/SMO Mosspar-H

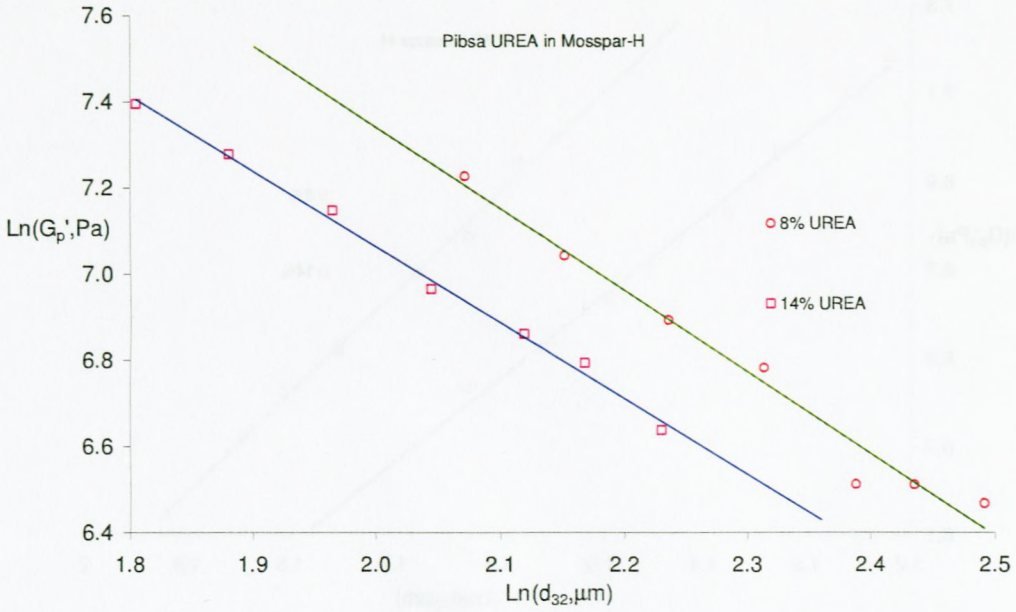

Figure K.9 Linearisation of G'_P vs. d_{32}: Pibsa UREA Mosspar-H

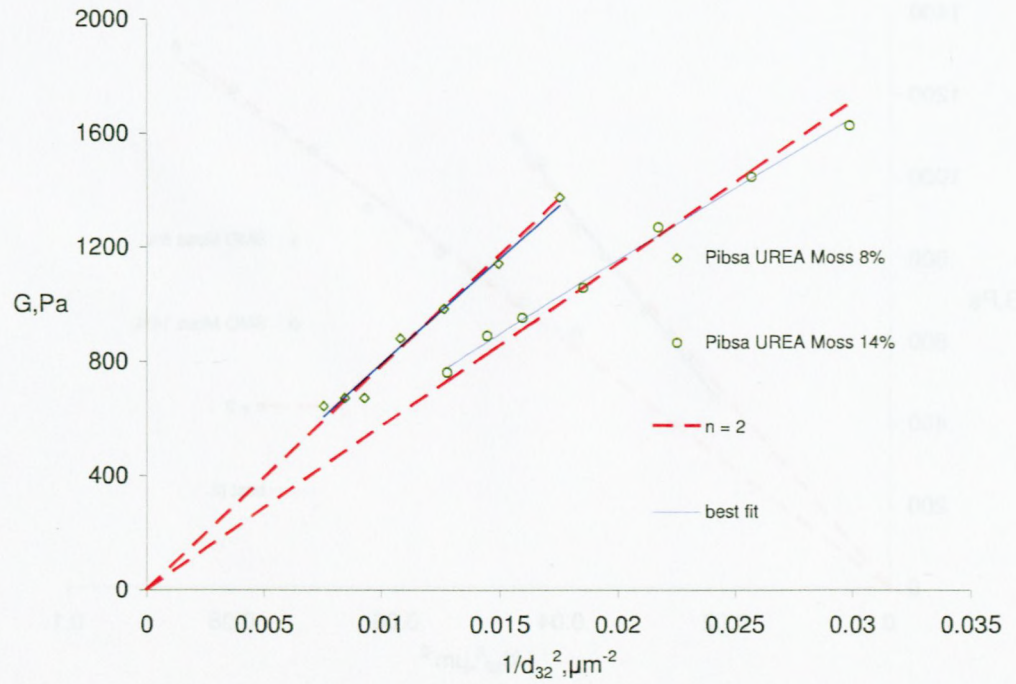

Figure K.10 Dependency of the elasticity on the droplet size, Pibsa UREA Mosspar-H

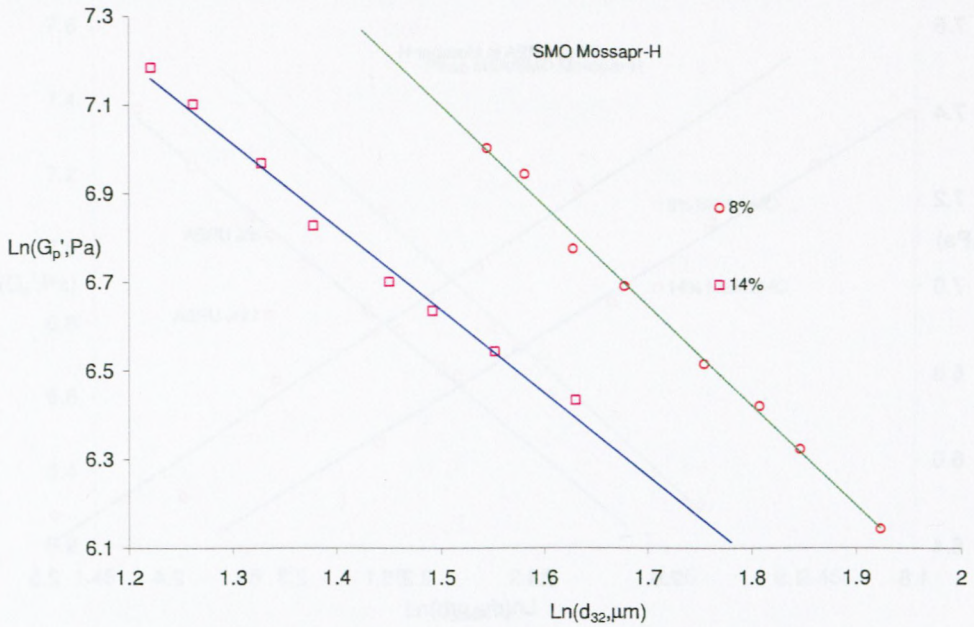

Figure K.11 Linearisation of G'_P vs. d_{32}: SMO Mosspar-H

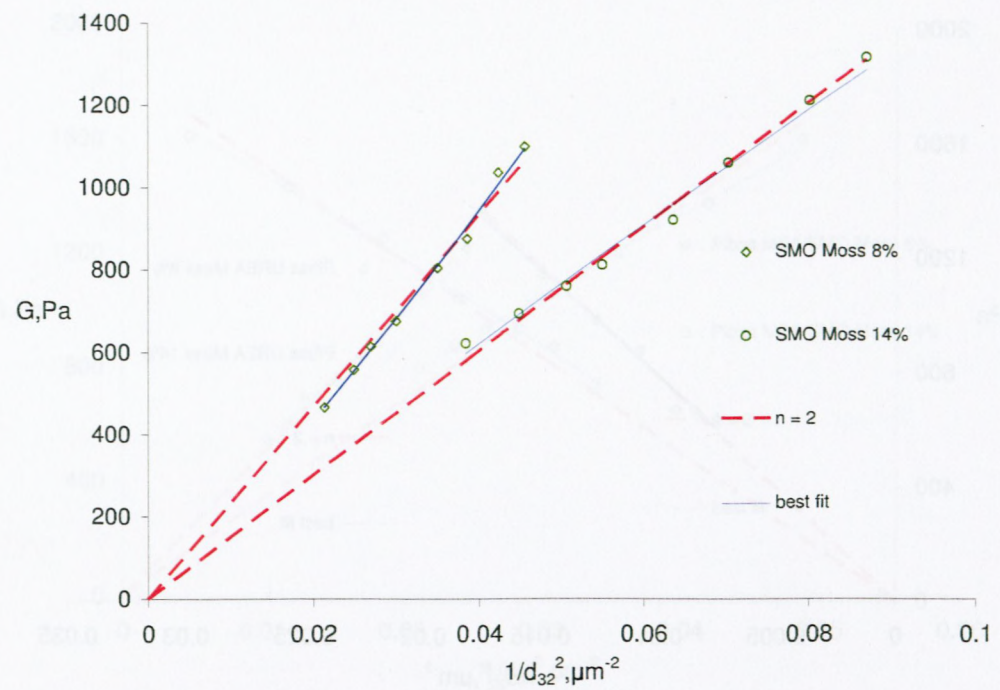

Figure K.12 Dependency of the elasticity on the droplet size, SMO Mosspar-H